Volume 15, Issue 4, December 2025
pISSN 2158-0510 eISSN - 2158-0529

IJBM

International Journal of BIOMEDICINE

www.ijbm.org

IJBM

INTERNATIONAL JOURNAL OF BIOMEDICINE

Aims and Scope: *International Journal of Biomedicine (IJBM)* publishes peer-reviewed articles on the topics of basic, applied, and translational research on biology and medicine. Original research studies, reviews, hypotheses, editorial commentary, and special reports spanning the spectrum of human and experimental and tissue research will be considered. All research studies involving animals must have been conducted following animal welfare guidelines such as the National Institutes of Health (NIH) Guide for the Care and Use of Laboratory Animals, or equivalent documents. Studies involving human subjects or tissues must adhere to the Declaration of Helsinki and Title 45, US Code of Federal Regulations, Part 46, Protection of Human Subjects, and must have received approval of the appropriate institutional committee charged with oversight of human studies. Informed consent must be obtained.

International Journal of Biomedicine endorses and behaves in accordance with the codes of conduct and international standards established by the Committee on Publication Ethics (COPE).

International Journal of Biomedicine (ISSN 2158-0510) is published four times a year by International Medical Research and Development Corp. (IMRDC), 767 Broadway #1549, Manhattan, NY 10003, USA

Customer Service: International Journal of Biomedicine, 767 Broadway #1549, Manhattan, NY 10003, USA; Tel: 1-917-740-3053; E-mail: editor@ijbm.org

Manuscript Submission: Original works will be accepted with the understanding that they are contributed solely to the Journal, are not under review by another publication, and have not previously been published except in abstract form. Accepted manuscripts become the sole property of the Journal and may not be published elsewhere without the consent of the Journal. A form stating that the authors transfer all copyright ownership to the Journal will be sent from the Publisher when the manuscript is accepted; this form must be signed by all authors of the article. All manuscripts must be submitted through the International Journal of Biomedicine`s online submission and review website. Authors who are unable to provide an electronic version or have other circumstances that prevent online submission must contact the Editorial Office prior to submission to discuss alternate options (editor@ijbm.org).

IJBM

INTERNATIONAL JOURNAL OF BIOMEDICINE

ACVC
Association for
Acute CardioVascular Care

ESC ACUTE CARDIOVASCULAR CARE 2026

20-21 MARCH
LISBON, PORTUGAL

#ACVC26

ESC
European Society
of Cardiology

IJBM
INTERNATIONAL JOURNAL OF BIOMEDICINE
www.ijbm.org
Volume 15 Issue 4 December 2025

CONTENTS

CONTENTS

EAPC
European Association
of Preventive Cardiology

ESC Preventive Cardiology 2026

EAPC Annual Congress

23-25 April
Ljubljana, Slovenia

#ESCPrev26

ESC
European Society
of Cardiology

International Journal of Biomedicine 15(4) (2025) 627-633
http://dx.doi.org/10.21103/Article15(4)_RA1

REVIEW ARTICLE

INTERNATIONAL JOURNAL OF BIOMEDICINE

The Complex Interplay Between Alcohol Consumption and Diabetes Mellitus: Insights from Experimental Models and Clinical Studies

N. Kocharyan[1], I. Sahakyan[1*], L. Grigoryan[1], S. Abrahamyan[1], N. Tumasyan[1]

[1]*Institute of Biochemistry after H. Buniatyan, NAS RA, Yerevan, Armenia*

Abstract

Background: This review examines how different patterns of alcohol consumption—moderate, acute, and chronic—affect the development and management of diabetes mellitus, based on experimental and clinical studies.
Methods and Results: A comprehensive literature search was conducted across PubMed, Scopus, Web of Science, Google Scholar, and gray literature sources. Alcohol impacts diabetes pathophysiology, notably insulin resistance and β-cell function. Chronic heavy drinking worsens glucose tolerance and promotes diabetes progression. In contrast, moderate intake with meals may enhance insulin sensitivity and reduce cardiovascular risk. Acute alcohol use, especially without food, can cause hypoglycemia. Effects vary depending on the dose, timing, and individual health.
Conclusions: Alcohol has both beneficial and harmful effects on diabetes. Moderate consumption may help, but chronic use increases risks. Personalized medical advice is essential for safe alcohol use in diabetic patients.(**International Journal of Biomedicine. 2025;15(4):627-633.**)

Keywords: alcohol consumption • insulin sensitivity • diabetes mellitus • cardiovascular diseases

For citation: Kocharyan N, Sahakyan I, Grigoryan L, Abrahamyan S, Tumasyan N. The Complex Interplay Between Alcohol Consumption and Diabetes Mellitus: Insights from Experimental Models and Clinical Studies. International Journal of Biomedicine. 2025;15(4):627-633. doi:10.21103/Article15(4)_RA1

Abbreviations

AT, adipose tissue; **BDNF**, brain-derived neurotrophic factor; **CNS**, central nervous system; **DM**, diabetes mellitus; **DRW**, dealcoholized red wine; **HDL-C**, high-density lipoprotein cholesterol; **LDL-C**, low-density lipoprotein cholesterol; **ROS**, reactive oxygen species; **RW**, red wine; **STZ**, streptozotocin; **T1DM**, type 1 diabetes mellitus; **T2DM**, type 2 diabetes mellitus.

Introduction

Despite extensive research on diabetes mellitus (DM) and the application of modern treatment methods, the disease persists in its progression, particularly in industrialized nations. According to the World Health Organization (WHO) DM is classified into several types: Type 1 diabetes mellitus (T1DM); Type 2 diabetes mellitus (T2DM); Hybrid forms of diabetes (Slowly evolving immune-mediated diabetes of adults, so called Latent autoimmune diabetes in adults (LADA) and Ketosis-prone type 2 diabetes); Hyperglycemia first detected during pregnancy (DM in pregnancy and Gestational DM); Specific types of diabetes (Monogenic diabetes, Diseases of the exocrine pancreas, Endocrine disorders, Drug- or chemical-induced Infections); Unclassified diabetes.[1] But the two major types are T1DM and T2DM. T1DM, also known as the insulin-dependent form, develops as a consequence of the autoimmune-mediated gradual destruction of pancreatic β-cells responsible for insulin production.[2] Approximately, 5-10% of all DM cases are attributed to T1DM. T2DM is a non-insulin-dependent acquired metabolic disorder characterized by diminished insulin sensitivity in tissue cells.[3] In adults, T2DM accounts for 90-95% of all DM cases. Its prevalence is on the rise, particularly among people over 40.[1] According to the WHO, the number of adults with diabetes worldwide in 2014 has doubled in recent decades, reaching 422 million, with projections estimating a rise to 629 million by 2045. The surge is predominantly observed in children and adolescents with T2DM. T1DM is defined by an absolute deficiency in insulin production, while T2DM involves both diminished insulin

secretion and increased insulin resistance.[4] In contrast to T1DM, where insulin replacement therapy is highly effective, managing T2DM necessitates addressing insulin resistance alongside impaired insulin secretion. Gestational diabetes is associated with high blood glucose during pregnancy.[5]

The manifestations of diabetes encompass a spectrum of disorders, including hyperglycemia, altered metabolism of lipids, carbohydrates, and proteins, as well as complications related to vascular injuries,[6] strokes, heart and kidney diseases, impaired immune function, changes in intestinal processes, neuropathy,[7] retinopathy, and gangrene of the extremities.[8] These complications contribute to premature disability and mortality.

It is recognized that during DM, the body's antioxidant defenses are weakened.[9] This, in combination with hyperglycemia and lipid metabolism disorders, contributes to a decrease in the permeability of phospholipid membranes in peripheral tissue cells, as well as in the islets of Langerhans of the pancreas. This disorder ultimately leads to damage to the β-cells of the islets.[10]

Although alcohol consumption is approached cautiously by both clinicians and diabetes patients due to risks like hypoglycemia, metabolic imbalance, and long-term complications, recent biomedical research highlights potential benefits of moderate ethanol intake. Alcohol-related disorders often precede diabetes and remain a public health concern, prompting growing interest in managing diabetes among individuals with alcohol dependence. Epidemiological data suggest a possible inverse link between moderate alcohol use and atherosclerotic risk, raising questions about its role in diabetes care. Alcohol consumption over time is linked to a lower risk of T2DM in initially light or rare drinkers, evident within four years.[11]

This review summarizes recent scientific findings on the complex relationship between alcohol consumption and diabetes mellitus, recognizing their shared impact on multiple physiological systems. A comprehensive literature search was conducted across PubMed, Scopus, Web of Science, Google Scholar, and gray literature sources.

Experimental Models of Diabetes

Analyzing and summarizing recent scientific research on the link between alcohol consumption and DM requires data integrating from both experimental models and clinical studies. Ethical constraints significantly limit diabetes research in humans, as deliberately inducing the disease is strictly prohibited. Research in experimental diabetology plays a crucial role in elucidating pathogenesis, clinical presentation, prevention, and treatment of diabetes. Experimental models of DM provide valuable insights into the pathophysiology of the disease and explain the antidiabetic mechanisms of various drugs through targeted use. Consequently, experimental animal models play a vital role in biomedical studies, offering valuable insights into the mechanisms and potential treatments for human diabetes. Numerous experimental models of DM have been developed,[12,13] with significant ones being:

• Surgical model: The complete or partial removal of the pancreas.

• Chemical model: Injections of chemicals that selectively target the β-cells of the islets of Langerhans, such as alloxan and streptozotocin (STZ).

• Endocrine model: Metapituitary diabetes from prolonged use of somatotropic hormone or adrenocorticotropic hormone, or metasteroid diabetes from glucocorticoid use.

• Immune model: Administering anti-insulin antibodies to animals.

• Genetic model: Employing pure animal lines with hereditary diabetes mellitus.

The development of diabetes in animals depends on the experimental model and the type of chemical used. Chemical-induced diabetes models, particularly using alloxan or STZ, have shown effective results. Alloxan is used to model T1DM, leading to β-cell destruction and insulin deficiency,[14] possibly via the generation of cytotoxic hydroxyl radicals (·OH). Developing an animal model that accurately represents human T2DM poses significant challenges. Nevertheless, such models are crucial for advancing comprehensive diabetes research. Otsuka Long-Evans Tokushima Fatty (OLETF) rats are a common model for studying T2DM, as they exhibit obesity, hyperglycemia, and insulin resistance. In contrast, Long-Evans Tokushima Otsuka (LETO) rats serve as their non-diabetic counterparts, genetically resistant to diabetes. STZ induces both T1DM and T2DM, depending on the dose and administration scheme.[15] Despite their utility, none of these models fully replicates the time-consuming processes of DM in humans.

Impact of Ethanol on Carbohydrate Metabolism

The impact of ethanol on carbohydrate metabolism is complicated and not yet fully elucidated. Specific effects are directly linked to ethanol or its metabolites, acetaldehyde and acetate, while others arise from ethanol-mediated elevation of the NADH/NAD+ ratio in hepatic cells. This alteration in redox balance is driven by the enzymatic conversion of ethanol to acetaldehyde, which is subsequently converted to acetate via dehydrogenase activity. Consequently, this shift in the redox state suppresses the citric acid cycle and fatty acid oxidation, thereby favoring the conversion of pyruvate to lactate.[16] Normally, the liver releases glucose from its glycogen reserves in response to an anticipated glucose deficit. However, alcohol can interfere with this glycogenolysis process. Chronic ethanol consumption significantly impairs glucose release from the liver, leading to a marked reduction in glycogen levels, potentially due to decreased synthesis or increased breakdown, ultimately contributing to hypoglycemia.[17] Findings indicate that prolonged alcohol consumption causes a substantial decrease in hepatic gluconeogenesis when ethanol is present in hepatocytes, with women exhibiting a greater effect than men.[18] Studies reveal that ethanol acutely impacts pancreatic microcirculation, causing redistribution in blood flow from the exocrine to the endocrine regions of the pancreas by mechanisms involving nitric oxide and vagal nerve activity.[19] As a result, late-phase insulin secretion is enhanced, leading to the development of hypoglycemia. Ethanol selectively

increases blood flow to the pancreatic islets by nearly fourfold without significantly altering overall pancreatic blood flow. These effects may help explain the hypoglycemic action of alcohol commonly observed in individuals with diabetes or in those with liver dysfunction associated with chronic alcohol consumption. Reactive hypoglycemia occurred more frequently following the simultaneous consumption of ethanol and glucose than of glucose alone.[20]

In a study by our group, a single intraperitoneal injection of ethanol in alloxan-induced diabetic animals resulted in hypoglycemia, significantly reducing peripheral blood glucose levels by 26%.[21] In summary, alcohol's impact on carbohydrate metabolism is multifaceted, involving various pathways and factors that contribute to complex outcomes.

Some Pathophysiological Mechanisms of the Influence of Ethanol on Diabetes Pathogenesis

The metabolic breakdown of ethanol generates free radicals, primarily targeting mitochondrial membranes. This process hinders oxidative phosphorylation, disrupts the coupling between oxidation and phosphorylation, and depletes energy within the mitochondrial matrix.[22]

The primary metabolite of ethanol, acetaldehyde, has a strong tendency to covalently bind to amino and sulfhydryl groups of proteins, forming Schiff bases and disrupting protein function. Since the inner mitochondrial membrane consists of a substantial proportion of proteins, it is considered the main target of reactive oxygen species (ROS) inside mitochondria.[23] Elevated alcohol intake has been linked to increased ROS production due to disturbances in the mitochondrial oxidative chain by two main enzymes, cytochrome P450 2E1 (CYP2E1) and catalase, two key enzymes that metabolize alcohol to acetaldehyde. This could contribute to pancreatic β-cell dysfunction in individuals with diabetes.

Long-term alcohol consumption has been increasingly linked to T2DM, disrupting glucose metabolism and promoting pancreatic β-cell dysfunction and apoptosis. Even low-to-moderate alcohol intake can structurally alter glucokinase through tyrosine nitration, thereby reducing its enzymatic activity. Prolonged ethanol exposure has been shown to downregulate and inactivate glucokinase via nitration of Tyr residues, contributing to β-cell dysfunction and apoptosis.[24] A study demonstrated that treatment of the rat β-cell line RINm5F with ethanol causes β-cell death by apoptosis.[25] Such findings underscore the harmful consequences of excessive alcohol consumption, including disruptions in lipid metabolism associated with diabetes, driven by oxidative stress and metabolic dysregulation linked to impaired insulin sensitivity.

It is known that diabetes produces various dysfunctions of the central nervous system (CNS), including increased stroke risk, altered brain transport, blood flow disturbances, and metabolic disruptions that may lead to chronic encephalopathy. Acute glycemic fluctuations can trigger coma, seizures, focal neurological deficits, and impaired consciousness.[26] Elevated blood glucose levels in DM negatively impact brain function and cognitive abilities, leading to various neurological and neuropsychiatric disorders, including chronic neurodegeneration and cognitive decline.[27] Alcohol indirectly affects DNA and histone methylation by altering one-carbon metabolism from which methyl groups are derived.[28] A possible pathway by which chronic alcohol consumption could impact various processes associated with the interactions between the nervous and the endocrine systems in T2DM is by influencing appetite-regulating peptides, specifically ghrelin and leptin.

Ghrelin, a gastric-derived peptide, has a dual function in pancreatic β-cells. Beyond its role as a negative regulator of insulin secretion, the findings imply that ghrelin enhances β-cell regeneration in newborn rats treated with STZ. Therefore, early ghrelin administration could potentially aid in preventing diabetes in individuals at risk following β-cell depletion.[29] Ghrelin regulates glucose metabolism and insulin secretion in a variety of species. Consistent with its ability to suppress insulin secretion in vivo, ghrelin-deficient mice generally exhibit lower blood glucose levels than wild-type controls. Ghrelin receptor antagonism has been explored as a potential therapeutic strategy to reduce obesity-related weight gain and improve glucose metabolism in T2DM.[30] Research has demonstrated that ethanol elevates serum ghrelin levels while lowering insulin levels in male Wistar rats, leading to increased mobilization of free fatty acids from adipose tissue to the liver and contributing to hepatic steatosis.[31]

Leptin, the circulating hormone encoded by the obese gene, is produced in adipose tissue (AT) and is a crucial regulator of overall glucose metabolism. Leptin inhibits appetite, increases energy expenditure, and helps stabilize blood glucose, primarily by decreasing hepatic glucose production and increasing glucose utilization in peripheral tissues. It has been demonstrated that excessive leptin levels can contribute to the development of metabolic imbalances, such as dysfunction of pancreatic β-cells, insulin resistance, obesity, and impaired glucose metabolism, all of which contribute to the development of T2DM.[32] Insulin therapy over extended periods has been associated with weight gain and rising leptin concentrations, indicating a regulatory interplay between insulin and leptin secretion. Together, ghrelin and leptin seem to engage in a broad functional interplay, potentially playing an important role in the overall consequences of diabetes with long-term alcohol ingestion.

Recent studies highlight that AT is a key target of ethanol.[33] Adipose tissue plays a significant role in ethanol's effects, as adipocytes release adipokines- biologically active molecules. Ethanol disrupts the secretion of these cell-signaling proteins, thereby altering liver function. Studies show that chronic alcohol consumption in animals and humans increases inflammatory mediators in AT, such as cytokines and chemokines.[34] This alcohol-induced AT dysfunction contributes to liver inflammation by releasing pro-inflammatory molecules like tumor necrosis factor-alpha, which raises circulating inflammatory cytokine levels and induces hepatocyte apoptosis.[35] This subsequently leads to alcohol-associated liver disease, which includes conditions such as steatosis, steatohepatitis, fibrosis, and cirrhosis.[36]

The brain is susceptible to toxicity induced by alcohol. Chronic alcohol consumption significantly impacts neurological function and memory, contributing to cognitive

impairments in affected populations.[37] It is known that the development of depression is observed during DM.[38] Moreover, ethanol's impact on various physiological and mental functions is well-documented. Long-term alcohol consumption can progressively impair psychological well-being, potentially resulting in varying levels of cognitive dysfunction, with severe cases leading to dementia.[39] DM is often considered an accelerator of cognitive decline. Like alcohol exposure, diabetes may also be associated with cognitive impairment.[40]

Researchers have explored the influence of ethanol on the onset of T2DM, focusing on the impact of altered Brain-Derived Neurotrophic Factor (BDNF) levels.[41] Studies on TrkB.T1-deficient mouse model and mouse cell lines reveal that the BDNF receptor TrkB.T1 is present in pancreatic β-cells and in skeletal muscles, and it is crucial for insulin secretion, suggesting a metabolic role separate from CNS influence. These findings highlight BDNF's potential as a key regulator of insulin secretion and a promising target for diabetes treatment.

Studies have revealed that prolonged heavy administration of ethanol induces a reduction in blood BDNF levels in T2DM animals. Specifically, rats treated with ethanol exhibited considerably lower plasma BDNF levels than controls, indicating a possible combined effect of chronic excessive alcohol use and T2DM on reducing BDNF.[42] Moreover, these animals had lower fasting glucose levels but elevated postprandial glucose, highlighting the role of BDNF not only in alcohol metabolism but also in glucose homeostasis and insulin resistance.

Chronic ethanol exposure impairs glucose regulation through mitochondrial dysfunction, oxidative stress, and disrupted insulin secretion. These effects highlight the harmful impact of excessive alcohol on pancreatic β-cell function and underscore the need for strategies to address alcohol-related metabolic risks in diabetes.

Ethanol Consumption and Health Outcomes

According to the WHO, 2.6 million deaths worldwide were related to alcohol consumption in 2019, of which 2 million were among men and 0.6 million among women. Ethanol's impact on health is multifaceted, with effects varying based on the amount consumed and drinking patterns. While most studies quantify alcohol intake in grams, some investigations employ standard drink units, which contain approximately 12 grams of ethanol. Recent publication with a large sample size (n~300,000) reported that spirit drinking was associated with 25% higher risk of mortality and 48% higher risk of liver cirrhosis compared with red wine drinkers.[43] The 2020-2025 U.S. Dietary Guidelines states that for adults heavy or binge alcohol consumption is >60 or 100 g of ethanol per day, or, five or more drinks on any day for men and four or more on any day for women, and moderate alcohol intake is <60 g/day for men, <50 g/day for women, or two drinks or less in a day for men and one drink or less in a day for women.[44] Increased alcohol intake has been shown to be positively correlated with an increased incidence of T2DM.[45] Similar results were found in a study among Japanese men.[46]

On the other hand, moderate alcohol intake has been associated with a lower risk of diabetes, with the strongest inverse correlation observed at 22–24 g/day.[47] A meta-analysis of 15 studies found that moderate drinkers had a reduced risk of developing T2DM compared to abstainers or heavy drinkers, regardless of the beverage type.[48] However, a study on healthy women indicated a stronger protective effect from wine and beer compared to liquor.[49] A government-funded study from the Korean Genome and Epidemiology Study (2001–2012) analyzed data from 1,772 middle-aged Korean men and found a J-shaped relationship between alcohol consumption and T2DM risk.[50] Among white British populations, light to moderate alcohol intake appeared to offer protection against diabetes, whereas excessive drinking heightened the risk.[51] Additionally, alcohol consumption had minimal influence on insulin sensitivity, except in cases of heavy intake, suggesting that ethanol primarily affects diabetes risk through its impact on β-cell function rather than insulin sensitivity.

A separate meta-analysis suggests that moderate alcohol consumption may improve glucose metabolism and contribute to T2DM prevention in men, particularly when compared to lower intake levels.[52] Another recent meta-analysis found no significant impact of alcohol consumption on insulin sensitivity overall, although a potential improvement was observed among women, with no similar effect detected in men.[53] While moderate alcohol intake has been linked to a reduced risk of T2DM, some studies indicate that in some Asian groups, even minimal consumption may still contribute to disease development.[54]

Research shows that polyphenols in wine have antioxidant properties, while ethanol promotes oxidative stress. In one clinical trial, participants consumed 30 g of alcohol daily for 4 weeks, either as red wine (rich in polyphenols) or gin (poor in polyphenols); red wine showed more potent antioxidant effects due to its polyphenol content.[55] Another study found that daily intake of 400 mL of red wine increased plasma total antioxidant status compared to abstention.[56] However, the effects of different alcoholic beverages on antioxidant status remain incompletely understood.

Studies indicate that the non-alcoholic components of red wine, particularly polyphenols, may improve insulin resistance, suggesting that red wine offers greater cardiovascular protection than other alcoholic beverages. Key findings show that red wine, whether alcoholic (RW) or dealcoholized (DRW), enhances glucose metabolism, whereas gin, which lacks polyphenols, does not. Additionally, RW, but not DRW or gin, was found to lower lipoprotein(a) levels in men at high cardiovascular risk.[57] However, caution should be taken when making recommendations related to alcohol consumption.

Moderate alcohol consumption was shown to be associated with a decreased incidence of DM, primarily due to its positive impact on atherosclerotic conditions, notably coronary heart disease in persons with diabetes.[58] In 6745 Framingham Heart Study (FHS) participants (mean age 49 years; 53% women), this effect is believed to involve alterations in lipid metabolism, blood clotting, blood pressure, and insulin sensitivity.[59]

Epidemiological studies have linked moderate alcohol intake to reduced cardiovascular risk and elevated HDL-C levels, although it does not significantly influence total cholesterol, LDL-C, triglycerides, or lipoprotein(a) concentrations.[58,60]

Research consistently shows a dose-dependent relationship between alcohol consumption and hypertension risk.[61] While heavy drinking elevates hypertension risk, moderate consumption appears to have a protective effect, similar to the pattern observed for cardiovascular disease.

Age-related differences in alcohol's effects on LDL-C levels have also been noted. A recent cross-sectional study found a negative correlation between alcohol intake and LDL-C concentration in young women, whereas older men exhibited a positive association.[62] These findings suggest that moderate alcohol consumption provides the most significant cardiovascular benefits for postmenopausal women and adult men. In another investigation, it was shown that moderate red wine consumption has beneficial effects on hemorheological parameters, which may contribute to the "French Paradox."[63]

Heavy or binge drinking increases the risk of death and poses serious social and economic challenges. In contrast, moderate alcohol intake-particularly wine and beer-may offer cardioprotective benefits. However, interpreting epidemiological data requires caution due to confounding factors like ethnicity, age, gender, and drinking patterns. Therefore, recommendations on alcohol use must consider beverage type and population specifics.

Conclusions

The relationship between alcohol consumption and diabetes mellitus is multifaceted, with both harmful and potentially beneficial effects. This review highlights the significant impact of chronic alcohol use on glucose tolerance and insulin resistance, which may contribute to diabetes development. However, moderate alcohol intake, when consumed responsibly and with food, may help reduce cardiovascular risks and support glycemic stability.

Appetite-regulating peptides such as ghrelin, leptin, and BDNF may mediate the link between alcohol and T2DM, though further research is needed to clarify these mechanisms. The complexity of alcohol's metabolic effects underscores the importance of personalized medical guidance. There is no universal rule for safe alcohol use in diabetes; clinicians must consider individual health status, treatment plans, and lifestyle factors.

Ultimately, a deeper understanding of these interactions may inform more effective therapeutic strategies for managing both alcohol use disorder and diabetes, emphasizing the need for open, patient-centered communication in clinical practice.

Competing Interests

The authors declare that they have no financial/commercial conflicts of interest concerning this article.

References

1. World Health Organization. Classification of diabetes mellitus. 21 April 2019. https://www.who.int/publications/i/item/classification-of-diabetes-mellitus
2. Tang W, Liang H, Cheng Y, Yuan J, Huang G, Zhou Z, Yang L. Diagnostic value of combined islet antigen-reactive T cells and autoantibodies assays for type 1 diabetes mellitus. J Diabetes Investig. 2021 Jun;12(6):963-969. doi: 10.1111/jdi.13440.
3. Kahn SE, Cooper ME, Del Prato S. Pathophysiology and treatment of type 2 diabetes: perspectives on the past, present, and future. Lancet. 2014 Mar 22;383(9922):1068-83. doi: 10.1016/S0140-6736(13)62154-6.
4. Ke C, Narayan KMV, Chan JCN, Jha P, Shah BR. Pathophysiology, phenotypes and management of type 2 diabetes mellitus in Indian and Chinese populations. Nat Rev Endocrinol. 2022 Jul;18(7):413-432. doi: 10.1038/s41574-022-00669-4.
5. ElSayed NA, Aleppo G, Aroda VR, Bannuru RR, Brown FM, Bruemmer D, et al. Summary of Revisions: Standards of Care in Diabetes-2023. Diabetes Care. 2023 Jan 1;46(Suppl 1):S5-S9. doi: 10.2337/dc23-Srev.
6. Mota RI, Morgan SE, Bahnson EM. Diabetic vasculopathy: macro and microvascular injury. Curr Pathobiol Rep. 2020 Mar;8(1):1-14. doi: 10.1007/s40139-020-00205-x.
7. Mizukami H. Pathological evaluation of the pathogenesis of diabetes mellitus and diabetic peripheral neuropathy. Pathol Int. 2024 Aug;74(8):438-453. doi: 10.1111/pin.13458.
8. Peng L, Wang Y, Zhao C, Zhao Z, Fei Q, Xin P, et al. Comparative Study of Xi's Tendon Gangrene (Nonischemic Type of Diabetic Foot) and Gangrene (Diabetic Foot Ischemic Type). Comput Math Methods Med. 2022 Jun 28;2022:8114073. doi: 10.1155/2022/8114073. Retraction in: Comput Math Methods Med. 2023 Jun 28;2023:9865264. doi: 10.1155/2023/9865264.
9. Román-Pintos LM, Villegas-Rivera G, Rodríguez-Carrizalez AD, Miranda-Díaz AG, Cardona-Muñoz EG. Diabetic Polyneuropathy in Type 2 Diabetes Mellitus: Inflammation, Oxidative Stress, and Mitochondrial Function. J Diabetes Res. 2016;2016:3425617. doi: 10.1155/2016/3425617.
10. de M Bandeira S, da Fonseca LJ, da S Guedes G, Rabelo LA, Goulart MO, Vasconcelos SM. Oxidative stress as an underlying contributor in the development of chronic complications in diabetes mellitus. Int J Mol Sci. 2013 Feb 5;14(2):3265-84. doi: 10.3390/ijms14023265.
11. Joosten MM, Chiuve SE, Mukamal KJ, Hu FB, Hendriks HF, Rimm EB. Changes in alcohol consumption and subsequent risk of type 2 diabetes in men. Diabetes. 2011 Jan;60(1):74-9. doi: 10.2337/db10-1052.
12. Yagihashi S. Contribution of animal models to diabetes research: Its history, significance, and translation to humans. J Diabetes Investig. 2023 Sep;14(9):1015-1037. doi: 10.1111/jdi.14034.
13. Janapati YK, Junapudi S. Progress in experimental models to investigate the in vivo and in vitro antidiabetic activity of drugs. Animal Model Exp Med. 2024 Jun;7(3):297-309. doi: 10.1002/ame2.12442.
14. Han Q, Sun J, Xie W, Bai Y, Wang S, Huang J, et al. Repeated Low-Dose Streptozotocin and Alloxan Induced

Long-Term and Stable Type 1 Diabetes Model in Beagle Dogs. Biomed Res Int. 2022 Aug 8;2022:5422287. doi: 10.1155/2022/5422287.
15. Furman BL. Streptozotocin-Induced Diabetic Models in Mice and Rats. Curr Protoc. 2021 Apr;1(4):e78. doi: 10.1002/cpz1.78.
16. Seitz HK, Bataller R, Cortez-Pinto H, Gao B, Gual A, Lackner C, et al. Alcoholic liver disease. Nat Rev Dis Primers. 2018 Aug 16;4(1):16. doi: 10.1038/s41572-018-0014-7. Erratum in: Nat Rev Dis Primers. 2018 Aug 28;4(1):18. doi: 10.1038/s41572-018-0021-8.
17. Steiner JL, Crowell KT, Lang CH. Impact of Alcohol on Glycemic Control and Insulin Action. Biomolecules. 2015 Sep 29;5(4):2223-46. doi: 10.3390/biom5042223.
18. Sumida KD, Cogger AA, Matveyenko AV. Alcohol-induced suppression of gluconeogenesis is greater in ethanol fed female rat hepatocytes than males. Alcohol. 2007 Mar;41(2):67-75. doi: 10.1016/j.alcohol.2007.02.002.
19. Huang Z, Sjöholm A. Ethanol acutely stimulates islet blood flow, amplifies insulin secretion, and induces hypoglycemia via nitric oxide and vagally mediated mechanisms. Endocrinology. 2008 Jan;149(1):232-6. doi: 10.1210/en.2007-0632.
20. Oba-Yamamoto C, Takeuchi J, Nakamura A, Takikawa R, Ozaki A, Nomoto H, Kameda H, Cho KY, Atsumi T, Miyoshi H. Combination of alcohol and glucose consumption as a risk to induce reactive hypoglycemia. J Diabetes Investig. 2021 Apr;12(4):651-657. doi: 10.1111/jdi.13375.
21. Kocharyan NV, Khachatryan HS, Sahakyan IK, Tumasyan NV. Effects of ethanol and the amino acids mixture on pathophysiological processes in rats with alloxan-induced diabetes. Biol J Arm. 2021;3:102-8
22. Ganesan R, Jeong JJ, Kim DJ, Suk KT. Recent Trends of Microbiota-Based Microbial Metabolites Metabolism in Liver Disease. Front Med (Lausanne). 2022 May 9;9:841281. doi: 10.3389/fmed.2022.841281.
23. Mantena SK, King AL, Andringa KK, Eccleston HB, Bailey SM. Mitochondrial dysfunction and oxidative stress in the pathogenesis of alcohol- and obesity-induced fatty liver diseases. Free Radic Biol Med. 2008 Apr 1;44(7):1259-72. doi: 10.1016/j.freeradbiomed.2007.12.029.
24. Kim JY, Lee DY, Lee YJ, Park KJ, Kim KH, Kim JW, Kim WH. Chronic alcohol consumption potentiates the development of diabetes through pancreatic β-cell dysfunction. World J Biol Chem. 2015 Feb 26;6(1):1-15. doi: 10.4331/wjbc.v6.i1.1.
25. Dembele K, Nguyen KH, Hernandez TA, Nyomba BL. Effects of ethanol on pancreatic beta-cell death: interaction with glucose and fatty acids. Cell Biol Toxicol. 2009 Apr;25(2):141-52. doi: 10.1007/s10565-008-9067-9.
26. Acherjya GK, Uddin MM, Chowdhury MJ, Srinivasan A. Central Nervous System Manifestations in Diabetes Mellitus - A Review. J Medicine. 2017 Aug 24;18(2):109–12.
27. Chavda V, Yadav D, Patel S, Song M. Effects of a Diabetic Microenvironment on Neurodegeneration: Special Focus on Neurological Cells. Brain Sci. 2024 Mar 15;14(3):284. doi: 10.3390/brainsci14030284.
28. Fowler AK, Hewetson A, Agrawal RG, Dagda M, Dagda R, Moaddel R, et al. Alcohol-induced one-carbon metabolism impairment promotes dysfunction of DNA base excision repair in adult brain. J Biol Chem. 2012 Dec 21;287(52):43533-42. doi: 10.1074/jbc.M112.401497.
29. Irako T, Akamizu T, Hosoda H, Iwakura H, Ariyasu H, Tojo K, Tajima N, Kangawa K. Ghrelin prevents development of diabetes at adult age in streptozotocin-treated newborn rats. Diabetologia. 2006 Jun;49(6):1264-73. doi: 10.1007/s00125-006-0226-3.
30. Liang Y, Yin W, Yin Y, Zhang W. Ghrelin Based Therapy of Metabolic Diseases. Curr Med Chem. 2021;28(13):2565-2576. doi: 10.2174/0929867327666200615152804.
31. Rasineni K, Thomes PG, Kubik JL, Harris EN, Kharbanda KK, Casey CA. Chronic alcohol exposure alters circulating insulin and ghrelin levels: role of ghrelin in hepatic steatosis. Am J Physiol Gastrointest Liver Physiol. 2019 Apr 1;316(4):G453-G461. doi: 10.1152/ajpgi.00334.2018.
32. Pereira S, Cline DL, Glavas MM, Covey SD, Kieffer TJ. Tissue-Specific Effects of Leptin on Glucose and Lipid Metabolism. Endocr Rev. 2021 Jan 28;42(1):1-28. doi: 10.1210/endrev/bnaa027.
33. Gopal T, Ai W, Casey CA, Donohue TM Jr, Saraswathi V. A review of the role of ethanol-induced adipose tissue dysfunction in alcohol-associated liver disease. Alcohol Clin Exp Res. 2021 Oct;45(10):1927-1939. doi: 10.1111/acer.14698.
34. Voican CS, Njiké-Nakseu M, Boujedidi H, Barri-Ova N, Bouchet-Delbos L, Agostini H, et al. Alcohol withdrawal alleviates adipose tissue inflammation in patients with alcoholic liver disease. Liver Int. 2015 Mar;35(3):967-78. doi: 10.1111/liv.12575.
35. Slevin E, Baiocchi L, Wu N, Ekser B, Sato K, Lin E, et al. Kupffer Cells: Inflammation Pathways and Cell-Cell Interactions in Alcohol-Associated Liver Disease. Am J Pathol. 2020 Nov;190(11):2185-2193. doi: 10.1016/j.ajpath.2020.08.014.
36. Carr RM, Dhir R, Yin X, Agarwal B, Ahima RS. Temporal effects of ethanol consumption on energy homeostasis, hepatic steatosis, and insulin sensitivity in mice. Alcohol Clin Exp Res. 2013 Jul;37(7):1091-9. doi: 10.1111/acer.12075.
37. Mira RG, Lira M, Tapia-Rojas C, Rebolledo DL, Quintanilla RA, Cerpa W. Effect of Alcohol on Hippocampal-Dependent Plasticity and Behavior: Role of Glutamatergic Synaptic Transmission. Front Behav Neurosci. 2020 Jan 24;13:288. doi: 10.3389/fnbeh.2019.00288.
38. Bădescu SV, Tătaru C, Kobylinska L, Georgescu EL, Zahiu DM, Zăgrean AM, Zăgrean L. The association between Diabetes mellitus and Depression. J Med Life. 2016 Apr-Jun;9(2):120-5.
39. Kwok CL. Central Nervous System Neurotoxicity of Chronic Alcohol Abuse. Asia Pac J Med Toxicol. 2016;2:70-71.
40. Bordier L, Doucet J, Boudet J, Bauduceau B. Update on cognitive decline and dementia in elderly patients with diabetes. Diabetes Metab. 2014 Nov;40(5):331-7. doi: 10.1016/j.diabet.2014.02.002.
41. Chao MV. Neurotrophins and their receptors: a convergence point for many signalling pathways. Nat Rev Neurosci. 2003 Apr;4(4):299-309. doi: 10.1038/nrn1078.
42. Yamanaka M, Itakura Y, Inoue T, Tsuchida A, Nakagawa T, Noguchi H, Taiji M. Protective effect of brain-derived neurotrophic factor on pancreatic islets in obese diabetic mice. Metabolism. 2006 Oct;55(10):1286-92. doi: 10.1016/j.metabol.2006.04.017.
43. Jani BD, McQueenie R, Nicholl BI, Field R, Hanlon P, Gallacher KI, et al. Association between patterns of alcohol

consumption (beverage type, frequency and consumption with food) and risk of adverse health outcomes: a prospective cohort study. BMC Med. 2021 Jan 12;19(1):8. doi: 10.1186/s12916-020-01878-2.
44. U.S. Department of Agriculture and U.S. Department of Health and Human Services. Dietary Guidelines for Americans, 2020-2025. 9th Edition. December 2020. Available at DietaryGuidelines.gov.
45. Cullmann M, Hilding A, Östenson CG. Alcohol consumption and risk of pre-diabetes and type 2 diabetes development in a Swedish population. Diabet Med. 2012 Apr;29(4):441-52. doi: 10.1111/j.1464-5491.2011.03450.x.
46. Song J, Lin WQ. Association between alcohol consumption and incidence of type 2 diabetes mellitus in Japanese men: a secondary analysis of a Retrospective Cohort Study. BMC Endocr Disord. 2023 Apr 25;23(1):91. doi: 10.1186/s12902-023-01350-1.
47. Cordain L, Melby CL, Hamamoto AE, O'Neill DS, Cornier MA, Barakat HA, Israel RG, Hill JO. Influence of moderate chronic wine consumption on insulin sensitivity and other correlates of syndrome X in moderately obese women. Metabolism. 2000 Nov;49(11):1473-8. doi: 10.1053/meta.2000.17672.
48. Naissides M, Pal S, Mamo JC, James AP, Dhaliwal S. The effect of chronic consumption of red wine polyphenols on vascular function in postmenopausal women. Eur J Clin Nutr. 2006 Jun;60(6):740-5. doi: 10.1038/sj.ejcn.1602377.
49. Kim SH, Abbasi F, Lamendola C, Reaven GM. Effect of moderate alcoholic beverage consumption on insulin sensitivity in insulin-resistant, nondiabetic individuals. Metabolism. 2009 Mar;58(3):387-92. doi: 10.1016/j.metabol.2008.10.013.
50. Lee DY, Yoo MG, Kim HJ, Jang HB, Kim JH, Lee HJ, Park SI. Association between alcohol consumption pattern and the incidence risk of type 2 diabetes in Korean men: A 12-years follow-up study. Sci Rep. 2017 Aug 4;7(1):7322. doi: 10.1038/s41598-017-07549-2.
51. Thompson A, Cook J, Choquet H, Jorgenson E, Yin J, Kinnunen T, et al. Functional validity, role, and implications of heavy alcohol consumption genetic loci. Sci Adv. 2020 Jan 15;6(3):eaay5034. doi: 10.1126/sciadv.aay5034.
52. Zhang S, Liu Y, Wang G, Xiao X, Gang X, Li F, Sun C, Gao Y, Wang G. The Relationship between Alcohol Consumption and Incidence of Glycometabolic Abnormality in Middle-Aged and Elderly Chinese Men. Int J Endocrinol. 2016;2016:1983702. doi: 10.1155/2016/1983702.
53. Schrieks IC, Heil AL, Hendriks HF, Mukamal KJ, Beulens JW. The effect of alcohol consumption on insulin sensitivity and glycemic status: a systematic review and meta-analysis of intervention studies. Diabetes Care. 2015 Apr;38(4):723-32. doi: 10.2337/dc14-1556.
54. Knott C, Bell S, Britton A. Alcohol Consumption and the Risk of Type 2 Diabetes: A Systematic Review and Dose-Response Meta-analysis of More Than 1.9 Million Individuals From 38 Observational Studies. Diabetes Care. 2015 Sep;38(9):1804-12. doi: 10.2337/dc15-0710.
55. Estruch R, Sacanella E, Mota F, Chiva-Blanch G, Antúnez E, Casals E, et al. Moderate consumption of red wine, but not gin, decreases erythrocyte superoxide dismutase activity: a randomised cross-over trial. Nutr Metab Cardiovasc Dis. 2011 Jan;21(1):46-53. doi: 10.1016/j.numecd.2009.07.006.
56. Micallef M, Lexis L, Lewandowski P. Red wine consumption increases antioxidant status and decreases oxidative stress in the circulation of both young and old humans. Nutr J. 2007 Sep 24;6:27. doi: 10.1186/1475-2891-6-27.
57. Chiva-Blanch G, Urpi-Sarda M, Ros E, Valderas-Martinez P, Casas R, Arranz S, et al. Effects of red wine polyphenols and alcohol on glucose metabolism and the lipid profile: a randomized clinical trial. Clin Nutr. 2013 Apr;32(2):200-6. doi: 10.1016/j.clnu.2012.08.022.
58. Ronksley PE, Brien SE, Turner BJ, Mukamal KJ, Ghali WA. Association of alcohol consumption with selected cardiovascular disease outcomes: a systematic review and meta-analysis. BMJ. 2011 Feb 22;342:d671. doi: 10.1136/bmj.d671.
59. Sun X, Ho JE, Gao H, Evangelou E, Yao C, Huan T, et al. Associations of Alcohol Consumption with Cardiovascular Disease-Related Proteomic Biomarkers: The Framingham Heart Study. J Nutr. 2021 Sep 4;151(9):2574-2582. doi: 10.1093/jn/nxab186.
60. Brien SE, Ronksley PE, Turner BJ, Mukamal KJ, Ghali WA. Effect of alcohol consumption on biological markers associated with risk of coronary heart disease: systematic review and meta-analysis of interventional studies. BMJ. 2011 Feb 22;342:d636. doi: 10.1136/bmj.d636.
61. Taylor B, Irving HM, Baliunas D, Roerecke M, Patra J, Mohapatra S, Rehm J. Alcohol and hypertension: gender differences in dose-response relationships determined through systematic review and meta-analysis. Addiction. 2009 Dec;104(12):1981-90. doi: 10.1111/j.1360-0443.2009.02694.x.
62. Whitfield JB, Heath AC, Madden PA, Pergadia ML, Montgomery GW, Martin NG. Metabolic and biochemical effects of low-to-moderate alcohol consumption. Alcohol Clin Exp Res. 2013 Apr;37(4):575-86. doi: 10.1111/acer.12015.
63. Toth A, Sandor B, Papp J, Rabai M, Botor D, Horvath Z, et al. Moderate red wine consumption improves hemorheological parameters in healthy volunteers. Clin Hemorheol Microcirc. 2014;56(1):13-23. doi: 10.3233/CH-2012-1640.

***Corresponding author**: Inesa Sahakyan, PhD, Senior Researcher, Head of Group of Histochemistry and Functional Morphology, Institute of Biochemistry after H. Buniatyan, NAS RA. E-mail: inesasahakyan5@gmail.com*

International Journal of Biomedicine 15(4) (2025) 634-638
http://dx.doi.org/10.21103/Article15(4)_RA2

REVIEW ARTICLE

INTERNATIONAL JOURNAL OF BIOMEDICINE

Oxidative Stress and Oral Microbiota in Periodontitis (Brief-Review)

Marina A. Darenskaya[1*], Ivan S. Goncharov[1,2], Natalya A. Yuzvak[1], Sergey I. Kolesnikov[1], Natalya E. Bolshedvorskaya[2], Lyubov I. Kolesnikova[1]

[1]*Scientific Centre for Family Health and Human Reproduction Problems, Irkutsk, Russian Federation*
[2]*Irkutsk State Medical University, Irkutsk, Russian Federation*

Abstract

The investigation of periodontitis pathogenesis is critically important due to its global prevalence. It has been established that periodontitis is associated with chronic periodontal inflammation, alveolar bone loss, the development of oxidative stress, and oral microbiota dysbiosis. Oxidative stress biomarkers (e.g., malondialdehyde, 8-OHdG) and genetic factors (CXCR4, SELL, ITGAL) exacerbate tissue damage and osteoclastogenesis. The oral microbiota plays a significant role in the development and progression of periodontitis through complex interactions with host immune responses, mediated by pathogenic bacteria like Porphyromonas gingivalis and their metabolic byproducts. Emerging therapies targeting OS (e.g., resveratrol, curcumin) and microbial balance highlight the need for integrated treatment strategies. In this context, it is particularly relevant to investigate the interplay between oxidative stress and microbial dysbiosis to develop targeted therapeutic strategies for the prevention and treatment of periodontitis and its systemic complications. (**International Journal of Biomedicine. 2025;15(4):634-638.**)

Keywords: periodontitis • pathogenesis • oxidative stress • inflammation • oral microbiome • systemic links

For citation: Darenskaya MA, Goncharov IS, Yuzvak NA, Kolesnikov SI, Bolshedvorskaya NE, Kolesnikova LI. Oxidative Stress and Oral Microbiota in Periodontitis (Brief-Review). International Journal of Biomedicine. 2025;15(4):634-638. doi:10.21103/Article15(4)_RA2

Abbreviations

8-OhdG, 8-hydroxy-2-deoxyguanosine; **AH**, arterial hypertension; **AOD**, antioxidant defense; **CAT**, catalase; **GPx**, glutathione peroxidase; **GR**, glutathione reductase; **GSH**, reduced glutathione; **LPO**, lipid peroxidation; **NO**, nitric oxide; **OS**, oxidative stress; **ROS**, reactive oxygen species; **SOD**, superoxide dismutase; **TBARs**, thiobarbituric acid reactants; **WHO**, World Health Organization.

Relevance of Studying Periodontitis

Periodontitis is one of the most common diseases, affecting between 50% and 90% of individuals in developing countries and between 4% and 76% in developed countries [1] According to the World Health Organization (WHO). intact periodontitis occurs only in 2-10% of cases, while inflammatory periodontal diseases are detected in 90-95% of the adult population.[2]

Periodontitis is characterized by prolonged periodontal inflammation, including the gum, periodontal ligament, and alveolar bone, with loss of the latter.[3] The main cause, as a rule, is pathogenic microorganisms contained in plaque.[4] The decisive predisposing factors are the fact of smoking, poor oral hygiene, genetic component, gastrointestinal disorders, etc.[5] At a young age, traumatic effects, bleeding gums, partial dentition, low bone mineral density, and obesity are added.[6] It was also noted that disorders in the immune system, local changes in acid-base balance, hypoxia, and other adverse factors contribute to the proliferation of pathogenic microorganisms, an increase in the activity of opportunistic infection, and the progression of inflammatory and destructive periodontal diseases.[7] In recent years, it has been proven that periodontitis, as an inflammatory process, can be epidemiologically related to other chronic diseases, which include cardiovascular, neurodegenerative, autoimmune, oncological, and others.[8-10] Understanding the pathology and etiology of periodontitis is crucial to developing effective approaches to periodontitis treatment.

Oxidative Stress in Periodontitis Genesis

Currently, more than 200 diseases associated with the involvement of free radicals are known. They are characterized by changes in the internal environment and vascular disorders, which indicate a single mechanism of development – an

imbalance in the "lipid peroxidation (LPO) – antioxidant defense (AOD) "LPO – AOD system. The term oxidative stress (OS) is widely used to describe this imbalance.[11] LPO-AOD plays an important role in adaptive reactions, reducing the activity of inflammatory processes, pathology, and maintaining homeostasis.[12] The predominant role of this type of reaction in modifying cell membrane structure, xenobiotic metabolism, regulating the immune response, cell proliferation, vascular permeability, and receptor sensitivity is well established.[13] The activation of LPO reactions in the membranes of the endoplasmic reticulum, mitochondria, and lysosomes undoubtedly plays a crucial role in the functioning of normal cellular systems, presumably determining overall reactivity and resistance to pathogenic factors.[14]

Modern studies confirm that the insufficiency of AOD factors contributes to the uncontrolled intensification of LPO processes, which play a crucial role in the development of various pathologies, including those associated with periodontal disorders.[15] Moreover, the development of OS occurs not only due to a decrease in the buffer capacity of the AOD system, but also due to a violation of its mobilization in response to an increase in the activity of prooxidant factors. Protection of cells from LPO at different stages is implemented by various systems of both enzymatic and non-enzymatic nature.[16] At the same time, LPO reactions in the membranes of various cellular compartments play a crucial role in determining the overall reactivity of the body and its resistance to pathogenic influences.[17]

It was proven that OS plays a key role in the pathogenesis of periodontitis. Studies revealed changes in the expression of genes associated with oxidative stress (OS genes) in patients with periodontitis.[18,19] In total, 74 genes were isolated in periodontitis, the expression of which changes during OS, including 65 genes with increased expression and 9 genes with reduced expression. Six key genes (CXCR4, SELL, FCGR3B, FCGR2B, PECAM1, and ITGAL) are involved in leukocyte intercellular adhesion, phagocytosis, and cellular extravasation, which highlights their role in the pathogenesis of the disease.[20] CXCR4 is one of the most expressed OS genes in periodontal tissues. It plays a key role in podocyte damage, proteinuria, and glomerular sclerosis under oxidative stress. The neutralization of CXCR4 suppresses the resorption of the alveolar bone in periodontal inflammation. CXCR4 also suppresses the release of nitric oxide from macrophages and is involved in modulating mechanical sensitivity in periodontitis. The interaction of PECAM1 and CXCR4 genes enhances the transendothelial migration of leukocytes, promoting tissue infiltration by neutrophils and monocytes. The SELL and ITGAL genes ensure the adhesion of immune cells to the endothelium, which exacerbates periodontal damage.[20] Another study also identified the OS genes ITGAM, FCGR3A, and PECAM1, which perform a crucial function in the development of periodontitis.[21] Under the influence of pathogenic microflora, increased involvement and activation of neutrophils in periodontal tissues is noted, which, in turn, synthesize reactive oxygen species (ROS).[22] There is an aberrant activation of neutrophils, the increased release of pro-inflammatory mediators, which ultimately leads to tissue damage and disease progression.[23] It is interesting to discover the special structure of neutrophils – neutrophil extracellular traps (netosis), which they use for their function. Numerous studies indicate violations of local and/or systemic OS indicators.[24] Thus, clinical studies demonstrate an increase in the levels of LPO products, such as diene conjugates and malondialdehyde, in saliva and gingival fluid in patients with periodontitis.[25,26] These changes correlate with the severity of the disease and can serve as markers of its progression.[25,27] In periodontitis, there was also an increase in other markers of OS – 8-OHdG, carbonylated proteins, nitric oxide (NO), and 8-isoprostanes.[28,29] Several studies have investigated the level of nitrosative stress in the saliva of patients with periodontitis.[30] Basically, an increased level of these biomarkers was found, correlating with the risk of developing comorbidity of periodontal pathology and cardiovascular diseases.[24] Patients with periodontitis also exhibited an increase in less common markers, such as those indicating nuclear abnormalities and shortening of leukocyte telomeres.[31,32] Periodontitis-induced OS can trigger pro-inflammatory mechanisms and, significantly, osteoclastogenesis, which then leads to bone loss observed in patients with periodontitis.[20] Studies of the AOD system in periodontitis primarily focus on the activity of GR, SOD, CAT, GPx, myeloperoxidase, vitamin C, uric acid, GSH, melatonin, and the integral indicator of overall antioxidant status.[23] Negative changes in periodontitis often occur in the saliva. In patients with periodontitis, there were disturbances in glutathione homeostasis in peripheral blood neutrophils, which significantly impaired the chemotactic ability of these cells to combat infectious agents.[33] In patients with stage IV periodontitis, vitamin C levels were significantly lower than those in patients with early-stage periodontitis.[34] It was also noted that vitamin D deficiency led to a decrease in bone density, osteoporosis, and, as a result, the progression of periodontal diseases.[35] It is believed that the traditional treatment of periodontitis, which aims to combat bacterial pathogens, is insufficient. The use of additional antioxidants, such as resveratrol, quercetin, biochanin A, pyonol, and curcumin, which react stoichiometrically with ROS, has become a promising method for treating periodontitis.[36]

Oral Microbiota and Periodontitis

The human oral cavity is home to a diverse array of microorganisms that form a complex ecosystem, which, in terms of the number of species and complexity of organization, is second only to the microbiota of the gastrointestinal tract.[37] The complexity of the microbiota is due to the diverse environmental conditions in various parts of the oral cavity, which form microenvironments for colonization and growth of specific microorganisms forming highly organized surface-associated communities (biofilms) immersed in an extracellular polymer matrix, which consists of a complex of extracellular polymeric substances (water, polysaccharides, proteins, lipids, and DNA).[38] The oral microbiota plays a key role in the development and progression of periodontitis.[39] Plaque bacteria are the main culprits of periodontal diseases.[40] Plaque is present in both the supra-gingival and sub-gingival regions, forming microbial biofilms that multiply on the tooth surface. The slit-like epithelium and gingival fissure serve as the main

habitats of microbes, supported by gingival slotted fluid and a favorable anaerobic environment.[41] It has been identified that the subgingival plaque, comprising more than 500 species, changes composition as the disease progresses.[42] In healthy conditions, gram-positive cocci and rods predominate as early colonizers, while *Fusobacterium nucleatum* promotes bacterial coagulation.[43] Pathogenic microorganisms, such as *Porphyromonas gingivalis* and *Aggregatibacter actinomycetemcomitans*, are capable of triggering a systemic inflammatory response and exacerbating the course of the disease.[44] It was found that OS can suppress the tolerance of macrophages to endotoxins induced by lipopolysaccharides produced by *Porphyromonas gingivalis* bacteria, thereby contributing to the progression of periodontitis through the suppression of tolerance to endotoxins.[45] It is known that *Aggregatibacter actinomycetemcomitans* can migrate from stress factors to a more protected subgingival region due to the activation of hexosaminidase, which attacks matrix polysaccharides containing hexosamine.[46] When faced with an innate subgingival reaction, *Aggregatibacter actinomycetemcomitans* can activate complement resistance genes and leukotoxin production to modulate the host's local immune response and ensure the proliferation of a consortium of pathobionts. Working together, the consortium can suppress the natural resistance of the host organism and produce inflammatory cytokines, which can lead to loss of connective tissue and bone tissue, as well as impaired attachment.[47]

Microbial imbalance (dysbiosis) contributes to the activation of OS and chronic inflammation. The formation of ROS, which has primarily antimicrobial effects, can be considered a double-edged sword, as ROS can help destroy invading pathogens during treatment; however, when overactivated, they can become cytotoxic to host cells. ROS play an essential role in cell signaling, gene regulation, and antimicrobial defense. Still, an overabundance of reactive oxygen species leads to increased oxidative stress, along with unchanged or reduced antioxidant capacity, which in turn leads to OS in the affected tissues. This subsequently results in pathological changes and, consequently, cell destruction of the host tissues.[48]

Periodontitis and Systemic Diseases

Periodontitis is often associated with systemic pathologies such as oral cancer, Alzheimer's disease, Parkinson's disease, hypertension, diabetes mellitus, and chronic kidney disease.[49] The connection arises from chronic low-grade inflammation, bacterial dissemination, and shared pathogenic mechanisms between periodontal and systemic diseases. Every year, the dentists' interest in disorders of systemic and local hemodynamics is expanding, and the links between periodontal pathology and cardiovascular diseases were established. The presence of systemic diseases, taking medications, and hormonal changes can certainly have a significant effect on periodontal tissue. Thus, it was established that comorbid associations of periodontitis, particularly with arterial hypertension (AH) in adolescence, are accompanied by disorders of systemic hemodynamics and contribute to a more active course of inflammatory processes in periodontal tissues.[50] Circulatory disorders in periodontal diseases correlate with the severity and degree of hypertension, as manifested by changes in vascular tone and permeability, endothelial dysfunction in the arterial network, and impaired autonomic regulation of vascular tone in tissues.[50] The risk factors for periodontal disease on the background of hypertension include common factors: socio-economic, smoking, stress, and age; hence, hypertension and periodontitis have a common mechanism of development.[51] In particular, the dynamic balance in the LPO-AOD underlies the functioning of systems that regulate the contraction of vascular smooth muscle cells and, consequently, systemic blood pressure.[52] It was established that the disorganization of the homeostatic mechanisms of the microvascular periodontal bed in arterial hypertension causes chronic hypoxia of the periodontal complex tissues, in which the processes of LPO of biomolecules are activated, leading to a violation of the structure and function of periodontal biomembranes correlations between the parameters of blood flow of the microcirculatory bed of the periodontium and the content of the final products of LPO thiobarbituric acid reactants (TBARs). The reinforcing effect of damaging factors may be due to the accumulation of prooxidants in periodontal tissues, their subsequent decomposition, leading to the formation of free radicals that have a destructive effect on the vascular wall, resulting in fibrosis, thickening of capillaries, and partial or complete obliteration.[53]

Oxidative stress plays a key mediating role, as stress-related overproduction of ROS overwhelms antioxidant defenses, accelerating periodontal tissue breakdown and worsening systemic disease progression. Stress factors play a significant role in the development of periodontitis. It is known that adaptation to stress is associated with the activation of stress-limiting systems, including prostaglandin and antioxidant systems, as well as an increase in the number of adenosinergic receptors. This suggests that the protective effects under stress are based on the coordinated activation of central and local stress-limiting systems. At the same time, adaptation to stress factors is impossible in cases where the regulatory stress systems responsible for implementing stress reactions have congenital or acquired defects. It can be assumed that an innate predisposition to hypertension reduces the body's functional reserves, which may serve as a risk factor for further disease progression.[54]

In conclusion, periodontitis is a multifactorial disease, the pathogenesis of which is influenced by oxidative stress, dysbiosis of the oral microbiota, and systemic inflammation. The relationship of periodontitis with cardiovascular and other chronic diseases was established, which underlines the need for an integrated approach to its prevention and treatment. Further studies of the pathogenetic mechanisms of periodontitis will help develop personalized therapies aimed at correcting oxidative stress and restoring microbial balance.

Conflicts of Interest

The authors declare that they have no competing interests.

References

1. Ayati A, Khodabandelu S, Khaleghi S, Nourmohammadi A, Jafari F, Ahmadianghalehsorkh M, et al. A systematic review and network meta-analysis of the association between periodontitis and inflammatory bowel diseases. BMC Oral Health. 2025;25(1):463. doi: 10.1186/s12903-025-05830-9.
2. World Health Organization. Global oral health status report: towards universal health coverage for oral health by 2030; 2022.
3. de Pablo P, Chapple IL, Buckley CD, Dietrich T. Periodontitis in systemic rheumatic diseases. Nature reviews. Rheumatology. 2009; 5(4):218–224. doi: 10.1038/nrrheum.2009.28
4. Wang Z, Saxena A, Yan W, Uriarte SM, Siqueira R, Li X. The impact of aging on neutrophil functions and the contribution to periodontitis. International journal of oral science. 2025;17(1):10. doi: 10.1038/s41368-024-00332-w
5. Ray RR. Periodontitis: an oral disease with severe consequences. Applied biochemistry and biotechnology. 2023;195(1):17-32. doi: 10.1007/s12010-022-04127-9
6. Hung M, Kelly R, Mohajeri A, Reese L, Badawi S, Frost C, et al. Factors associated with periodontitis in younger individuals: A scoping review. Journal of Clinical Medicine. 2023;12(20):6442. doi: 10.3390/jcm12206442
7. Orlandi M, Munoz Aguilera E, Marletta D, Petrie A, Suvan J, D'Aiuto F. Impact of the treatment of periodontitis on systemic health and quality of life: A systematic review. Journal of Clinical Periodontology. 2022;49:314-327. doi: 10.1111/jcpe.13554.
8. Schenkein HA, Papapanou PN, Genco R, Sanz M. Mechanisms underlying the association between periodontitis and atherosclerotic disease. Periodontology 2000. 2020;83(1):90–106. doi: 10.1111/prd.12304.
9. Genco RJ, Sanz M. Clinical and public health implications of periodontal and systemic diseases: An overview. Periodontology. 2000. 2020;83(1):7–13. doi: 10.1111/prd.12344.
10. Ishai A, Osborne MT, El Kholy K, Takx RAP, Ali A, Yuan N, et al. Periodontal Disease Associates With Arterial Inflammation Via Potentiation of a Hematopoietic-Arterial Axis. JACC Cardiovasc. Imaging. 2019;12:2271–2273. doi: 10.1016/j.jcmg.2019.05.015.
11. Kolesnikova LI, Darenskaya MA, Kolesnikov SI. [Free radical oxidation: a pathophysiologist's view]. Bulletin of Siberian Medicine. 2017;16(4):16-29. doi: 10.20538/1682-0363-2017-4-16-29. [Article in Russian].
12. Darenskaya MA, Grebenkina LA, Sholokhov LF, Rashidova MA., Semenova NV, Kolesnikov SI, et al. Lipid peroxidation activity in women with chronic viral hepatitis. Free Radical Biology & Medicine. 2016;100(S):192. doi: 10.1016/j.freeradbiomed.2016.10.525.
13. Darenskaya MA, Kolesnikova LR, Rychkova LV, Grebenkina LA, Semenova NV, Druzhinina EB, et al. Comparative Analysis of Lipid Peroxidation System in Humans and Rats with Arterial Hypertension. International Journal of Biomedicine. 2019;9(4):292-296. doi: 10.21103/Article9(4)_OA3
14. Darenskaya M, Kolesnikova L, Kolesnikov S. The association of respiratory viruses with oxidative stress and antioxidants. implications for the COVID-19 pandemic. Current Pharmaceutical Design. 2021;27(13):1618-1627. doi: 10.2174/1381612827666210222113351
15. Kolesnikova LR, Darenskaya MA, Pogodina AV, Grebenkina LA, Natyaganova LV, Kolesnikova LI, et al. [The relationship of hemodynamic parameters of periodontal microvascular bed and lipid peroxidation products in adolescents with arterial hypertension]. Stomatology. 2020;99(4):914. doi: 10.17116/stomat2020990419 [Article in Russian]
16. Kolesnikova LI, Darenskaya MA, Grebenkina LA, Osipova EV, Dolgikh MI, Semenova NV. [Analysis of antioxidant status and actual diet of students]. Voprosy pitaniia. 2015;84(4):66-73.[Article in Russian]
17. Kolesnikova LI, Rychkova LV, Kolesnikova LR, Darenskaya MA, Natyaganova LV, Grebenkina LA., et al. Coupling of lipoperoxidation reactions with changes in arterial blood pressure in hypertensive isiah rats under conditions of chronic stress. Bulletin of Experimental Biology and Medicine. 2018;164(6):712-715.doi: 10.1007/s10517-018-4064-3
18. Halliwell B. Understanding mechanisms of antioxidant action in health and disease. Nature Reviews Molecular Cell Biology. 2024;25(1):13-33. doi:10.1038/s41580-023-00645-4
19. Sies H, Mailloux RJ, Jakob U. Fundamentals of redox regulation in biology. Nature Reviews Molecular Cell Biology. 2024;25(9):701-719. doi:10.1038/s41580-024-00730-2
20. Zhang Z, ZhengY, Bian X, Wang M, Chou J, Haifeng L, et al. Identification of key genes and pathways associated with oxidative stress in periodontitis. Oxidative Medicine and Cellular Longevity, 2022;(1):1-27. doi: 10.1155/2022/9728172.
21. Zhou W, Zhang P, Li H. Identifying Oxidative Stress-Related Genes (OSRGs) as Potential Target for Treating Periodontitis Based on Bioinformatics Analysis. Comb Chem High Throughput Screen. 2024;27(8):1191-1204. doi:10.2174/1386207326666230821102623
22. Bassani B, Cucchiara M, Butera A, Kayali O, Chiesa A, Palano MT, et al. Neutrophils' contribution to periodontitis and periodontitis-associated cardiovascular diseases. International Journal of Molecular Sciences. 2023;24(20):15370. doi: 10.3390/ijms242015370
23. Palomino-Segura M, Sicilia J, Ballesteros I, Hidalgo A. Strategies of neutrophil diversification. Nature Immunology. 2023;24(4):575-584. doi: 10.1038/s41590-023-01452-x
24. Patil RT, Dhadse PV, Salian SS, Punse SD, Dhadse P, Salian SS. Role of Oxidative Stress in Periodontal Diseases. Cureus. 2024;16(5). doi: 10.7759/cureus.60779
25. Mohideen K, Chandrasekaran K, Veeraraghavan H, Faizee SH, Dhungel S, Ghosh S. Meta-Analysis of Assessment of Total Oxidative Stress and Total Antioxidant Capacity in Patients with Periodontitis. Disease Markers. 2023;2023(1):9949047. doi: 10.1155/2023/9949047
26. Skutnik-Radziszewska A, Zalewska A. Salivary redox biomarkers in the course of caries and periodontal disease. Applied Sciences. 2020;10(18):6240. doi: 10.3390/app10186240
27. Leong XF, Ng CY, Badiah B, Das S. Association between hypertension and periodontitis: possible mechanisms. The Scientific World Journal. 2014;(1):11-41. doi:10.1155/2014/768237
28. Goriuc A, Cojocaru KA, Luchian I, Ursu RG, Butnaru O, Foia L. Using 8-Hydroxy-2′-Deoxiguanosine (8-OHdG) as a Reliable Biomarker for Assessing Periodontal Disease Associated with Diabetes. International Journal of Molecular Sciences. 2024;25(3):1425. doi: 10.3390/ijms25031425
29. Maciejczyk M, Zalewska A, Ładny JR. Salivary antioxidant barrier, redox status, and oxidative damage to proteins and

lipids in healthy children, adults, and the elderly. Oxidative Medicine and Cellular Longevity. 2019;2019(1):4393460. doi: 10.1155/2019/4393460
30. Toczewska J, Konopka T, Zalewska A, Maciejczyk M. Nitrosative Stress Biomarkers in the Non-Stimulated and Stimulated Saliva, as well as Gingival Crevicular Fluid of Patients with Periodontitis: Review and Clinical Study. Antioxidants. 2020;9(3):259. doi: 10.3390/antiox9030259
31. de Mello Lobro WJ, Zajdenverg L, Lopes GC, de Barros MCM, Sansone C, Silva-Boghossian CM. Redox biomarkers in saliva and nuclear abnormalities in jugal epithelial cells of individuals with type 2 diabetes mellitus and periodontitis. Archives of Oral Biology. 2024;161:105915. doi: 10.1016/j.archoralbio.2024.105915
32. Sonoki K, Muraoka K, Morishita M, Awano S, Nakashima K. Periodontal Disease Shortens the Telomere Length in Human Gingival Crevicular Epithelium Cells and Human Umbilical Endothelial Cells. Journal of Biomedical Research & Environmental Sciences. 2024;5(9):1168-1175. doi: 10.37871/jbres2005
33. Binti Badlishah Sham NI, Grant MM. Role of Glutathione in Neutrophil Chemotaxis in Periodontitis. Oral. 2023;3(4):526-538. doi: 10.3390/oral3040043
34. Munday MR, Rodricks R, Fitzpatrick M, Flood VM, Gunton JE. A Pilot Study Examining Vitamin C Levels in Periodontal Patients. Nutrients. 2020;12(8):2255. doi: 10.3390/nu12082255
35. Nascimento GG, Leite FR, Gonzalez-Chica DA, Peres KG, Peres MA. Dietary vitamin D and calcium and periodontitis: A population-based study. Frontiers in Nutrition. 2022;9:1016763. doi: 10.3389/fnut.2022.1016763
36. Wu Y, Zhang X, Chen Y, Chen W, Qian W. Identification the Low Oxidative Stress Subtype of Periodontitis. International Dental Journal. 2024;74(1):119-128. doi:10.1016/j.identj.2023.07.011
37. Huttenhower C, Gevers D, Knight R, Abubucker S, Badger JH, Chinwalla AT, et al. Structure, function and diversity of the healthy human microbiome. Nature. 2012;486:207–214. doi: 10.1038/nature11234.
38. Di Stefano M, Polizzi A, Santonocito S, Romano A, Lombardi T, Isola G. Impact of Oral Microbiome in Periodontal Health and Periodontitis: A Critical Review on Prevention and Treatment. International Journal of Molecular Sciences. 2022;23(9):5142. doi: 10.3390/ijms23095142
39. Gao L, Xu T, Huang G, Jiang S, Gu Y, Chen F. Oral microbiomes: More and more importance in oral cavity and whole body. Protein Cell. 2018;9:488–500. doi: 10.1007/s13238-018-0548-1.
40. Lu M, Xuan S, Wang Z. Oral microbiota: A new view of body health. Food Sci. Hum. Wellness. 2019;8:8–15. doi: 10.1016/j.fshw.2018.12.001
41. Malla MA, Dubey A, Kumar A, Yadav S, Hashem A, Abd Allah EF. Exploring the Human Microbiome: The Potential Future Role of Next-Generation Sequencing in Disease Diagnosis and Treatment. Front. Immunol. 2019;9:2868. doi: 10.3389/fimmu.2018.02868.
42. Moore WE, Moore LV. The bacteria of periodontal diseases. Periodontology 2000. 1994;5:66–77. doi: 10.1111/j.1600-0757.1994.tb00019.x.
43. Rajasekaran JJ, Krishnamurthy HK, Bosco J, Jayaraman V, Krishna K, Wang T, et al. Oral Microbiome: A Review of Its Impact on Oral and Systemic Health. Microorganisms. 2024;12(9):1797. doi: 10.3390/microorganisms12091797
44. Mukherjee S, Chopra A, Karmakar S, Bhat, SG. Periodontitis increases the risk of gastrointestinal dysfunction: an update on the plausible pathogenic molecular mechanisms. Critical Reviews in Microbiology. 2024;51(1):187–217.doi: 10.1080/1040841X.2024.2339260
45. Yamaguchi T, Yamamoto Y, Egashira K, Sato A, Kondo Y, Saiki S, et al. Oxidative Stress Inhibits Endotoxin Tolerance and May Affect Periodontitis. Journal of Dental Research. 2022;102(3):331-339. doi:10.1177/00220345221138523
46. Ramasubbu N, Thomas LM, Ragunath C, Kaplan JB. Structural analysis of dispersin B, a biofilm-releasing glycoside hydrolase from the periodontopathogen Actinobacillus actinomycetemcomitans. Journal of Molecular Biology. 2005;349(3):475-486. doi:10.1016/j.jmb.2005.03.082
47. Fine DH, Patil AG and Velusamy SK. Aggregatibacter actinomycetemcomitans (Aa) Under the Radar: Myths and Misunderstandings of Aa and Its Role in Aggressive Periodontitis. Front. Immunol. 2019;10:728. doi: 10.3389/fimmu.2019.00728
48. Sczepanik FSC, Grossi ML, Casati M, Goldberg M, Glogauer M, Fine N, et al. Periodontitis is an inflammatory disease of oxidativestress: We should treat it that way. Periodontol 2000. 2020;84:45-68. doi: 10.1111/prd.12342
49. Albahri J, Allison H, Whitehead KA, Muhamadali H. The role of salivary metabolomics in chronic periodontitis: bridging oral and systemic diseases. Metabolomics. 2025;21(1):24. doi:10.1007/s11306-024-02220-0
50. Kolesnikova LR, Darenskaya MA, Kolesnikova LI, Grebenkina LA, Kolesnikov SI, Korytov LI, et al. Morphofunctional state of the periodontal tissues in humans and rats with arterial hypertension. Bulletin of Experimental Biology and Medicine. 2020;169(6):831-835. doi: 10.1007/s10517-020-04990-8
51. Stepanov EA, Kurashvili LV, Mikulyak NI, Moiseev YaP, Kinzirskiy AS. [The features of parodentium's microcirculation in various systemic diseases (a literature review)]. Izvestiya Vysshikh Uchebnykh Zavedeniy. Povolzhskiy region. Meditsinskie Nauki. 2021;2:137–150. doi:10.21685/2072-3032-2021-2-13. [Article in Russian]
52. Bairova TA, Kolesnikov SI, Kolesnikova LI, Pervushina OA, Darenskaya MA, Grebenkina LA. Lipid peroxidation and mitochondrial superoxide dismutase-2 gene in adolescents with essential hypertension. Bulletin of Experimental Biology and Medicine. 2015;158(2):181-184. doi: 10.1007/s10517-014-2717-4
53. Kolesnikova LR, Darenskaya MA, Pogodina AV, Grebenkina LA, Natyaganova LV, Kolesnikova LI, et al. [The relationship of hemodynamic parameters of periodontal microvascular bed and lipid peroxidation products in adolescents with arterial hypertension]. Stomatology. 2020;99(4):914. doi: 10.17116/stomat2020990419 [Article in Russian]
54. Kolesnikova LI, Kolesnikova LR, Darenskaya MA, Natyaganova LV, Grebenkina LA, Korytov LI, et al. Comparison of Reactivity of the Lipid Peroxidation–Antioxidant Defense System in Normal and Hypertensive Rats at Different Stages of Stress-Reaction. Bulletin of Experimental Biology and Medicine. 2019;166(5):613-616. doi: 10.1007/s10517-019-04403-5

***Corresponding author**: Prof. Marina Darenskaya, PhD, ScD. E-mail: marina_darenskaya@inbox.ru,*

International Journal of Biomedicine 15(4) (2025) 639-644
http://dx.doi.org/10.21103/Article15(4)_RA3

BRIEF REVIEW

INTERNATIONAL JOURNAL OF BIOMEDICINE

Regional Lymphatic Status in Oral Squamous Cell Carcinoma: A Brief Review

A. D. Dadamov[1, 2*], A. M. Gizatullina[1], Sh. N. Yakubov[1], R. Kh. Nabiev[1], Zh. E. Dusmatov[1]

[1]*Tashkent State Medical University, Tashkent, Uzbekistan*
[2]*Tashkent Regional Branch of the Republican Specialized Scientific and Practical Medical Center of Oncology and Radiology, Tashkent, Uzbekistan*

Abstract

Oral squamous cell carcinoma (OSCC) is a common type of head and neck malignancy, leading to high morbidity and mortality rates. This brief review focuses on the regional lymphatic status in patients with OSCC. The lymphatic system plays a key role in the dissemination of malignant cells from the primary tumor. Tumor cell migration into the lymphatic system is a complex process involving multiple mechanisms and interactions within the tumor microenvironment. This multistep process is associated with the complex role of lymphatic endothelial cells in the tumor microenvironment, lymphangiogenesis, lymphatic invasion, and the modulation of the immune response. Despite recent advances, the precise role of the regional lymphatic system in the progression of OSCC remains unclear, highlighting the need for further in-depth study.(**International Journal of Biomedicine. 2025;15(4):639-644.**)

Keywords: oral cancer • lymph node • lymphangiogenesis • lymphovascular invasion • metastases

For citation: Dadamov AD, Gizatullina AM, Yakubov ShN, Nabiev RKh, Dusmatov ZhE. Regional Lymphatic Status in Oral Squamous Cell Carcinoma: A Brief Review. International Journal of Biomedicine. 2025;15(4):639-644. doi:10.21103/Article15(4)_RA3

Abbreviations

CT, computed tomography; **DWI**, diffusion-weighted imaging; **DCE-PWI**, dynamic contrast-enhanced perfusion-weighted imaging; **DKI**, diffusion kurtosis imaging; **DTI**, diffusion tensor imaging; **FGF**, fibroblast growth factor; **LVI**, lymphovascular invasion; **LN**, lymph node; **LEC**, lymphatic endothelial cell; **LLNs**, lingual lymph nodes; **LYVE-1**, lymphatic vessel endothelial hyaluronic acid receptor 1; **MRS**, magnetic resonance spectroscopy; **MRI**, magnetic resonance imaging; **OSCC**, oral squamous cell carcinoma; **RLS**, regional lymphatic status; **VEGF,** vascular endothelial growth factor.

Oral squamous cell carcinoma (OSCC), originating from the flat squamous cells that line the mouth, lips, and tongue, accounts for more than 90% of all oral malignancies.[1] OSCC dramatically impacts patients' quality of life, resulting in high morbidity and mortality rates. Early diagnosis and complete tumor removal are considered the mainstays of treatment for OSCC.[2,3] Despite improvements in diagnosis and treatment over the past 30 years, the five-year survival rate for OSCC remains only 50%.[4,5] Cervical lymph node (LN) involvement (N-status) is one of the most important independent prognostic factors in OSCC.[6,7]

This review focuses on the regional lymphatic status (RLS) of patients with OSCC.

Regional lymphatic status in patients with oral cavity carcinoma is crucial for determining the stage of the disease, prognosis, and treatment strategy. The drainage and transport functions of the lymphatic system are essential to oral cancer, as they serve as the primary pathway for metastasis.

Lymphatic endothelial cells (LECs), a specialized subset of endothelial cells, play multiple roles in the tumor microenvironment in addition to lining lymphatic vessels.[8,9] Lymphatic endothelial cells interact with innate and adaptive immune cells in both tissues and lymph nodes. These cells produce chemokines to attract immune cells to lymph nodes; specifically, CCL21 is involved in recruiting dendritic cells, which, in turn, promotes lymph node enlargement.[10-12]

Lymphatic endothelial cells play a crucial role in the formation of new lymphatic vessels observed in highly active tumors, a process known as tumor-associated lymphangiogenesis.[13] Tumor-associated lymphangiogenesis also involves various lymphangiogenic factors secreted by tumor cells or host cells present in the tumor microenvironment. These include vascular endothelial growth factor (VEGF) C and D, known primarily for stimulating lymphatic vessel growth, angiopoietin-2, fibroblast growth factor (FGF), and others.[14]

Importantly, the discovery of specific markers for LEC, such as the lymphatic vessel endothelial hyaluronic acid receptor 1 (LYVE-1) and podoplanin (D2-40), has enabled the distinction between lymphatic and blood vessels.[15-17] LYVE-1 exhibits a high degree of lymphatic vessel specificity and has been an essential component in numerous studies on tumor-induced lymphangiogenesis.[17,18] Furthermore, LYVE-1 is closely associated with lymph node metastasis in OSCC.[19]

The complex role of lymphatic endothelial cells in the tumor microenvironment and recent advances in this field require in-depth study.

The lingual, sublingual, and submental nodes provide lymphatic drainage from the tongue and surrounding tissues, playing a crucial role in local immunity. Lymphatic metastases in oral cavity carcinoma are a sign of a more aggressive course of the disease and make the prognosis less favorable.

Lymphovascular invasion (LVI), in which cancer cells invade the lumen of endothelial-lined lymphatic and blood vessels, is considered an important step in lymph node metastasis.[8,20] Lymphatic invasion is the main mechanism by which cancer cells in oral squamous cell carcinoma disseminate to regional lymph nodes.[21] Blood vessel invasion is considered a secondary route of distant metastasis, although it does not appear to be associated with lymph node metastasis.[22]

Michikawa et al.[23] reported a multivariate analysis of 63 patients with oral tongue squamous cell carcinoma, which showed that lymphatic vessel invasion was an independent risk factor for the presence of lymph node metastasis, although blood vessel invasion was not.

Several retrospective studies have also reported a significant positive association between LVI and lymph node metastasis.[24,25] A meta-analysis by Huang et al.[21] included 36 studies involving 17,109 patients with squamous cell carcinoma. It concluded that LVI can serve as a prognostic indicator of metastasis and prognosis in OSCC.

In oral carcinoma, due to its location and the characteristics of the vessels and lymphatic pathways that pass through the glossopharyngeal neuromuscular complex, metastasis and lymphatic drainage occur under high pressure, which can influence the rate of tumor growth and dissemination.[26] Recently, numerous studies have shown that abnormal tumor vasculature can create significant pressure on the tumor microenvironment, collectively referred to as hydrostatic stress.[27] Typically, fluid stress is generated by blood flow and interstitial blood flow, which includes microvascular fluid pressure, interstitial fluid pressure, and shear stress.[28] Due to increased interstitial fluid pressure in the central regions of the tumor, interstitial fluid flows from the center to the periphery and carries proangiogenic factors such as VEGF, promoting tumor hemangiogenesis. These proangiogenic factors also lead to increased lymph node metastasis by promoting lymphangiogenesis.[29] Shear stress in lymphatic vessels has also been shown to activate YAP1 (Yes-associated protein 1), thereby stimulating cancer cell migration.[30]

In oral carcinoma, lymphatic pathways lead to metastasis to regional lymph nodes, including the submandibular and cervical nodes, located outside the muscular structures in the subcutaneous tissue.[31,32] Lymph node metastasis is the most adverse prognostic factor of OSCC, with an incidence rate of approximately 40%.[33,34]

Having precise knowledge of the regional spread can be highly beneficial before initiating any definitive treatment. There are approximately 300 lymph nodes in the head and neck region, which are classified according to various criteria, such as superficial and deep or medial and lateral.[35-37]

Lymph from the tongue drains along a specific pathway: the anterior third to the submental lymph nodes (level IA), the middle third to the submandibular lymph nodes (level IB), and the posterior third and root of the tongue to the deep lymph nodes of the neck located along the internal jugular vein (levels IIB and III, less commonly IV).[38,39]

The intraoral areas have a rich lymphatic supply and are a typical site of metastasis in oral cancer.[40] There is a predictable pattern of spread from upper to lower lymph node levels: submental (IA), submandibular (IB), superior jugular (II), middle jugular (III), inferior jugular (IV), and posterior cervical (V).

In oral cavity carcinomas, the submandibular lymph nodes (level IB) and the superior deep jugular lymph nodes (level II) are the most frequent sentinel lymph nodes. Metastasis to the lateral lingual lymph nodes (LLNs), located lateral to the hyoglossus muscle behind the submandibular gland, has not been frequently reported in English literature. This group of LLNs was illustrated by Rouvière.[41] Lingual lymph nodes are intervening lymph nodes that appear inconstantly within the fascial/intermuscular spaces of the floor of the mouth.[42,43] Rouvière classified LLNs into median LLNs located between the genioglossus muscles and lateral LLNs located lateral to the genioglossus muscle or the hyoglossus muscle.[41]

Ozeki et al.[44] first reported a case of LLN metastasis in 1985, and subsequent cases have been reported since then.[45-48] According to studies, the incidence of metastases to the medial and lateral LLNs in patients with squamous cell carcinoma of the tongue was 0.7-3.0%[45,49,50] and 1.4-14.3% [44,49-52], respectively.

Suzuki et al.[42] presented the first case of metastasis to the lateral LLN located behind the submandibular gland from squamous cell carcinoma of the tongue. Eguchi et al.[53] presented a clinical case of a 55-year-old man with squamous cell carcinoma of the tongue (stage T4aN0M0) who underwent hemiglossectomy with cervical dissection and free flap reconstruction. An 8-mm lesion was present in the lingual septum, which, upon histopathological examination, was diagnosed as a metastasis to the medial lingual lymph node. The patient developed multiple distant metastases and died of the disease 18 months after the initial surgery. The presence

of metastases to the medial lymph node could have led to metastases to the contralateral neck and worsened the prognosis.

In a study by Kuroshima et al.,[54] a 5-year disease-specific survival was significantly lower in patients with squamous cell carcinoma of the tongue and LLN metastasis than in patients without LLN metastasis (49.0% vs. 88.4%, $P<0.01$). Cox proportional hazards analysis revealed that cervical lymph node metastases at levels IV or V and LLN metastasis were independent prognostic factors for 5-year survival. LLN metastasis had a strong negative impact on survival in patients with squamous cell carcinoma of the tongue.

In a letter to the editors, Calabrese et al.[55] stated that LLN metastases may worsen prognosis and may have the same effect as level I lymph node metastases.

However, data on the clinical significance and prognostic value of LLNs in patients with squamous cell carcinoma of the tongue are insufficient, as LLNs have received little attention until recently.

Median LLNs, located in the muscularis propria of the tongue, are a rare anatomical structure, and their presence can be variable. Their unique location, directly within the muscularis propria of the tongue rather than in the submandibular glands, may serve as a site for metastasis in tongue cancer, a poorly understood issue. A study by Tomblinson et al.[48] estimated the prevalence of median LLN metastases from oral cavity squamous cell carcinoma. In the study group, a solitary metastasis to the median LLN from a tumor on the lateral surface of the tongue (T4aN2c) was detected in 1 of 105 cases of OSCC (0.95%).

Assessment of regional lymphatic status in oral carcinoma includes a clinical examination to palpate the nodes, a combination of instrumental methods (ultrasound, CT, MRI, PET-CT) to detect metastases in deep lymph nodes, and a biopsy of an enlarged lymph node for histological verification of the diagnosis.

Magnetic resonance imaging (MRI) has a high degree of soft tissue discrimination, making it the preferred method for assessing oral soft tissue conditions. The use of advanced MRI techniques, such as diffusion-weighted imaging (DWI), dynamic contrast-enhanced perfusion-weighted imaging (DCE-PWI), magnetic resonance spectroscopy (MRS), diffusion tensor imaging (DTI), and diffusion kurtosis imaging (DKI) (an advanced DWI technique that focuses on the non-Gaussian diffusion of water molecules in heterogeneous tissue microstructures), can improve diagnostic accuracy. These advanced functional MRI techniques enable noninvasive assessment of the biochemical, structural, and metabolic characteristics of tissues, which is crucial for the diagnosis, staging, and monitoring of oral cancer treatment.

For example, Shaukat et al.[56] investigated the accuracy of DWI for diagnosing oral cancer metastases to cervical lymph nodes. Magnetic resonance imaging, including a DWI sequence, in a 1.5-T scanner with a phased-array head and neck coil, was performed in 150 patients diagnosed with oral cancer. In the DWI sequence, the area scanned included the lymph nodes from the suprasternal notch to the base of the skull. Histopathological examination of the lymph nodes was used as the gold standard. The sensitivity, specificity, positive predictive value, negative predictive value, and accuracy of DWI for diagnosing oral cancer metastasis to cervical lymph nodes, using histopathology as the gold standard, were 90.57%, 91.75%, 94.68%, 90.57% and 91.33%, respectively.

Innovative lymphography methods, such as radionuclide and fluorescence, have made it possible to visualize the process of lymph movement. Fluorescence lymphography, which visualizes the lymphatic system using a fluorescent dye such as indocyanine green, enables the assessment of the condition of lymphatic vessels and nodes, which is particularly important in oncological diseases.[57] Fluorescence imaging visualizes biological processes occurring during the early stages of carcinogenesis and can facilitate the detection of small tumors at early stages. Due to its high sensitivity and spatial resolution, fluorescence imaging can aid in assessing resection margins during surgery.[58]

Recently, near-infrared (NIR) fluorescence has been introduced intraoperatively to detect lymph nodes, tumors, and vital structures.[59] A study by van der Vorst et al.[36] demonstrated the feasibility of detecting draining lymph nodes in patients with head and neck cancer using NIR fluorescence imaging.

Yang et al.[35] evaluated the capability of indirect computed tomography and magnetic resonance lymphography (CT/MR-LG) with gadolinium-loaded gold nanoprobes embedded in polyethyleneimine (Gd-Au PENP) to assess sentinel lymph node metastasis in the VX2 tongue carcinoma model. They found that indirect CT/MR-LG with Gd-Au PENP can be used to diagnose sentinel lymph node metastasis in tongue cancer.

Conclusion

The lymphatic system plays a key role in the dissemination of malignant cells from the primary tumor. Tumor cell migration into the lymphatic system is a complex process involving multiple mechanisms and interactions within the tumor microenvironment. This multistep process is associated with the complex role of lymphatic endothelial cells in the tumor microenvironment, lymphangiogenesis, characterized by the expression of MMPs, VEGF, FGF, and PDGF, promoted by adhesion molecules and cytokines, including CCR7, CCL21, MMPs, and VCAM-1.[60,61] A key step in cancer cell invasion and metastasis is the destruction of the basement membrane. Basement membrane destruction through targeted secretion of matrix metalloproteinases can lead to increased adhesion of migrating cells, as well as the release and activation of various growth factors necessary for angiogenesis, tumor growth, and metastasis. Lymphatic invasion and lymphatic metastasis are significant prognostic factors determining tumor survival and progression. Despite recent advances, the exact role of the regional lymphatic system in the progression of oral squamous cell carcinoma remains unclear, underscoring the need for further in-depth study.

Competing Interests

The author declares that there are no conflicts of interest regarding the publication of this paper.

References

1. Chamoli A, Gosavi AS, Shirwadkar UP, Wangdale KV, Behera SK, Kurrey NK, Kalia K, Mandoli A. Overview of oral cavity squamous cell carcinoma: Risk factors, mechanisms, and diagnostics. Oral Oncol. 2021 Oct;121:105451. doi: 10.1016/j.oraloncology.2021.105451. Epub 2021 Jul 28. PMID: 34329869.
2. Mitchell DA, Kanatas A, Murphy C, Chengot P, Smith AB, Ong TK. Margins and survival in oral cancer. Br J Oral Maxillofac Surg. 2018 Nov;56(9):820-829. doi: 10.1016/j.bjoms.2018.06.021. Epub 2018 Sep 13. PMID: 30220612.
3. Woolgar JA, Triantafyllou A. A histopathological appraisal of surgical margins in oral and oropharyngeal cancer resection specimens. Oral Oncol. 2005 Nov;41(10):1034-43. doi: 10.1016/j.oraloncology.2005.06.008. Epub 2005 Aug 29. PMID: 16129652.
4. Leoncini E, Vukovic V, Cadoni G, Giraldi L, Pastorino R, Arzani D, Petrelli L, Wünsch-Filho V, Toporcov TN, Moyses RA, Matsuo K, Bosetti C, La Vecchia C, Serraino D, Simonato L, Merletti F, Boffetta P, Hashibe M, Lee YA, Boccia S. Tumour stage and gender predict recurrence and second primary malignancies in head and neck cancer: a multicentre study within the INHANCE consortium. Eur J Epidemiol. 2018 Dec;33(12):1205-1218. doi: 10.1007/s10654-018-0409-5. Epub 2018 May 19. PMID: 29779202; PMCID: PMC6290648.
5. Warnakulasuriya S. Global epidemiology of oral and oropharyngeal cancer. Oral Oncol. 2009 Apr-May;45(4-5):309-16. doi: 10.1016/j.oraloncology.2008.06.002. Epub 2008 Sep 18. PMID: 18804401.
6. Bernier J, Domenge C, Ozsahin M, Matuszewska K, Lefèbvre JL, Greiner RH, Giralt J, Maingon P, Rolland F, Bolla M, Cognetti F, Bourhis J, Kirkpatrick A, van Glabbeke M; European Organization for Research and Treatment of Cancer Trial 22931. Postoperative irradiation with or without concomitant chemotherapy for locally advanced head and neck cancer. N Engl J Med. 2004 May 6;350(19):1945-52. doi: 10.1056/NEJMoa032641. PMID: 15128894.
7. Voss JO, Freund L, Neumann F, Mrosk F, Rubarth K, Kreutzer K, Doll C, Heiland M, Koerdt S. Prognostic value of lymph node involvement in oral squamous cell carcinoma. Clin Oral Investig. 2022 Nov;26(11):6711-6720. doi: 10.1007/s00784-022-04630-7. Epub 2022 Jul 27. PMID: 35895143; PMCID: PMC9643253.
8. Fujimoto N, Dieterich LC. Mechanisms and Clinical Significance of Tumor Lymphatic Invasion. Cells. 2021 Sep 29;10(10):2585. doi: 10.3390/cells10102585. PMID: 34685565; PMCID: PMC8533989.
9. He M, He Q, Cai X, Chen Z, Lao S, Deng H, Liu X, Zheng Y, Liu X, Liu J, Xie Z, Yao M, Liang W, He J. Role of lymphatic endothelial cells in the tumor microenvironment-a narrative review of recent advances. Transl Lung Cancer Res. 2021 May;10(5):2252-2277. doi: 10.21037/tlcr-21-40. PMID: 34164274; PMCID: PMC8182726.
10. Bromley SK, Thomas SY, Luster AD. Chemokine receptor CCR7 guides T cell exit from peripheral tissues and entry into afferent lymphatics. Nat Immunol. 2005 Sep;6(9):895-901. doi: 10.1038/ni1240. Epub 2005 Aug 14. PMID: 16116469.
11. Tal O, Lim HY, Gurevich I, Milo I, Shipony Z, Ng LG, Angeli V, Shakhar G. DC mobilization from the skin requires docking to immobilized CCL21 on lymphatic endothelium and intralymphatic crawling. J Exp Med. 2011 Sep 26;208(10):2141-53. doi: 10.1084/jem.20102392. Epub 2011 Sep 19. PMID: 21930767; PMCID: PMC3182054.
12. Weber M, Hauschild R, Schwarz J, Moussion C, de Vries I, Legler DF, Luther SA, Bollenbach T, Sixt M. Interstitial dendritic cell guidance by haptotactic chemokine gradients. Science. 2013 Jan 18;339(6117):328-32. doi: 10.1126/science.1228456. PMID: 23329049.
13. Dieterich LC, Detmar M. Tumor lymphangiogenesis and new drug development. Adv Drug Deliv Rev. 2016 Apr 1;99(Pt B):148-160. doi: 10.1016/j.addr.2015.12.011. Epub 2015 Dec 17. PMID: 26705849.
14. Kataru RP, Jung K, Jang C, Yang H, Schwendener RA, Baik JE, Han SH, Alitalo K, Koh GY. Critical role of CD11b+ macrophages and VEGF in inflammatory lymphangiogenesis, antigen clearance, and inflammation resolution. Blood. 2009 May 28;113(22):5650-9. doi: 10.1182/blood-2008-09-176776. Epub 2009 Apr 3. PMID: 19346498.
15. Karinen S, Juurikka K, Hujanen R, Wahbi W, Hadler-Olsen E, Svineng G, Eklund KK, Salo T, Åström P, Salem A. Tumour cells express functional lymphatic endothelium-specific hyaluronan receptor in vitro and in vivo: Lymphatic mimicry promotes oral oncogenesis? Oncogenesis. 2021 Mar 5;10(3):23. doi: 10.1038/s41389-021-00312-3. PMID: 33674563; PMCID: PMC7977063.
16. Zhang Z, Helman JI, Li LJ. Lymphangiogenesis, lymphatic endothelial cells and lymphatic metastasis in head and neck cancer--a review of mechanisms. Int J Oral Sci. 2010 Mar;2(1):5-14. doi: 10.4248/IJOS10006. PMID: 20690413; PMCID: PMC3475589.
17. Banerji S, Ni J, Wang SX, Clasper S, Su J, Tammi R, Jones M, Jackson DG. LYVE-1, a new homologue of the CD44 glycoprotein, is a lymph-specific receptor for hyaluronan. J Cell Biol. 1999 Feb 22;144(4):789-801. doi: 10.1083/jcb.144.4.789. PMID: 10037799; PMCID: PMC2132933.
18. Jackson DG. Biology of the lymphatic marker LYVE-1 and applications in research into lymphatic trafficking and lymphangiogenesis. APMIS. 2004 Jul-Aug;112(7-8):526-38. doi: 10.1111/j.1600-0463.2004.apm11207-0811.x. PMID: 15563314.
19. Arimoto S, Hasegawa T, Takeda D, Saito I, Amano R, Akashi M, Komori T. Lymphangiogenesis and Lymph Node Metastasis in Oral Squamous Cell Carcinoma. Anticancer Res. 2018 Nov;38(11):6157-6162. doi: 10.21873/anticanres.12968. PMID: 30396932.
20. Moore AE, Alvi SA, Tarabichi O, Zhu VL, Buchakjian MR. Role of Lymphovascular Invasion in Oral Cavity Squamous Cell Carcinoma Regional Metastasis and Prognosis. Ann Otol Rhinol Laryngol. 2024 Mar;133(3):300-306. doi: 10.1177/00034894231211116. Epub 2023 Nov 5. PMID: 37927046; PMCID: PMC11578272.
21. Huang S, Zhu Y, Cai H, Zhang Y, Hou J. Impact of lymphovascular invasion in oral squamous cell carcinoma: A meta-analysis. Oral Surg Oral Med Oral Pathol Oral Radiol. 2021 Mar;131(3):319-328.e1. doi: 10.1016/j.oooo.2020.10.026. Epub 2020 Nov 5. PMID: 33309267.
22. Shivamallappa SM, Venkatraman NT, Shreedhar B, Mohanty L, Shenoy S. Role of angiogenesis in oral

squamous cell carcinoma development and metastasis: an immunohistochemical study. Int J Oral Sci. 2011 Oct;3(4):216-24. doi: 10.4248/IJOS11077. PMID: 22010580; PMCID: PMC3469979.
23. Michikawa C, Uzawa N, Kayamori K, Sonoda I, Ohyama Y, Okada N, Yamaguchi A, Amagasa T. Clinical significance of lymphatic and blood vessel invasion in oral tongue squamous cell carcinomas. Oral Oncol. 2012 Apr;48(4):320-4. doi: 10.1016/j.oraloncology.2011.11.014. Epub 2011 Dec 16. PMID: 22178206.
24. Jones HB, Sykes A, Bayman N, Sloan P, Swindell R, Patel M, Musgrove B. The impact of lymphovascular invasion on survival in oral carcinoma. Oral Oncol. 2009 Jan;45(1):10-5. doi: 10.1016/j.oraloncology.2008.03.009. Epub 2008 Jul 11. PMID: 18620889.
25. Sahoo A, Panda S, Mohanty N, Jena D, Mishra N, Surabhi, Baisakh MR. Perinerural, lymphovascular and depths of invasion in extrapolating nodal metastasis in oral cancer. Clin Oral Investig. 2020 Feb;24(2):747-755. doi: 10.1007/s00784-019-02921-0. Epub 2019 May 28. PMID: 31139977.
26. Borodin JuI. [Lymphatic system and aging]. Fundamental Research. 2011;(5):11-15. [Article in Russian].
27. Zhou H, Wang M, Zhang Y, Su Q, Xie Z, Chen X, Yan R, Li P, Li T, Qin X, Yang H, Wu C, You F, Li S, Liu Y. Functions and clinical significance of mechanical tumor microenvironment: cancer cell sensing, mechanobiology and metastasis. Cancer Commun (Lond). 2022 May;42(5):374-400. doi: 10.1002/cac2.12294. Epub 2022 Apr 26. PMID: 35470988; PMCID: PMC9118059.
28. Jain RK, Martin JD, Stylianopoulos T. The role of mechanical forces in tumor growth and therapy. Annu Rev Biomed Eng. 2014 Jul 11;16:321-46. doi: 10.1146/annurev-bioeng-071813-105259. PMID: 25014786; PMCID: PMC4109025.
29. Rofstad EK, Galappathi K, Mathiesen BS. Tumor interstitial fluid pressure-a link between tumor hypoxia, microvascular density, and lymph node metastasis. Neoplasia. 2014 Jul;16(7):586-94. doi: 10.1016/j.neo.2014.07.003. PMID: 25117980; PMCID: PMC4198829.
30. Lee HJ, Diaz MF, Price KM, Ozuna JA, Zhang S, Sevick-Muraca EM, Hagan JP, Wenzel PL. Fluid shear stress activates YAP1 to promote cancer cell motility. Nat Commun. 2017 Jan 18;8:14122. doi: 10.1038/ncomms14122. PMID: 28098159; PMCID: PMC5253685.
31. Kiss F., Szentagothai J. Anatomical atlas of the human body. Hungarian Academy of Sciences: Medicine; 1966, v.3.
32. Sinelnikov RD, Sinelnikov YaR, Sinelnikov AYa. [Atlas of human anatomy. Lymph nodes and vessels]. 2017, v.3. [In Russian].
33. Ferlito A, Silver CE, Rinaldo A. Neck dissection in the new era. J Am Coll Surg. 2007 Mar;204(3):466-8. doi: 10.1016/j.jamcollsurg.2006.11.016. Epub 2007 Jan 25. PMID: 17324783.
34. Noguti J, De Moura CF, De Jesus GP, Da Silva VH, Hossaka TA, Oshima CT, Ribeiro DA. Metastasis from oral cancer: an overview. Cancer Genomics Proteomics. 2012 Sep-Oct;9(5):329-35. PMID: 22990112.
35. Yang Y, Zhou B, Zhou J, Shi X, Sha Y, Wu H. Assessment of lingual sentinel lymph nodes metastases using dual-modal indirect CT/MR lymphography with gold-gadolinium-based nanoprobes in a tongue VX_2 carcinoma model. Acta Otolaryngol. 2018 Aug;138(8):727-733. doi: 10.1080/00016489.2018.1441544. Epub 2018 Mar 7. PMID: 29513120.
36. van der Vorst JR, Schaafsma BE, Verbeek FP, Keereweer S, Jansen JC, van der Velden LA, Langeveld AP, Hutteman M, Löwik CW, van de Velde CJ, Frangioni JV, Vahrmeijer AL. Near-infrared fluorescence sentinel lymph node mapping of the oral cavity in head and neck cancer patients. Oral Oncol. 2013 Jan;49(1):15-9. doi: 10.1016/j.oraloncology.2012.07.017. Epub 2012 Aug 28. PMID: 22939692; PMCID: PMC3608510.
37. Norris CD, Anzai Y. Anatomy of Neck Muscles, Spaces, and Lymph Nodes. Neuroimaging Clin N Am. 2022 Nov;32(4):831-849. doi: 10.1016/j.nic.2022.07.027. Epub 2022 Sep 21. PMID: 36244726.
38. Parkinson EK, James EL, Prime SS. Senescence-Derived Extracellular Molecules as Modulators of Oral Cancer Development: A Mini-Review. Gerontology. 2016;62(4):417-24. doi: 10.1159/000440954. Epub 2015 Dec 3. PMID: 26629698.
39. Chen J, Zhang Z, Liu J, Li C, Yin M, Nie L, Song B. Multiparametric Magnetic Resonance Imaging of the Kidneys: Effects of Regional, Side, and Hydration Variations on Functional Quantifications. J Magn Reson Imaging. 2023 May;57(5):1576-1586. doi: 10.1002/jmri.28477. Epub 2022 Oct 11. PMID: 36219465; PMCID: PMC10079549.
40. Patel S, Singh I, Gulati A, Khurana N. A Study on Neck Nodes in Oral Cancers, with Special Reference to Skip Metastasis. Indian J Otolaryngol Head Neck Surg. 2019 Oct;71(Suppl 1):474-481. doi: 10.1007/s12070-018-1360-1. Epub 2018 Apr 16. PMID: 31742006; PMCID: PMC6848720.
41. Rouvière H. Lymphatics of the tongue and of the salivary gland. In: Anatomy of the human lymphatic system. Ann Arbor, MI: Edward Brothers, Inc.; 1938:44-51.
42. Suzuki M, Eguchi K. Metastasis to the lateral lingual lymph node located behind the submandibular gland: A case of squamous cell carcinoma of the tongue. Clin Case Rep. 2021 Feb 9;9(3):1763-1766. doi: 10.1002/ccr3.3898. PMID: 33768931; PMCID: PMC7981743.
43. Ananyan SG, Gvetadze SR, Ilkaev KD, Mochalnikova VV, Zairatyants GO, Mkhitarov VA, et al. Anatomical and histological examination of the bottom of the oral cavity: lingual lymph nodes. J Clin Oncol. (Jpn) 2015;45:547-554.
44. Ozeki S, Tashiro H, Okamoto M, Matsushima T. Metastasis to the lingual lymph node in carcinoma of the tongue. J Maxillofac Surg. 1985 Dec;13(6):277-81. doi: 10.1016/s0301-0503(85)80064-3. PMID: 3866823.
45. Ando M, Asai M, Asakage T, Oyama W, Saikawa M, Yamazaki M, Miyazaki M, Ugumori T, Daiko H, Hayashi R. Metastatic neck disease beyond the limits of a neck dissection: attention to the 'para-hyoid' area in T1/2 oral tongue cancer. Jpn J Clin Oncol. 2009 Apr;39(4):231-6. doi: 10.1093/jjco/hyp001. Epub 2009 Feb 12. PMID: 19213806.
46. Dutton JM, Graham SM, Hoffman HT. Metastatic cancer to the floor of mouth: the lingual lymph nodes. Head Neck. 2002 Apr;24(4):401-5. doi: 10.1002/hed.10026. PMID: 11933183.
47. Han W, Yang X, Huang X, Hu Q, Wang Z. Metastases to lingual lymph nodes from squamous cell carcinoma of the tongue. Br J Oral Maxillofac Surg. 2008 Jul;46(5):376-8. doi: 10.1016/j.bjoms.2007.12.002. Epub 2008 Jan 18. PMID: 18207615.

48. Tomblinson CM, Nagel TH, Hu LS, Zarka MA, Hoxworth JM. Median Lingual Lymph Nodes: Prevalence on Imaging and Potential Implications for Oral Cavity Cancer Staging. J Comput Assist Tomogr. 2017 Jul/Aug;41(4):528-534. doi: 10.1097/RCT.0000000000000568. PMID: 28099223.
49. Woolgar JA. Histological distribution of cervical lymph node metastases from intraoral/oropharyngeal squamous cell carcinomas. Br J Oral Maxillofac Surg. 1999 Jun;37(3):175-80. doi: 10.1054/bjom.1999.0036. PMID: 10454023.
50. Jia J, Jia MQ, Zou HX. Lingual lymph nodes in patients with squamous cell carcinoma of the tongue and the floor of the mouth. Head Neck. 2018 Nov;40(11):2383-2388. doi: 10.1002/hed.25340. Epub 2018 Jul 26. PMID: 30051610.
51. Yang W, Sun M, Jie Q, Zhou H, Zhang P, Zhu J. Lingual Lymph Node Metastasis in cT1-2N0 Tongue Squamous Cell Carcinoma: Is It an Indicator for Elective Neck Dissection. Front Oncol. 2020 Apr 7;10:471. doi: 10.3389/fonc.2020.00471. PMID: 32318349; PMCID: PMC7154091.
52. Fang Q, Li P, Qi J, Luo R, Chen D, Zhang X. Value of lingual lymph node metastasis in patients with squamous cell carcinoma of the tongue. Laryngoscope. 2019 Nov;129(11):2527-2530. doi: 10.1002/lary.27927.
53. Eguchi K, Kawai S, Mukai M, Nagashima H, Shirakura S, Sugimoto T, Asakage T. Medial lingual lymph node metastasis in carcinoma of the tongue. Auris Nasus Larynx. 2020 Feb;47(1):158-162. doi: 10.1016/j.anl.2019.03.003. Epub 2019 Mar 29. PMID: 30929928.
54. Kuroshima T, Onozato Y, Oikawa Y, Ohsako T, Kugimoto T, Hirai H, Tomioka H, Michi Y, Miura M, Yoshimura R, Harada H. Prognostic impact of lingual lymph node metastasis in patients with squamous cell carcinoma of the tongue: a retrospective study. Sci Rep. 2021 Oct 15;11(1):20535. doi: 10.1038/s41598-021-99925-2.
55. Calabrese L, Renne G, De Cicco C, Chiesa F. Metastatic cancer to the floor of mouth: the lingual lymph nodes. Head Neck. 2003 Apr;25(4):341-2; author reply 342. doi: 10.1002/hed.10259. PMID: 12658740.
56. Shaukat S, Mansoor A, Rashid N, Shaukat Z, Amin U, Mazhar S. Diagnostic accuracy of diffusion-weighted magnetic resonance imaging for cervical lymph node metastasis from oral cancer. Radiol Bras. 2025 Apr 11;58:e20240064. doi: 10.1590/0100-3984.2024.0064. PMID: 40248573; PMCID: PMC12005712.
57. Firsov DF, Zhila ES, Atroshchenko AO, Ganova TD, Ganov DI. [History and applications of indocyanine green in medical practice. Literature Review]. Bulletin of Medical Science. 2024;3(35):96-100. doi:10.31684/25418475-2024-3-96. [Article in Russian].
58. Vonk J, de Wit JG, Voskuil FJ, Witjes MJH. Improving oral cavity cancer diagnosis and treatment with fluorescence molecular imaging. Oral Dis. 2021 Jan;27(1):21-26. doi: 10.1111/odi.13308. Epub 2020 Mar 13. PMID: 32072691; PMCID: PMC7818506.
59. Schaafsma BE, Mieog JS, Hutteman M, van der Vorst JR, Kuppen PJ, Löwik CW, Frangioni JV, van de Velde CJ, Vahrmeijer AL. The clinical use of indocyanine green as a near-infrared fluorescent contrast agent for image-guided oncologic surgery. J Surg Oncol. 2011 Sep 1;104(3):323-32. doi: 10.1002/jso.21943. Epub 2011 Apr 14. PMID: 21495033; PMCID: PMC3144993.
60. Chambers AF, Matrisian LM. Changing views of the role of matrix metalloproteinases in metastasis. J Natl Cancer Inst. 1997 Sep 3;89(17):1260-70. doi: 10.1093/jnci/89.17.1260. PMID: 9293916.
61. Jacob A, Jing J, Lee J, Schedin P, Gilbert SM, Peden AA, Junutula JR, Prekeris R. Rab40b regulates trafficking of MMP2 and MMP9 during invadopodia formation and invasion of breast cancer cells. J Cell Sci. 2013 Oct 15;126(Pt 20):4647-58. doi: 10.1242/jcs.126573. Epub 2013 Jul 31. PMID: 23902685; PMCID: PMC3795337.

***Corresponding author**: Prof. Ashot D. Dadamov. E-mail: dadamdent@yandex.com*

International Journal of Biomedicine 15(4) (2025) 645-648
http://dx.doi.org/10.21103/Article15(4)_RA4

MINI REVIEW

INTERNATIONAL JOURNAL OF BIOMEDICINE

Electrosurgery: Principles, Risks, Safety Considerations, and Modeling of Thermal Effects

Branislav Radjenović, Marija Radmilović-Radjenović*

Institute of Physics, University of Belgrade, Belgrade, Serbia

Abstract

Electrosurgery has significantly transformed modern surgical practices, offering a versatile and effective approach for cutting, coagulating, and desiccating biological tissue with remarkable precision. This review provides a comprehensive exploration of the fundamental principles that underpin electrosurgery, including the electrical mechanisms, tissue interactions, and the various types of thermal injuries that may arise during procedures. It categorizes thermal injuries into direct and indirect types, elucidating the unique risks associated with patients who have implantable electromagnetic devices. Furthermore, the review emphasizes the critical role of modeling thermal effects in electrosurgical procedures, highlighting how computational simulations can predict tissue damage and enhance safety measures. By deepening the understanding of these intricate concepts, surgeons are better equipped to optimize patient outcomes, minimize complications, and ensure the safe application of electrosurgical techniques. Ultimately, this review aims to bridge existing knowledge gaps and promote best practices in the field of electrosurgery, reinforcing its role as a vital tool in contemporary surgical settings.(**International Journal of Biomedicine. 2025;15(4):645-648.**)

Keywords: electrosurgery • thermal injures • electromagnetic devices

For citation: Radjenović B, Radmilović-Radjenović M. Electrosurgery: Principles, Risks, Safety Considerations, and Modeling of Thermal Effects. International Journal of Biomedicine. 2025;15(4):645-648. doi:10.21103/Article15(4)_RA4

Introduction

Electrosurgery has revolutionized surgical practices by providing a versatile and effective tool for cutting, coagulating, and desiccating biological tissue[1-3] By harnessing the effects of electric current, this technique enhances precision and efficiency in a wide range of surgical procedures, from minimally invasive laparoscopic surgeries to complex open surgeries. The ability to manipulate tissue with high accuracy not only improves surgical outcomes but also reduces recovery times and complications associated with traditional surgical methods.

However, the use of electrosurgery is not without its challenges. As with any surgical technology, it introduces inherent risks and complications, particularly in the form of thermal injuries.[4,5] These injuries can have significant consequences for patient safety, ranging from minor burns to severe internal damage. Understanding the underlying principles of electrosurgery—including electrical fundamentals, tissue interactions, and the mechanisms of potential hazards—is essential for surgeons striving to optimize patient outcomes and minimize risks.

Electric currents flowing through the human body can lead to severe tissue injuries, commonly classified as direct and indirect thermal injuries.[6] Direct injuries occur when an active electrode inadvertently contacts any part of the body outside the intended surgical site. In contrast, indirect injuries occur when the electrode unintentionally comes into contact with other metal instruments, causing the current to divert and affect surrounding tissues. Additionally, patients with implantable electromagnetic devices face unique risks, as electrosurgical devices can interact adversely with these implants, leading to specific injuries.

Given these complexities, this review aims to explore the principles of electrosurgery, examine the factors that influence its effectiveness, and emphasize the importance of safety considerations in its application. By enhancing our understanding of electrosurgery, we can better equip surgeons to utilize this powerful tool safely and effectively, ultimately improving patient care in surgical settings.

***Corresponding author**: Dr. Marija Radmilović-Radjenović, Institute of Physics, University of Belgrade, Pregrevica 118, 11080 Belgrade, Serbia, E-mail: marija@ipb.ac.rs*

Principles of Electrosurgery

Electrical Fundamentals

The mechanics of electrosurgery are grounded in electrical principles. It employs alternating current, which causes cellular ions to oscillate, generating frictional heat. This process transforms electrical energy into mechanical and then thermal energy within the cells. Electrode arrangements used in electrosurgery can be roughly divided into two categories: unipolar and bipolar (Figure 1).[7,8]

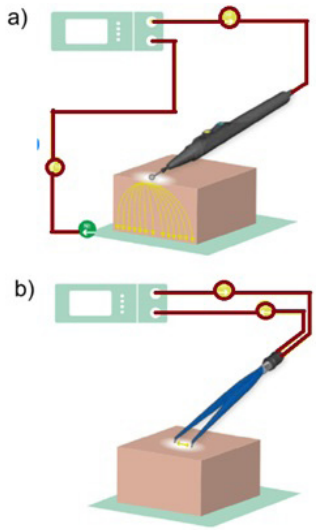

Figure 1. *Schematic view of dipole circuits: a) a small active electrode - unipolar (monopolar) and b) two equal-sized electrodes - bipolar.*

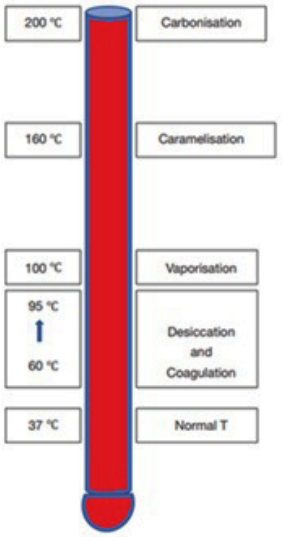

Figure 2. *Tissue effects result from the changes that biological tissues undergo when exposed to heat or cold.*

The primary difference between these modalities lies in the pathway of the current. The unipolar circuit consists of a small active electrode placed at the surgical site and a patient return electrode placed on the patient's body. The current's likely path is from the active electrode to the ground electrode and back to the electrosurgical generator, completing the circuit. The high current density produced at the active electrode creates a pronounced diathermic effect, causing tissue destruction at the operative site. On the other hand, a bipolar circuit uses two electrodes of equal size, creating a dipole circuit at the site of application. Upon applying a high current density through bipolar forceps, the small amount of tissue contained between the tips of the forceps is coagulated with minimal effect on surrounding tissue.

Thermal Tissue Effects

Figure 2 illustrates thermal tissue effects, which refer to the changes that occur in biological tissues when they are exposed to heat or cold.[9] Electrosurgical cutting occurs when temperatures exceed 100°C, leading to cellular vaporization. The gradual temperature rise between 60°C and 95°C results in desiccation and coagulation. Desiccation is achieved through the loss of cellular water, while coagulation arises from thermal protein denaturation. The use of wider active electrodes generally reduces current density, making it more conducive to coagulation and desiccation. Fulguration is a specialized application of the coag waveform, executed with the active electrode positioned away from the tissue. This technique generates electric arcing that bridges the air gap, producing temperatures above 200°C and resulting in carbonization. The low duty cycle ensures rapid diminishment of current, thus preventing excessive heat accumulation in deeper tissues. Fulguration proves effective in controlling bleeding from raw surfaces, providing a valuable tool for surgical hemostasis.

Tissue Factors

Tissues with high impedance, such as fat and scar tissue, will require higher power to achieve the desired tissue effects compared to those with low impedance, such as muscles and skin.[10] Generally, obese or emaciated patients need more power output to cause the same tissue effects as in lean and muscular patients. Patients with vascular diseases such as atherosclerosis, liver cirrhosis, diabetes, and collagen disorders may not be suitable for electrosurgical hemostasis, and alternative hemostatic techniques may be required. Eschar build-up on the active electrode poses a high impedance to current; hence, higher power will be needed to achieve the desired tissue effects. It is good practice to keep the electrode clean at all times or to use non-stick electrodes (Teflon or silicone-coated).

Hazards of Electrosurgery

Although advanced technology has significantly reduced electrosurgical complications, severe internal burns still occur.[11] The estimated incidence of such burns is 3.6 per 1,000 laparoscopic procedures. The majority of such burns are not recognized at the time of surgery, which can lead to severe morbidity or even mortality postoperatively. Additionally, they are associated with increased costs due to repeated surgeries, prolonged hospitalizations, and

malpractice claims. Table 1 shows a practical classification of electrosurgical hazards.

Table 1.

Overview of the electrosurgical hazards (unintended burns, electrical shock and glove burns, surgical plume, explosion, surgical fire, and electromagnetic interference with other devices).

Unintended burns		
Active electrode	***Dispersive electrode***	***Current diversion***
Lateral thermal spread	Poor skin contact	Insulation failure
Residual heat	Poor lead connection	Direct coupling
Inadverten activation		Capacitive coupling
Direct thermal extension		Antenna coupling
		Alternate site injury
Electrical shock and glove burns		
Surgical plume		
Explosion		
Surgical fire		
Electromagnetic interference with other devices		
Implantable electronic devices	***Electrocardiogram***	***Video imaging system***

Modelling of Thermal Effect

Accurate modeling of electrosurgical heating of soft tissues requires a fundamental understanding of how the applied energy distributes and dissipates within the tissue. Electrosurgery involves the application of an alternating current to cut and coagulate tissues simultaneously.[12] When higher power settings are applied, the tissue is rapidly heated to 100°C within seconds. In an electrosurgical procedure, the vicinity of the electrode is a region of high-power density as the electric field intensity drops off as the square of the distance from it, resulting in sharp temperature and pressure gradients with large evaporation losses.[13] The challenge of accurately modeling electrosurgical heating of hydrated soft tissues arises from the need to capture energy dissipation that is significantly affected by changes in temperature-dependent properties, latent heat loss, and phase change within the tissue that is heterogeneous and contains than 70% water by mass. Computational models are frequently employed to evaluate the safety of electrosurgical procedures, predict tissue damage, and inform the development of new instrument designs.[14,15] In the modeling of thermal effects on the tissue, several factors have to be considered:

• *Penetration of Electric Field into Tissue* – The distribution of the electric field is determined by the geometry of the electrodes. For spherical and cylindrical electrode configurations, the penetration depth of the electric field in tissue is approximately equal to the electrode radius.

• *Heat Diffusion* – The penetration of heat into the tissue by diffusion depends on pulse duration. If repetitive pulses are applied, heat accumulation should be prevented by providing a sufficient delay between pulses for energy dissipation from the heated area.

• *Cavitation* – In pulsed ablation, tissue can also be damaged by the mechanical effects of the rapidly expanding and collapsing cavitation bubbles. During the collapse of the cavitation bubbles, fast water jets can form near the tissue boundaries, extending the range of mechanical tissue damage.

• *Electroporation* – Another potentially damaging mechanism is the direct effect of the electric field on cellular membranes. Due to the polarization of the cell in an electric field, its transmembrane potential is increased on the anodic side (hyperpolarization) and decreased on the cathodic side (depolarization).

• *Tissue Modelling* – The significant discrepancies found between model predictions and experimental data in the literature show that accurately modelling the radio-frequency heating of soft tissue requires capturing the interactions between the heterogeneous phases that comprise soft tissue, including heat transfer, mass transport, phase change, and mechanics.

• *Evolution of Tissue Damage* – Modeling of electrosurgical procedures is complicated because the models must also include the motion of the electrosurgical tool. The actual depth and extent of tissue injury depend on several factors, including power density, electrode size and shape, and the nature of the tissue being dissected.

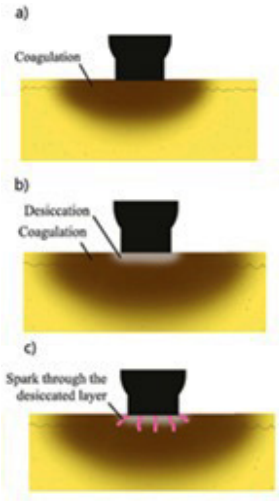

Figure 3. *Graphical illustration of the sparking that occurs during the electrocoagulation with desiccation.*

The computational model plays a significant role in predicting electrosurgical outcomes, thereby enhancing electrosurgery, as illustrated in Figure 3, which depicts the stages of electrocoagulation. a) The process starts with coagulation. b) At the end of coagulation, the more superficial coagulated tissue dries out (desiccation) and becomes less electrically conductive, potentially preventing the current from continuing to flow. c) Sparking may then occur through the nonconductive desiccated layer, leading to disruption of this layer, passage of more current, more heat production, and deeper thermal damage. The timing of desiccation occurrence during coagulation depends on the current density. With lower current density, there may be deep

coagulation before desiccation happens. Therefore, for deep coagulation, a relatively low power should be chosen to provide slow coagulation and a late occurrence of desiccation, keeping in mind that a very low power may not be able to ensure the coagulation. In such cases, simulations may provide accurate values of the current density that enable the desired coagulation with late desiccation.

Conclusions and Future Outlook

In conclusion, electrosurgery represents a significant advancement in surgical technology, enabling the performance of complex procedures with greater efficiency and precision. The capability to simultaneously cut and coagulate tissue has transformed surgical protocols, reducing operation times and improving patient recovery. However, risks such as thermal injuries and complications for patients with implantable devices remain concerns.

This review highlights the importance of ongoing research in enabling surgical teams to understand the complexities of electrosurgical techniques and their associated risks. Implementing rigorous safety protocols and updating best practices based on current research will be vital in mitigating complications. Looking ahead, advancements in technology and computational modeling promise to further enhance the capabilities of electrosurgery. An improved understanding of tissue interactions and thermal dynamics through simulation may enable more tailored surgical approaches, thereby minimizing damage to surrounding tissues. The integration of artificial intelligence and machine learning could also revolutionize precision and safety, offering real-time feedback for dynamic adjustments during procedures.

As the field evolves, interdisciplinary collaboration among engineers, surgeons, and researchers will drive innovation, keeping electrosurgery at the forefront of surgical technology and ultimately enhancing patient care and outcomes. The future of electrosurgery is promising, with potential for even greater advancements in surgical practices and patient safety.

Sources of Funding

Marija Radmilović-Radjenović acknowledges that this research was supported by the Slovak Academic Information Agency through the National Scholarship Program of the Slovak Republic.

Conflicts of Interest

The authors declare that they have no competing interests.

References

1. Meeuwsen F, Guédon A, Klein J, Elst MV, Dankelman J, Van Den Dobbelsteen J. Electrosurgery: short-circuit between education and practice. Minim Invasive Ther Allied Technol. 2019 Aug;28(4):247-253. doi: 10.1080/13645706.2018.1513945.

2. Biradar M, Dode P. Principles of electrosurgery in laparoscopy - A review. International Journal of Biomedical and Advance Research. 2019;10:e5163. Doi:10.21037/gpm

3. Radmilović-Radjenović M, Sabo M, Radjenović B. Application of multi-component fluid model in studies of the origin of skin burns during electrosurgical procedures. Comput Methods Biomech Biomed Engin. 2021 Oct;24(13):1409-1418. doi: 10.1080/10255842.2021.1890721. Epub 2021 Mar 5. PMID: 33667151.

4. Bisinotto FMB, Dezena RA, Martins LB, Galvão MC, Sobrinho JM, Calçado MS. Queimaduras relacionadas à eletrocirurgia – Relato de dois casos [Burns related to electrosurgery - Report of two cases]. Rev Bras Anestesiol. 2017;67:527-534. Portuguese. doi: 10.1016/j.bjan.2016.03.003.

5. Ho CWG, Yang SH, Wong CH, Chong SJ. High-voltage electrical injury complicated by compartment syndrome and acute kidney injury with successful limb salvage: A case report and review of the literature. Int J Surg Case Rep. 2018;48:38-42. doi: 10.1016/j.ijscr.2018.04.039. Epub 2018 May 16.

6. Huschak G, Steen M, Kaisers UX. Elektrochirurgie--Grundlagen und Risiken [Principles and risks of electrosurgery]. Anasthesiol Intensivmed Notfallmed Schmerzther. 2009 Jan;44(1):10-3. German. doi: 10.1055/s-0028-1128179. Epub 2008 Dec 29. PMID: 19115182.

7. Vilos GA, Rajakumar C. Electrosurgical generators and monopolar and bipolar electrosurgery. J Minim Invasive Gynecol. 2013 May-Jun;20(3):279-87. doi: 10.1016/j.jmig.2013.02.013.

8. Takahashi Y, Enatsu R, Kanno A, Imataka S, Komura S, Tamada T, et al. Comparison of Thresholds between Bipolar and Monopolar Electrical Cortical Stimulation. Neurol Med Chir (Tokyo). 2022 Jun 15;62(6):294-299. doi: 10.2176/jns-nmc.2021-0389. Epub 2022 Apr 22.

9. El-Sayed MM, Saridogan E. Principles and safe use of electrosurgery in minimally invasive surgery. Gynecol Pelvic Med 2021;4:6(1-14). doi: 10.21037/gpm-2020-pfd-10

10. Frivalssky M, Pavlek M. Electro-Thermal Model of Liver Tissue and its Approximation. Biomedical Eng. 2019; 17:187-193. doi: 10.15598/aeee.v17i2.2872

11. Hurst RD, Stewart CL. Hazards of surgical smoke from electrocautery: A critical review of the data. Am J Surg. 2024 Jul;233:29-36. doi: 10.1016/j.amjsurg.2024.02.017. Epub 2024 Feb 9.

12. Dufaye G, Cherouat A, Bachmann JM. Advanced modelling of the mechanical behaviour of biological tissues: application to 3D breast deformation. Comput Methods Biomech Biomed Engin. 2013;16 Suppl 1:305-7. doi: 10.1080/10255842.2013.815917. PMID: 23923952.

13. Morrison TM, Dreher ML, Nagaraja S, Angelone LM, Kainz W. The Role of Computational Modeling and Simulation in the Total Product Life Cycle of Peripheral Vascular Devices. J Med Device. 2017;11(2):024503. doi: 10.1115/1.4035866. Epub 2017 Jan 23. PMID: 29479395; PMCID: PMC5823268.

14. Lin CL, Lan GJ. A computational approach to investigate optimal cutting speed configurations in rotational needle biopsy cutting soft tissue. Comput Methods Biomech Biomed Engin. 2019 Jan;22(1):84-93. doi: 10.1080/10255842.2018.1535060. Epub 2018 Nov 6. PMID: 30398374.

15. Radmilović-Radjenović M, Radjenović B. 2020. Studies of the origin of skin burns during electrocautery based on a multi-component plasma fluid model. J. Surg. Surgical Research 2020;6:27-29. doi:10.17352/2455-2968.000091

International Journal of Biomedicine 15(4) (2025) 649-652
http://dx.doi.org/10.21103/Article15(4)_RA5

MINI REVIEW

INTERNATIONAL JOURNAL OF BIOMEDICINE

Impact of Herpes Zoster Vaccine on Postherpetic Neuralgia: A Comprehensive Review

Ramadan S. Hussein[1*], Salman Bin Dayel[1], Othman Abahussein[1], Waled Kamal Abdelbasset[2], Osama Mahfouz[3]

[1]*Department of Dermatology, College of Medicine, Prince Sattam Bin Abdulaziz University, Al-Kharj, Saudi Arabia*
[2]*Department of Physical Therapy, College of Health Sciences, University of Sharjah, Sharjah, United Arab Emirates*
[3]*Department of Emergency, King Saud University medical city, Riyadh, Saudi Arabia*

Abstract

Background: Herpes zoster (HZ), also known as shingles, is often complicated by postherpetic neuralgia (PHN), a chronic pain condition that significantly impairs quality of life. Vaccination against HZ has become a key preventive strategy to lower the risk of PHN. This review evaluates the effectiveness of HZ vaccines in reducing the incidence of PHN.
Methods and Results: In accordance with PRISMA guidelines, a systematic search was conducted across PubMed, Embase, Web of Science, and the Cochrane Library up to May 2024. Eligible studies included randomized controlled trials (RCTs), cohort studies, and observational studies that reported quantitative outcomes on the occurrence of PHN after vaccination.
The included studies encompassed diverse populations, primarily older adults. The recombinant zoster vaccine (RZV) demonstrated a substantial reduction in PHN incidence, with effectiveness approaching 60%. In contrast, the live zoster vaccine (ZVL) showed notable early protection, though its efficacy declined over time. The recombinant zoster vaccine (RZV) was associated with higher rates of mild, self-limiting adverse reactions compared with ZVL.
Conclusions: Both HZ vaccines, particularly RZV, are effective in preventing PHN and exhibit acceptable safety profiles. Broader vaccine uptake could decrease the public health burden of PHN. Long-term data on the duration of immunity and the potential role of booster doses remain areas for future investigation.(**International Journal of Biomedicine. 2025;15(4):649-652.**)

Keywords: herpes zoster • neuralgia • vaccine

For citation: Hussein RS, Dayel SB, Abahussein O, Abdelbasset WK, Mahfouz O. Impact of Herpes Zoster Vaccine on Postherpetic Neuralgia: A Comprehensive Review. International Journal of Biomedicine. 2025;15(4):649-652. doi:10.21103/Article15(4)_RA5

Abbreviations

HZ, herpes zoster; **PHN**, postherpetic neuralgia; **RZV**, recombinant zoster vaccine; **RCTs**, randomized controlled trials; **VZV**, varicella-zoster virus; **ZVL**, live zoster vaccine.

Introduction

Herpes zoster (HZ), also known as shingles, is caused by the reactivation of the latent varicella-zoster virus (VZV), the same virus responsible for causing chickenpox. Following primary infection, usually in childhood, VZV remains dormant within sensory ganglia and can reactivate later in life. Age-related immune decline, immunosuppression, and psychosocial stress are among the major triggers of viral reactivation, leading to the development of HZ. Clinically, HZ presents as a painful, vesicular rash in a dermatomal distribution, often preceded by prodromal symptoms such as itching, burning, or tingling sensations.[1]

The most common and burdensome complication of HZ is postherpetic neuralgia (PHN), a chronic neuropathic pain syndrome that may persist for months or years after rash resolution. PHN significantly impairs quality of life, contributing to ongoing pain, functional limitations, sleep

disturbances, and psychological distress. Beyond individual suffering, PHN imposes a considerable healthcare and economic burden due to prolonged treatment needs and increased healthcare utilization[2,3]

Because PHN is difficult to treat and often refractory to available therapies, prevention has become a major clinical priority. Vaccination against HZ has emerged as an effective strategy to reduce both the incidence and severity of HZ and, by extension, the risk of PHN. By enhancing VZV-specific immunity, vaccines aim to prevent reactivation or attenuate disease severity, thereby lowering the likelihood of PHN development.[4,5] Current recommendations target older adults, the population at greatest risk, with evidence suggesting a meaningful reduction in HZ and its complications following vaccination.[6] Nonetheless, questions remain regarding the degree of protection specifically against PHN, underscoring the need for a systematic evaluation of available evidence.

In this review, we assess the impact of HZ vaccination on the incidence of PHN. By synthesizing data across clinical trials and observational studies, we aim to clarify the effectiveness of HZ vaccines in mitigating one of the most persistent and debilitating outcomes of HZ.

Methods

We systematically searched PubMed, Embase, Web of Science, and the Cochrane Library for studies published up to May 2024, and screened reference lists of relevant articles.

Eligible studies included randomized controlled trials, cohort, case-control studies, and observational studies that assessed herpes zoster (HZ) vaccination and reported quantitative data on postherpetic neuralgia (PHN) incidence in humans. Reviews, editorials, case reports, and studies without relevant outcomes were excluded.

Search terms combined keywords and MeSH headings for "herpes zoster," "shingles," "postherpetic neuralgia," and "vaccine." Two reviewers independently screened records, extracted data, and resolved discrepancies by consensus. Extracted variables included study and participant characteristics, vaccine type and regimen, and outcomes (PHN incidence, follow-up duration, vaccine efficacy, and adverse events).

The primary outcome was the incidence of PHN after vaccination; secondary outcomes included the incidence of HZ, vaccine efficacy, and safety. The methods followed the PRISMA guidelines.

Results

Across randomized trials, cohort, and observational studies, herpes zoster (HZ) vaccination consistently reduced postherpetic neuralgia (PHN) incidence. Most studies involved adults aged ≥50 years from the United States, New Zealand, and Southeast Asia, with sample sizes up to >30,000.

The recombinant zoster vaccine (RZV) lowered PHN incidence by ~60% in older adults, with durable protection over several years. By contrast, live zoster vaccine (ZVL) showed strong early efficacy but declined markedly over time, suggesting a need for booster strategies.[6-9]

Recombinant zoster vaccine (RZV) was associated with higher rates of mild local and systemic reactions than ZVL, but serious adverse events were rare.[10-13]

Modeling studies predicted substantial public health gains: raising RZV coverage to 65% in Southeast Asia could prevent hundreds of thousands of PHN cases over 15 years, with significant healthcare cost savings.[12,13]

Subgroup analyses confirmed benefits across age groups and health statuses, with particularly strong protection in older and immunocompromised populations.[13-15]

Discussion

Herpes zoster (HZ) results from reactivation of latent varicella-zoster virus (VZV) within sensory ganglia. Following primary infection, the virus persists in neuronal cell bodies in a transcriptionally quiescent state, thereby evading immune detection.[15] Reactivation is primarily driven by immunosenescence, with age-related declines in T-cell-mediated immunity rendering older adults particularly vulnerable. Immunocompromised states such as HIV infection, organ transplantation, or long-term immunosuppressive therapy further disrupt the host–virus balance, permitting viral replication and clinical disease. In addition, stress, trauma, or neurological injury can alter the local ganglionic microenvironment via neuroendocrine and inflammatory signaling, creating conditions favorable to reactivation. Viral factors, including mutations in latency- or reactivation-associated genes, may also modulate the risk of reactivation.[15,16]

Host immune responses play a decisive role in determining disease outcomes. VZV-specific T cells are central to viral control; memory T cells maintain immune surveillance in sensory ganglia and can rapidly eliminate reactivated virus.[17] When this surveillance is compromised, viral spread along sensory nerves initiates acute HZ, characterized by a painful dermatomal rash and robust inflammatory infiltration of cytokines, chemokines, and immune cells.[15] This inflammation, while necessary for viral clearance, also contributes to neuronal injury and heightened nociceptive signaling. Persistent neuroinflammation, combined with ongoing antigenic stimulation, aberrant nociceptive processing, and neuronal sensitization, provides the basis for postherpetic neuralgia (PHN).[18]

Several risk factors predispose to PHN. Advanced age remains the strongest predictor, owing to diminished immune function, reduced regenerative capacity, and heightened neuroinflammation. Severe acute pain during HZ also strongly correlates with PHN onset, highlighting the importance of early and effective pain control.[19] Pathophysiologically, PHN is sustained by persistent inflammation, structural nerve injury (including demyelination and axonal loss), and central sensitization that amplifies pain signaling within the central nervous system.[19,20]

Management of HZ focuses on limiting viral replication and alleviating acute pain. Antivirals such as acyclovir, valacyclovir, and famciclovir, when administered early, reduce viral replication and accelerate lesion healing.[21] Pain management strategies include NSAIDs, opioids, anticonvulsants, and

topical agents such as lidocaine patches.[22] Once established, PHN requires a multimodal approach involving tricyclic antidepressants, gabapentin or pregabalin, topical capsaicin or lidocaine, and, in refractory cases, interventional procedures such as nerve blocks or spinal cord stimulation.[23] Despite these options, PHN remains challenging to treat, emphasizing the importance of preventive strategies.

Vaccination has emerged as the most effective intervention for reducing both HZ and PHN. The live attenuated vaccine (Zostavax) demonstrated efficacy in lowering disease incidence in older adults, although its protective effect wanes within a few years.[5,10,25] In contrast, the recombinant subunit vaccine (Shingrix), which contains VZV glycoprotein E and the AS01B adjuvant system, has shown superior efficacy and durability across age groups, including individuals over 70 years.[24] Shingrix induces both humoral and cell-mediated responses without viral replication, making it safer for immunocompromised populations.[5,25]

Evidence from randomized clinical trials consistently demonstrates the efficacy of vaccines. The ZOE-50 trial and related studies showed that Shingrix significantly reduces both HZ incidence and PHN risk compared to placebo, with efficacy exceeding 90% in older adults.[24] In contrast, the protective effect of Zostavax declines markedly within the first year, raising questions about the need for boosters [10,25] Both vaccines are generally safe, with adverse events limited to transient injection-site reactions and mild systemic symptoms, although live vaccines carry higher risks for immunocompromised individuals.[5,24,25]

Beyond clinical trials, real-world effectiveness studies confirm that HZ vaccination programs substantially reduce the incidence of HZ and PHN, lower healthcare utilization, and improve quality of life for older adults.[26] Population-based data further show declines in PHN rates following widespread vaccine adoption, with the greatest benefit observed in older adults and individuals with immunocompromising conditions.[7,10,14,15] Modeling and cost-effectiveness analyses suggest that the broader use of recombinant subunit vaccines could prevent a substantial proportion of PHN cases and yield significant public health benefits.[8,10]

Taken together, these findings underscore that PHN arises from a complex interplay of immune decline, neuroinflammation, and neuronal injury, which makes it difficult to manage once established. Vaccination, particularly with Shingrix, represents the most effective strategy to prevent HZ and its chronic complications. Continued efforts to expand vaccination coverage, particularly among high-risk groups, are crucial for reducing the burden of PHN at both the individual and population levels.

Challenges and Future Directions

Despite proven efficacy, herpes zoster vaccines remain underutilized due to hesitancy, cost, and limited access. Addressing these barriers through physician engagement, public education, and expanded delivery models (e.g., pharmacies, mobile clinics) will be essential to improve uptake.[27,28] Key research priorities include defining long-term immunity, optimizing booster strategies, and refining cost-effectiveness models for high-risk groups. Sustained real-world surveillance of safety and effectiveness will be crucial to maintain confidence and maximize public health impact. [10,29,30]

Limitations

Only articles written in English and with available full texts were included. Studies featuring both adult and pediatric data were considered only if they provided individual-level data specifically for pediatric patients. No meta-analysis was performed.

Conclusion

The herpes zoster vaccine, particularly RZV, represents a significant advancement in the prevention of PHN. The evidence supports its widespread use, given its effectiveness, safety profile, and potential to reduce the public health burden of HZ. Continued research and public health efforts are essential to maximize the benefits of vaccination and improve the quality of life for older adults.

Acknowledgments

“This study is supported via funding from Prince Sattam bin Abdulaziz University project number (PSAU/2023/R/1444).”

Conflicts of Interest

The authors declare that they have no competing interests.

Generative AI Disclosure

OpenAI’s ChatGPT (GPT-4, July 2025) was used for language editing and text refinement. All AI-assisted text was reviewed for accuracy and originality, and the AI is not listed as an author.

References

1. Kawai K, Gebremeskel BG, Acosta CJ. Systematic review of incidence and complications of herpes zoster: towards a global perspective. BMJ Open. 2014 Jun 10;4(6):e004833. doi: 10.1136/bmjopen-2014-004833. PMID: 24916088.
2. Johnson RW, Rice AS. Clinical practice. Postherpetic neuralgia. N Engl J Med. 2014 Oct 16;371(16):1526-33. doi: 10.1056/NEJMcp1403062. PMID: 25317872.
3. Harpaz R, Ortega-Sanchez IR, Seward JF; Advisory Committee on Immunization Practices (ACIP) Centers for Disease Control and Prevention (CDC). Prevention of herpes zoster: recommendations of the Advisory Committee on Immunization Practices (ACIP). MMWR Recomm Rep. 2008 Jun 6;57(RR-5):1-30; quiz CE2-4. PMID: 18528318.
4. Schmader KE, Oxman MN. Varicella and herpes zoster. In: Bennett JE, Dolin R, Blaser MJ, editors. Mandell, Douglas, and Bennett's Principles and Practice of Infectious Diseases. 9th ed. Elsevier; 2020. p. 1665-77.

5. Cunningham AL, Lal H, Kovac M, Chlibek R, Hwang SJ, Díez-Domingo J, et al.; ZOE-70 Study Group. Efficacy of the Herpes Zoster Subunit Vaccine in Adults 70 Years of Age or Older. N Engl J Med. 2016 Sep 15;375(11):1019-32. doi: 10.1056/NEJMoa1603800. PMID: 27626517.
6. Curran D, Bitetti J, Catterall I, Wincott S. Herpes zoster in older adults: Impact on carbon footprint in the United States. Hum Vaccin Immunother. 2024 Dec 31;20(1):2335722. doi: 10.1080/21645515.2024.2335722. Epub 2024 May 3. PMID: 38698759; PMCID: PMC11073404.
7. Tseng HF, Harpaz R, Luo Y, Hales CM, Sy LS, Tartof SY, et al. Declining Effectiveness of Herpes Zoster Vaccine in Adults Aged ≥60 Years. J Infect Dis. 2016 Jun 15;213(12):1872-5. doi: 10.1093/infdis/jiw047. Epub 2016 Feb 9. PMID: 26908728.
8. Gagliardi AM, Andriolo BN, Torloni MR, Soares BG. Vaccines for preventing herpes zoster in older adults. Cochrane Database Syst Rev. 2016 Mar 3;3(3):CD008858. doi: 10.1002/14651858.CD008858.pub3. Update in: Cochrane Database Syst Rev. 2019 Nov 7;2019(11). doi: 10.1002/14651858.CD008858.pub4. PMID: 26937872; PMCID: PMC6516976.
9. Drolet M, Levin MJ, Schmader KE, et al. A National Study of the Impact of Herpes Zoster Vaccine on the Burden of Disease. J Infect Dis. 2016;213(12):1876-1882. doi:10.1093/infdis/jiv641.
10. Dooling KL, Guo A, Patel M, Lee GM, Moore K, Belongia EA, Harpaz R. Recommendations of the Advisory Committee on Immunization Practices for Use of Herpes Zoster Vaccines. MMWR Morb Mortal Wkly Rep. 2018 Jan 26;67(3):103-108. doi: 10.15585/mmwr.mm6703a5. PMID: 29370152.
11. Li Y, Fang L, Zhang Q, Zhang J, Xia N, Wang Q. Effectiveness of Herpes Zoster Vaccine in Reducing the Incidence of Postherpetic Neuralgia: A Meta-Analysis. BMC Geriatr. 2020;20(1):310. doi:10.1186/s12877-020-01675-1.
12. Schmader KE, Levin MJ, Gnann JW Jr, McNeil SA, Vesikari T, Betts RF, et al.. Efficacy, safety, and tolerability of herpes zoster vaccine in persons aged 50-59 years. Clin Infect Dis. 2012 Apr;54(7):922-8. doi: 10.1093/cid/cir970. Epub 2012 Jan 30. PMID: 22291101; PMCID: PMC4542655.
13. Lal H, Cunningham AL, Godeaux O, Chlibek R, Diez-Domingo J, Hwang SJ, et al.; ZOE-50 Study Group. Efficacy of an adjuvanted herpes zoster subunit vaccine in older adults. N Engl J Med. 2015 May 28;372(22):2087-96. doi: 10.1056/NEJMoa1501184. Epub 2015 Apr 28. PMID: 25916341.
14. Cunningham AL, Heineman TC, Lal H, Godeaux O, Chlibek R, Hwang SJ, et al.; ZOE-50/70 Study Group. Immune Responses to a Recombinant Glycoprotein E Herpes Zoster Vaccine in Adults Aged 50 Years or Older. J Infect Dis. 2018 May 5;217(11):1750-1760. doi: 10.1093/infdis/jiy095. PMID: 29529222; PMCID: PMC5946839.
15. Gilden DH, Kleinschmidt-DeMasters BK, LaGuardia JJ, Mahalingam R, Cohrs RJ. Neurologic complications of the reactivation of varicella-zoster virus. N Engl J Med. 2000 Mar 2;342(9):635-45. doi: 10.1056/NEJM200003023420906. Erratum in: N Engl J Med 2000 Apr 6;342(14):1063. PMID: 10699164.
16. Oaklander AL, Cohen SP, Raju SV. Intractable postherpetic itch and cutaneous deafferentation after facial shingles. Pain. 2002 Mar;96(1-2):9-12. doi: 10.1016/s0304-3959(01)00400-6.
17. Kawai K, Gebremeskel BG, Acosta CJ. Systematic review of incidence and complications of herpes zoster: towards a global perspective. BMJ Open. 2014 Jun 10;4(6):e004833. doi: 10.1136/bmjopen-2014-004833. PMID: 24916088.
18. Johnson RW, Wasner G, Saddier P, Baron R. Postherpetic neuralgia: epidemiology, pathophysiology and management. Expert Rev Neurother. 2007 Nov;7(11):1581-95. doi: 10.1586/14737175.7.11.1581. PMID: 17997705.
19. Cohen JI. Clinical practice: Herpes zoster. N Engl J Med. 2013 Jul 18;369(3):255-63. doi: 10.1056/NEJMcp1302674.
20. Yawn BP, Saddier P, Wollan PC, St Sauver JL, Kurland MJ, Sy LS. A population-based study of the incidence and complication rates of herpes zoster before zoster vaccine introduction. Mayo Clin Proc. 2007 Nov;82(11):1341-9. doi: 10.4065/82.11.1341. Erratum in: Mayo Clin Proc. 2008 Feb;83(2):255. PMID: 17976353.
21. Dworkin RH, Johnson RW, Breuer J, Gnann JW, Levin MJ, Backonja M, et al. Recommendations for the management of herpes zoster. Clin Infect Dis. 2007 Jan 1;44 Suppl 1:S1-26. doi: 10.1086/510206. PMID: 17143845.
22. Lapolla W, Digiorgio C, Haitz K, Magel G, Mendoza N, Grady J, Lu W, Tyring S. Incidence of postherpetic neuralgia after combination treatment with gabapentin and valacyclovir in patients with acute herpes zoster: open-label study. Arch Dermatol. 2011 Aug;147(8):901-7. doi: 10.1001/archdermatol.2011.81. Epub 2011 Apr 11. PMID: 21482862.
23. Attal N, Cruccu G, Baron R, Haanpää M, Hansson P, Jensen TS, Nurmikko T. EFNS guidelines on the pharmacological treatment of neuropathic pain: 2010 revision. Eur J Neurol. 2010 Sep;17(9):1113-e88. doi: 10.1111/j.1468-1331.2010.02999.x. Epub 2010 Apr 9. PMID: 20402746.
24. GlaxoSmithKline. Shingrix (Zoster Vaccine Recombinant, Adjuvanted) [package insert]. Research Triangle Park, NC: GlaxoSmithKline; 2019.
25. Oxman MN, Levin MJ, Johnson GR, Schmader KE, Straus SE, Gelb LD, et al.; Shingles Prevention Study Group. A vaccine to prevent herpes zoster and postherpetic neuralgia in older adults. N Engl J Med. 2005 Jun 2;352(22):2271-84. doi: 10.1056/NEJMoa051016. PMID: 15930418.
26. Langan SM, Minassian C, Smeeth L, Thomas SL. Risk of herpes zoster in patients with altered immune function. Epidemiol Infect. 2018;146(4):419-429.
27. Weinberg A, Popmihajlov Z, Schmader KE, Johnson MJ, Caldas Y, Salazar AT, et al. Persistence of Varicella-Zoster Virus Cell-Mediated Immunity After the Administration of a Second Dose of Live Herpes Zoster Vaccine. J Infect Dis. 2019 Jan 7;219(2):335-338. doi: 10.1093/infdis/jiy514.
28. Giannelos N, Ng C, Curran D. Cost-effectiveness of the recombinant zoster vaccine (RZV) against herpes zoster: An updated critical review. Hum Vaccin Immunother. 2023 Dec 31;19(1):2168952. doi: 10.1080/21645515.2023.2168952. Epub 2023 Mar 14. PMID: 36916240; PMCID: PMC10054181.
29. Williams WW, Lu PJ, O'Halloran A, Bridges CB, Kim DK, Pilishvili T, Hales CM, Markowitz LE; Centers for Disease Control and Prevention (CDC). Vaccination coverage among adults, excluding influenza vaccination - United States, 2013. MMWR Morb Mortal Wkly Rep. 2015 Feb 6;64(4):95-102. PMID: 25654611.
30. Hechter RC, Tartof SY, Jacobsen SJ, Smith N, Tseng HF. Trends and disparity in zoster vaccine uptake in a managed care population. Vaccine. 2013 Sep 23;31(41):4564-8. doi: 10.1016/j.vaccine.2013.07.053.

***Corresponding author**: Ramadan S. Hussein. Department of Dermatology, College of Medicine, Prince Sattam Bin Abdulaziz University, Alkharj, Saudi Arabia. E-mail: ramadangazeera@yahoo.com*

International Journal of Biomedicine 15(4) (2025) 653-659
http://dx.doi.org/10.21103/Article15(4)_OA1

ORIGINAL ARTICLE

Cardiology

INTERNATIONAL JOURNAL OF BIOMEDICINE

Significance of Clinical and Biochemical Markers in Predicting Atrial Fibrillation Recurrence after Catheter Ablation

Khasan I. Uralov[1*], Nodir U. Zakirov[1], Baxtiyor Dj. Amirkulov[1], Ravshanbek D. Kurbanov[1]

[1]*Republican Specialized Cardiology Scientific Practical Medicine Center, Tashkent, Uzbekistan*

Abstract

Background: Pulmonary vein isolation, particularly via radiofrequency ablation (RFA), is a well-established and effective treatment strategy recommended in international clinical guidelines for patients with symptomatic, drug-resistant atrial fibrillation (AF). This study aimed to investigate the incidence and risk factors of early and late recurrence of AF following RFA.

Methods and Results: This prospective, randomized, open-label study included 67 patients (70.1% male) diagnosed with recurrent AF. Any atrial tachyarrhythmia episode lasting more than 30 seconds was defined as a recurrence. All patients underwent RFA of the pulmonary veins (without the CARTO system) between 2022 and 2025. Clinical and laboratory parameters were analyzed before ablation for their association with recurrence.

Early recurrence (ER) was observed in 30 (44.8%) patients, while late recurrence (LR) occurred in 32 (47.8%) patients. Multivariate logistic regression revealed that diabetes mellitus and C-reactive protein (CRP) level at the end of the blanking period remained the only independent predictors of ER. CRP levels demonstrated strong predictive value for early recurrences (AUC = 0.93), with a cutoff point of 1.95 mg/L, a sensitivity of 90%, and a specificity of 85.7% (P<0.001). In ROC analysis for CRP and diabetes combined, the AUC reached 0.957, demonstrating a very high discriminative capacity. The sensitivity was 96.7%, and the specificity was 90.9%, confirming the high accuracy and reliability of the prognostic model (P<0.001).

For late recurrence, multivariate logistic regression revealed that CRP, AF duration, left atrial volume index (LAVI), and erythrocyte sedimentation rate (ESR) were identified as independent predictors of the outcome. In the ROC analysis of 12-month recurrence predictors, the model demonstrated strong statistical significance (P=0.000), with an AUC of 0.83. Although ER was not identified as an independent predictor in the logistic regression model, the ROC analysis demonstrated the predictive relevance of CRP, AF duration, LAVI, ESR, and ER rate, with sensitivity exceeding 75% and specificity above 80%

Conclusion: Elevated CRP levels and diabetes are strong independent predictors of early AF recurrence after catheter ablation. Longer AF duration, larger left atrial size, increased ESR, and early recurrence rate also contribute to late recurrence. Combined clinical and biochemical evaluation may enhance individualized risk stratification and post-ablation management.(**International Journal of Biomedicine. 2025;15(4):653-659.**)

Keywords: atrial fibrillation • radiofrequency ablation • recurrence • C-reactive protein • diabetes mellitus

For citation: Uralov KhI, Zakirov NU, Amirkulov BDj, Kurbanov RD. Significance of Clinical and Biochemical Markers in Predicting Atrial Fibrillation Recurrence after Catheter Ablation. International Journal of Biomedicine. 2025;15(4):653-659. doi:10.21103/Article15(4)_OA1

Abbreviations

AH, arterial hypertension; **AF**, atrial fibrillation; **AI**, atherogenic index; **CRP**, C-reactive protein; **DM**, diabetes mellitus; **ESR**, erythrocyte sedimentation rate; **ER**, early recurrence; **eGFR**, estimated glomerular filtration rate; **ESR**, erythrocyte sedimentation rate; **HDL-C**, high-density lipoprotein cholesterol; **IHD**, ischemic heart disease; **IVS**, interventricular septum; **LA**, left atrium; **LVEF**, left ventricular ejection fraction; **LVEDD**, left ventricular end-diastolic diameter; **LVESD**, left ventricular end-systolic diameter; **LVMI**, left ventricular mass index; **LR**, late recurrence; **LAVI**, left atrial volume index; **LDL-C**, low-density lipoprotein cholesterol; **PW**, posterior wall; **PVI**, pulmonary vein isolation; **RBC**, red blood cells; **RFA**, radiofrequency ablation; **RA**, right atrium; **TSH**, thyroid-stimulating hormone; **TC**, total cholesterol; **TG**, triglycerides; **WBC**, white blood cells.

Introduction

Atrial fibrillation (AF) is the most common cardiac arrhythmia encountered in clinical practice, and its global prevalence continues to rise each year. In 2021, approximately 52.5 million people worldwide were reported to have AF or atrial flutter, representing a 137% increase over 1990. The age-standardized global prevalence rate was estimated at 620.5 cases per 100,000 population.[1] According to other sources, the number of AF cases globally increased from 33.5 million in 2010 to nearly 59 million in 2019.[2] The presence of AF increases the risk of stroke by at least fivefold, with more than 20% of cardioembolic strokes being directly related to AF. Moreover, AF is characterized by its recurrent nature, reduced quality of life, and substantial healthcare costs.[3]

Pulmonary vein isolation (PVI), particularly via radiofrequency ablation (RFA), is a well-established and effective treatment strategy recommended in international clinical guidelines for patients with symptomatic, drug-resistant AF. In some cases, especially for paroxysmal AF, ablation is also considered as a first-line rhythm control strategy. Compared with pharmacological therapy, catheter ablation has demonstrated superior efficacy in maintaining sinus rhythm, improving quality of life, reducing hospitalizations due to heart failure, and lowering the risk of stroke and cardiovascular mortality.[4]

Despite these benefits, AF recurrence after PVI remains a significant clinical challenge. Long-term rhythm control after a single ablation procedure is achieved in only about half of patients, with most recurrences occurring within the first year—the period considered to be the most vulnerable.[5] Early recurrence (ER) (within 3 months after RFA) is reported in 20%–40% of patients, depending on the type of AF (paroxysmal or persistent), the patient population, and the monitoring method. Although these arrhythmias were previously regarded as clinically insignificant, growing evidence now supports ER as a strong predictor of subsequent relapse and long-term procedural failure. In other words, the presence of ER markedly increases the likelihood of late recurrence (LR) (between 3 and 12 months after RFA).[6]

The one-year recurrence rate varies among studies. Meta-analyses have reported that 25%–40% of patients experience recurrence within a year after a single ablation procedure, depending on the monitoring methods, AF type, and recurrence definition criteria. Continuous or implantable monitoring devices often detect asymptomatic paroxysms, leading to higher reported recurrence rates.[6]

Various predictors of AF recurrence have been proposed in the literature, including clinical, social, and lifestyle characteristics, as well as procedural parameters, laboratory findings, and echocardiographic markers. However, methodological and clinical heterogeneity among studies has led to inconsistent results. Therefore, identifying reliable clinical and biochemical predictors of AF recurrence after PVI is crucial for optimizing patient selection, tailoring post-procedural management, and improving long-term outcomes.

This study aimed to investigate the incidence and risk factors of early and late AF recurrence following RFA.

Materials and Methods

This prospective, randomized, open-label study included 67 patients (70.1% male) diagnosed with recurrent AF. Among them, 46 had paroxysmal and 21 had persistent AF. All patients underwent RFA of the pulmonary veins (without the CARTO system) between 2022 and 2025.

Before RFA, all patients underwent the standard examination: 12-lead ECG, transthoracic echocardiography, transesophageal echocardiography to exclude left atrial appendage thrombus, 24-hour Holter monitoring, complete blood count, biochemical tests (ALT, AST, urea, creatinine, glucose, lipid profile, and CRP). In patients over 50 years of age, coronary angiography was performed to diagnose coronary artery disease. All patients received anticoagulant therapy before surgery in accordance with current guidelines.[7] Patients who had previously taken amiodarone discontinued it at least 40 days before the procedure. To assess the presence of inflammation at the end of the blanking period, CRP levels were re-measured. Clinical and laboratory parameters were analyzed before ablation for their association with recurrence.

Electrophysiological Study and RFA

The procedure was performed under fluoroscopic guidance (C-arm Siemens) and local anesthesia (0.5% novocaine or lidocaine). The right jugular and bilateral femoral veins were punctured, and transseptal access to the left atrium was achieved via PREFACE introducers (Biosense Webster). Pulmonary vein anatomy and size were assessed using an angiographic catheter, then replaced with a Lasso catheter. Circular mapping of the pulmonary veins was performed to evaluate the size and electrical activity of the muscular sleeves. During sinus rhythm, double or multicomponent potentials were recorded along the pulmonary vein ostia—low-frequency components representing the left atrium and high-frequency components representing pulmonary vein activity. In complex cases, coronary sinus pacing was used to differentiate them. Electrical isolation was achieved by circumferential ablation around the venous ostia, starting from the earliest activation site, divided into 12 segments (Biosense Webster Stockert 70 Ablation System). Ablation parameters: temperature 40–44 °C, power 30–35 W, irrigation rate 17–30 mL/min. Post-procedural assessments of pulmonary vein refractoriness, AF inducibility, fragmented activity, and conduction times were performed.

After the procedure, patients received class IC antiarrhythmic drugs (propafenone, n=33; lappaconitine hydrobromide, n=34) for three months, anticoagulant therapy, and additional symptomatic management as indicated. Outpatient follow-up lasted 12 months after ablation.

During follow-up, patients were evaluated at 3, 6, 9, and 12 months with 24-hour Holter monitoring and echocardiography. Unscheduled visits were performed in cases of recurrent arrhythmia, hospital admission, or emergency service contact, with reasons for hospitalization verified via phone interviews. Any atrial tachyarrhythmia episode lasting more than 30 seconds (AF, atrial flutter, or atrial tachycardia) was defined as a recurrence. Patients were categorized into two groups based on recurrence timing: the ER group and the LR group.

Statistical analysis was conducted using IBM SPSS Statistics, version 27. Quantitative variables with normal distribution were expressed as mean ± standard deviation (M ± SD); non-normally distributed variables—as median (interquartile range); categorical variables—as absolute numbers and percentages. Comparisons between two independent groups were made using the Student's t-test (for normally distributed data) or the Mann–Whitney U test (for non-normal data). Categorical variables were analyzed using Fisher's exact test or Pearson's χ^2 test, as appropriate. Predictors of AF recurrence were assessed using ROC curve analysis and logistic regression. ROC analysis was used to evaluate the predictive performance of key variables and to determine the optimal cut-off points, along with their corresponding sensitivity and specificity. Logistic regression was performed to identify independent predictors of recurrence; variables with $P < 0.25$ in univariate analysis were entered into the multivariate model. Statistical significance was set at $P < 0.05$.

Results

Baseline clinical characteristics of the study patients are presented in Table 1. Early recurrence was observed in 30 (44.8%) patients, while late recurrence occurred in 32 (47.8%) patients.

The median number of AF-free days was 142 days (range: 17.5–600 days). Among patients with recurrence, the proportion of males was 60% in the ER group and 56.3% in the LR group. The mean age of the cohort was 51.5±11.9 years. Patients with recurrence tended to be older: 54.43 ± 9.1 vs. 49.1 ± 13.4 years (P=0.06) at 3 months and 54.78 ± 9.9 vs. 48.5 ± 12.8 years (P=0.029) at 12 months (Table 1).

A history of COVID-19 infection was present in 61% of patients, with no significant difference between groups. Among patients with recurrence, the duration of AF was significantly longer at 12 months (5 [3–8] years vs. 2 [1–6] years, P=0.008). Arterial hypertension and ischemic heart disease were observed in 74.6% of all patients and were more frequent in those with recurrence, though without statistical significance. Myocarditis and idiopathic AF were reported in 15% and 10.4% of cases, respectively.

Diabetes mellitus was significantly more prevalent in the recurrence groups at 3 months (26.7% vs. 5.4%, P=0.034) and at 12 months (25% vs. 5.7%, P=0.039). Echocardiographic evaluation revealed that patients with recurrence had larger LA diameters and LAVI at 3 months (4.45 (4.15-4.7) cm vs. 41.5 (3.85-4.35) mm, P=0.004; 27 (24-32.7 vs. 23 (21-28) mL/m², P=0.004). These differences remained more pronounced at 12 months (P<0.001 in both cases). IVS and PW thickness tended to be greater in the recurrence groups, though not statistically significant. LVEF was preserved in both groups.

Table 1.

Baseline clinical characteristics of the study patients.

Characteristics	Total n=67	3 months		*P*-value	12 months		*P*-value
		Recurrence n= 30	No recurrence n= 37		Recurrence n=32	No recurrence n=35	
Men, n (%)	47 (70.1%)	18 (60%)	29 (78.37%)	0.11	18 (56.3%)	29 (82.9%)	0.03
Women, n (%)	20 (29.9%)	12 (40%)	8 (21.63%)		14 (43.8%)	6 (17.1%)	
Mean age, years	51.52±11.88	54.43±9.1	49.1±13.4	0.06	54.78±9.9	48.5±12.8	0.029
COVID 19, n (%)	41 (61%)	16 (53.3%)	25 (67.6%)	0.23	19 (59.4%)	22 (62.9%)	0.77
Rural residence, n (%)	36 (53.7%)	16 (53.3%)	20 (54%)	1.0	18 (56.2%)	18 (51.4%)	0.7
Follow-up duration, month Me [IQR]	22 (19-31)	20 (19-25)	27 (18-32)	0.196	21 (19-28)	23 (15-31)	0.8
AF duration, month Me [IQR]	4 (2-7)	4 (3-6)	2 (1-8)	0.64	5 (3-8)	2 (1-6)	0.008
Paroxysmal, n (%)	46 (68.7%)	20 (66.7%)	26 (70.3%)	0.79	19 (59.4%)	27 (77.1%)	0.18
Persistent, n (%)	21(31.3%)	10 (33.3%)	11 (29.7%)		13 (40.6%)	8 (22.9%)	
CHA2DS2VASc score, Me [IQR]	2 (0-3)	2 (1-4)	1 (0-2)	0.011	2 (1-4)	1 (0-2)	0.014
HASBLED score, Me [IQR]	1 (0.5-2)	2 (1-2)	1 (0-2)	0.011	2 (1-2)	1 (0-2)	0.004
AH/IHD, n (%)	50 (74.6%)	26 (86.7%)	24 (64.9)	0.1	27 (84.4%)	23 (65.7%)	0.15
Myocarditis, n (%)	10 (15%)	3 (10%)	7 (18.9%)		2 (6.3%)	8 (22.9%)	
Idiopathic AF, n (%)	7 (10.4%)	6 (16.2%)	1 (3.3%)		3 (9.4%)	4 (11.4%)	
DM, n (%)	10 (14.9%)	8 (26.7%)	2 (5.4%)	0.034	8 (25%)	2 (5.7%)	0.039
BMI, Me [IQR]	29.2 (27.5-31.24)	28.9 (27.6-31.6)	29.4(27.5-31.4)	0.73	29.3 (26.7-32.3)	29.3 (27.6-30.9)	0.4
Obesity, n (%)	27 (40.3%)	11 (36.7%)	16 (43.2%)	0.58	15 (46.9%)	12 (34.3%)	0.29

Table 1 (continued).

Baseline clinical characteristics of the study patients.

Characteristics	Total n=67	3 months		*P*-value	12 months		*P*-value
		Recurrence n= 30	No recurrence n= 37		Recurrence n=32	No recurrence n=35	
Echocardiographic Parameters							
IVS, cm Me [IQR]	1 (0.9-1.15)	1.07 (0.95-1.2)	1 (0.89-1.12)	0.06	1.07 (0.95-1.2)	1 (0.9-1.11)	0.158
PW, cm Me [IQR]	0.95 (0.9-1.05)	0.97 (0.91-1.1)	0.93 (0.9-1.0)	0.09	0.95 (0.9-1.1)	0.93 (0.9-1.0)	0.316 0.13
LAD, cm Me [IQR]	4.3 (3.95-4.55)	4.45 (4.15-4.7)	4.15 (3.85-4.35)	0.004	4.45 (4.2-4.6)	4.0 (3.8-4.35)	<0.001
LAVI, mL/m^2 Me [IQR]	25.9 (22-30.4)	27 (24-32.7)	23 (21-28)	0.004	28 (25.3-34.6)	22.1 (20.5-26.7)	<0.001
LVEDD, cm Me [IQR]	4.9 (4.8-5.2)	4.9 (4.8-5.3)	4.9 (4.7-5.2)	0.62	4.9 (4.75-5.3)	4.9 (4.8-5.1)	0.626
LVESD, cm Me [IQR]	3.4 (3.2-3.6)	3.4 (3.3-3.6)	3.4 (3.2-3.7)	0.86	3.45 (3.25-3.6)	3.4 (3.2-3.5)	0.4
LVEF, % Me [IQR]	60.45 (58.8-62.5)	60.3 (56.4-62.2)	61.5 (59.3-62.8)	0.177	60.3 (56.3-62.2)	62 (59.3-62.7)	0.1
RA med, cm Me [IQR]	4 (3.85-4.2)	4 (3.9-4.25)	4 (3.8-4.1)	0.7	4.05 (3.95-4.25)	3.95 (3.7-4.1)	0.056
LVMI, g/m^2 Me [IQR]	86 (75-102)	95 (82.3-102.8)	81.2 (66.1-90.2)	0.03	97.4 (81.2-102.7)	80.9 (72.7-	0.01
Biochemical Parameters							
CRP, mg/L Me [IQR]	0.5 (0.5-5)	5 (5-5)	0.5 (0.5-0.5)	<0.001	5 (1.95-5)	0.5 (0.5-0.5)	<0.001
TSH, mIU/mL (M±SD)	2.31±1.11	2.48±1.32	2.16±0.91	0.265	2.59±0.99	2.05±1.17	0.05
Free T4, pmol/mL (M±SD)	17.84±2.7	18.9±2.9	16.9±2.17	0.002	18.7±3.1	17±1.95	0.008
TC, mg/dL (M±SD)	192.4±42.1	198.6±26.2	187.8±51.47	0.28	195.9±32.3	189.2±49.6	0.5
TG, mg/dL Me [IQR]	139 (97-202)	148 (104-178)	131 (97-202)	0.6	139 (92-170.5)	131 (98-204)	0.37
HDL-C, mg/dl (M±SD)	44.7±10.7	44.7±12.5	44.7±9.1	0.98	45.2±12.8	44.2±8.5	0.7
VLDL-C, mg/dL Me [IQR]	31 (20-40)	29.5 (21-36)	31 (20-41)	0.57	28 (18.5-34.5)	33 (20.5-44)	0.13
LDL-C, mg/dL (M±SD)	115.37±42	121.73±31	110.2±49	0.27	119.3±33.83	111.8±48.6	0.46
AI (M±SD)	3.4 (2.3-4.2)	3.67±1.13	3.35±1.3	0.3	3.6±1.25	3.4±1.22	0.5
Glucose, mmol/L Me [IQR]	5.1 (4.8-5.8)	5 (4.4-5.5)	5.3 (4.9-5.8)	0.48	5 (4.5-5.65)	5.3 (4.8-5.8)	0.51
Urea, mmol/L (M±SD)	6±1.39	6.4±1.36	5.66±1.35	0.027	6.44±1.3	5.6±1.37	0.013
Creatinine, µmol/L (M±SD)	90.7±21.5	98.5±18.6	84.38±21.8	0.007	98.97±21.1	83.14±19.1	0.002
eGFR, mL/min/1.73m^2 Me [IQR]	79 (65-100)	71 (64-79)	98 (73-110)	<0.001	67.5 (54.5-79)	88 (76.5-106)	<0.001
Uric acid, mg/dL, Me [IQR]	5 (4.3-5.7)	5.6 (4.5-6.9)	4.9 (4.3-5.2)	0.01	5.2 (4.4-5.8)	5.0 (4.3-5.6)	0.27
Complete Blood Count							
Platelets, ×10^9/L Me [IQR]	255 (228-308)	255 (232-296)	242 (221-343)	0.96	255 (227-293)	242 (228-342)	0.67
WBC, ×10^9/L (M±SD)	6.4±1.40	6.3±1.52	6.5±1.32	0.6	6.4±1.52	6.4±1.32	0.9
RBC, ×10^{12}/L (M±SD)	4.83±0.55	4.78±0.58	4.87±0.52	0.5	4.7±0.56	4.95±0.52	0.059
ESR, mm/60min Me [IQR]	3 (2-15)	2 (2-18)	3 (2-11)	0.8	4 (2-23)	3 (2-11)	0.014

Among laboratory parameters, CRP levels were significantly higher in the recurrence groups at both 3 and 12 months (P<0.001 in both cases). Baseline urea and creatinine were also higher in patients with recurrence at 3 months

(6.4±1.36 vs. 5.66±1.35 mmol/L, *P*=0.027; 98.5±18.6 vs. 84.38±21.8 µmol/L, *P*=0.007) and 12 months (6.44±1.3 vs. 5,6±1,37 mmol/L, *P*=0.013; 98.97±21.1 vs. 83.14±19.1 µmol/L; *P*=0.002). eGFR was significantly lower in patients with recurrence at 3 months (71 (64-79) vs. 98 (73-110) mL/min/1.73m^2, *P*<0.001). This difference remained significant at 12 months (*P*<0.001). Serum uric acid levels were elevated only in the recurrence group at 3 months (5.6 (4.5-6.9) vs. 4.9 (4.3-5.2) mg/dL; *P*=0.01). Lipid profile parameters did not differ significantly between groups.

Thyroid hormones showed notable variation: free T4 levels were higher in the recurrence group at 3 months (18.9±2.9 vs. 16.9±2.17 pmol/mL; *P*=0.002) and 12 months (18.7±3,1 vs. 17±1,95 pmol/mL; *P*=0.008). Complete blood count parameters were comparable between groups. However, at 12 months, the recurrence group showed a trend toward a lower erythrocyte count (4.7±0.56 vs. 4.95±0.52×10^{12}/L; *P*=0.059) and a significantly higher ESR (4 (2-23) vs. 3 (2-11) mm/60min; *P*=0.014).

Overall, analysis of the blanking period and the subsequent 12-month follow-up after RFA identified several clinical, echocardiographic, and biochemical variables associated with AF recurrence. Notably, higher CHA_2DS_2-VASc and HAS-BLED scores, presence of DM, left atrial enlargement and remodeling, and elevated left ventricular mass index were found to be important recurrence predictors.

Among biochemical markers, elevated CRP levels at the end of the ER period, increased free T4, and renal dysfunction parameters were significantly associated with recurrence. Additionally, elevated serum uric acid levels were associated with the end of the ER period. At 12 months, recurrence was more frequent among older and female patients, and those with longer AF duration, higher TSH levels, and elevated ESR values.

Logistic regression analysis was performed to identify independent predictors of AF recurrence after RFA. While several factors showed significance in univariate analysis, multivariate logistic regression revealed that DM and CRP level at the end of the blanking period remained the only independent predictors of ER. The obtained logistic regression model was found to be statistically significant (P<0.001). The Nagelkerke pseudo-R² value was 0.81, indicating that the model has a strong explanatory power for the outcome variable. According to the regression coefficient analysis, the presence of DM and elevated CRP levels during the blanking period were identified as factors directly associated with an increased likelihood of AF recurrence. Specifically, the presence of DM increased the odds of recurrence by 26-fold (95% CI: 1.93–351.8), while each 1mg/L rise in CRP level increased the risk of recurrence by 3.58 times (95% CI: 2.1–6.1) (Figure 1a). The model demonstrated strong predictive performance: sensitivity - 96.7%, specificity - 89.2%, and overall accuracy - 92.5%.

For late recurrence, CRP, AF duration, LAVI, and ESR were identified as independent predictors of the outcome. The obtained logistic regression model was found to be statistically significant (*P*<0.001), with a Nagelkerke pseudo-R² value of 0.71.

- Each 1 mg/L rise in CRP level increased the recurrence risk by 2.14 times (95% CI: 1.4–3.2; *P*<0.01)
- Each additional year of AF duration increased the recurrence risk by 1.26 times (95% CI: 1.05–1.52; *P*<0.05)
- Each 1 mL rise in LAVI increased the recurrence risk by 1.18 times (95% CI: 1.04–1.35; *P*<0.05)
- Each 1 mm/h rise in ESR increased the recurrence risk by 1.10 times (95% CI: 1.01–1.20; *P*<0.05) (Figure 1b).

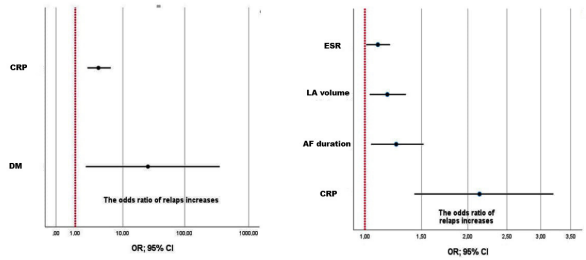

(a) *(b)*

Fig. 1. *Logistic regression analysis: (a) ER and (b) LR.*

The model demonstrated strong predictive performance: sensitivity – 84.4%, specificity – 80.0%, and overall accuracy – 82.1%.

The area under the ROC curve (AUC) reflecting the relationship between 3-month AF recurrence and CRP level was 0.93, indicating excellent discriminative ability. The obtained model was statistically significant (*P*=0.000). The cutoff value for CRP was 1.95mg/L; thus, patients with CRP ≥1.95mg/L were predicted to have a high risk of recurrence. At this threshold, the sensitivity and specificity were 90% and 85.7%, respectively (Figure 2A). When ROC analysis was performed for CRP and DM combined, the AUC reached 0.957, demonstrating a very high discriminative capacity. The sensitivity was 96.7%, and the specificity was 90.9%, confirming the high accuracy and reliability of the prognostic model (*P*<0.001) (Figure 2b).

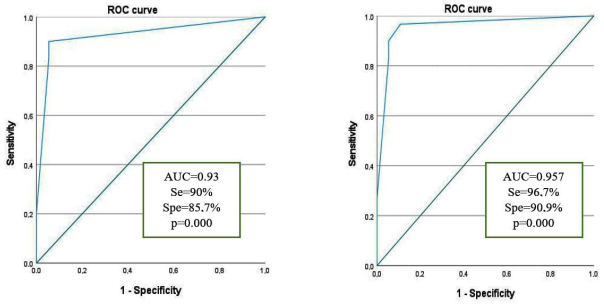

(a) *(b)*

Fig. 2. *ROC analysis of 3-month recurrence predictors: (a) CRP and (b) CRP+DM.*

In the ROC analysis of 12-month recurrence predictors, the model demonstrated strong statistical significance (*P*=0.000), with an AUC of 0.83. Although ER was not

identified as an independent predictor in the logistic regression model, the ROC analysis demonstrated the predictive relevance of CRP, AF duration, LAVI, ESR, and ER rate, with sensitivity exceeding 75% and specificity above 80% (Figure 3).

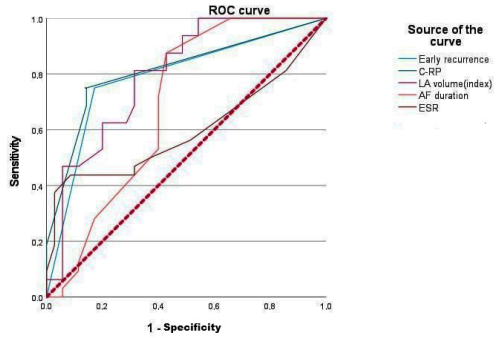

Fig. 3. *ROC analysis of 12-month recurrence predictors.*

Discussion

The findings of this study provide important insights into the clinical and biochemical factors associated with AF recurrences during both the early post–RFA blanking period and the subsequent 12-month follow-up. Recurrences were observed in nearly half of the patients within the early and late phases, underscoring the clinical relevance of recurrence. The study identified DM and elevated CRP levels as independent predictors of AF recurrence after RFA. Previous research has consistently shown DM to be an independent risk factor for AF development.[8,9] Chronic hyperglycemia leads to oxidative stress, accumulation of advanced glycation end-products, myocardial fibrosis, and remodeling of ion channels and gap junctions in the atrial myocardium. These changes reduce conduction velocity, impair homogeneity of impulse propagation, and prolong the action potential duration, thereby creating a substrate conducive to AF initiation and maintenance.[10] High CRP levels were also identified as a strong predictor, consistent with prior studies.[11] Elevated CRP reflects ongoing myocardial inflammation and fibrotic activity, which promote post-ablation electrical remodeling. In ROC analysis, CRP showed an AUC of 0.93 (95% CI: 0.85–0.99), indicating excellent discriminatory power. The cutoff value of 1.95 mg/L was identified as an optimal threshold; patients with CRP ≥1.95 mg/L were at a significantly higher risk of recurrence. Additionally, ESR also indicates the inflammation process and is identified as an LR predictor in our study. Among echocardiographic parameters, increased LA size and LAVI were also significantly associated with recurrence, in line with previous literature.[7] LA enlargement is recognized as a key marker of both electrical and mechanical remodeling. Increased LVMI and impaired renal function were noted, suggesting a multifactorial mechanism of recurrence.[12] During a 12-month follow-up, female sex and older age were associated with a higher recurrence risk, partially consistent with prior studies.[13,14] Although some discrepancies exist as population, genetic, or structural differences.[15]

Conclusion

Analysis of the blanking period and 12-month follow-up after RFA revealed several clinical, echocardiographic, and biochemical parameters associated with AF recurrence. Specifically, higher CHA_2DS_2-VASc and HAS-BLED scores, the presence of DM, LA remodeling, increased LV mass, as well as elevated CRP, free T_4, and markers of renal dysfunction, were found to be significantly correlated with recurrence. According to multivariate logistic regression analysis, DM and CRP levels at the end of the blanking period remained independent predictors of recurrence.

Although several factors influenced LR, only LA enlargement, longer AF history, and elevated levels of CRP, ESR, and ER rate were identified as independent predictors of LR. These findings indicate that the above factors serve as reliable prognostic markers of AF recurrence after RFA and should be considered in clinical practice for patient follow-up and management. Combined clinical and biochemical evaluation may enhance individualized risk stratification and post-ablation management.

Ethical Approval

This study was approved by the Ethics Committee at Republican Specialized Cardiology Scientific Practical Medicine Center; Protocol No. 5 dated June 10, 2025. Written informed consent was obtained from all the participants.

Competing Interests

The authors declare that they have no conflicts of interest.

References

1. Li X, Li Z, He H, Wang S, Su H, Kang G. Global burden and health inequality of atrial fibrillation/atrial flutter from 1990 to 2021. Front Cardiovasc Med. 2025 May 21;12:1585980. doi: 10.3389/fcvm.2025.1585980. PMID: 40469078; PMCID: PMC12133759.

2. Linz D, Gawalko M, Betz K, Hendriks JM, Lip GYH, Vinter N, Guo Y, Johnsen S. Atrial fibrillation: epidemiology, screening and digital health. Lancet Reg Health Eur. 2024 Feb 1;37:100786. doi: 10.1016/j.lanepe.2023.100786. PMID: 38362546; PMCID: PMC10866942.

3. Hindricks G, Potpara T, Dagres N, Arbelo E, Bax JJ, Blomström-Lundqvist C, et al.; ESC Scientific Document Group. 2020 ESC Guidelines for the diagnosis and management of atrial fibrillation developed in collaboration with the European Association for Cardio-Thoracic Surgery (EACTS): The Task Force for the diagnosis and management of atrial fibrillation of the European Society of Cardiology (ESC) Developed with the special contribution of the European Heart Rhythm Association (EHRA) of the ESC. Eur Heart J. 2021 Feb 1;42(5):373-498. doi: 10.1093/eurheartj/ehaa612. Erratum in: Eur Heart J. 2021 Feb 1;42(5):507. doi: 10.1093/eurheartj/ehaa798. Erratum in: Eur Heart J. 2021 Feb 1;42(5):546-547. doi: 10.1093/eurheartj/ehaa945. Erratum in:

Eur Heart J. 2021 Oct 21;42(40):4194. doi: 10.1093/eurheartj/ehab648. PMID: 32860505.
4. Mark DB, Anstrom KJ, Sheng S, Peterson ED, Poole JE, Piccini JP, et al. Catheter ablation versus medical therapy for atrial fibrillation: long-term follow-up of the CABANA trial. J Am Coll Cardiol. 2023;81(5):479–492. doi:10.1016/j.jacc.2022.11.037.
5. Stauffer N, Knecht S, Badertscher P, Krisai P, Hennings E, Serban T, et al. Repeat catheter ablation after very late recurrence of atrial fibrillation after pulmonary vein isolation. Europace. 2024 May 2;26(5):euae096. doi: 10.1093/europace/euae096. PMID: 38607938; PMCID: PMC11068271.
6. Darby AE, DiMarco JP. Recurrent atrial fibrillation after catheter ablation: incidence and predictors. *Heart Rhythm.* 2016;13(2):281–287. doi:10.1016/j.hrthm.2015.08.024.
7. Tzeis S, Gerstenfeld EP, Kalman J, Saad EB, Sepehri Shamloo A, Andrade JG, et al. 2024 European Heart Rhythm Association/Heart Rhythm Society/Asia Pacific Heart Rhythm Society/Latin American Heart Rhythm Society expert consensus statement on catheter and surgical ablation of atrial fibrillation. Europace. 2024 Mar 30;26(4):euae043. doi: 10.1093/europace/euae043. Corrected and republished in: Heart Rhythm. 2024 Sep;21(9):e31-e149. doi: 10.1016/j.hrthm.2024.03.017. PMID: 38587017; PMCID: PMC11000153.
8. Aune D, Feng T, Schlesinger S, Janszky I, Norat T, Riboli E. Diabetes mellitus, blood glucose and the risk of atrial fibrillation: A systematic review and meta-analysis of cohort studies. J Diabetes Complications. 2018 May;32(5):501-511. doi: 10.1016/j.jdiacomp.2018.02.004. Epub 2018 Feb 17. PMID: 29653902.
9. Creta A, Providência R, Adragão P, de Asmundis C, Chun J, Chierchia G, et al. Impact of Type-2 Diabetes Mellitus on the Outcomes of Catheter Ablation of Atrial Fibrillation (European Observational Multicentre Study). Am J Cardiol. 2020 Mar 15;125(6):901-906. doi: 10.1016/j.amjcard.2019.12.037. Epub 2019 Dec 30. PMID: 31973808.
10. Liu C, Fu H, Li J, Yang W, Cheng L, Liu T, Li G. Hyperglycemia aggravates atrial interstitial fibrosis, ionic remodeling and vulnerability to atrial fibrillation in diabetic rabbits. Anadolu Kardiyol Derg. 2012 Nov;12(7):543-50. doi: 10.5152/akd.2012.188. Epub 2012 Aug 8. PMID: 22877897.
11. Meyre PB, Sticherling C, Spies F, Aeschbacher S, Blum S, Voellmin G, et al. C-reactive protein for prediction of atrial fibrillation recurrence after catheter ablation. BMC Cardiovasc Disord. 2020 Sep 29;20(1):427. doi: 10.1186/s12872-020-01711-x. PMID: 32993521; PMCID: PMC7526257.
12. Boyalla V, Harling L, Snell A, Kralj-Hans I, Barradas-Pires A, Haldar S, et al. Biomarkers as predictors of recurrence of atrial fibrillation post ablation: an updated and expanded systematic review and meta-analysis. Clin Res Cardiol. 2022 Jun;111(6):680-691. doi: 10.1007/s00392-021-01978-w.
13. Wesselink R, Mossink B, Meulendijks ER, van den Berg NWE, Neefs J, Kawasaki M, et al. Women Have More Recurrences of Atrial Fibrillation than Men after Thoracoscopic Ablation and Suffer More from Established Risk Factors. J Clin Med. 2023 Apr 2;12(7):2650. doi: 10.3390/jcm12072650.
14. Kawamura I, Aikawa T, Yokoyama Y, Takagi H, Kuno T. Catheter ablation for atrial fibrillation in elderly patients: Systematic review and a meta-analysis. Pacing Clin Electrophysiol. 2022 Jan;45(1):59-71. doi: 10.1111/pace.14413. Epub 2021 Dec 9. PMID: 34816458.
15. Nielsen J, Kragholm KH, Christensen SB, Johannessen A, Torp-Pedersen C, Kristiansen SB, et al. Periprocedural complications and one-year outcomes after catheter ablation for treatment of atrial fibrillation in elderly patients: a nationwide Danish cohort study. J Geriatr Cardiol. 2021 Nov 28;18(11):897-907. doi: 10.11909/j.issn.1671-5411.2021.11.005. PMID: 34908927; PMCID: PMC8648543.

***Corresponding author**: Khasan I. Uralov. E-mail: hasan.uralov0319@gmail.com*

International Journal of Biomedicine 15(4) (2025) 660-667
http://dx.doi.org/10.21103/Article15(4)_OA2

ORIGINAL ARTICLE

Endocrinology

INTERNATIONAL JOURNAL OF BIOMEDICINE

Prediabetes in Overweight Adult Men: Serum Testosterone Variations

Omar Babateen[1], Zahir Hussain[1*]

[1]*Department of Physiology, Faculty of Medicine, Umm Al-Qura University (UQU), Makkah 21955, Saudi Arabia*

Abstract

Background: Prediabetes (PD), an intermediate stage between normoglycemia and diabetes mellitus (DM), is characterized by elevated blood glucose levels, but not enough to be to be diagnosed as DM. Some studies show that men with hypogonadism are at an increased risk for insulin resistance (IR) and PD. This study aimed to evaluate the variation of testosterone levels in adult Saudi men with normal weight (NW) and PD (NW-PD) and men with overweight (OW) and PD (OW-PD).

Methods and Results: This case-control study comprised 391 adult Saudi males (age range: 35-40 years). The subjects in the current study had a body mass index (BMI) of 18.5-29.9 kg/m². The adult subjects were categorized into four groups: 1) NW control (NW-C), 2) OW control (OW-C), 3) men with NW and PD (NW-PD), and 4) men with OW and PD (OW-PD). The serum testosterone level was determined using ELISA kits. Testosterone levels in the OW-PD group were significantly lower than those in the NW-PD group (P=0.03). BMI plotted against serum testosterone for the OW-PD group showed a significant negative linear correlation between BMI and testosterone (R^2=0.05, P=0.03).

Conclusion: The present study provides helpful information about the overweight status in association with decreased serum testosterone in men with prediabetes.(**International Journal of Biomedicine. 2025;15(4):660-667.**)

Keywords: prediabetes • adult men • overweight • body mass index • testosterone

For citation: Babateen O, Hussain Z. Prediabetes in Overweight Adult Men: Serum Testosterone Variations. International Journal of Biomedicine. 2025;15(4):660-667. doi:10.21103/Article15(4)_OA2

Abbreviations

ADA, American Diabetes Association; **BMI,** body mass index; **BW,** body weight; **DM,** diabetes mellitus; **FBG,** fasting blood glucose; **IFG**, impaired fasting glucose; **Hb,** hemoglobin; **IGT,** impaired glucose tolerance; **IR,** insulin resistance; **MetS,** metabolic syndrome; **NW,** normal weight; **OW,** overweight; **PD,** prediabetes; **SHBG,** sex hormone-binding globulin; **T2D,** type 2 diabetes; **TES,** testosterone.

Introduction

Diabetes mellitus (DM)and prediabetes (PD) are global health challenges.[1,2] Prediabetes (PD), an intermediate stage between normoglycemia and diabetes mellitus (DM), is characterized by elevated blood glucose levels, but not enough to be to be diagnosed as DM.[3-5] The main factors that characterize PD are impaired fasting glucose (IFG) and impaired glucose tolerance (IGT).[6,7]

Lifestyle modifications, particularly effective diet, exercise, and other weight management programs, are key factors in preventing PD and type 2 diabetes (T2D).[8-13] According to recent studies, the rate of progression from PD to T2D is about 25% in 3–5 years, and it is estimated that 70% of individuals with PD will develop T2D in their lifetime.[3,14-19]

Prediabetes was initially recommended and defined by the ADA in 1997 as a fasting blood glucose (FBG) level of 110-125 mg/dL or IFG.[20] The World Health Organization adopted this criterion. In 2003, the ADA lowered the FBG threshold to 100–125 mg/dL;[21] however, the WHO did not adopt this lower cutoff and maintained its 110–125 mg/dL standard. The diagnosis of PD also includes IGT, which is based on a 2-hour oral glucose tolerance test (OGTT), with a 2-hour plasma glucose level of 140–199 mg/dL being the diagnostic range for IGT.[22]

Prediabetes is included in the International Classification of Diseases, Tenth Revision.[23] Prediabetes is associated with insulin resistance (IR), obesity, fatty liver disease, metabolic syndrome (MetS), T2D, cardiovascular complications, and all-cause mortality.[24-29] Early intervention by dietary and lifestyle changes helps prevent it and its progression to other diseases, especially T2D.[30]

Among the main factors influencing the progression of PD to T2D, along with genetic factors, diet, lifestyle, obesity, and IR, one can also highlight the low level of testosterone in the blood serum in men.[30-33] Various reports document decreased testosterone levels in men with obesity, PD, and T2D, and the effectiveness of testosterone intervention for preventing PD and T2D.[34-43] A study by Souteiro et al.[44] showed that IR, and not hyperglycemia and weight per se, seems to be the main determinant of low testosterone levels in obese males. Harrington et al.[45] showed a 39% increase in HOMA-IR after one year of androgen deprivation therapy.

Serum testosterone levels may vary across populations with different lifestyles/behaviors, and the role of testosterone in long-term outcomes and causation remains complex.

In this study, we evaluated the variation of testosterone levels in adult Saudi men with normal weight (NW) and PD (NW-PD) and men with overweight (OW) and PD (OW-PD), and investigated the correlation between body mass index (BMI) and serum testosterone in men with PD.

Materials and Methods

This case-control study comprised 391 adult Saudi males (age range: 35-40 years) and was conducted at Umm Al-Qura University (UQU) and UQU-related hospitals in Makkah, Kingdom of Saudi Arabia (KSA), from January 20, 2024, to January 20, 2025. The adult subjects were categorized into four groups: 1) NW control (NW-C, n=99), 2) OW control (OW-C, n=98), 3) men with NW and PD (NW-PD, n=99), and 4) men with OW and PD (OW-PD, n=95)

All groups of the subjects comprising NW-C, OW-C, NW-PD, and OW-PD were age-matched. None of the patients had T2D, anemia, cardiovascular disorders, or other complicated conditions. Only the subjects with normal hemoglobin levels were included in the current study. The subjects in the present study included only non-smokers with no reproductive/endocrine complications. It was confirmed by estimating sex hormone-binding globulin (SHBG) that they have no hypogonadism-related symptoms. The subjects in the current study had a BMI of 18.5-29.9 kg/m². Sample size was evaluated at the start of the study. The BMI ranges for the NW-C, OW-C, NW-PD, and OW-PD groups were 18.5-24.9 kg/m², 25.0-29.9 kg/m², 18.5-24.9 kg/m², and 25.0-29.9 kg/m², respectively.

A questionnaire was prepared to measure general features and the history of the male subjects. Fasting was defined as ≥10 hours since the last meal. The PD was defined based on the FBG levels in the range of 110-125 mg/dL. Hemoglobin (Hb) levels were determined using the Sysmex XN-100i hematology analyzer (Sysmex Europe SE, Norderstedt, Germany). The serum SHBG and testosterone levels were determined using ELISA kits.

Statistical analysis was performed using the statistical software package SPSS version 24.0 (IBM Corp., Armonk, NY). For the descriptive analysis, results are presented as mean (M) ± standard deviation (SD). For data with a normal distribution, inter-group comparisons were performed using Student's t-test. Multiple comparisons were performed with one-way ANOVA. The coefficient of determination R^2 was estimated to measure the strength of the linear relationship. The probability value of $P \leq 0.05$ was considered statistically significant.

Results

Table 1 presents characteristic variables in NW and OW men with PD. Age of the subject groups varied non-significantly. Variation in BMI was significant for NW-C vs. OW-C ($P<0.0001$) and NW-PD vs OW-PD ($P<0.0001$).

Table 1.

Characteristic variables in NW and OW men with prediabetes.

Variables	Normal weight and overweight men with prediabetes											
	NW-C vs. OW-C			NW-C vs. NW-PD			OW-C vs. OW-PD			NW-PD vs OW-PD		
	NW-C	OW-C	*P*-value	NW-C	NW-PD	*P*-value	OW-C	OW-PD	P-value	NW-PD	OW-PD	*P*-value
Number of subjects (n)	99	98	-	99	99	-	98	95	-	99	95	-
Age (years)	37.56 ± 1.74	37.78 ±1.66	0.37	37.56 ±1.74	37.68 ±1.68	0.62	37.78 ±1.66	37.93 ±1.65	0.53	37.68 ±1.68	37.93 ±1.65	0.30
BMI (kg/m²)	21.76 ±2.04	27.47 ±1.51	<0.0001	21.76 ±2.04	21.78 ±2.01	0.96	27.47 ±1.51	27.39 ±1.48	0.71	21.78 ±2.01	27.39 ±1.48	<0.0001
Hb (g/dL)	13.76 ±1.02	13.78 ±1.22	0.89	13.76 ±1.02	13.82 ±1.21	0.73	13.78 ±1.22	13.70 ±1.32	0.63	13.82 ±1.21	13.70 ±1.32	0.51
TES (ng/dl)	454.06 ±150.41	418.80 ±123.51	0.07	454.06 ±150.41	451.96 ±149.21	0.92	418.80 ±123.51	412.34 ±104.05	0.70	451.96 ±149.21	412.34 ±104.05	0.03

An unpaired two–sample t–test was employed for obtaining a two-tailed P-value.

Testosterone levels in the OW-PD group were significantly lower than those in the NW-PD group (P=0.03).

Other comparisons (NW-C vs. OW-C, NW-C vs. NW-PD and OW-C vs. OW-PD) did not show significant variation of testosterone levels (Table 1).

BMI plotted against serum testosterone for the OW-PD group presented a significant negative linear correlation of BMI with testosterone (R^2= 0.05, P=0.03, Fig.1). Other groups did not show a significant correlation between BMI and testosterone.

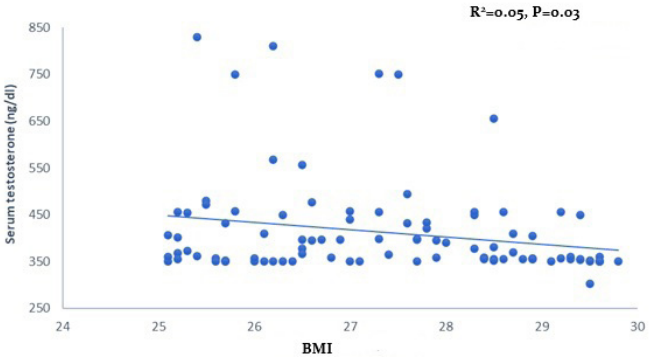

Fig.1. *Association of BMI with serum testosterone in overweight men with prediabetes.*

A one-way analysis of variance (ANOVA) revealed no statistically significant differences in age or hemoglobin levels between the NW-C, OW-C, NW-PD, and OW-PD groups. In contrast, BMI showed highly significant differences between groups (P=0.0001). Testosterone levels also differed significantly between groups (P=0.05) (Table 2).

Table 2.

Analysis of variance for variables in NW and OW men with prediabetes.

Variables	Normal weight and overweight men with prediabetes				Significance level	
	NW-C	OW-C	NW-PD	OW-PD	F-value	*P*-value
Number of subjects (n)	99	98	99	95	-	-
Age (years)	37.56 ±1.74	37.78 ±1.66	37.68 ±1.68	37.93 ±1.65	0.84	0.47
BMI (kg/m^2)	21.76 ±2.04	27.47 ±1.51	21.78 ±2.01	27.39 ±1.48	329.56	<0.0001
HB (g/dL)	13.76 ±1.02	13.78 ±1.22	13.82 ±1.21	13.70 ±1.32	0.17	0.92
TES (ng/dl)	454.06 ±150.41	418.80 ±123.51	451.96 ±149.21	412.34 ±104.05	2.61	0.05

The P-values were obtained using one way ANOVA.

The subjects' ages were found to be highly significantly correlated with BMI, with a positive linear association across all groups (P=0.0001) (Table 3). Age did not correlate significantly with hemoglobin or testosterone in any group. The BMI negative correlated significantly with testosterone in OW-PD (P=0.03) (Table 4). However, the other groups (NW-C, OW-C, NW-PD) did not present a significant correlation with testosterone. The BMI did not show a significant correlation with hemoglobin in all groups.

Table 3.

Association of age with the other parameters in NW and OW men with prediabetes.

Variables	Association of age with the other parameters				
	R^2 & *P*-value	NW-C	OW-C	NW-PD	OW-PD
BMI (kg/m^2)	R^2	0.30	0.22	0.28	0.14
	P-value	0.00	0.00	0.00	0.00
Hb (g/dL)	R^2	0.00	0.01	0.00	0.00
	P-value	0.55	0.47	0.65	0.75
TES (ng/dL)	R^2	0.02	0.01	0.02	0.01
	P-value	0.23	0.37	0.20	0.25

Table 4.

Association of BMI with the other parameters in NW and OW men with prediabetes.

Variables	Association of BMI with the other parameters				
	R^2 & *P*-value	NW-C	OW-C	NW-PD	OW-PD
Age (years)	R^2	0.30	0.22	0.28	0.14
	P-value	0.00	.0.00	0.00	0.00
HB (g/dL)	R^2	0.01	0.01	0.00	0.01
	P-value	0.43	0.42	0.99	0.44
TES (ng/dL)	R^2	0.00	0.02	0.00	0.05
	P-value	0.61	0.13	0.63	0.03

Discussion

The overweight status and obesity are considered important risk factors that may increase insulin resistance, causing prediabetes and T2D. An OW-PD progression to T2D was investigated in a study by Duan et al.[30] A combined effect of hyperglycemia and OW status on the development of T2D has been shown. A meta-analysis by Jiang et al.[31] examined the impact of sedentary behavior accompanying overweight and obesity, which increases the prevalence of T2D originating from prediabetes, and the significance of

lifestyle intervention on glucose regulation in prediabetes or impaired glucose tolerance.

In a population-based cohort study by de Ritter et al.,[46] both men and women with T2D had greater fat and lean body mass, as well as greater hip circumference, than healthy participants. However, the role of lean body mass in the development of hyperglycemic states is not fully understood. In a study by Yeung et al.,[47] women with low lean body mass had a higher risk of diabetes, whereas men with T2D showed a more pronounced increase in visceral adipose tissue than women.

Some of the reports reached the same conclusion for the role of testosterone in OW-PD men as inferred in the present investigation. The overweight or obese men frequently have low levels of serum testosterone and reveal an increased risk for T2D.[48] Obesity has a greater effect on the levels of testosterone than the levels of testosterone have on the status of obesity.[49] Overweight and obese men are advised to make lifestyle changes, including exercise programs and weight loss measures, to elevate testosterone levels.[50] Lopez et al.[51] showed that men with co-occurrence of testosterone deficiency and abdominal obesity have a higher risk of mortality.

A series of studies have found that insulin resistance, rather than hyperglycemia and weight per se, appears to be the main factor leading to low testosterone levels in obese men, although some reports do not fully support this.[48-51]

In our study, testosterone levels in PD men with obesity resembled the results obtained in several studies.[33,38,39,52] Low serum testosterone levels in men are associated with the development of insulin resistance.[33] Low serum testosterone is a novel and modifiable biomarker/risk factor for prediabetes.[38,39]

The decrease in testosterone levels in adolescents and adult men, investigated during the last two decades, indicates the possibility of the development of various complications, including prediabetes and T2D. Sex steroids, especially testosterone and estradiol, are involved in the metabolic processes, and the resulting complications may lead to metabolic disorders.[34,37] Patients with T2D and prediabetes had lower free testosterone levels than those with standard glucose tolerance. At the same time, a study by Ho et al.[53] concluded that prediabetes is associated with an increased risk of testosterone deficiency, independent of obesity and MetS.

Many studies have shown a higher risk of T2D in men with low serum testosterone levels, which indicates the importance of testosterone in the development of T2D.[52,54-57] Serum testosterone levels had opposite effects on impaired fasting glucose and T2D in males and females, as reported by Liu et al.[58] With higher serum testosterone levels, dysglycemia progression decreased among males and increased among females.

Several studies provide excellent evidence for the involvement of serum testosterone levels in overweight status/obesity[41,49,50] and prediabetes.[33,38,39,52] The current study demonstrated a significant negative linear correlation between BMI and testosterone in PD patients with overweight. And in a study by Smith et al.,[40] BMI/obesity and type 2 diabetes were both significantly and independently associated negatively with testosterone. In sum, low levels of testosterone are found commonly in men with obesity, prediabetes, and type 2 diabetes.

Many experimental/interventional studies provide evidence for the present investigations. Long-term therapy with testosterone prevents progression from prediabetes to diabetes.[43] It is known that testosterone administration increases skeletal muscle mass and decreases fat mass, leading to beneficial metabolic effects, but testosterone treatment has inconsistent effects on glycemic measures.[41]

The testosterone therapy has been employed in men with T2D and PD, which improved the testosterone levels mainly through weight loss and physical activities.[59,60] Although the declining levels of testosterone in men are a strong prediction of the occurrence of T2D in the future, further studies are required to establish the duration of testosterone benefit and long-term safety measures for testosterone treatment.

The influence of hyperglycemia on testosterone levels provides interesting results. It has been found that a glucose load or a mixed meal transiently lowers testosterone for 1-2 hours, independent of changes in luteinizing hormone or prolactin, in healthy, non-diabetic men without hypogonadism.[61] Since serum testosterone exhibits a diurnal rhythm, with peak levels in the morning,[62,63] levels are checked in the morning after fasting.[64] Although it has been recommended that the subject sample be collected in a fasting state,[64] this recommendation is controversial. The most significant factor in accurate measurement remains the timing of the blood draw, given the hormone's diurnal rhythm. Some studies did not estimate sex hormone-binding globulin, others used less reliable methods to measure testosterone, some used mixed population data, and some had small sample sizes of men.[65-67] Further studies with a multidisciplinary approach are needed that may clarify the precise role of testosterone in overweight, prediabetes, and OW-PD subjects.

Conclusion

The present study provides helpful information about the overweight status in association with decreased serum testosterone in men with prediabetes. Hopefully, the current information will serve as a potential approach for understanding the progression of prediabetes to diabetes in future studies for clinical, pathophysiological, and therapeutic purposes.

Ethical Approval

This study was approved by the Ethics Committee at the College of Medicine, Umm Al-Qura University; Approval Number: HAPO-02-K-012-2022-01-1069. All methods and procedures employed were in accordance with the Declaration of Helsinki of 1964, as revised in 2013. Written informed consent was obtained from all the participants.

Competing Interests

The authors declare that they have no conflicts of interest.

Acknowledgments

The authors acknowledge the honorary help of medical consultants, other medical experts, and laboratory personnel for their help and assistance.

Sources of Funding

This research received no external funding.

References

1. Zimmet PZ, Magliano DJ, Herman WH, Shaw JE. Diabetes: a 21st century challenge. Lancet Diabetes Endocrinol. 2014 Jan;2(1):56-64. doi: 10.1016/S2213-8587(13)70112-8. Epub 2013 Dec 3. PMID: 24622669.
2. Tuorila K, Ollila MM, Järvelin MR, Tapanainen JS, Franks S, Puukka K, Piltonen TT, Morin-Papunen L. Hyperandrogenemia in Early Adulthood Is an Independent Risk Factor for Abnormal Glucose Metabolism in Middle Age. J Clin Endocrinol Metab. 2021 Oct 21;106(11):e4621-e4633. doi: 10.1210/clinem/dgab456. PMID: 34153097; PMCID: PMC8530724.
3. Tabák AG, Herder C, Rathmann W, Brunner EJ, Kivimäki M. Prediabetes: a high-risk state for diabetes development. Lancet. 2012 Jun 16;379(9833):2279-90. doi: 10.1016/S0140-6736(12)60283-9. Epub 2012 Jun 9. PMID: 22683128; PMCID: PMC3891203.
4. Vas PRJ, Alberti KG, Edmonds ME. Prediabetes: moving away from a glucocentric definition. Lancet Diabetes Endocrinol. 2017 Nov;5(11):848-849. doi: 10.1016/S2213-8587(17)30234-6. Epub 2017 Aug 3. PMID: 28781065.
5. Hostalek U. Global epidemiology of prediabetes - present and future perspectives. Clin Diabetes Endocrinol. 2019 May 9;5:5. doi: 10.1186/s40842-019-0080-0. PMID: 31086677; PMCID: PMC6507173.
6. Echouffo-Tcheugui JB, Selvin E. Prediabetes and What It Means: The Epidemiological Evidence. Annu Rev Public Health. 2021 Apr 1;42:59-77. doi: 10.1146/annurev-publhealth-090419-102644. Epub 2021 Dec 23. PMID: 33355476; PMCID: PMC8026645.
7. Echouffo-Tcheugui JB, Perreault L, Ji L, Dagogo-Jack S. Diagnosis and Management of Prediabetes: A Review. JAMA. 2023 Apr 11;329(14):1206-1216. doi: 10.1001/jama.2023.4063. PMID: 37039787.
8. Lean ME, Leslie WS, Barnes AC, Brosnahan N, Thom G, McCombie L, Peters C, Zhyzhneuskaya S, Al-Mrabeh A, Hollingsworth KG, Rodrigues AM, Rehackova L, Adamson AJ, Sniehotta FF, Mathers JC, Ross HM, McIlvenna Y, Stefanetti R, Trenell M, Welsh P, Kean S, Ford I, McConnachie A, Sattar N, Taylor R. Primary care-led weight management for remission of type 2 diabetes (DiRECT): an open-label, cluster-randomised trial. Lancet. 2018 Feb 10;391(10120):541-551. doi: 10.1016/S0140-6736(17)33102-1. Epub 2017 Dec 5. PMID: 29221645.
9. Taheri S, Zaghloul H, Chagoury O, Elhadad S, Ahmed SH, El Khatib N, Amona RA, El Nahas K, Suleiman N, Alnaama A, Al-Hamaq A, Charlson M, Wells MT, Al-Abdulla S, Abou-Samra AB. Effect of intensive lifestyle intervention on bodyweight and glycaemia in early type 2 diabetes (DIADEM-I): an open-label, parallel-group, randomised controlled trial. Lancet Diabetes Endocrinol. 2020 Jun;8(6):477-489. doi: 10.1016/S2213-8587(20)30117-0. PMID: 32445735.
10. Barua S, Upadhyay D, Berube LT, Popp CJ, Curran M, Pompeii ML, Hu L, Aleman JO, Bergman M, Sevick MA. Weight loss is associated with improved daytime time in range in adults with prediabetes and non-insulin-treated type 2 diabetes undergoing dietary intervention. Diabet Med. 2025 Aug;42(8):e70052. doi: 10.1111/dme.70052. Epub 2025 Jun 3. PMID: 40460001.
11. Castillo-Hernandez IM, Wilson HK, Williams ER, Berg AC, Evans EM. EXERCISE BENEFITS AND BARRIERS IN AN EXTENSION-DELIVERED DIABETES PREVENTION PROGRAM. Fam Consum Sci Res J. 2025 Mar;53(3):e70000. doi: 10.1111/fcsr.70000. Epub 2025 Feb 21. PMID: 40453509; PMCID: PMC12121941.
12. Dansinger ML, Gleason JA, Maddalena J, Asztalos BF, Diffenderfer MR. Lifestyle Modification in Prediabetes and Diabetes: A Large Population Analysis. Nutrients. 2025 Apr 11;17(8):1333. doi: 10.3390/nu17081333. PMID: 40284198; PMCID: PMC12030603.
13. Zhang S, Wang Y, Wang X, Leng M, Liu R, Li Z, Li J, Xiao J, Hou D, Gao X, Li C. Effect of hypoglycemic agents with weight loss effect plus a high protein diet and moderate exercise on diabetes remission in adults with obesity and type 2 diabetes: a randomized controlled trial. BMC Med. 2025 May 7;23(1):270. doi: 10.1186/s12916-025-04072-4. PMID: 40336033; PMCID: PMC12060396.
14. Diabetes Prevention Program Research Group. The prevalence of retinopathy in impaired glucose tolerance and recent-onset diabetes in the Diabetes Prevention Program. Diabet Med. 2007 Feb;24(2):137-44. doi: 10.1111/j.1464-5491.2007.02043.x. PMID: 17257275; PMCID: PMC2267935.
15. Lee CC, Perkins BA, Kayaniyil S, Harris SB, Retnakaran R, Gerstein HC, Zinman B, Hanley AJ. Peripheral Neuropathy and Nerve Dysfunction in Individuals at High Risk for Type 2 Diabetes: The PROMISE Cohort. Diabetes Care. 2015 May;38(5):793-800. doi: 10.2337/dc14-2585. Epub 2015 Feb 9. PMID: 25665810.
16. Echouffo-Tcheugui JB, Narayan KM, Weisman D, Golden SH, Jaar BG. Association between prediabetes and risk of chronic kidney disease: a systematic review and meta-analysis. Diabet Med. 2016 Dec;33(12):1615-1624. doi: 10.1111/dme.13113. Epub 2016 Apr 24. PMID: 26997583.
17. Huang Y, Cai X, Mai W, Li M, Hu Y. Association between prediabetes and risk of cardiovascular disease and all cause mortality: systematic review and meta-analysis. BMJ. 2016 Nov 23;355:i5953. doi: 10.1136/bmj.i5953. PMID: 27881363; PMCID: PMC5121106.
18. HAPO Study Cooperative Research Group; Metzger BE,

Lowe LP, Dyer AR, Trimble ER, Chaovarindr U, Coustan DR, Hadden DR, McCance DR, Hod M, McIntyre HD, Oats JJ, Persson B, Rogers MS, Sacks DA. Hyperglycemia and adverse pregnancy outcomes. N Engl J Med. 2008 May 8;358(19):1991-2002. doi: 10.1056/NEJMoa0707943. PMID: 18463375.

19. Souza CF, Gross JL, Gerchman F, Leitão CB. Pré-diabetes: diagnóstico, avaliação de complicações crônicas e tratamento [Prediabetes: diagnosis, evaluation of chronic complications, and treatment]. Arq Bras Endocrinol Metabol. 2012 Jul;56(5):275-84. Portuguese. doi: 10.1590/s0004-27302012000500001. PMID: 22911279.

20. Report of the Expert Committee on the Diagnosis and Classification of Diabetes Mellitus. Diabetes Care. 1997 Jul;20(7):1183-97. doi: 10.2337/diacare.20.7.1183. PMID: 9203460.

21. Genuth S, Alberti KG, Bennett P, Buse J, Defronzo R, Kahn R, Kitzmiller J, Knowler WC, Lebovitz H, Lernmark A, Nathan D, Palmer J, Rizza R, Saudek C, Shaw J, Steffes M, Stern M, Tuomilehto J, Zimmet P; Expert Committee on the Diagnosis and Classification of Diabetes Mellitus. Follow-up report on the diagnosis of diabetes mellitus. Diabetes Care. 2003 Nov;26(11):3160-7. doi: 10.2337/diacare.26.11.3160. PMID: 14578255.

22. American Diabetes Association. Diagnosis and classification of diabetes mellitus. Diabetes Care. 2010 Jan;33 Suppl 1(Suppl 1):S62-9. doi: 10.2337/dc10-S062. Erratum in: Diabetes Care. 2010 Apr;33(4):e57. PMID: 20042775; PMCID: PMC2797383.

23. Rett K, Gottwald-Hostalek U. Understanding prediabetes: definition, prevalence, burden and treatment options for an emerging disease. Curr Med Res Opin. 2019 Sep;35(9):1529-1534. doi: 10.1080/03007995.2019.1601455. Epub 2019 Apr 15. PMID: 30935247.

24. Mahat RK, Singh N, Rathore V, Arora M, Yadav T. Cross-sectional correlates of oxidative stress and inflammation with glucose intolerance in prediabetes. Diabetes Metab Syndr. 2019 Jan-Feb;13(1):616-621. doi: 10.1016/j.dsx.2018.11.045. Epub 2018 Nov 14. PMID: 30641776.

25. Luc K, Schramm-Luc A, Guzik TJ, Mikolajczyk TP. Oxidative stress and inflammatory markers in prediabetes and diabetes. J Physiol Pharmacol. 2019 Dec;70(6). doi: 10.26402/jpp.2019.6.01. Epub 2020 Feb 19. PMID: 32084643.

26. Aktas G. Association between the Prognostic Nutritional Index and Chronic Microvascular Complications in Patients with Type 2 Diabetes Mellitus. J Clin Med. 2023 Sep 13;12(18):5952. doi: 10.3390/jcm12185952. PMID: 37762893; PMCID: PMC10531521.

27. Kosekli MA, Aktas G. The systemic immune inflammation index is a reliable and novel risk factor for metabolic dysfunction-associated fatty liver disease. Curr Med Res Opin. 2025 Feb;41(2):247-251. doi: 10.1080/03007995.2025.2463952. Epub 2025 Feb 12. PMID: 39912740.

28. Dedemen B, Duman TT, Dedemen MM, Aktas G. Effect of sodium glucose Co-transporter 2 inhibitor use on anthropometric measurements and blood glucose in obese and non-obese type 2 diabetic patients. Clin Nutr ESPEN. 2024 Oct;63:515-519. doi: 10.1016/j.clnesp.2024.07.016. Epub 2024 Jul 22. PMID: 39047870.

29. Cai X, Zhang Y, Li M, Wu JH, Mai L, Li J, Yang Y, Hu Y, Huang Y. Association between prediabetes and risk of all cause mortality and cardiovascular disease: updated meta-analysis. BMJ. 2020 Jul 15;370:m2297. doi: 10.1136/bmj.m2297. PMID: 32669282; PMCID: PMC7362233.

30. Duan D, Kengne AP, Echouffo-Tcheugui JB. Screening for Diabetes and Prediabetes. Endocrinol Metab Clin North Am. 2021 Sep;50(3):369-385. doi: 10.1016/j.ecl.2021.05.002. Epub 2021 Jul 12. PMID: 34399951; PMCID: PMC8375583.

31. Jiang Q, Li JT, Sun P, Wang LL, Sun LZ, Pang SG. Effects of lifestyle interventions on glucose regulation and diabetes risk in adults with impaired glucose tolerance or prediabetes: a meta-analysis. Arch Endocrinol Metab. 2022 Apr 28;66(2):157-167. doi: 10.20945/2359-3997000000441. Epub 2022 Mar 14. PMID: 35289514; PMCID: PMC9832886.

32. Satman I. Prediabetes and diabetes: main characteristics. Pol Arch Intern Med. 2023 Mar 29;133(3):16469. doi: 10.20452/pamw.16469. Epub 2023 Mar 29. PMID: 36994495.

33. Bhasin S, Lincoff AM, Nissen SE, Wannemuehler K, McDonnell ME, Peters AL, Khan N, Snabes MC, Li X, Li G, Buhr K, Pencina KM, Travison TG. Effect of Testosterone on Progression From Prediabetes to Diabetes in Men With Hypogonadism: A Substudy of the TRAVERSE Randomized Clinical Trial. JAMA Intern Med. 2024 Apr 1;184(4):353-362. doi: 10.1001/jamainternmed.2023.7862. PMID: 38315466; PMCID: PMC10845044.

34. Corona G, Rastrelli G, Vignozzi L, Barbonetti A, Sforza A, Mannucci E, Maggi M. The Role of testosterone treatment in patients with metabolic disorders. Expert Rev Clin Pharmacol. 2021 Sep;14(9):1091-1103. doi: 10.1080/17512433.2021.1938548. Epub 2021 Jun 21. PMID: 34085587.

35. Lokeshwar SD, Patel P, Fantus RJ, Halpern J, Chang C, Kargi AY, Ramasamy R. Decline in Serum Testosterone Levels Among Adolescent and Young Adult Men in the USA. Eur Urol Focus. 2021 Jul;7(4):886-889. doi: 10.1016/j.euf.2020.02.006. Epub 2020 Feb 18. PMID: 32081788.

36. Yin L, Luo M, Wang R, Ye J, Wang X. Mitochondria in Sex Hormone-Induced Disorder of Energy Metabolism in Males and Females. Front Endocrinol (Lausanne). 2021 Dec 20;12:749451. doi: 10.3389/fendo.2021.749451. PMID: 34987473; PMCID: PMC8721233.

37. Ali Hamza M, Abdulhameed A, Ali Mansour A. Total Testosterone to Estradiol Ratio as a Predictor Marker of Metabolic Syndrome in Males. Arch Razi Inst. 2022 Feb 28;77(1):351-357. doi: 10.22092/ARI.2021.356607.1878. PMID: 35891738; PMCID: PMC9288628.

38. Beckmann K, Crawley D, Nelson WG, Platz EA, Selvin E, Van Hemelrijck M, Rohrmann S. Hormonal patterns in men with prediabetes and diabetes in NHANES III: possible links with prostate cancer. Cancer Causes Control. 2022 Mar;33(3):429-440. doi: 10.1007/s10552-021-01538-7. Epub 2022 Jan 21. PMID: 35059918; PMCID: PMC9066414.

39. Wang J, Yan AF, Cheskin LJ, Shi Z. Higher Serum

Testosterone Level Was Associated with a Lower Risk of Prediabetes in US Adults: Findings from Nationally Representative Data. Nutrients. 2022 Dec 20;15(1):9. doi: 10.3390/nu15010009. PMID: 36615670; PMCID: PMC9824532.
40. Smith SJ, Bekele D, Lopresti AL, Fairchild TJ. Examining the associations between testosterone and biomarkers as men age. Am J Hum Biol. 2023 Nov;35(11):e23942. doi: 10.1002/ajhb.23942. Epub 2023 Jun 21. PMID: 37341438.
41. Grossmann M, Wittert GA. Testosterone in prevention and treatment of type 2 diabetes in men: Focus on recent randomized controlled trials. Ann N Y Acad Sci. 2024 Aug;1538(1):45-55. doi: 10.1111/nyas.15188. Epub 2024 Jul 22. PMID: 39039746.
42. Liu X, Chen X, Wang C, Song J, Xu J, Gao Z, Huang Y, Suo H. Mechanisms of probiotic modulation of ovarian sex hormone production and metabolism: a review. Food Funct. 2024 Mar 18;15(6):2860-2878. doi: 10.1039/d3fo04345b. PMID: 38433710.
43. Dandona P, Dhindsa S, Ghanim H, Saad F. Mechanisms underlying the metabolic actions of testosterone in humans: A narrative review. Diabetes Obes Metab. 2021 Jan;23(1):18-28. doi: 10.1111/dom.14206. Epub 2020 Oct 19. PMID: 32991053.
44. Souteiro P, Belo S, Oliveira SC, Neves JS, Magalhães D, Pedro J, Bettencourt-Silva R, Costa MM, Varela A, Queirós J, Freitas P, Carvalho D; AMTCO Group. Insulin resistance and sex hormone-binding globulin are independently correlated with low free testosterone levels in obese males. Andrologia. 2018 Sep;50(7):e13035. doi: 10.1111/and.13035. Epub 2018 May 9. PMID: 29744905.
45. Harrington JM, Schwenke DC, Epstein DR, Bailey DE Jr. Androgen-deprivation therapy and metabolic syndrome in men with prostate cancer. Oncol Nurs Forum. 2014 Jan 1;41(1):21-9. doi: 10.1188/14.ONF.21-29. PMID: 24368236.
46. de Ritter R, Sep SJS, van Greevenbroek MMJ, Kusters YHAM, Vos RC, Bots ML, Kooi ME, Dagnelie PC, Eussen SJPM, Schram MT, Koster A, Brouwers MCG, van der Sangen NMR, Peters SAE, van der Kallen CJH, Stehouwer CDA. Sex differences in body composition in people with prediabetes and type 2 diabetes as compared with people with normal glucose metabolism: the Maastricht Study. Diabetologia. 2023 May;66(5):861-872. doi: 10.1007/s00125-023-05880-0. Epub 2023 Feb 20. PMID: 36805778; PMCID: PMC10036428.
47. Yeung CHC, Au Yeung SL, Fong SSM, Schooling CM. Lean mass, grip strength and risk of type 2 diabetes: a bi-directional Mendelian randomisation study. Diabetologia. 2019 May;62(5):789-799. doi: 10.1007/s00125-019-4826-0. Epub 2019 Feb 23. PMID: 30798333.
48. Wittert G, Bracken K, Robledo KP, Grossmann M, Yeap BB, Handelsman DJ, Stuckey B, Conway A, Inder W, McLachlan R, Allan C, Jesudason D, Fui MNT, Hague W, Jenkins A, Daniel M, Gebski V, Keech A. Testosterone treatment to prevent or revert type 2 diabetes in men enrolled in a lifestyle programme (T4DM): a randomised, double-blind, placebo-controlled, 2-year, phase 3b trial. Lancet Diabetes Endocrinol. 2021 Jan;9(1):32-45. doi: 10.1016/S2213-8587(20)30367-3. PMID: 33338415.
49. Grossmann M. Hypogonadism and male obesity: Focus on unresolved questions. Clin Endocrinol (Oxf). 2018 Jul;89(1):11-21. doi: 10.1111/cen.13723. Epub 2018 May 16. PMID: 29683196.
50. Kanakis GA, Pofi R, Goulis DG, Isidori AM, Armeni E, Erel CT, Fistonić I, Hillard T, Hirschberg AL, Meczekalski B, Mendoza N, Mueck AO, Simoncini T, Stute P, van Dijken D, Rees M, Lambrinoudaki I. EMAS position statement: Testosterone replacement therapy in older men. Maturitas. 2023 Dec;178:107854. doi: 10.1016/j.maturitas.2023.107854. Epub 2023 Oct 15. PMID: 37845136.
51. Lopez DS, Qiu X, Advani S, Tsilidis KK, Khera M, Kim J, Morgentaler A, Wang R, Canfield S. Double trouble: Co-occurrence of testosterone deficiency and body fatness associated with all-cause mortality in US men. Clin Endocrinol (Oxf). 2018 Jan;88(1):58-65. doi: 10.1111/cen.13501. Epub 2017 Nov 20. PMID: 29067698.
52. Feng Y, Jin X, Zhu J, Yuan M, Zhu L, Ye D, Shen Y. Association between endogenous estradiol, testosterone, and long-term mortality in adults with prediabetes and diabetes: Evidence from NHANES database. J Diabetes Investig. 2025 Mar;16(3):481-491. doi: 10.1111/jdi.14367. Epub 2024 Dec 20. PMID: 39705158; PMCID: PMC11871383.
53. Ho CH, Yu HJ, Wang CY, Jaw FS, Hsieh JT, Liao WC, et al. Prediabetes is associated with an increased risk of testosterone deficiency, independent of obesity and metabolic syndrome. PLoS One. 2013;8(9):e74173. doi: 10.1371/journal.pone.0074173. Erratum in: PLoS One. 2013;8(12). doi:10.1371/annotation/c226aa64-8d3b-4c29-971b-84f87b618291.
54. Ding EL, Song Y, Malik VS, Liu S. Sex differences of endogenous sex hormones and risk of type 2 diabetes: a systematic review and meta-analysis. JAMA. 2006 Mar 15;295(11):1288-99. doi: 10.1001/jama.295.11.1288. PMID: 16537739.
55. Grossmann M. Low testosterone in men with type 2 diabetes: significance and treatment. J Clin Endocrinol Metab. 2011 Aug;96(8):2341-53. doi: 10.1210/jc.2011-0118. Epub 2011 Jun 6. PMID: 21646372.
56. Atlantis E, Fahey P, Martin S, O'Loughlin P, Taylor AW, Adams RJ, Shi Z, Wittert G. Predictive value of serum testosterone for type 2 diabetes risk assessment in men. BMC Endocr Disord. 2016 May 27;16(1):26. doi: 10.1186/s12902-016-0109-7. PMID: 27230668; PMCID: PMC4882776.
57. Yao QM, Wang B, An XF, Zhang JA, Ding L. Testosterone level and risk of type 2 diabetes in men: a systematic review and meta-analysis. Endocr Connect. 2018 Jan;7(1):220-231. doi: 10.1530/EC-17-0253. Epub 2017 Dec 12. PMID: 29233816; PMCID: PMC5793809.
58. Liu X, Jiang J, Liu X, Luo Z, Wang Y, Dong X, Wei D, Li R, Wang Y, Huo W, Yu S, Li L, Jin S, Wang C, Mao Z. Association of serum testosterone with different classes of glucose metabolism and the mediation effect of obesity: The Henan Rural Cohort Study. Diabetes Metab Res Rev. 2019 Jul;35(5):e3133. doi: 10.1002/dmrr.3133. Epub 2019 Feb 21. PMID: 30715782.
59. Corona G, Maggi M. Testosterone Therapy With a Man With Equivocal Testosterone Levels. J Sex Med. 2022

Nov;19(11):1587-1590. doi: 10.1016/j.jsxm.2022.03.601. Epub 2022 Apr 10. PMID: 35414487.
60. Corona G, Vena W, Pizzocaro A, Vignozzi L, Sforza A, Maggi M. Testosterone therapy in diabetes and pre-diabetes. Andrology. 2023 Feb;11(2):204-214. doi: 10.1111/andr.13367. Epub 2022 Dec 29. PMID: 36542412.
61. Gagliano-Jucá T, Li Z, Pencina KM, Beleva YM, Carlson OD, Egan JM, Basaria S. Oral glucose load and mixed meal feeding lowers testosterone levels in healthy eugonadal men. Endocrine. 2019 Jan;63(1):149-156. doi: 10.1007/s12020-018-1741-y. Epub 2018 Sep 6. PMID: 30191441; PMCID: PMC6445266.
62. Bremner WJ, Vitiello MV, Prinz PN. Loss of circadian rhythmicity in blood testosterone levels with aging in normal men. J Clin Endocrinol Metab. 1983 Jun;56(6):1278-81. doi: 10.1210/jcem-56-6-1278. PMID: 6841562.
63. Brambilla DJ, O'Donnell AB, Matsumoto AM, McKinlay JB. Intraindividual variation in levels of serum testosterone and other reproductive and adrenal hormones in men. Clin Endocrinol (Oxf). 2007 Dec;67(6):853-62. doi: 10.1111/j.1365-2265.2007.02976.x. PMID: 18052942.
64. Bhasin S, Brito JP, Cunningham GR, Hayes FJ, Hodis HN, Matsumoto AM, Snyder PJ, Swerdloff RS, Wu FC, Yialamas MA. Testosterone Therapy in Men With Hypogonadism: An Endocrine Society Clinical Practice Guideline. J Clin Endocrinol Metab. 2018 May 1;103(5):1715-1744. doi: 10.1210/jc.2018-00229. PMID: 29562364.
65. Iranmanesh A, Lawson D, Veldhuis JD. Glucose ingestion acutely lowers pulsatile LH and basal testosterone secretion in men. Am J Physiol Endocrinol Metab. 2012 Mar 15;302(6):E724-30. doi: 10.1152/ajpendo.00520.2011. Epub 2012 Jan 17. PMID: 22252939; PMCID: PMC3311294.
66. Lehtihet M, Arver S, Bartuseviciene I, Pousette A. S-testosterone decrease after a mixed meal in healthy men independent of SHBG and gonadotrophin levels. Andrologia. 2012 Dec;44(6):405-10. doi: 10.1111/j.1439-0272.2012.01296.x. Epub 2012 Apr 23. PMID: 22524522.
67. Caronia LM, Dwyer AA, Hayden D, Amati F, Pitteloud N, Hayes FJ. Abrupt decrease in serum testosterone levels after an oral glucose load in men: implications for screening for hypogonadism. Clin Endocrinol (Oxf). 2013 Feb;78(2):291-6. doi: 10.1111/j.1365-2265.2012.04486.x. PMID: 22804876.

***Corresponding author**: Prof. Dr. Zahir Hussain, PhD. Department of Physiology, Faculty of Medicine, Umm Al-Qura University, Makkah 21955, Saudi Arabia. E-mail: zahirhussa@gmail.com*

International Journal of Biomedicine 15(4) (2025) 668-673
http://dx.doi.org/10.21103/Article15(4)_OA3

ORIGINAL ARTICLE

Dyslipidemia

INTERNATIONAL JOURNAL OF BIOMEDICINE

Age- and Gender-Specific Dyslipidemia in Omani Young Adults: Metabolic Links to Cardiovascular Risk

Gulam Saidunnisa Begum[1], Anshoo Agarwal[2], Nida Suhail[3*], Mariah N. Hafiz[3], Mohammed M. Jawad[3], Awadh Elkareem Abass[3], Shefa A. Hejazy[4]

[1]Department of Biochemistry, National University of Science and Technology, College of Medicine and Health Sciences, Sohar Campus, Oman
[2]Pathology Department, Faculty of Medicine, Northern Border University, Arar, Saudi Arabia
[3]Department of Medical Laboratory Technology, Faculty of Applied Medical Sciences, Northern Border University, Arar, Saudi Arabia
[4]Diagnostic Hematology, Clinical Laboratory Sciences, College of Applied Medical Sciences, Umm Al Qura University, Makkah, Saudi Arabia

Abstract

Background: Dyslipidemia is a key modifiable risk factor for atherosclerotic cardiovascular disease that often remains undiagnosed in young adults due to its asymptomatic nature. Early detection and management are crucial to preventing long-term complications. This study aimed to determine the prevalence and patterns of dyslipidemia among young adults and examine its association with age and gender.
Materials and Methods: A cross-sectional analysis was conducted among 1,436 individuals (742 females and 694 males). Lipid profiles were assessed using established clinical thresholds, and gender differences were analyzed with the chi-square test.
Results: Dyslipidemia was present in 69.8% of participants, with the most common abnormalities being high total cholesterol (41.2%), low HDL-C (36.4%), and high LDL-C (34.5%). Low HDL-C was more frequent in females, while males exhibited higher triglycerides and mixed dyslipidemia. Prevalence increased with age, from 53.8% in those aged 20–24 years to 76.6% in the group 36–40 years.
Conclusion: Dyslipidemia is highly prevalent among young adults, with gender-specific and age-related variations. These findings emphasize the importance of early screening, lifestyle modification, and public health interventions to mitigate future cardiovascular disease risk.(**International Journal of Biomedicine. 2025;15(4):668-673.**)

Keywords: cardiovascular risk • dyslipidemia • young adults

For citation: Begum GS, Agarwal A, Suhail N, Hafiz MN, Jawad MM, Abass AE, Hejazy SA. Age- and Gender-Specific Dyslipidemia in Omani Young Adults: Metabolic Links to Cardiovascular Risk. International Journal of Biomedicine. 2025;15(4):668-673. doi:10.21103/Article15(4)_OA3

Abbreviations

ACS, acute coronary syndrome; **CAD**, coronary artery disease; **CVDs**, cardiovascular diseases; **HDL-C**, high-density lipoprotein cholesterol; **LDL-C**, low-density lipoprotein cholesterol; **NCDs**, non-communicable diseases; **TC**, total cholesterol; **TG**, triglycerides; **T2DM**, type 2 diabetes mellitus.

Introduction

Globally, cardiovascular diseases (CVDs) remain the leading cause of mortality and disability among non-communicable diseases (NCDs), accounting for approximately 12 million deaths annually and 40–45% of all global deaths. [1–3] Despite global preventive efforts, CVDs continue to be the major cause of death in many countries. Atherosclerosis,

thrombosis, coronary heart disease, and ischemic stroke are major complications associated with dyslipidemia, which plays a critical role in the CVD pathogenesis.[4] According to a study by Saeed et al.,[5] each unit increase in total blood cholesterol triples the risk of CVDs in both men and women. Dyslipidemia, defined by elevated total cholesterol (TC), low-density lipoprotein cholesterol (LDL-C), triglycerides (TG), and reduced high-density lipoprotein cholesterol (HDL-C), is a significant, independent, and modifiable risk factor for CVD, metabolic syndrome, and type 2 diabetes mellitus (T2DM).[6–9] Even minor lipid abnormalities markedly increase coronary artery disease (CAD) risk, particularly when combined with other factors like T2DM.[10] In Oman, the National Cholesterol Education Program Adult Treatment Panel III (ATP III) reported an age-adjusted metabolic syndrome prevalence of 21.0%, higher among women (23.0%) than men (19.5%). Low HDL-C (75.4%) and abdominal obesity (24.6%) were the most common components, the latter being significantly more frequent in women.[11]

Lipids are vital for energy storage, hormone synthesis, vitamin absorption, and cell membrane formation. However, their accumulation in the arteries can cause vascular obstruction and organ dysfunction.[12] Among young adults, premature CAD is closely linked to dyslipidemia, hypertension, and smoking.[13] A study at Sultan Qaboos University Hospital (SQUH), Muscat, found a high prevalence of dyslipidemia among young Omanis.[14] Similarly, studies in younger Middle Eastern patients with acute coronary syndrome (ACS) reveal higher rates of modifiable risk factors, notably smoking and hypercholesterolemia, than in older groups.[15]

Given its asymptomatic nature and early contribution to atherosclerosis, early detection and management of dyslipidemia are critical to reducing future cardiovascular burden.

This study aimed to determine the prevalence and patterns of dyslipidemia among young adults and examine its association with age and gender.

Material and Methods

A retrospective cross-sectional observational study was conducted by reviewing the medical records of individuals who were treated at Sohar Hospital, Oman, between January 2024 and December 2024.

Sample Size

The minimum required sample size was calculated using Cochran's formula for estimating a proportion in a population, assuming a 95% confidence level (Z=1.96), a 5% margin of error (e=0.05), and a conservative estimated prevalence (*P*=0.5) to yield the maximum sample size. The initial calculated sample size was 385. However, the present study included 1436 individuals, which significantly exceeds the minimum requirement. This larger sample enhances precision, providing strong generalizability and statistical power to detect significant associations.

Study Design

One thousand four hundred thirty-six subjects were categorized into four age groups: 20-24 years, 25-30 years, 31-35 years, and 36-40 years. This age-based categorization enabled the identification of age-specific trends in dyslipidemia prevalence and associated factors among young adults. The control group was also included and comprised of individuals without dyslipidemia, selected from the same hospital records using matching criteria such as age and sex.

A STEPwise approach was employed to ensure systematic data extraction, facilitate trend identification, and support the development of targeted public health strategies to address non-communicable diseases (NCDs) effectively.[16]

Step 1: Questionnaire-Based Assessment (Information from Case Files): Demographic information, including age and gender, was collected from patient case files.

Step 2: Biochemical Profile: Biochemical data were extracted to assess dyslipidemia prevalence. This included serum lipid profile values, such as TC, LDL-C, HDL-C, and TG.

Data from patient case files dated between January 2024 and December 2024 were extracted from the electronic medical records system using a pre-designed Excel sheet to fulfill the study's objectives. Dyslipidemia was defined using the National Cholesterol Education Program-Adult Treatment Panel III (NCEP-ATP III) criteria, based on the cut-off values outlined below.[16] It was identified by the presence of at least one of six lipid abnormality patterns in the serum lipid profile. According to the NCEP-ATP III classification, dyslipidemia was categorized into six types—four isolated and two combined (or mixed) patterns as outlined below:

- Elevated TC (≥5.2 mmol/L)
- Lowered HDL-C (<1.04 mmol/L in men and <1.3 mmol/L in women)
- Elevated TG (≥1.7 mmol/L)
- Elevated LDL-C (≥3.4 mmol/L)
- Combined (mixed) dyslipidemia (high TG + low HDL-C)
- Combined (mixed) dyslipidemia (high TG + high TC)

Inclusion and Exclusion Criteria

The study included adults of both genders aged 20–40 years with complete records, including lipid profiles (TC, LDL-C, HDL-C, and TG). Exclusion criteria: patients younger than 20 or older than 40 years, incomplete records, pregnancy, CVDs, chronic kidney disease, liver disease, and lipid-lowering drug use.

Statistical Analysis

Data were analyzed using descriptive statistics to determine prevalence rates and inferential statistics to explore associations between variables. The data was entered into Microsoft Excel and coded. The coded data were analysed in SPSS Version 21. The data were further categorized according to age group. Post-stratification, Chi-square and Student t-test were applied. *P*-value <0.05 was considered significant.

Results

A total of 1436 patients were enrolled: 742 (51.7%) were females and 694 (48.3%) were males. The majority of participants were Omani nationals (90.5%), followed by Indians (5.8%) and Egyptians (1.0%). Other nationalities, including Bangladeshi, Filipino, Sudanese, Syrian, and Nepali, each accounted for less than 1% of the study population.

The age distribution of participants showed that 41.0% were between 36 and 40 years, 29.5% between 31 and 35 years, 21.3% between 25 and 30 years, and 8.1% between 20 and 24 years. The mean age was 33.12±5.27 years, with a range of 20–40 years (Table 1). In the study population, dyslipidemia was observed in 69.8% of participants, indicating a high overall burden, whereas 30.2% demonstrated a normal lipid profile (Table 2). Among the various dyslipidemia components, isolated high TC was the most prevalent abnormality, observed in 41.2% of participants, followed by isolated low HDL-C (36.4%) and isolated high LDL-C (34.5%). Isolated hypertriglyceridemia was present in 26.3% of subjects. Combined abnormalities were less common, with TG+TC present in 15.5% and TG+HDL-C in 14.4% of the population (Table 3). Gender-wise analysis showed that the overall prevalence of dyslipidemia was comparable between females (70.2%) and males (69.3%), with a *P*-value of 0.708 (Table 4). However, significant differences were observed in specific components. Low HDL-C was more common among females (39.9% vs. 32.6%, *P*=0.004), whereas high TG was significantly more prevalent in males (33.9% vs. 19.3%, *P*=0.001). Combined abnormalities were also more frequent in males, with higher proportions of TG+HDL-C (17.4% vs. 11.6%, *P*=0.002) and TG+TC (20.0% vs. 11.3%, *P*=0.001). No significant gender differences were found in the prevalence of high TC or high LDL-C. Age-wise distribution revealed a progressive increase in dyslipidemia prevalence with advancing age (Table 5). Overall, dyslipidemia was detected in 53.8% of participants aged 20–24 years, rising to 65.4% in those aged 25–30 years, 67.9% in those aged 31–35 years, and 76.6% in those aged 36–40 years (*P*=0.001). High TC and high LDL-C were significantly more common in older age groups (*P*=0.001 for both), while high TG also showed a significant upward trend with age (*P*=0.004). Combined abnormalities (TG+HDL-C and TG+TC) were more frequent in participants aged ≥31 years (*P*=0.017 and *P*=0.029, respectively). In contrast, the prevalence of low HDL-C did not differ significantly across age groups (*P*=0.201).

Table 1.

Distribution of subjects according to different age groups.

Age group (years)	Frequency	Percentage
20-24	117	8.1
25-30	306	21.3
31-35	424	29.5
36-40	589	41.0
Total	1436	100.0

Table 2.

Overall prevalence of dyslipidemia.

Dyslipidemia	Frequency	Percentage
Yes	1002	69.8
No	434	30.2
Total	1436	100.0

Table 3.

Prevalence of dyslipidemia components.

Dyslipidemia components	Frequency	Percentage
Isolated high TC	591	41.2
Isolated low HDL-C	522	36.4
Isolated high LDL-C	495	34.5
Isolated high TG	378	26.3
Combined abnormal TG+HDL-C	207	14.4
Combined abnormal TG+TC	223	15.5

Table 4.

Prevalence of dyslipidemia according to gender.

Dyslipidemia components	Female (n=742) n (%)	Male (n=694) n (%)	*P*-value
High TC	298 (40.2)	293 (42.2)	0.429
Low HDL-C	296 (39.9)	226 (32.6)	0.004
High LDL-C	239 (32.2)	256 (36.9)	0.062
High TG	143 (19.3)	235 (33.9)	0.001
Abnormal TG+HDL-C	86 (11.6)	121 (17.4)	0.002
Abnormal TG+TC	84 (11.3)	139 (20.0)	0.001
Overall dyslipidemia	521 (70.2)	481 (69.3)	0.708

Table 5.

Prevalence of dyslipidemia according to age group.

Dyslipidemia components	20-24 (n=117) n (%)	25-30 (n=306) n (%)	31-35 (n=424) n (%)	36-40 (n=589) n (%)	*P*-value
High TC	25 (21.4)	119 (38.9)	180 (42.5)	267 (45.3)	0.001
Low HDL-C	37 (31.6)	99 (32.4)	160 (37.7)	226 (38.4)	0.201
High LDL-C	21 (17.9)	97 (31.7)	156 (36.8)	221 (37.5)	0.001
High TG	17 (14.5)	77 (25.2)	106 (25.0)	178 (30.2)	0.004
Abnormal TG+HDL-C	8 (6.8)	35 (11.4)	68 (16.0)	96 (16.3)	0.017
Abnormal TG+TC	7 (6.0)	49 (16.0)	68 (16.0)	99 (16.8)	0.029
Overall dyslipidemia	63 (53.8)	200 (65.4)	288 (67.9)	451 (76.6)	0.001

Discussion

This study found a high prevalence of dyslipidemia (69.8%) among young adults aged 20–40 years, slightly higher in females (70.2%) than males (69.3%). Similar gender trends have been reported elsewhere. Talpur et al.[17] observed dyslipidemia in 75.9% of young adults, with a higher prevalence in females (76.0%) than males (74.2%). Studies from China and Iran also reported higher rates in women—37.6% vs. 34.4% and 55.4% vs. 37.4%, respectively.[18,19] Although our findings did not show a statistically significant difference, the

consistent pattern suggests possible hormonal, metabolic, or lifestyle influences.

Regional comparisons further support these findings. A Middle Eastern meta-analysis reported pooled prevalence rates of 54.08% for dyslipidemia, 32.51% for hypertriglyceridemia, 29.44% for hypercholesterolemia, 32.09% for high LDL-C, and 44.71% for low HDL-C.[20] These values align with our results showing elevated TC (40–42%), LDL (32–37%), TG (19–34%), and low HDL-C (33–40%). Similar patterns were observed by Talpur et al.,[17] who reported high rates of low HDL-C and hypertriglyceridemia among young adults. The high burden of combined lipid abnormalities (TG+HDL, TG+TC) in our cohort also reflects regional trends.

Low HDL-C was significantly more frequent among females (39.9%, P=0.004). Although estrogen generally raises HDL and provides cardiovascular protection, this effect can be offset by poor lifestyle factors. Diets high in saturated fats and sugars, physical inactivity, central obesity, and stress-induced cortisol elevation may suppress HDL-C production while increasing LDL-C and triglycerides.[21] These findings emphasize the interplay between metabolic and behavioral determinants of dyslipidemia, particularly among women.

Dyslipidemia remains a major pathogenic factor for atherosclerotic CVDs.[22] Evidence from China indicates that proper lipid management substantially reduces ischemic CVD incidence and mortality.[23] However, its asymptomatic nature often delays diagnosis, highlighting the need for routine screening and preventive interventions.[24]

Although dyslipidemia prevalence rises with age, its presence in younger adults is clinically significant.[25] The Bogalusa Heart Study demonstrated that early elevations in LDL-C and triglycerides are linked to premature atherosclerosis,[26] suggesting that lipid abnormalities during early adulthood contribute to later cardiovascular events.

In the Arabian Gulf, high rates of diabetes and metabolic syndrome among ACS patients reflect a pattern of atherogenic dyslipidemia characterized by elevated TG, low HDL-C, and small dense LDL particles.[27,28] Even with optimal LDL-C control, these patients face substantial residual cardiovascular risk.[29,30] A study by Al-Rasadi et al.,[31] found that 62% of ACS patients had low HDL-C—the highest reported in regional cohorts. Additionally, familial hypercholesterolemia, a common but underdiagnosed genetic condition, contributes to persistently high LDL-C and increased risk of premature coronary artery disease.[32,33]

Overall, the study highlights a major public health concern in Oman, revealing a high prevalence of dyslipidemia among young adults aged 20–40 years. Of the 1,436 participants, 69.8% had at least one lipid abnormality. Dyslipidemia increased with age, from 53.8% in the 20–24 age group to 76.6% among those aged 36–40, suggesting early onset and progressive worsening. Gender variations were observed, with women showing lower HDL-C and men exhibiting higher TG and mixed dyslipidemia.

These findings underscore the need for early lipid screening, preventive lifestyle modifications, and targeted public health strategies to mitigate future cardiovascular disease risk among young adults.

The study's retrospective cross-sectional nature limits the ability to establish causal relationships between dyslipidemia and demographic or lifestyle factors. It only reflects associations at a single point in time. Additionally, all data were obtained from a single healthcare facility, which may not fully represent the broader young adult population in Oman or in other regions with different socioeconomic and lifestyle backgrounds.

Ethical Considerations

This study was approved by the college ethics and biosafety committee (EBC) NU/COMHS/EBC0018/2025 and the Ministry of Health Research and Ethical Review Committee, North Batinah Governorate (RERAC-NBG) MH/DGHS/NBG: MoH/CSR/25/29558 and was conducted according to Helsinki Declaration Principles. The Ethics Committee waived the consent requirement for participation due to the study's retrospective nature and the use of anonymized, de-identified patient data.

Acknowledgements

The authors thank the staff at Sohar Hospital, particularly those in the clinical biochemistry and pathology laboratories, for providing access to the electronic medical records system (Al-Shifa'a).

Funding Sources

The author (Nida Suhail) extends her appreciation to the Deanship of Scientific Research at Northern Border University, Arar, KSA, for funding this research work through the project number NBU-FFR-2025-2143-04.

Competing Interests

The authors have no conflicts of interest to declare.

References

1. Ghazwani M, Mahmood SE, Gosadi IM, Bahri AA, Ghazwani SH, Khmees RA. Prevalence of Dyslipidemia and Its Determinants Among the Adult Population of the Jazan Region. Int J Gen Med. 2023 Sep 18;16:4215-4226. doi: 10.2147/IJGM.S429462. PMID: 37745134; PMCID: PMC10516128.
2. Blacher J, Gabet A, Vallée A, Ferrières J, Bruckert E, Farnier M, Olié V. Prevalence and management of hypercholesterolemia in France, the Esteban observational study. Medicine (Baltimore). 2020 Dec 11;99(50):e23445. doi: 10.1097/MD.0000000000023445. PMID: 33327276; PMCID: PMC7738064.
3. Rifin HM, Lourdes TR, Ab Majid NL, Abd Hamid HA, Hasani WR, Ling MY, et al. Hypercholesterolemia prevalence, awareness, treatment and control among adults in Malaysia: the 2015 national health and morbidity survey, Malaysia.

Glob J Health Sci. 2018;10(11):10-5539. doi: 10.5539/gjhs.v10n7p11
4. Akbartabar Toori M PhD, Kiani F MSc, Sayehmiri F PhD, Sayehmiri K PhD, Mohsenzadeh Y MD, Ostovar R PhD, Angha P MSc, Mohsenzadeh Y MSc. Prevalence of Hypercholesterolemia, High LDL, and Low HDL in Iran: A Systematic Review and Meta-Analysis. Iran J Med Sci. 2018 Sep;43(5):449-465. PMID: 30214097; PMCID: PMC6123550.
5. Saeed E, Ali R, Jalal-ud-din M, Saeed A, Jadoon RJ, Moiz M. HYPERCHOLESTEROLEMIA IN PATIENTS OF ISCHEMIC STROKE. J Ayub Med Coll Abbottabad. 2015 Jul-Sep;27(3):637-9. PMID: 26721027.
6. Huang C, Zhang WQ, Tang WW, Liu Y, Liu JX, Xu RH, Zhao SP, Wang TD, Huang XB. Prevalence and related factors of dyslipidemia among urban adults aged 35 to 79 years in Southwestern China. Sci Rep. 2021 Sep 2;11(1):17579. doi: 10.1038/s41598-021-96864-w. PMID: 34475467; PMCID: PMC8413428.
7. Song PK, Li H, Man QQ, Jia SS, Li LX, Zhang J. Trends in Determinants of Hypercholesterolemia among Chinese Adults between 2002 and 2012: Results from theNational Nutrition Survey. Nutrients. 2017 Mar 15;9(3):279. doi: 10.3390/nu9030279. PMID: 28294966; PMCID: PMC5372942.
8. Pappan N, Awosika AO, Rehman A. Dyslipidemia. 2024 Mar 4. In: StatPearls [Internet]. Treasure Island (FL): StatPearls Publishing; 2025 Jan–. PMID: 32809726.
9. Abujbara M, Batieha A, Khader Y, Jaddou H, El-Khateeb M, Ajlouni K. The Prevalence of Dyslipidemia among Jordanians. J Lipids. 2018 Oct 28;2018:6298739. doi: 10.1155/2018/6298739. PMID: 30510803; PMCID: PMC6230384.
10. Qi L, Ding X, Tang W, Li Q, Mao D, Wang Y. Prevalence and Risk Factors Associated with Dyslipidemia in Chongqing, China. Int J Environ Res Public Health. 2015 Oct 26;12(10):13455-65. doi: 10.3390/ijerph121013455. PMID: 26516874; PMCID: PMC4627042.
11. Khader YS, Batieha A, El-Khateeb M, Al Omari M, Ajlouni K. Prevalence of dyslipidemia and its associated factors among Jordanian adults. J Clin Lipidol. 2010 Jan-Feb;4(1):53-8. doi: 10.1016/j.jacl.2009.12.004. Epub 2009 Dec 22. PMID: 21122627.
12. Raffee LA, Alawneh KZ, Ibdah RK, Rawashdeh SI, Zoghoul S, Ewais AS, Al-Mistarehi AH. Prevalence, Clinical Characteristics, and Risk Among Patients with Ischemic Heart Disease in the Young Jordanian Population. Open Access Emerg Med. 2020 Nov 16;12:389-397. doi: 10.2147/OAEM.S272961. PMID: 33235526; PMCID: PMC7678703.
13. Islam SM, Purnat TD, Phuong NT, Mwingira U, Schacht K, Fröschl G. Non-communicable diseases (NCDs) in developing countries: a symposium report. Global Health. 2014 Dec 11;10:81. doi: 10.1186/s12992-014-0081-9. PMID: 25498459; PMCID: PMC4267750.
14. Al-Waili K, Al-Rasadi K, Zadjali F, Al-Hashmi K, Al-Mukhaini S, Al-Kindi M, Al-Sabti H, Al-Hinai AT, Farhan H, Al-Zakwani I. Clinical and Genetic Characteristics of Familial Hypercholesterolemia at Sultan Qaboos University Hospital in Oman. Oman Med J. 2020 Jun 30;35(3):e141. doi: 10.5001/omj.2020.59. PMID: 32704389; PMCID: PMC7362724.
15. National Cholesterol Education Program (NCEP) Expert Panel on Detection, Evaluation, and Treatment of High Blood Cholesterol in Adults (Adult Treatment Panel III). Third Report of the National Cholesterol Education Program (NCEP) Expert Panel on Detection, Evaluation, and Treatment of High Blood Cholesterol in Adults (Adult Treatment Panel III) final report. Circulation. 2002 Dec 17;106(25):3143-421. PMID: 12485966.
16. Bonita R. Surveillance of Risk Factors for Non-Communicable Diseases. The WHO STEPwise Approach. Summary. 2001.
17. Talpur MT, Katbar MT, Shabir KU, Shabir KU, Yaqoob U, Jabeen S, et al. Prevalence of dyslipidemia in young adults. Prof Med J. 2020;27(5):987-93. doi: 10.29309/TPMJ/2020.27.05.4040
18. Qi L, Ding X, Tang W, Li Q, Mao D, Wang Y. Prevalence and Risk Factors Associated with Dyslipidemia in Chongqing, China. Int J Environ Res Public Health. 2015 Oct 26;12(10):13455-65. doi: 10.3390/ijerph121013455. PMID: 26516874; PMCID: PMC4627042.
19. Sadeghi M, Talaei M, Oveisgharan S, Rabiei K, Dianatkhah M, Bahonar A, Sarrafzadegan N. The cumulative incidence of conventional risk factors of cardiovascular disease and their population attributable risk in an Iranian population: The Isfahan Cohort Study. Adv Biomed Res. 2014 Nov 29;3:242. doi: 10.4103/2277-9175.145749. PMID: 25538928; PMCID: PMC4260292.
20. Kargar S, Ansari H. Prevalence of dyslipidemias in the Middle East region: A systematic review & meta-analysis study. Diabetes Metab Syndr. 2023 Nov;17(11):102870. doi: 10.1016/j.dsx.2023.102870. Epub 2023 Oct 11. PMID: 37844434.
21. Sessa WC. Estrogen Reduces LDL (Low-Density Lipoprotein) Transcytosis. Arterioscler Thromb Vasc Biol. 2018 Oct;38(10):2276-2277. doi: 10.1161/ATVBAHA.118.311620. PMID: 30354224; PMCID: PMC6448576.
22. Penalva RA, Huoya Mde O, Correia LC, Feitosa GS, Ladeia AM. Lipid profile and intensity of atherosclerosis disease in acute coronary syndrome. Arq Bras Cardiol. 2008 Jan;90(1):24-30. English, Portuguese. doi: 10.1590/s0066-782x2008000100005. PMID: 18317637.
23. Li JJ, Zhao SP, Zhao D, Lu GP, Peng DQ, Liu J, Chen ZY, Guo YL, Wu NQ, Yan SK, Wang ZW, Gao RL. 2023 China Guidelines for Lipid Management. J Geriatr Cardiol. 2023 Sep 28;20(9):621-663. doi: 10.26599/1671-5411.2023.09.008. PMID: 37840633; PMCID: PMC10568545.
24. He H, Yu YQ, Li Y, Kou CG, Li B, Tao YC, Zhen Q, Wang C, Kanu JS, Huang XF, Han M, Liu YW. Dyslipidemia awareness, treatment, control and influence factors among adults in the Jilin province in China: a cross-sectional study. Lipids Health Dis. 2014 Aug 3;13:122. doi: 10.1186/1476-511X-13-122. PMID: 25086650; PMCID: PMC4237893.
25. Chou R, Dana T, Blazina I, Daeges M, Bougatsos C, Jeanne TL. Screening for Dyslipidemia in Younger Adults: A Systematic Review for the U.S. Preventive Services Task Force. Ann Intern Med. 2016 Oct 18;165(8):560-564. doi: 10.7326/M16-0946. Epub 2016 Aug 9. PMID: 27538032.
26. Berenson GS, Srinivasan SR, Bao W, Newman WP 3rd, Tracy RE, Wattigney WA. Association between multiple

cardiovascular risk factors and atherosclerosis in children and young adults. The Bogalusa Heart Study. N Engl J Med. 1998 Jun 4;338(23):1650-6. doi: 10.1056/NEJM199806043382302. PMID: 9614255.

27. Thalib L, Zubaid M, Rashed W, Suwaidi JA, Almahmeed W, Alozairi E, Alanbaei M, Sulaiman K, Amin H, Al-Motarreb A. Impact of diabetic status on the hyperglycemia-induced adverse risk of short term outcomes in hospitalized patients with acute coronary syndromes in the Middle East: findings from the Gulf registry of Acute Coronary Events (Gulf RACE). Clin Med Res. 2011 Mar;9(1):32-7. doi: 10.3121/cmr.2010.946. Epub 2010 Sep 17. PMID: 20852085; PMCID: PMC3064757.

28. Al Suwaidi J, Zubaid M, El-Menyar AA, Singh R, Rashed W, Ridha M, Shehab A, Al-Lawati J, Amin H, Al-Mottareb A. Prevalence of the metabolic syndrome in patients with acute coronary syndrome in six middle eastern countries. J Clin Hypertens (Greenwich). 2010 Nov;12(11):890-9. doi: 10.1111/j.1751-7176.2010.00371.x. Epub 2010 Aug 30. PMID: 21054777; PMCID: PMC8816483.

29. Fruchart JC, Sacks FM, Hermans MP, Assmann G, Brown WV, Ceska R, Chapman MJ, Dodson PM, Fioretto P, Ginsberg HN, Kadowaki T, Lablanche JM, Marx N, Plutzky J, Reiner Z, Rosenson RS, Staels B, Stock JK, Sy R, Wanner C, Zambon A, Zimmet P; Residual Risk Reduction Initiative (R3I). The Residual Risk Reduction Initiative: a call to action to reduce residual vascular risk in dyslipidaemic patient. Diab Vasc Dis Res. 2008 Nov;5(4):319-35. doi: 10.3132/dvdr.2008.046. PMID: 18958843.

30. Hermans MP, Fruchart JC. Reducing Residual Vascular Risk in Patients with Atherogenic Dyslipidemia: Where do we go from here? Clin Lipidol. 2010;5:811-26 . doi: org/10.2217/clp.10.65

31. Al-Rasadi K, Al-Zakwani I, Zubaid M, Ali A, Bahnacy Y, Sulaiman K, Al Mahmeed W, Al Suwaidi J, Mikhailidis DP. Prevalence, Predictors, and Impact of Low High-Density Lipoprotein Cholesterol on in-Hospital Outcomes Among Acute Coronary Syndrome Patients in the Middle East. Open Cardiovasc Med J. 2011;5:203-9. doi: 10.2174/1874192401105010203. Epub 2011 Aug 30. PMID: 21966331; PMCID: PMC3178900.

32. Goldstein JK, Hobbs HH, Brown MS. Familial hypercholesterolemia. In: Scriver CR, Beaudet AL, Sly WS, Valle D (editors). The Metabolic & Molecular Bases of Inherited Disease. 8th ed. New York: McGraw-Hill Inc; 2001; p. 2863-913.

33. Austin MA, Hutter CM, Zimmern RL, Humphries SE. Genetic causes of monogenic heterozygous familial hypercholesterolemia: a HuGE prevalence review. Am J Epidemiol. 2004 Sep 1;160(5):407-20. doi: 10.1093/aje/kwh236. PMID: 15321837.

***Corresponding author**: Dr. Nida Suhail, E-mail: nsuhail123@gmail.com*

International Journal of Biomedicine 15(4) (2025) 674-678
http://dx.doi.org/10.21103/Article15(4)_OA4

ORIGINAL ARTICLE

Obstetrics and Gynecology

INTERNATIONAL JOURNAL OF BIOMEDICINE

Histopathological Evaluation of Endometrial Curettage in Patients with Abnormal Uterine Bleeding: A Retrospective Study in Al Kharj City, Saudi Arabia

Ali Hassan A. Ali[1, 2 *], Wafaey Badawy[3], Samah O. Mohager[1], Saud A. Alsharif[4], Rabie Elsayed I. Elshaer[5,6], Aryam Shudayyid R. Almutairi[7], Haya Abdulaziz M. Alwtaidy[7], Asma Muneer S. Alharthi[7], Arwa Ibrahim Alwabran[7], Shahad Mohammed S. Alkhashan[7], Amerah Omar Qirat[7], Mariyyah Abdulrahman Alnathir[7], Razan Saleh A. Hazzaa[7], Shahad Zaid M. Aloqayli[7]

[1]*Basic Medical Science Department, College of Medicine, Prince Sattam bin Abdulaziz University, Al-Kharj 11942, Saudi Arabia*
[2]*Anatomy Department, Faculty of Medicine, Al-Azhar University, Cairo, Egypt*
[3]*Department of Pathology, Military Industries Hospital, Al-Kharj, Saudi Arabia*
[4]*Department of Obstetrics & Gynecology, College of Medicine, Prince Sattam bin Abdulaziz University, Al-Kharj 11942, Saudi Arabia*
[5]*Pathology Department, Faculty of Medicine, Al-Azhar University, Cairo, Egypt*
[6]*Histopathology Department, Delta Medical Lab., Riyadh, Saudi Arabia*
[7]*College of Medicine, Prince Sattam bin Abdulaziz University, Al-Kharj 11942, Saudi Arabia*

Abstract

Background: One of the most common issues that adult females face is abnormal uterine bleeding (AUB). The preferred sampling method for identifying endometrial pathology is still uterine curettage or biopsy. Hormonal imbalance patterns, atrophic endometrium, endometritis, endometrial polyps, endometrial hyperplasia, and endometrial cancer are examples of common diseases. The purpose of this study was to identify the endometrial histological pattern in women of different ages who presented with AUB.

Methods and Results: In this retrospective study, the medical records of 309 women who had endometrial curettage for AUB were reviewed. Every endometrial curettage specimen received for histological examination between January 2025 and June 2025 by the histopathology department of the Al Kharj Military Industries Corporation Hospital, in cooperation with the Department of Obstetrics and Gynecology, PSA Hospital, is included in the study. Endometrial biopsies were taken using a dilation and curettage (D&C) procedure. Following hematoxylin and eosin staining, a microscopic analysis was conducted.

The most common histopathological finding was proliferative endometrial disorders (34.95%), followed by endometrial polyps (32.36%). Endometrial hyperplasia without atypia was found in 91 cases (29.45%). Endometrial adenocarcinoma was the sole diagnosis in four cases (1.29%).

Conclusion: Abnormal uterine bleeding may be the only complaint presented by patients with endometrial lesions. Endometrial curettage and biopsy are reliable procedures for detecting endometrial pathology.(**International Journal of Biomedicine. 2025;15(4):674-678.**)

Keywords: histopathology • abnormal uterine bleeding • endometrial curettage • Al Kharj

For citation: Ali AHA, Badawy W, Mohager SO, Alsharif SA, Elshaer REI, Almutairi ASR, Alwtaidy HAM, Alharthi AMS, Alwabran AI, Alkhashan SMS, Qirat AO, Alnathir MA, Hazzaa RSA, Aloqayli SZM. Histopathological Evaluation of Endometrial Curettage in Patients with Abnormal Uterine Bleeding: A Retrospective Study in Al Kharj City, Saudi Arabia. International Journal of Biomedicine. 2025;15(4):674-678. doi:10.21103/Article15(4)_OA4

Introduction

The most prevalent gynecologic symptom and complaint among gynecological outpatients is abnormal uterine bleeding (AUB), which affects women of all ages. [1] It has a noticeable impact on quality of life and places a significant financial strain on women's health care. Healthcare professionals routinely deal with this issue. There are several classifications and definitions for AUB. A loose definition of it would be a deviation from the typical menstrual cycle. Variations may occur in the amount of blood loss, regularity, frequency, or length of the flow. Excessive monthly blood loss that interferes with a woman's physical, social, emotional, and/or material quality of life is sometimes referred to as "heavy" bleeding. Abnormal uterine bleeding can have a variety of reasons, including systemic, anatomical, and drug-related ones. Chronic endometritis, endometrial polyps, and endometrial hyperplasia are common reasons for AUB. Patients who have a malignant or premalignant endometrial lesion may present with AUB.[2] Thyroid issues, submucosal fibroids, and coagulation abnormalities can all contribute to ovulatory AUB, or menorrhagia.[3] Following examination and ruling out premalignant and malignant etiology, many of the treatment strategies are the same.[4] Menstrual cycles may be regulated by treatment with progestins or combination oral contraceptives. Treatment options for histologic evidence of hyperplasia without atypia include continuous or cyclic progestin. Gynecologists or gynecologic oncologists should be consulted for women with hyperplasia with atypia or adenocarcinoma, respectively. The most reliable method for determining the causes of atypical uterine bleeding is still endometrial biopsy followed by histological analysis. Endometrial curettage is a simple and safe method for endometrial collection, and its histopathological analysis is regarded as the gold standard for diagnosing the cause of AUB. It also has a fair turnaround time and high diagnostic accuracy.[5]

The purpose of this study was to identify the endometrial histological pattern in women of different ages who presented with AUB.

Materials and Methods

The medical records of 309 women who underwent endometrial curettage for AUB were examined histopathologically in this retrospective study. Endometrial biopsies were taken using a dilation and curettage (D&C) procedure. The study includes every endometrial curettage specimen that was received for histological analysis in the Al Kharj Military Industries Corporation Hospital's histopathology department in collaboration with the Department of Obstetrics and Gynecology, PSA Hospital, between January 2025 and June 2025.

A 10% formalin solution was used to fix the specimens. Sections were collected from each representative area of specimens. Hematoxylin and eosin staining was applied to the tissue fragments after they underwent standard processing. The histological results and clinical information were recorded. All women, regardless of age, who complained of AUB were included. The study excluded patients who met the following criteria: unsatisfactory samples, such as only fibrin and blood clots and no endometrial glands or stroma; AUB from gestational causes, such as tubal pregnancy, molar pregnancy, or abortion; hormone therapy during the previous six months; and cervical pathology, such as cervical cancer. The cause of AUB was confirmed by microscopic examination of the slides. SPSS software was used for statistical analysis.

Results

This study included 309 patients, ranging in age from 34 to 81 years, with a mean age of 48.9±7.9 years. Among 309 patients, 236 (76.38%) were married, 33 (10.68%) were widows, and 40 (12.94%) were divorced. The majority of patients (73.79%) had a parity of three to four. 173 patients (55.99%) experienced AUB for less than six months (Table 1). The percentage of endometrial histological findings after uterine curettage in AUB patients is shown in Table 2.

Table 1.

Age, marital status, and obstetric history of the study population (n=309).

Parameter	Category	No. of patients	Percentage
Age	<40	11	3.56%
	40-50	189	61.16%
	51-60	99	32.04%
	> 60	10	3.24%
Duration of bleeding	<6 months	173	55.99%
	7-12 months	65	21.04%
	One-two years	39	12.62%
	> 2 years	32	10.36%
Marital status	Married	236	76.38%
	Divorced	40	12.94%
	Widow	33	10.68%
Parity	Nulliparous	7	2.27%
	1-2 children	48	15.53%
	3-4 children	228	73.79%
	≥ 5 children	26	8.41%

Table 2.

Histopathological findings after endometrial curettage.

Histopathological findings	No. of patients	Percentage
Disordered proliferative endometrium	108	34.95%
Endometrial hyperplasia without atypia	91	29.45%
Endometrial hyperplasia with focal atypia	4	1.29%
Acute endometritis	1	0.32%
Endometrial polyp	100	32.36%
Endometrial adenocarcinoma	4	1.29%
Endometrial serous adenocarcinoma	1	0.32%

In 108 (34.95%) patients, proliferative endometrial disorders were found. It displays proliferative endometrial glands sporadically scattered with cystically dilated glands (> 2 times normal size). More than 10% of all glands have been seen to be dilated, with dilated glands typically having irregular shapes (branched, convoluted, and scalloped exterior outlines). Furthermore, a relatively typical ratio of glands to stroma (glands occupying less than 50% of the surface area) is also displayed. No cytologic atypia is present (Figure 1).

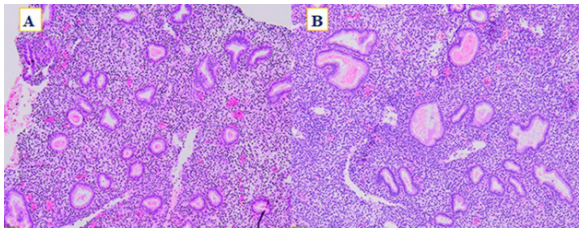

Fig. 1. *A) and B) Images of endometrium stained with H&E demonstrating disordered proliferative endometrium. Cystically dilated glands (> 2x normal size) randomly interspersed among proliferative endometrial glands are shown. Dilated glands usually have irregular shapes (branched, convoluted, and scalloped outer contours), which make up more than 10% of the total number of glands. In addition, a relatively normal gland-to-stroma ratio (glands occupy < 50% of the surface area) is also shown. There is a lack of cytologic atypia. A) (X 200). B) (X 400).*

In 100 patients, an endometrial polyp was discovered (32.36%). It was made up of varying numbers of glands and stroma and exhibits benign hyperplastic overgrowth of endometrial tissue that generates a localized projection into the uterine cavity. Cystically dilated glands and fibrovascular cores with thick-walled blood arteries are present in papillary proliferations (Figure 2).

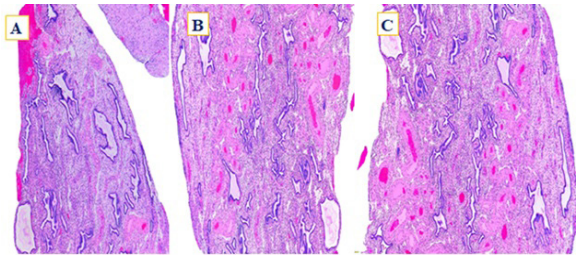

Fig. 2. *A), B), and C) Images of endometrium stained with H&E demonstrating endometrial polyps. It shows benign hyperplastic overgrowth of endometrial tissue that forms a localized projection into the endometrial cavity and is composed of variable amounts of glands and stroma. There are papillary proliferations with fibrovascular cores with thick-walled blood vessels and cystically dilated glands. A) B) and C) (X 400).*

Ninety-one (29.45%) had endometrial hyperplasia without atypia. It demonstrates endometrial gland proliferation, which raises the ratio of glands to stroma. Although there is still stroma between glandular basement membranes, the architecture displays densely packed glands with a gland-to-stroma ratio greater than 3:1. The background endometrium had the same cytologic characteristics as the packed glands. No cytologic atypia was present (Figure 3).

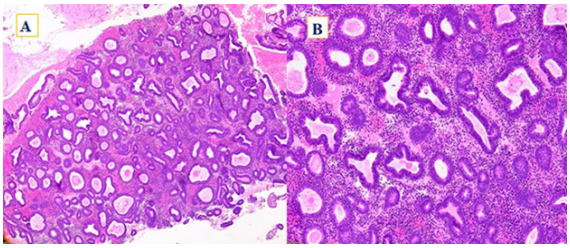

Fig. 3. *A) and B) Images of endometrium stained with H&E demonstrating endometrial hyperplasia without atypia. It shows Proliferation of endometrial glands with a resulting increase in the gland-to-stroma ratio. The Architecture shows closely packed glands such that the gland-to-stroma ratio is > 3:1, but stroma is still present between glandular basement membranes. The cytologic features of the crowded glands must be identical to those of the background endometrium. There is a lack of cytologic atypia. A) (X 200). B) (X 400).*

Endometrial adenocarcinoma was the sole diagnosis in four cases (1.29%). Confluent or back-to-back glands without an intermediate stroma are depicted in the architecture. Cribriform or microacinar layouts are available. There have been observations of intricate villoglandular, micropapillary, or papillary structures. Additionally, it exhibits cytoplasmic eosinophilia, lack of polarity, nuclear rounding (as opposed to elongation) with prominent nucleoli, and cellular or nuclear expansion (Figure 4).

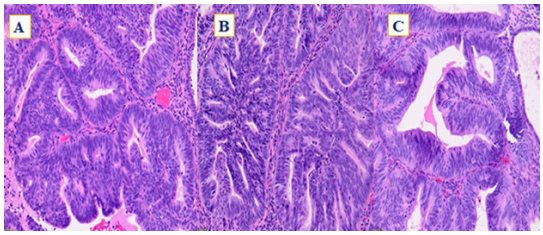

Fig. 4. *A), B), and C) Images of endometrium stained with H&E demonstrating endometrial adenocarcinoma. Architecture shows confluent or back-to-back glands lacking intervening stroma. There are cribriform or microacinar configurations. Complex papillary, micropapillary, or villoglandular structures have been seen. It also shows cellular or nuclear enlargement, nuclear rounding (rather than elongation) with prominent nucleoli, loss of polarity, and cytoplasmic eosinophilia. A) B) and C) (X 400).*

There was only one instance of acute endometritis. It depicts the endometrial epithelium being infiltrated and destroyed by neutrophils. The gland lumen is being filled by neutrophils, whether or not microabscesses are forming (Figure 5).

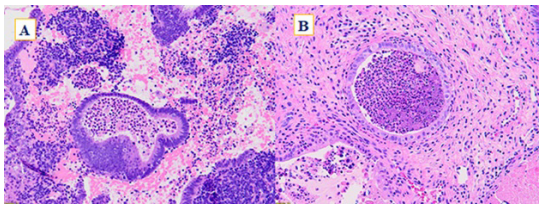

Fig. 5. *A) and B) Images of endometrium stained with H&E demonstrating acute endometritis. Neutrophils infiltrating and destroying the endometrial epithelium are shown. The neutrophils are filling the gland lumen with or without microabscess formation. A) and B) (X 400).*

Discussion

Unusual uterine bleeding is a complex problem that affects women of all ages. A key component of diagnosis and treatment is the endometrium's histopathological assessment. A total of 309 women with complaints of AUB were included in this study. About 61% of the cases in our study were in the 40–50 age range. In contrast, a previous study indicates that the age range of 35 to 39 years accounts for the greatest number of instances.[6] Abnormal uterine bleeding is generally not life-threatening, and from the point of view of the patient, the primary burden of this symptom is its effect on quality of life. Studies on AUB do not consistently evaluate quality of life, and there is a lack of data on how bleeding affects quality of life indicators at the national population level. According to the population-level research that is currently available, women who have uterine bleeding use health services more frequently than women who do not.[7]

An amplification of the typical proliferative phase without an apparent increase in the overall gland to stroma ratio is known as disordered proliferative endometrium. The majority of our cases, 108 (34.95%), had proliferative endometrial disorders. The results of other studies are consistent with this fact.[8] In the endometrium, endometrial polyps are epithelial proliferations made up of connective, fibromuscular, vascular, and glandular tissue.[9]

Compared with other studies,[10,11] the incidence of endometrial polyps in this study was significantly higher, reaching 32.36%. If the patient exhibits atypical uterine bleeding, it is crucial to obtain a history of her bleeding pattern to diagnose endometrial polyps. However, in contrast to other research, the frequency of endometrial cancer was lower in our study. The practice of early childbirth, multiparity, and early intervention may be the cause of the reduced incidence of endometrial cancer in this study.

Women's screening programs aimed at early detection of endometrial cancer precursors enable the development of preventive measures and timely treatment, thereby reducing mortality and morbidity from endometrial cancer.

Particularly for perimenopausal women who are at risk of developing cancer, the significance of endometrial biopsy or curettage performed to gather material for histological study, to aid in diagnosis and future care, cannot be overstated.[12] Determining the diagnostic value of curettage in diagnostically disordered proliferative endometrium was a novel component of this research, and identifying a high diagnostic rate for endometrial cancer by curettage was an essential component.

Conclusions

Abnormal uterine bleeding may be the only complaint presented by patients with endometrial lesions. A specific test that is reliable in identifying endometrial pathology is an endometrial biopsy. A detailed microscopic analysis of the tissue and a skilled endometrial sample are necessary for the final diagnosis.

Ethical Approval

All series of steps that were implemented in this study complied with the Ethics Committee of Prince Sattam bin Abdulaziz University Institutional Review Board (SCBR-444/2025).

Funding

This study has not received any external funding.

Availability of Data and Materials

The data are available upon request from the authors.

Conflicts of Interest

The authors declare that there are no conflicts of interest regarding the publication of this paper.

Acknowledgements

The authors are grateful to the Deanship of Scientific Research, Prince Sattam bin Abdulaziz University, Al-Kharj, Saudi Arabia, for its support and encouragement in conducting the research and publishing this report.

References

1. Almuhaitb RA, Alenazi RH, Almebki RA, Alshehri RA, Alemad MM, AlHarbi JM, AlAmro SA, Alshahrani RM, Bakhsh H. Management of Abnormal Uterine Bleeding Among Reproductive Age Group Women: A Cross-Sectional Study. J Clin Med. 2024 Nov 23;13(23):7086. doi: 10.3390/jcm13237086. PMID: 39685546; PMCID: PMC11642035.
2. Montgomery BE, Daum GS, Dunton CJ. Endometrial hyperplasia: a review. Obstet Gynecol Surv. 2004 May;59(5):368-78. doi: 10.1097/00006254-200405000-00025. PMID: 15097798.
3. Singh MN, Sasidharan A, Paul B, Puthen Parambath S. Histopathological Spectrum of Endometrium in Abnormal Uterine Bleeding in a Tertiary Care Centre: A Three-Year Retrospective Study. Cureus. 2025 Jan 16;17(1):e77542. doi: 10.7759/cureus.77542. PMID: 39958083; PMCID: PMC11829713.

4. Singh S, Best C, Dunn S, Leyland N, Wolfman WL; CLINICAL PRACTICE – GYNAECOLOGY COMMITTEE. Abnormal uterine bleeding in pre-menopausal women. J Obstet Gynaecol Can. 2013 May;35(5):473-475. English, French. doi: 10.1016/S1701-2163(15)30939-7. PMID: 23756279.
5. Karimi M, Alizadeh A, Mahmoodi M. Clinicopathological Pattern of Endometrial Specimens in Women with Abnormal Uterine Bleeding and Ultrasonography Correlation. Arch Iran Med. 2024 Apr 1;27(4):216-222. doi: 10.34172/aim.2024.31. PMID: 38685848; PMCID: PMC11097308.
6. Varun N, Gupta N, Khan S. A retrospective study of endometrial histopathology in abnormal uterine bleeding patients. International Journal of Reproduction, Contraception, Obstetrics and Gynecology. 2018 Oct 1;7(10):4116-20.
7. Warner PE, Critchley HO, Lumsden MA, Campbell-Brown M, Douglas A, Murray GD. Menorrhagia II: is the 80-mL blood loss criterion useful in management of complaint of menorrhagia? Am J Obstet Gynecol. 2004 May;190(5):1224-9. doi: 10.1016/j.ajog.2003.11.016. PMID: 15167822.
8. Pai AH, Kodandapani S. Abnormal Uterine Bleeding in Perimenopausal Women: Relevance of Transvaginal Ultrasound, Office Endometrial Biopsy, Dilatation and Curettage—An Observational Study. International Journal of Infertility & Fetal Medicine. 2018 Jun 1;9(1):10-3.
9. Tanos V, Berry KE, Seikkula J, Abi Raad E, Stavroulis A, Sleiman Z, Campo R, Gordts S. The management of polyps in female reproductive organs. Int J Surg. 2017 Jul;43:7-16. doi: 10.1016/j.ijsu.2017.05.012. Epub 2017 May 5. PMID: 28483662.
10. Shaheen U, Majeed S, Khan YN, Adnan HA, Khalid M, Shaheen H. Morphologic patterns of endometrium in biopsy/curetting specimen of patients with abnormal uterine bleeding. Pakistan Journal of Physiology. 2020 Mar 31;16(1):24-7.
11. Ali SS, Muhammad I, Shaukat J, Afzal S, Hashmi SN, Hamdani SN, Ahmed R. Histopathological spectrum of endometrial biopsies–a study of 378 cases at AFIP Pakistan. Editorial Advisory Board Chairman. 2016;66:194.
12. Dangal G. A study of endometrium of patients with abnormal uterine bleeding at Chitwan Valley. Kathmandu Univ Med J (KUMJ). 2003 Apr-Jun;1(2):110-2. PMID: 16388208.

***Corresponding author**: Prof. Ali Hassan A. Ali. E-mail: alihassan3750@yahoo.com, a.ali@psau.edu.sa*

International Journal of Biomedicine 15(4) (2025) 679-684
http://dx.doi.org/10.21103/Article15(4)_OA5

ORIGINAL ARTICLE

Surgery

INTERNATIONAL JOURNAL OF BIOMEDICINE

Clinical Features, Diagnostic Methods, and Treatment Approaches for Meckel's Diverticulum in Children and Adolescents: Experience of One Center

J. A. Djurayev [1,3], A. A. Ismatov[4], R. N. Ismailova[3], Sh. Z. Nizamxodjayev[3], M. A. G'aniyev[1], P. K. Sultanov [2,4*]

[1]*Republican Scientific Center of Emergency Medical Care, Tashkent, Uzbekistan*
[2]*Tashkent State Medical University, Tashkent, Uzbekistan*
[3]*Kimyo International University in Tashkent, Tashkent, Uzbekistan*
[4]*Republic Specialized Scientific-Practical Medical Center of Nephrology and Kidney Transplantation, Tashkent, Uzbekistan*

Abstract

Background: Meckel's diverticulum is one of the most common congenital anomalies of the gastrointestinal tract, which is often detected in children. This study aims to conduct a comparative analysis of the clinical manifestations of Meckel's diverticulum complications across different pediatric age groups, based on surgical interventions performed at the Emergency Medical Care Center.
Methods and Results: During the period from 2017 to 2024, at the Republican Scientific Center of Emergency Medical Care (RSCEMC), in the Department of Pediatric Emergency Surgery, surgical treatment was provided to 132 children and adolescents aged from 4 months to 18 years with various forms of complicated and uncomplicated Meckel's diverticulum. Taking into account the generally accepted pediatric age classification, the material was divided into three age groups: the infancy-to-toddler group (Group 1), from 4 months to 3 years – 39 (29.5%) children, mean age of 1.47±0.91 years; the early-to-middle childhood group (Group 2), 4–11 years – 64 (48.5%) patients, mean age of 8.6±2.29 years; the adolescence group (Group 3), 12–18 years – 29 (22%) children, mean age of 14.93±1.72 years. The study involved a retrospective analysis of patients' medical records, including clinical, instrumental, and laparoscopic methods.
The clinical manifestation of Meckel's diverticulum varies. In some cases, it mimics acute appendicitis, in others, acute intestinal obstruction, which depends on the patient's age and the time of admission from the onset of the disease. In children aged 0–3 years with gastrointestinal bleeding, Meckel's diverticulum is most often suspected. In children aged 0–3 years, when Meckel's diverticulum is suspected, it is advisable to begin the intervention with laparotomy, which is associated with a high proportion of complicated forms (diverticulitis, necrosis, intussusception). In older children, the choice of surgical access is determined by the clinical picture and the preliminary diagnosis. In children aged 4-11 years, it is more often possible to perform less traumatic interventions; complicated forms are less common; however, the diverticulum is frequently removed simultaneously with the appendix due to a similar clinical presentation. In adolescents aged 12-18 years, laparoscopic and combined interventions predominate, characterized by lower invasiveness; complicated forms are recorded much less frequently. (**International Journal of Biomedicine. 2025;15(4):679-684.**)

Keywords: Meckel's diverticulum • pediatric surgery • acute abdomen • complications

For citation: Djurayev JA, Ismatov AA, Ismailova RN, Nizamxodjayev ShZ, G'aniyev MA, Sultanov PK. Clinical Features, Diagnostic Methods, and Treatment Approaches for Meckel's Diverticulum in Children and Adolescents: Experience of One Center. International Journal of Biomedicine. 2025;15(4):679-684. doi:10.21103/Article15(4)_OA5

Introduction

Meckel's diverticulum is a congenital anomaly of the vitelline duct of the ileum.[1,2] First described in 1809 by the German anatomist J. Meckel, it resembles the vermiform appendix in shape. The prevalence of this pathology is about 2–3% in the general population, and it is most frequently identified in children and adolescents.[3] The diverticulum can

present in various forms, but most commonly appears as a protrusion of the ileal wall on the antimesenteric border, with a free communication to the intestinal lumen.[1] The clinical presentation of Meckel's diverticulum can vary widely, ranging from an asymptomatic course to serious complications such as gastrointestinal bleeding, intussusception, Meckelitis (intestinal inflammation), intestinal obstruction, or perforation.[3-5] Therefore, timely diagnosis and appropriate management are crucial in preventing complications of Meckel's diverticulum.

This study aims to conduct a comparative analysis of the clinical manifestations of Meckel's diverticulum complications across different pediatric age groups, based on surgical interventions performed at the Emergency Medical Care Center.

Materials and Methods

During the period from 2017 to 2024, at the Republican Scientific Center of Emergency Medical Care (RSCEMC), in the Department of Pediatric Emergency Surgery, surgical treatment was provided to 132 children and adolescents aged from 4 months to 18 years with various forms of complicated and uncomplicated Meckel's diverticulum. Taking into account the generally accepted pediatric age classification, the material was divided into three age groups: the infancy-to-toddler group (Group 1), from 4 months to 3 years – 39 (29.5%) children, mean age of 1.47±0.91 years; the early-to-middle childhood group (Group 2), 4–11 years – 64 (48.5%) patients, mean age of 8.6±2.29 years; the adolescence group (Group 3), 12–18 years – 29 (22%) children, mean age of 14.93±1.72 years. Among them, boys accounted for 99 (75%), which confirms the higher incidence of this pathology in males, whereas girls accounted for 33 (25%). The study involved a retrospective analysis of patients' medical records, including clinical, instrumental, and laparoscopic methods, and statistical analysis using IBM SPSS Statistics 23, with descriptive statistics applied. Baseline characteristics were summarized as frequencies and percentages for categorical variables. Group comparisons concerning categorical variables were performed using chi-square or Fisher's exact tests. A *P*-value of < 0.05 was considered statistically significant.

Results

According to data from the Statistics Department of the RSCEMC, a total of 107,976 emergency and delayed surgeries were performed from 2017 to 2024, of which 16,095 were performed in the Pediatric Surgery Department (Fig. 1).

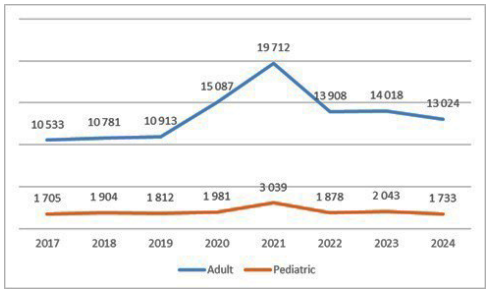

Fig. 1. *Number of surgeries at the RSCEMC in the Department of General Surgery and the Department of Pediatric Surgery for 2017–2024.*

From the analyzed surgical intervention data at the RSCEMC, surgeries performed due to complications of Meckel's diverticulum accounted for 0.82% (Fig. 2).

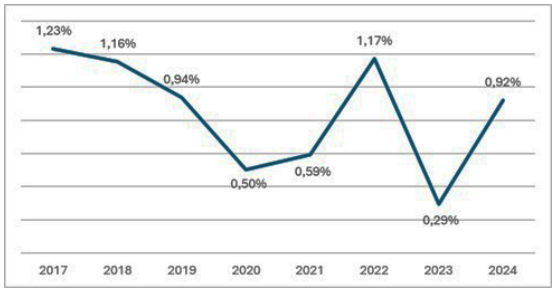

Fig. 2. *Dynamics of surgeries for complications of Meckel's diverticulum in children by year.*

In our series, the clinical presentation of Meckel's diverticulum was nonspecific, and most often patients were admitted under the guise of other acute surgical diseases of the abdominal cavity, including symptoms of complications of an undiagnosed underlying condition (Table 1).

Table 1.

Preoperative diagnosis in patients with Meckel's diverticulum.

Preoperative diagnosis	Group 1 n=39	Group 2 n=64	Group 3 n=29	*P-value*
Meckel's diverticulum			1 (3.4%)	
Bleeding from Meckel's diverticulum	15 (38.5%)	13 (20.3%)	3 (10.3%)	0.018
Acute appendicitis	7 (17.9%)	36 (56.3%)	12 (41.4%)	0.001
Acute intestinal obstruction	13 (33.3%)	9 (14.1%)	12 (41.4%)	0.009
Gastrointestinal bleeding of unknown etiology	2 (5.1%)	2 (3.1%)		>0.05
Peritonitis of unknown etiology		1 (1.6%)	1 (3.4%)	>0.05
Abscess of the abdominal cavity		2 (3.1%)		
Strangulated hernia: (inguinal and umbilical)	2 (5.1%)			
Colon developmental anomaly. Rectal form of Hirschsprung's disease Meckel's diverticulum		1 (1.6%)		

Bleeding from Meckel's diverticulum was found in 38.5%, 20.3% and 10.3% of patients in Groups 1, 2, and 3, respectively. The assumption of bleeding from Meckel's diverticulum was based on the following diagnostic signs: absence of a bleeding source in the large intestine during colonoscopy, absence of pathological changes in the stomach and duodenum on esophagogastroduodenoscopy, and presence of fresh blood in the terminal ileum during ileoscopy. In Group 1, complications of Meckel's diverticulum mainly manifested with symptoms of acute intestinal obstruction (33.3%) and

acute appendicitis (17.9%). In contrast, in Groups 2 and 3, the symptoms of acute appendicitis (56.3% and 41.4%, respectively) predominated over the symptoms of acute intestinal obstruction (14.4% and 41.4%, respectively). This may be explained by the fact that in younger children, Meckel's diverticulum is more often complicated by intussusception or perforation due to the smaller diameter of the ileal lumen, immaturity of the intestinal neuromuscular apparatus, and rapid development of mucosal edema and inflammation. These pathophysiological features contribute to the early onset of mechanical intestinal obstruction. In older age groups, by contrast, the inflammatory process in the diverticulum is more localized, mimicking acute appendicitis clinically. In addition, in older children, compensatory mechanisms of intestinal motility are better developed, and the ability to subjectively describe pain is more pronounced, facilitating differential diagnosis from obstructive forms of the disease.

The surgical approach depended on the preoperative diagnosis. In cases with a precise diagnosis of Meckel's diverticulitis, laparotomy was performed. If there were signs of bleeding, surgery was initiated laparoscopically, or laparotomy was performed. If acute appendicitis was suspected, surgery began with a McBurney incision, either laparoscopy or laparotomy. In the presence of clinical signs of acute intestinal obstruction, laparotomy was performed in most cases. In Group 1, the most common surgical approach for Meckel's diverticulitis was laparotomy (51.3%), compared with 26.6% and 34.5% in Groups 2 and 3, respectively (P=0.039) (Table 2). McBurney's incision was performed in 37.5% of cases in Group 2, and in 17.2% and 12.8% in Groups 3 and 2, respectively (P=0.010). In cases in which the operation was initiated laparoscopically, conversion to laparotomy was required in 28.2% of Group 1, 20.3% of Group 2, and 31.0% of Group 3 (P=0.466). In children under 3 years of age in Group 1, only one case was laparoscopic, in which a simple diverticulectomy was performed.

Table 2.

Surgical approach in the study groups.

Surgical approach	Group 1 n=39	Group 2 n=64	Group 3 n=29	*P-value*
McBurney's incision	5 (12.8%)	24 (37.5%)	5 (17.2%)	0.010
McBurney incision → → Laparotomy		1 (1.6%)		
Laparoscopy	1 (2.6%)	9 (14.1%)	5 (17.2%)	0.107
Laparoscopy → → Laparotomy	11 (28.2%)	13 (20.3%)	9 (31.0%)	0.466
Laparotomy	20 (51.3%)	17 (26.6%)	10 (34.5%)	0.039
Access through a strangulated hernia	2 (5.1%)			

Table 3 shows that in Group 1, the most common operation was laparotomy with diverticulectomy (28.2%), with a high proportion of bowel resection with anastomosis (25.6%) and bowel resection with ileostomy (12.8%), which indicates severe complications (gangrene, perforation, intussusception). Laparoscopy was performed in only 1 case (2.6%). In Group 2, the most frequent operations were laparotomy with diverticulectomy (26.6%) and appendectomy with diverticulectomy through the McBurney approach (28.1%). A smaller number of bowel resections were performed (6.3% with anastomosis, 4.7% with ileostomy). Laparoscopy was used more often than in the younger group (14.1% vs. 2.6%). In Group 3, the most significant proportion of laparoscopic interventions was observed (17.2%). Laparotomy with diverticulectomy accounted for 20.7%, which was lower than in Groups 1 and 2. Bowel resections were less common, but in cases of complications, they were performed both with anastomosis (10.3%) and with ileostomy (13.8%). A greater number of combined operations were noted (for example, appendectomy + diverticulectomy).

Table 3.

Types of operations performed in the study groups.

Operation	Group 1 n=39	Group 2 n=64	Group 3 n=29	*P-value*
McBurney. Appendectomy (diverticulum unchanged)		1 (3.1%)	1 (3.4%)	>0.05
McBurney. Appendectomy. Diverticulectomy	4 (10.3%)	18 (28.1%)	4 (13.8%)	0.056
McBurney. Appendectomy. Bowel resection with anastomosis.	1 (2.6%)	5 (7.8%)		>0.05
Laparoscopy. Diverticulectomy		5 (7.8%)	5 (17.2%)	>0.05
Laparoscopy. Appendectomy. Diverticulectomy.	1 (2.6%)	4 (6.3%)		>0.05
Laparotomy. Diverticulectomy	11 (28.2%)	17 (26.6%)	6 (20.7%)	0.766
Laparotomy. Appendectomy. Diverticulectomy.	3 (7.7)	2 (3.1%)	6 (20.7%)	0.018
Laparotomy. Bowel resection with anastomosis	10 (25.6%)	4 (6.3%)	3 (10.3%)	0.015
Laparotomy. Bowel resection with ileostomy	5 (12.8%)	3 (4.7%)	4 (13.8%)	0.231
Laparotomy. Appendectomy. Bowel resection with anastomosis.		2 (6.3%)		
Laparotomy. Intestinal disinvagination. Diverticulectomy	1 (2.6%)	3 (4.7%)		>0.05
Laparotomy. Diverticulectomy. Abdominoperineal procto-plasty with extraperitoneal resection of the colon with application of end-to-end colon-colonic anastomosis according to Swenson-Hiath-Isakov		1 (6.1%)		
Herniotomy. Diverticulectomy.	2 (5.1%)			

A comparative analysis of surgical interventions in children of different age groups revealed the following:

- •Laparotomy with diverticulectomy is the most common operation in all groups, but the proportion decreases with age (28.2% → 26.6% → 20.7%).
- •Appendectomy with diverticulectomy through the McBurney approach is more common in the early-to-

middle childhood group (28.1%), less in the infancy-to-toddler group (10.3%), and the adolescence group (13.8%).
•Bowel resection with anastomosis is typical mainly for the infancy-to-toddler group (25.6%) (*P*=0.015).
•Laparoscopy proportion increases with age (2.6% → 7.8% → 17.2%).

In Group 1, the most common postoperative diagnosis was bleeding from Meckel's diverticulum (38.5%), which confirms the anatomical and physiological features in younger children (thin mucosa, tendency to peptic ulcers) (Table 4). Acute catarrhal Meckel's diverticulum (28.2%), intussusception (7.7%) (Fig. 3), and strangulated intestinal obstruction (7.7%) indicated a severe course of complications. In Group 2, the leading diagnosis was phlegmonous Meckel's diverticulum (20.3%) and gangrenous Meckel's diverticulum (Fig. 4) (18.8%), reflecting more pronounced inflammatory complications. Catarrhal changes were rare (6.3%). Bleeding was detected in 20.3% of patients, a rate lower than in younger children. The incidence of intestinal obstruction decreased sharply, but isolated cases of strangulated intestinal obstruction (1.6%) and obstructive intestinal obstruction (3.1%) were noted. In Group 3, acute catarrhal Meckel's diverticulum (34.5%) (Fig. 5) and adhesive intestinal obstruction (20.7%) were more common, which were absent in the younger groups. Gangrenous Meckel's diverticulum was noted in 13.8% of adolescents, which was lower than in the early-to-middle childhood group. No bleeding was recorded in this group.

Table 4.

Postoperative diagnosis in the study groups.

Postoperative diagnosis	Group 1 n=39	Group 2 n=64	Group 3 n=29	*P-value*
Acute catarrhal Meckel's diverticulum	11 (28.2%)	4 (6.3%)	10 (34.5%)	0.001
Phlegmonous Meckel's diverticulum	4 (10.3%)	13 (20.3%)	2 (6.9%)	0.158
Gangrenous Meckel's diverticulum		12 (18.8%)	4 (13.8%)	0.558
Simple (unchanged) Meckel's diverticulum	6 (15.4%)	13 (20.3%)	9 (31.0%)	0.287
Acute appendicitis	9 (23.1%)	33(51.6%)	11 (37.9%)	0.016
Strangulated intestinal obstruction	3 (7.7%)	1 (1.6%)	4 (13.8%)	0.064
Obstructive intestinal obstruction	1 (2.6%)	2 (3.1%)		
Adhesive intestinal obstruction			6 (20.7%)	
Intussusception	3 (7.7%)	2 (3.1%)	1 (3.4%)	0.530
Meckel's diverticulum bleeding	15 (38.5%)	13 (20.3%)		0.045

A comparative analysis of postoperative diagnosis in children of different age groups revealed the following:

•Bleeding from Meckel's diverticulum is characteristic predominantly of the infancy-to-toddler group (38.5%), whereas it does not occur in the adolescence group (*P*=0.045).
•Phlegmonous and gangrenous forms were more frequently diagnosed in the early-to-middle childhood group (20.3% and 18.8%, respectively), confirming the age-related features of the inflammatory response.
•Acute catarrhal Meckel's diverticulum predominated in the infancy-to-toddler group (28.2%) and adolescence group (34.5%), but it was less common in the early-to-middle childhood group (6.3%) (*P*=0.001)
•Intestinal obstruction in the infancy-to-toddler group was represented by strangulation/intussusception (7.7%/2.6%), while in the adolescence group, adhesive intestinal obstruction was predominant (20.7%), indicating different mechanisms of complications.
•A simple (unchanged) diverticulum was found in all groups (15.4% in Group 1, 20.3% in Group 2, 31.0% in Group 3), without statistically significant differences.

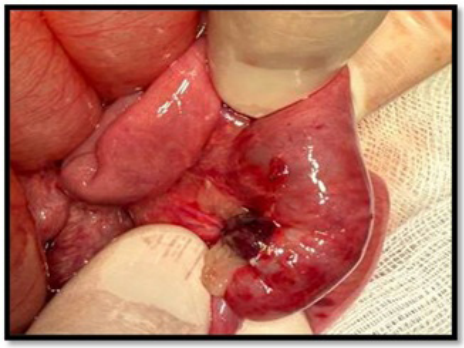

Fig. 3. *Intussusception of Meckel's diverticulum.*

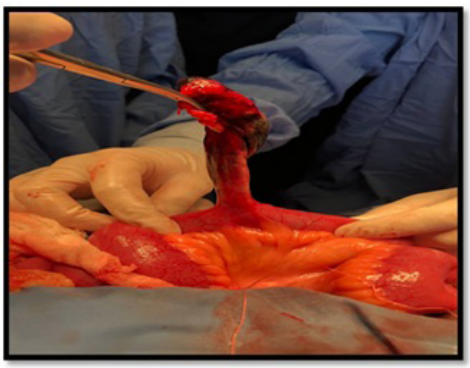

Fig. 4. *Gangrenous form of Meckel's diverticulitis.*

Fig. 5. *Catarrhal form of Meckel's diverticulitis.*

Discussion

According to several authors,[6,7] in children aged 0–3 years, performing a complete examination and establishing an accurate diagnosis in cases of "acute abdomen" is difficult. This is associated with the nonspecific nature of the clinical picture, the inability to fully communicate with the child, the rapid development of complications, and challenges in interpreting instrumental data due to the anatomical and physiological characteristics of the pediatric organism. Meckel's diverticulum often manifests only with signs of acute intestinal obstruction or internal bleeding, which significantly complicates differential diagnosis. Since preoperative diagnosis is virtually impossible, children frequently present to emergency surgical departments with suspected acute abdominal pathology. Indications for surgery most commonly include complicated forms of the diverticulum, such as inflammation mimicking appendicitis, gastrointestinal bleeding of unknown origin, the presence of free intraperitoneal air due to perforation, or intestinal obstruction.

In children aged 0–3 years, the preoperative diagnosis of Meckel's diverticulum coincided with the intraoperative finding in only 38.5% of cases. Almost always, this was associated with the presence of gastrointestinal bleeding, which prompted surgeons to suspect this pathology. In other cases, the clinical picture mimicked other acute surgical diseases of the abdominal cavity — primarily acute intestinal obstruction (33.3%) and acute appendicitis (17.9%). This confirms that in children of the infancy-to-toddler group, complicated forms of the diverticulum prevail, often requiring emergency bowel resection or ileostomy formation. Similar data are presented in a study by St-Vil et al.[8] In children under 4 years, intestinal obstruction, bleeding, and intussusception predominated, requiring more radical interventions.[8] In our study, the infancy-to-toddler group also showed a severe course and a high frequency of resections.

In adolescents (12–18 years), the concordance between the preoperative diagnosis and intraoperative findings was 13.7%. Despite the formally lower percentage, clinical diagnosis in this group was facilitated by clearer symptomatology, the possibility of using an extended set of instrumental methods (ultrasound, CT, laparoscopy), and a complete medical history. For this age group, the predominance of acute appendicitis (41.4%) and intestinal obstruction (41.4%) was characteristic, which allowed for a more targeted choice of surgical access already at the planning stage. At the same time, an increase in the proportion of laparoscopic interventions (up to 17.2%) was noted, which coincides with the conclusions of Shalaby et al.,[9] who demonstrated that laparoscopy for Meckel's diverticulum in children is safe, effective, and provides accurate diagnosis and treatment with minimal trauma and rapid recovery. Similarly, St-Vil et al.[8] noted that, in adolescents, less complex forms were more common, and laparoscopic access was used more frequently—a pattern that aligns fully with our results for Group 3.

Special attention should be given to the early-to-middle childhood group (4–11 years), where the concordance between preoperative and intraoperative diagnoses was observed in 20.3% of cases. In this cohort, the clinical picture most often resembled acute appendicitis (more than 50%), which explains the high percentage of combined interventions — removal of Meckel's diverticulum together with the appendix. Such a tactic allows the simultaneous elimination of both potential sources of inflammation and pain, reducing the risk of future repeat operations. This finding is consistent with data from a monographic review by Nissen et al.,[10] which indicated that in 62% of patients, the diagnosis was established before age 5, with obstruction (41%) and bleeding (27%) predominating. In older age groups, severe manifestations were less common, as evidenced in our study: in Group 1, bleeding and complications predominated, whereas in Groups 2 and 3, the proportion of severe forms was significantly lower.

Thus, the obtained data convincingly demonstrate that the patient's age decisively influences the clinical course and diagnostic accuracy in Meckel's diverticulum. In younger children, the disease predominantly presents in a complicated form, which complicates preoperative diagnosis and requires a more aggressive surgical approach (resections, open interventions). In adolescents, the proportion of laparoscopic and combined interventions increases, and preoperative diagnosis becomes more accurate as instrumental capabilities expand. The presented patterns are entirely consistent with the results of St-Vil et al., Shalaby et al., and Nissen et al.,[8-10] which confirm the reliability and reproducibility of our observations.

Conclusions

- The clinical manifestation of Meckel's diverticulum varies. In some cases, it mimics acute appendicitis, in others, acute intestinal obstruction, which depends on the patient's age and the time of admission from the onset of the disease.
- In children aged 0–3 years with gastrointestinal bleeding, Meckel's diverticulum is most often suspected.
- In children aged 0–3 years, when Meckel's diverticulum is suspected, it is advisable to begin the intervention with laparotomy. In contrast, in older children, the choice of surgical access is determined by the clinical picture and the preliminary diagnosis.
- In children aged 0–3 years, open surgeries predominate, which is associated with the high proportion of complicated forms (diverticulitis, necrosis, intussusception).
- In children aged 4-11 years, it is more often possible to perform less traumatic interventions; complicated forms are less common; however, the diverticulum is frequently removed simultaneously with the appendix due to a similar clinical presentation.
- In adolescents aged 12-18 years, laparoscopic and combined interventions predominate, characterized by lower invasiveness; complicated forms are recorded much less frequently.

Ethical Approval

This study was approved by the Ministry of Health of the Republic of Uzbekistan Ethical Committee (Approval No. 4/11-1878, dated 01.11.2025).

Competing Interests

The authors declare that they have no financial/ commercial conflicts of interest concerning this article.

References

1. Grona VN, Litovka VK, Zhurilo IP, Sopov GA, Vesely SV, K.V. Latyshov KV, Poshekhonov AS. [Acute bleeding into the lumen of the alimentary canal in children]. Child Health. 2010;4(28):30-32. [Article in Russian].
2. Isakov YuF, Dronov AF. Pediatric surgery: national guidelines. GEOTAR, Moscow. 2009. (In Russian)
3. Акilov HA, Djabbarov DA, Urmanov NT, Asadov ShY. Complete purulent fusion of Meckel's diverticulum, complicated by purulent-fibrinous peritonitisъ. Bulletin of Emergency Medicine. 2012.(3);56-57. [Article in Russian].
4. Snyder CL. Current management of umbilical abnormalities and related anomalies. Semin Pediatr Surg. 2007 Feb;16(1):41-9. doi: 10.1053/j.sempedsurg.2006.10.006. PMID: 17210482.
5. Yarustovsky PM. Laparoscopy in the diagnosis and treatment of Meckel diverticulum in children. Author's abstract. PhD Abstract. M. 2007. (In Russian)
6. Lin XK, Huang XZ, Bao XZ, Zheng N, Xia QZ, Chen CD. Clinical characteristics of Meckel diverticulum in children: A retrospective review of a 15-year single-center experience. Medicine (Baltimore). 2017 Aug;96(32):e7760. doi: 10.1097/MD.0000000000007760. PMID: 28796070; PMCID: PMC5556236.
7. Yusupov ShA, Atakulov JO, Mukhammadiev AA. Meckel's diverticulum: diagnostic and surgical criteria. Russian Bulletin of Pediatric Surgery, Anesthesiology and Resuscitation, 2020;10(3S). [Article in Russian].
8. St-Vil D, Brandt ML, Panic S, Bensoussan AL, Blanchard H. Meckel's diverticulum in children: a 20-year review. J Pediatr Surg. 1991 Nov;26(11):1289-92. doi: 10.1016/0022-3468(91)90601-o. PMID: 1812259.
9. Shalaby RY, Soliman SM, Fawy M, Samaha A. Laparoscopic management of Meckel's diverticulum in children. J Pediatr Surg. 2005 Mar;40(3):562-7. doi: 10.1016/j.jpedsurg.2004.11.032. PMID: 15793736.
10. Nissen M, Sander V, Rogge P, Alrefai M, Tröbs RB. Meckel's Diverticulum in Children: A Monocentric Experience and Mini-Review of Literature. Children (Basel). 2022 Jan 1;9(1):35. doi: 10.3390/children9010035.

***Corresponding author**: Dr. Pulat Sultanov, MD, PhD, DSc. E-mail: sultanovpk@gmail.com*

International Journal of Biomedicine 15(4) (2025) 685-689
http://dx.doi.org/10.21103/Article15(4)_OA6

ORIGINAL ARTICLE

Radiology

INTERNATIONAL JOURNAL OF BIOMEDICINE

Dosimetric Evaluation of 3D-CRT and IMRT Treatment Techniques in Medulloblastoma

Blerim Rrakaqi[1,3], Ervis Telhaj[2], Besim Xhafa[1], Ylli Kaçiu[3*], Armend Jashari[1,3*], Ramiz Ukaj[1,3]

[1]*Alma Mater Europae Campus College "REZONANCA," Prishtina, Kosovo*
[2]*Western Balkans University, Tirana, Albania*
[3]*University Clinical Center of Kosovo, Prishtina, Kosovo*

Abstract

A primitive neuroectodermal tumor (PNET) of the cerebellum, called medulloblastoma, is an aggressive, fast-growing brain tumor. This study aims to compare the dosimetric distribution of two radiotherapy techniques—three-dimensional conformal radiation therapy (3D-CRT) and intensity-mod ulated radiation therapy (IMRT)—in patients with medulloblastoma by evaluating planning target volume (PTV) and exposure of organs at risk (OARs).

In a 15-year retrospective analysis, considerable number of patients (aged 3–30 years) initially treated with 3D-CRT and subsequently with IMRT (volumetric modulated arc therapy is now used but not included in this comparison) were evaluated. Treatment plans were created in the planning system using the Monte Carlo Convolution/Superposition algorithm. Dose distributions were assessed via dose–volume histograms, and the maximum doses received by the hippocampus, brainstem, and spinal cord were compared between the two techniques.

Both 3D-CRT and IMRT achieved complete coverage of the PTV. IMRT demonstrated a significant reduction in dose to critical structures, thereby lowering the risk of neurocognitive and endocrine side effects, whereas 3D-CRT delivered higher radiation levels to surrounding normal tissues. Average treatment times for IMRT were approximately 20–30% longer than for 3D-CRT. IMRT provides a more conformal dose distribution, with enhanced protection of OAR, potentially permitting higher tumor doses and improved long-term outcomes in pediatric patients. However, the choice between 3D-CRT and IMRT should be made on a case-by-case basis, taking into account the contour delineation, technical availability, and the patient's tolerance for treatment duration. (**International Journal of Biomedicine. 2025;15(4):685-689.**)

Keywords: medulloblastoma • 3D-CRT • IMRT

For citation: Rrakaqi B, Telhaj E, Xhafa B, Kaçiu Y, Jashari A. Ukaj R. Dosimetric Evaluation of 3D-CRT and IMRT Treatment Techniques in Medulloblastoma. International Journal of Biomedicine. 2025;15(4):685-689. doi:10.21103/Article15(4)_OA6

Abbreviations

3D-CRT, three-dimensional conformal radiation therapy; **CSI**, craniospinal irradiation; **CT**, computer tomography; **CTV**, clinical target volume; **GTV**, gross tumor volume; **IMRT**, intensity-modulated radiation therapy; **MRI**, magnetic resonance imaging; **OAR**, organ at risk; **PTV**, planning target volume; **VMAT**, volumetric modulated arc therapy.

Introduction

Medulloblastoma is the most common malignant brain tumor in children, accounting for approximately 20% of all pediatric brain tumors. Any patient presenting with neurological symptoms should undergo a complete evaluation, including a neurological examination. If a brain tumor is suspected, the patient is typically referred for brain imaging.

Neuroimaging plays a key role in the diagnosis and assessment of medulloblastoma dissemination. Magnetic resonance imaging (MRI) and computed tomography (CT)

provide detailed images of the brain and spinal cord, enabling the detection of tumors and their anatomical relationships to surrounding structures.[1,2]

In pediatric patients, contrast administration improves lesion visualization, and sedation may be required to obtain high-quality images. In rare cases, a medulloblastoma or another primitive neuroectodermal tumor (PNET) can be detected by prenatal ultrasound.[3]

Some early studies suggested that the diagnosis could be established solely based on imaging without the need for a biopsy.[1,2,3] However, according to the WHO Classification of CNS Tumours 2021 and SIOP-Europe 2023 guidelines, final diagnosis requires histopathological verification and molecular characterization, which are essential for accurate risk stratification and optimal treatment planning.

The modern classification system divides medulloblastomas into four main molecular groups: WNT-activated – very favorable prognosis; often eligible for reduced CSI dose, HH-activated, TP53-wildtype – intermediate prognosis, SHH-activated, TP53-mutant – poor prognosis; often treatment-resistant, Non-WNT/Non-SHH – includes Group 3 and Group 4, with diverse molecular profiles and prognoses.[4,5]

This molecular classification, combined with histological and clinical features, has enabled a more personalized approach to treatment.

Radiotherapy, combined with surgery and chemotherapy, is a cornerstone in the management of medulloblastoma. For standard-risk patients, this multimodal approach achieves 5-year survival rates of 75–85%.[1] Age is a key factor in risk stratification: patients under 3 years of age are treated with specific protocols to avoid or reduce craniospinal irradiation due to the high risk of long-term side effects.

One of the most common and detrimental late effects of treatment is neurocognitive decline, which is directly related to the radiation dose delivered to the brain.[6,7] The hippocampus and temporal lobes are critical structures for memory formation and cognitive function. Studies in both animal models and patients have demonstrated that radiation-induced disruption of hippocampal neurogenesis leads to significant cognitive deficits.

For this reason, modern radiotherapy techniques such as intensity-modulated radiation therapy (IMRT), volumetric modulated arc therapy (VMAT), and proton therapy are increasingly used to limit the dose to critical structures while maintaining tumor control. Hippocampal-sparing craniospinal irradiation (CSI) is an emerging strategy designed to reduce the risk of long-term cognitive impairment.

In standard treatment, craniospinal irradiation (CSI) is delivered at a dose of 23.4–36 Gy, followed by a boost to the posterior fossa up to 54–55.[8] Gy.1,7 Typical margins for the gross tumor volume (GTV) and clinical target volume (CTV) range from 0.5cm to 1.5 cm, with an additional 0.5 cm added to generate the planning target volume (PTV). In WNT-activated and standard-risk patients, protocols with reduced CSI doses are being investigated to minimize toxicity without compromising survival.

Methodology

Over 15 years at our center, a considerable number of patients diagnosed with primitive neuroectodermal tumors (PNET), including medulloblastoma, were treated. The patients' ages ranged from 3 to 30 years, encompassing both pediatric and young adult populations. Initially, treatments were delivered using the three-dimensional conformal radiation therapy (3D-CRT) technique, followed by the introduction of IMRT, and more recently, VMAT.[8] Since the majority of treatments (about 90%) were performed using either 3D-CRT or IMRT, the present study focuses on a comparative evaluation of these two techniques using representative clinical cases. Both 3D-CRT and IMRT are established modalities in the treatment of medulloblastoma; however, they differ in terms of dose distribution, organ-at-risk sparing, acute and late toxicity profiles, and potential long-term outcomes (Table 1).[9-13]

Table 1.

Comparative features of IMRT and 3D-CRT in the treatment of medulloblastoma.

Feature	IMRT	3D-CRT	Notes / Evidence
Precision	Higher precision with inverse planning; better dose sculpting around the PTV and improved conformity	Less precise; often results in higher dose to surrounding healthy tissue	Difference most pronounced in boost fields; less marked in large-field CSI
Dose to normal tissue	Potentially reduces mean dose to brain, cochlea, and spinal cord when OAR constraints are applied	Higher dose to adjacent normal tissues; limited sparing capacity	IMRT may increase low-dose bath (V5–V10) to larger body volumes
Toxicity	Lower potential risk of neurocognitive decline, ototoxicity, and endocrine dysfunction when OAR sparing is implemented	Higher incidence of late effects, especially neurocognitive and endocrine toxicity	Benefits depend on plan quality; CSI without hippocampal/cochlear sparing may show minimal difference
Effectiveness	Similar tumor control compared to 3D-CRT; better quality-of-life outcomes when sparing OARs	Effective tumor control but with a higher risk of late toxicities	No survival advantage demonstrated for IMRT
Use in CSI	May allow better sparing of critical organs (thyroid, esophagus, cochlea); requires more complex planning and QA	Standard CSI technique historically; exposes more normal tissue to moderate–high doses	IMRT/VMAT CSI more sensitive to setup errors; requires daily IGRT

For pediatric patients, IMRT is often preferred due to its ability to reduce radiation dose to developing brain structures, the cochlea (lowering the risk of hearing loss), and endocrine glands, thereby reducing the risk of long-term neurocognitive, auditory, and hormonal dysfunction.[9,11] IMRT achieves highly conformal dose distributions, precisely targeting the PTV while minimizing exposure to organs at risk (OARs).

3D-CRT remains in routine use, especially for craniospinal irradiation (CSI), due to its simplicity, robustness, and effectiveness in covering the entire neuroaxis. This technique delivers a uniform dose across large target volumes but provides less sparing of OARs compared to IMRT or proton therapy, resulting in higher radiation exposure to normal tissues.[15,16,17]

For this study, treatment plans were created using both techniques for comparative purposes. Dose–volume histograms (DVHs) were generated, and dose metrics for the PTV and all relevant OARs were analyzed to identify potential advantages and disadvantages of each approach.

All patients undergo immobilization using pediatric thermoplastic masks and vacuum cushions. Simulation CT scans encompass the entire craniospinal axis with slice thicknesses of 1–2 mm. Target volumes are contoured according to international pediatric radiotherapy guidelines (SIOP-Europe, 2023).

Stage 1 – CSI: Standard-risk patients typically receive 23.4–36 Gy to the craniospinal axis, while high-risk patients may receive up to 36 Gy, depending on age and risk profile.

Stage 2 – Boost An additional 15–20 Gy is delivered to the posterior fossa or tumor bed, bringing the total dose to \~54–55.8 Gy for standard-risk cases.

For low-risk WNT-activated patients, dose de-escalation to 18–23.4 Gy CSI is considered, as per current protocols.

"Step-by-step" or "moving junction" techniques are applied for 3D-CRT CSI to avoid overdose/underdose at field junctions. IMRT/VMAT CSI eliminates the need for manual junction shifts.

All patients are managed within a multidisciplinary pediatric oncology team comprising radiation oncologists, neurosurgeons, pediatric oncologists, anesthesiologists, medical physicists, and radiation therapists.

Surgery: Maximal safe resection is performed before radiotherapy to obtain histopathological and molecular diagnosis and to debulk the tumor.

Chemotherapy: Administered pre- or post-radiotherapy in high-risk patients, those under 3 years of age, or in relapsed disease. Standard regimens include vincristine, etoposide, carboplatin, and cyclophosphamide.

Patients are classified according to a combination of clinical, radiological, and molecular features:

Low-risk: Residual tumor <1.5 cm², negative CSF cytology, no metastases, favorable molecular subgroup (e.g., WNT-activated). Expected 5-year survival >75%.

High-risk: Age <4 years, disseminated disease, incomplete resection, unfavorable histology, or molecular subgroup (e.g., Group 3). Expected 5-year survival 35–50%.[5,17]

Method 1: In this study, the first treatment approach involved the use of 3D-CRT for a patient diagnosed with medulloblastoma. The craniospinal irradiation (CSI) dose was 36 Gy, delivered in three different sequential treatment plans within the same session each day. This approach was chosen to optimize target coverage and minimize the occurrence of hot spots. To ensure optimal and reproducible patient positioning, Civco blue vacuum cushions were used for immobilization. Treatment was delivered on an Elekta Synergy linear accelerator. For the secondary beams, a motorized wedge was employed to achieve the desired dose distribution and improve homogeneity across the target volume Figure 1.

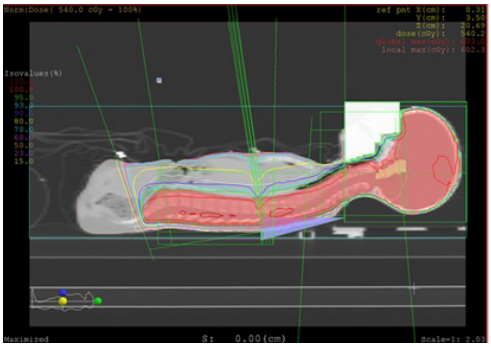

Fig. 1. *Medulloblastoma 3D-CRT treatment plans.*

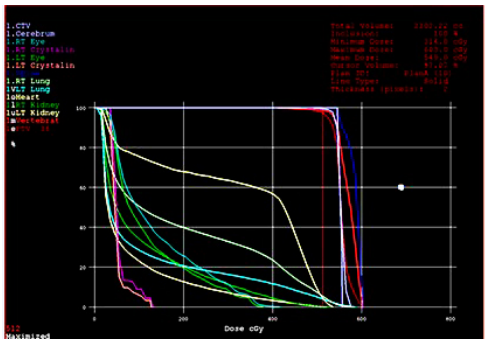

Fig. 2. *DVH for 3D-CRT medulloblastoma treatment.*

During treatment with this method, more precise results are expressed in the dose-volume histogram (Figure 2).

During 3D-CRT treatment for medulloblastoma, the minimum, maximum, and mean doses received by OARs were analyzed to assess their protection and exposure during therapy (Table 2).

Table 2.

The minimum, average, and maximum doses for OAR during 3D-CRT treatment.

Dose /OAR	Min Dose (cGy)	Max Dose (cGy)	Mean Dose (cGy)
Crystalline left	314	605	320
Crystalline right	314	605	320
Left Eye	310	605	335
Right Eye	310	605	330
Heart	320	605	550
Left Lung	314	610	350
Right Lung	315	610	350
Left Kidney	310	610	340
Right Kidney	310	610	340

The data show that the left and right crystalline lenses received a minimum dose of 314 cGy and a maximum dose of 605 cGy, with a mean dose of 320 cGy. The left and right eyes were exposed to minimum doses of 310 cGy and maximum doses of 605 cGy, with mean doses of 335 cGy and 330 cGy, respectively.

Regarding other vital organs, the heart received a relatively high mean dose of 550 cGy, ranging from 320 cGy to 605 cGy. The left and right lungs had minimum doses of \~314–315 cGy and maximum doses of 610 cGy, with equal mean doses of 350 cGy each. The left and right kidneys received minimum doses of 310 cGy and maximum doses of 610 cGy, with a mean dose of 340 cGy.

These results indicate that, although the dose distribution to the OARs was maintained within acceptable limits according to international protocols, there is considerable variability among the organs, with thoracic structures, such as the heart and lungs, being exposed to higher levels compared to ocular and renal structures. This dose profile is characteristic of 3D-CRT techniques, which provide uniform coverage of the target volume but have limitations in optimally sparing certain OARs compared to more advanced techniques such as IMRT or proton therapy.

Method 2: In this case, the IMRT technique was employed to maximize protection for OARs and surrounding healthy tissues. IMRT utilizes modulated beam intensities, enabling a non-uniform dose distribution, unlike the uniform distribution characteristic of 3D-CRT. This allows for the delivery of higher doses to the tumor target while minimizing exposure to OARs.[18,19]

IMRT is widely applied in the treatment of head and neck tumors. In the case of medulloblastoma, this technique enables precise dose escalation to the target volume, allowing delivery of up to 5600 cGy to the posterior fossa, while ensuring that doses to critical structures remain within recommended tolerance limits Figure 3.

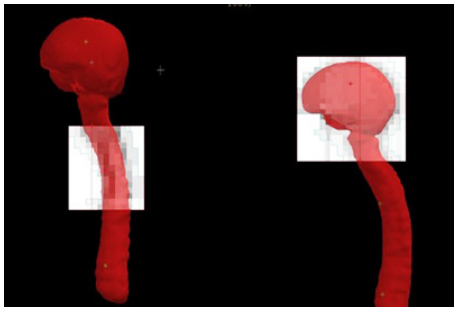

Fig. 3. *Delivery of radiation by IMRT beams.*

The IMRT treatment plan is delivered at multiple angles and divided into many small isodoses Figure 4.

During treatment with this method, more precise results are expressed in the dose-volume histogram (Figure 5).

Table 3 presents the minimum, maximum, and mean doses (in cGy) delivered to various OARs during IMRT for medulloblastoma. The crystalline lenses of both eyes received a maximum dose of 605–605 cGy, with a mean dose of 300 cGy, reflecting adequate sparing of these radiosensitive structures. The left and right eyes received similar maximum doses (605 cGy and 600 cGy, respectively) with mean doses limited to 300 cGy. The heart received a minimum dose of 220 cGy, a maximum dose of 605 cGy, and the highest mean dose among all OARs (≈350 cGy), indicating partial exposure due to its proximity to the inferior treatment fields. The left and right lungs showed maximum doses of 610 cGy and mean doses of 310–311 cGy, respectively. Renal exposure was kept minimal, with both kidneys receiving maximum doses of 600 cGy and mean doses limited to 300 cGy. Overall, the IMRT technique demonstrated effective dose modulation, ensuring OAR doses remained within clinically acceptable limits while optimizing target coverage.

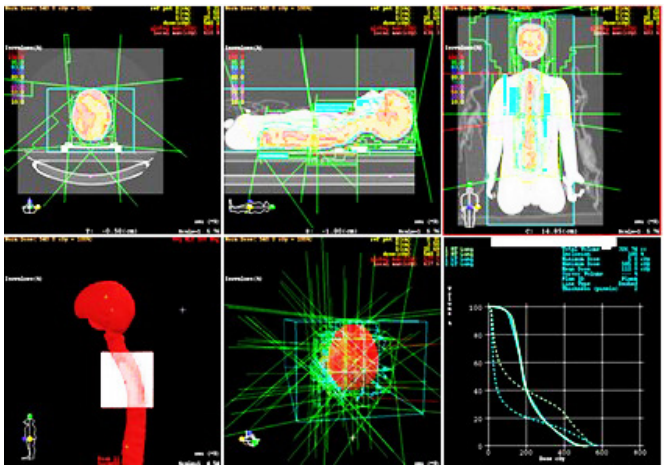

Fig. 4. *Medulloblastoma IMRT treatment plans.*

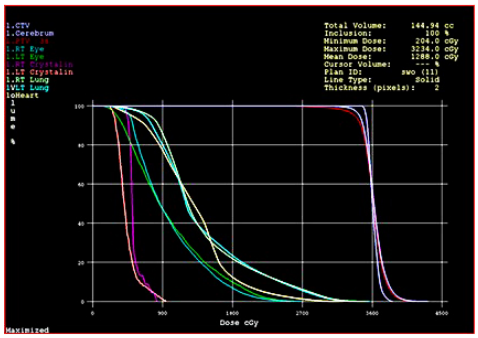

Fig. 5. *DVH for IMRT medulloblastoma treatment.*

Table 3.

The minimum, average, and maximum doses for OAR during IMRT treatment.

Dose /OAR	Min Dose (cGy)	Max Dose (cGy)	Mean Dose (cGy)
Crystalline left	300	600	300
Crystalline right	300	605	300
Left Eye	310	605	300
Right Eye	300	600	300
Heart	320	605	550
Left Lung	314	610	310
Right Lung	315	610	311
Left Kidney	310	600	300
Right Kidney	310	600	300

Conclusions

For a patient diagnosed with medulloblastoma, treatment plans were generated using both three-dimensional conformal radiotherapy (3D-CRT) and intensity-modulated radiation therapy (IMRT) techniques. In both approaches, the prescribed dose adequately covered the PTV. The plans were compared using dose–volume histograms (DVHs) and by evaluating the doses received by organs at risk (OARs).

This comparison aimed to evaluate the advantages and disadvantages of the two three-dimensional radiotherapy planning methods and to determine the optimal approach based on patient-specific characteristics, total prescribed dose to the PTV, and contour delineation defined by the radiation oncologist.

1. OAR sparing: IMRT provided superior protection for critical organs compared to 3D-CRT, resulting in lower expected side effects.

2. Dose escalation potential: Greater OAR sparing with IMRT may allow safe escalation of the tumor dose, potentially improving tumor control and clinical outcomes.

3. Treatment time: IMRT generally requires a more extended treatment delivery time compared to 3D-CRT.

The DVH comparison shows that for the same prescribed tumor dose, the OARs received lower radiation exposure with IMRT compared to 3D-CRT.

IMRT offers an optimized dose distribution for medulloblastoma by reducing radiation exposure to critical organs while maintaining effective tumor coverage. However, for craniospinal irradiation (CSI), proton therapy remains the most effective modality in reducing long-term toxicity.

3D-CRT, while capable of delivering a uniform dose to the craniospinal axis, exposes more normal tissue to radiation. It remains an effective and widely accessible technique, but when available, IMRT or proton therapy is preferred to reduce the risk of late side effects.

Conflicts of Interest

The authors declare that they have no competing interests.

References

1. Packer RJ, Goldwein J, Nicholson HS, Vezina LG, Allen JC, Ris MD, et al. Treatment of children with medulloblastomas with reduced-dose craniospinal radiation therapy and adjuvant chemotherapy: A Children's Cancer Group Study. J Clin Oncol. 1999 Jul;17(7):2127-36. doi: 10.1200/JCO.1999.17.7.2127.

2. Huber JF, Bradley K, Spiegler BJ, Dennis M. Long-term effects of transient cerebellar mutism after cerebellar astrocytoma or medulloblastoma tumor resection in childhood. Childs Nerv Syst. 2006 Feb;22(2):132-8. doi: 10.1007/s00381-005-1223-4.

3. Mulhern RK, Kepner JL, Thomas PR, Armstrong FD, Friedman HS, Kun LE. Neuropsychologic functioning of survivors of childhood medulloblastoma randomized to receive conventional or reduced-dose craniospinal irradiation: a Pediatric Oncology Group study. J Clin Oncol. 1998 May;16(5):1723-8. doi: 10.1200/JCO.1998.16.5.1723.

4. Louis DN, Perry A, Wesseling P, Brat DJ, Cree IA, Figarella-Branger D, et al. The 2021 WHO Classification of Tumors of the Central Nervous System: a summary. Neuro Oncol. 2021 Aug 2;23(8):1231-1251. doi: 10.1093/neuonc/noab106.

5. Louis DN, Perry A, Wesseling P, Brat DJ, Cree IA, Figarella-Branger D. et al. WHO Classification of Tumors Editorial Board. Central Nervous System Tumours (5th ed., Vol. 6). Lyon, France: International Agency for Research on Cancer, 2021. ISBN: 978-92-832-4508-7

6. Ris MD, Packer R, Goldwein J, Jones-Wallace D, Boyett JM. Intellectual outcome after reduced-dose radiation therapy plus adjuvant chemotherapy for medulloblastoma: a Children's Cancer Group study. J Clin Oncol. 2001 Aug 1;19(15):3470-6. doi: 10.1200/JCO.2001.19.15.3470. PMID: 11481352.

7. Spoudeas HA. Growth and endocrine function after chemotherapy and radiotherapy in childhood. Eur J Cancer. 2002 Sep;38(13):1748-59; discussion 1760-1. doi: 10.1016/s0959-8049(02)00169-7. PMID: 12175691.

8. Xhafa B, Telhaj E, Selimi F, Kaçiu Y, Elezaj N, Rrakaqi B. Utilizing the VMAT Technique for Treating Head and Neck Cancer with Fixed Collimator Jaws. International Journal of Biomedicine. 2024;14(3):474-477. doi: 10.21103/Article14(3)_OA14

9. Merchant TE, et al. Clinical and dosimetric advantages of IMRT for pediatric medulloblastoma. International Journal of Radiation Oncology • Biology • Physics. 2016;96(5), 985–992.

10. Murray L, et al. Dosimetric comparison of IMRT and 3D-CRT in craniospinal irradiation for medulloblastoma. Clinical Oncology. 2017;29(1):e21–e28.

11. Spampinato S, et al. IMRT vs 3D-CRT in pediatric brain tumors: Dosimetric and clinical results. Radiotherapy and Oncology. 2019;134:145–153.

12. Merchant TE, Li C, Xiong X, Kun LE, Boop FA, Sanford RA. Conformal radiotherapy after surgery for paediatric ependymoma: a prospective study. Lancet Oncol. 2009 Mar;10(3):258-66. doi: 10.1016/s1470-2045(08)70342-5.

13. Vogelius IR, Bentzen SM, Maraldo MV, Petersen PM, Specht L. Risk factors for radiation-induced hypothyroidism: a literature-based meta-analysis. Cancer. 2011 Dec 1;117(23):5250-60. doi: 10.1002/cncr.26186.

14. Vogelius IR, et al. Craniospinal irradiation with IMRT: Potential improvements and trade-offs. Acta Oncologica. 2011;50(3):370–378.

15. Carrie C, et al. Conformal radiotherapy after surgery for pediatric medulloblastoma. International Journal of Radiation Oncology • Biology • Physics. 1999:45(5), 927–938.

16. Goldwein JW. Advances in the radiotherapy of medulloblastoma. Cancer Treatment and Research. 1996;87:139–158.

17. Bailey S, Jacobs S, Kourti M, Massimino M, André N, Doz F, et al. Medulloblastoma therapy: Consensus treatment recommendations from SIOP-Europe and the European Research Network. EJC Paediatric Oncology.2025;5, 100205.

18. Telhaj E, Rrakaqi B, Xhafa B, Kaciu Y, Elezaj N. Dosimetry of Medical Linear and Its Use in The Treatment Planning System. J Surg Care. 2025;4(2), 01-05.

19. Telhaj E, Rrakaqi B, Xhafa B, Elezaj N, Kaçiu Y. Algorithmical Applications in the XiO Treatment Plan Based on Dosimetric Measurements. International Journal of Biomedicine. 2025;15(1):162-166. doi: 10.21103/Article15(1)_OA18

***Corresponding authors**:
Ylli Kaçiu: ylli.kaciu@gmail.com
Armend Jashari: armend.jashari@rezonanca-rks.com

International Journal of Biomedicine 15(4) (2025) 690-694
http://dx.doi.org/10.21103/Article15(4)_OA7

ORIGINAL ARTICLE

Radiology

INTERNATIONAL JOURNAL OF BIOMEDICINE

The Two-Dimensional Shear Wave Elastography (2D-SWE) in Assessing Abdominal Aortic Wall Stiffness

Salahaden R. Sultan[1*], Lojain Alsayegh[1], Hajer B. Almsaari[1], Mohammad Khalil[2], Abrar Alfatni[1], Reham Kaifi[3,4,5], Mohammed Alkharaiji[6], Adel Alzahrani[7], Mohammed Aslam[8]

[1]*Department of Radiologic Sciences, Faculty of Applied Medical Sciences, King Abdulaziz University, Jeddah, Saudi Arabia*
[2]*Department of Radiology, Faculty of Medicine, King Abdulaziz University, Jeddah, Saudi Arabia*
[3]*College of Applied Medical Sciences, King Saud bin Abdulaziz University for Health Sciences, Jeddah, Saudi Arabia*
[4]*King Abdullah International Medical Research Center, Jeddah, Saudi Arabia*
[5]*Medical Imaging Department, Ministry of the National Guard—Health Affairs, Jeddah, Saudi Arabia*
[6]*Department of Public Health, College of Health Sciences, Saudi Electronic University, Riyadh, Saudi Arabia*
[7]*Department of Diagnostic Radiology, King Abdullah Medical City, Makkah, Saudi Arabia*
[8]*Vascular Laboratory, Hammersmith Hospital, Imperial College NHS Healthcare Trust, London, UK*

Abstract

Background: Ultrasound elastography, a non-invasive imaging modality, holds promise for assessing tissue stiffness, offering potential applications in the evaluation of cardiovascular disease. This study aimed to quantify local stiffness of the abdominal aortic wall using two-dimensional shear wave elastography (2D-SWE) in adults without underlying medical conditions, and to evaluate its reproducibility.

Methods and Results:2D-SWE measurements of infra-renal posterior wall of the abdominal aorta (PWoAA) were obtained from 50 subjects. For intra- and inter-observer reproducibility, five 2D-SWE measurements of PWoAA were averaged, and the measurements were performed two times by observer A and once by observer B (n=750). Intraclass correlation coefficient (ICC) and Bland-Altman plot were used to establish bias and limit of agreement (LoA) between PWoAA elasticity measurements.

Ultrasound 2D-SWE of PWoAA was 3.87±0.99 kPa. Intra-observer agreement of PWoAA ultrasound 2D-SWE elasticity measurements was moderate with an ICC value of 0.69 (95% CI: 0.56–0.82, $P<0.001$). Bias in intra-observer measurements was 0.18±0.92 kPa (95% LoA: -1.62–1.99). Similarly, inter-observer agreement was moderate with an ICC value of 0.56 (95% CI: 0.22–0.75, $P=0.002$). Bias in inter-observer measurements was -0.02±1.09 kPa (95% LoA: -2.16–2.11). There was no significant difference in the 2D-SWE measurements of the aortic walls, both within the same observer (mean difference [MD] 0.17, 95% CI: 0.07–0.44, $P=0.16$)) and between two different observers (MD=0.02, 95% CI: 0.33–0.28, $P=0.86$).

Conclusion: Our findings demonstrated moderate reproducibility of ultrasound 2D-SWE in assessing abdominal aortic wall elasticity, with no significant differences within or between observers. Further research is warranted to optimize the clinical application of this method for assessing arterial wall stiffness, particularly in patients with cardiovascular disease, including those with abdominal aortic aneurysms.(**International Journal of Biomedicine. 2025;15(4):690-694.**)

Keywords: ultrasound elastography • 2D-SWE • aortic stiffness

For citation: Sultan SR, Alsayegh L, Almsaari HB, Khalil M, Alfatni A, Kaifi R, Alkharaiji M, Alzahrani A, Aslam M. The Two-Dimensional Shear Wave Elastography (2D-SWE) in Assessing Abdominal Aortic Wall Stiffness. International Journal of Biomedicine. 2025;15(4):690-694. doi:10.21103/Article15(4)_OA7

Abbreviations

AS, aortic stiffness; **ICC**, intraclass correlation coefficient; **LoA**, limit of agreement; **PWoAA**, posterior wall of the abdominal aorta.

Introduction

Aortic stiffness (AS) characterizes elastic resistance to deformation. It is intricately influenced by the dynamic interplay between vascular smooth muscle cells and extracellular matrix components, including fibrillin fibers, elastin, and collagen.[1] This biomechanical property assumes significance, as elevated AS reflects maladaptive responses to hemodynamic stress and imposes an increased afterload on the heart. It is considered a non-invasive indicator of metabolic disorders and a critical factor in assessing cardiovascular risk.[2,3]

Several methodologies have been used to assess AS non-invasively.[2] Pulse wave velocity (PWV) is a widely utilized approach that calculates the speed of the pressure wave along the aorta. This is achieved by measuring the pulse transit time between the carotid and femoral sites and determining the distance between them.[4] In addition, ultrasound-based techniques, including aortic arch pulse wave velocity (aaPWV) and carotid-femoral pulse wave velocity (cfPWV), by assessing pulse wave Doppler, have been reported to provide valuable insights for measuring AS.[5,6]

Ultrasound two-dimensional shear wave elastography (2D-SWE) enables quantitative measurements of tissue stiffness in real-time.[7] It employs acoustic radiation force impulses induced into tissues through focused ultrasonic beams, capturing the real-time propagation of resultant shear waves.[8] This enables the display of elasticity as a colored map overlay on a B-mode image, providing a holistic visualization of tissue stiffness.[9] Although ultrasound 2D-SWE is promising a diagnostic tool in assessing liver diseases, thyroid nodules, and breast conditions, its potential for evaluating abdominal aortic wall stiffness remains an underexplored. Therefore, in this study, we aimed to quantify the local stiffness of the abdominal aortic wall using 2D-SWE ultrasound in adults without underlying medical conditions, and to evaluate its reproducibility.

Materials and Methods

This observational pilot study was approved by the Research Ethics Committee at King Abdulaziz University (Reference No 202-23). The study was conducted in accordance with the ethical principles outlined in the Declaration of Helsinki (2000; revised October 2013, Fortaleza, Brazil). Written informed consent was obtained from all the participants. Subjects at least 18 years old, with no underlying medical conditions, not on regular medications, and not regular smokers were included in the study. Exclusion criteria included diagnosed with cardiovascular diseases, diabetes, on regular medicines, a regular smoker, and pregnancy. Participants were recruited between April and August 2023

Each participant was asked to attend a research clinical assessment room at the Department of Radiologic Sciences, Faculty of Applied Medical Sciences, King Abdulaziz University, once in the morning following an overnight fasting period.[10,11] The participants were screened for eligibility during the visit, and their heights and weights were taken. Then, they were asked to lie in a supine position for approximately 20 minutes. Afterward, brachial blood pressure and heart rate were measured by placing a Microlife monitor cuff on the upper arm, followed by ultrasound imaging of the abdominal aorta for normality assessment. The ultrasound imaging procedures were conducted using a high-resolution ultrasound system, EPIQ Elite (Philips Health Care ultrasound imaging system), with 2D-SWE capability using a 5-1MHz curvilinear transducer for optimal image acquisition. Ultrasound 2D-SWE was assessed in real-time.

Ultrasound 2D-SWE of infra-renal PWoAA were obtained by placing the ultrasound transducer along the midline of the abdomen in the longitudinal plane. A sufficient amount of gel was applied while participants lay in a supine position with their arms resting by their sides, and they were instructed to hold their breath at an end-expiratory level to ensure uniform depth of aorta visualization during assessments and the acquisition of high-quality elastography images. Measurements were taken during diastole in kPa. The dual-screen mode of 2D-SWE was activated, displaying both the confidence map and the stiffness map overlaid on the B-mode ultrasound image. A sample gate of 1mm in size was placed on the PWoAA under the guidance of the confident map to ensure reliable data is acquired (Figure 1). Aortic wall elasticity from each patient was estimated from the average value of five 2D-SWE measurements. Five 2D-SWE measurements from each participant were repeated three times by two certified clinical sonographers with efficient training on ultrasound 2D-SWE (twice by observer A and once by observer B). Both observers were blinded to their own measurements and those of the other observer to ensure unbiased data collection.

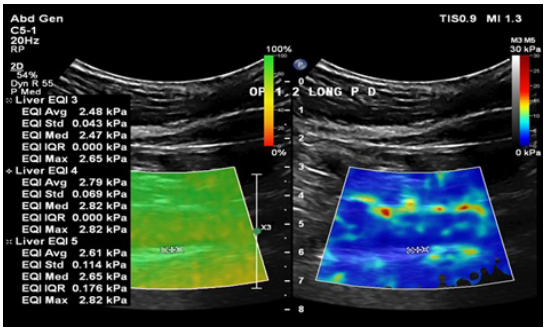

Figure 1. *Ultrasound confidence map and elastography images of 2D SWE measurements from the posterior wall of the infra-renal abdominal aorta. (Reprinted by permission of Elsevier from "Reproducibility of ultrasound 2D shear-wave elastography on abdominal aortic wall" by Alsayegh et al. Ultrasound in Medicine and Biology, 2024;50:S30-S31, World Federation for Ultrasound in Medicine and Biology Congress).*

Statistical analysis was performed using the intraclass correlation coefficient (ICC) and Bland-Altman plots to evaluate intra- and inter-observer reproducibility and establish bias and limit of agreement (LoA) between PWoAA elasticity measurements. A paired t-test was used to compare the mean elasticity measurements taken from the same individuals by the observers. Analysis was performed using

SPSS Statistics (Version 21.0, Armonk, NY: IBM Corp) and PRISM 7 (GraphPad Software, La Jolla, CA, USA). Statistical significance was set at a *P*-value ≤0.05.

Results

A total of 50 subjects (24 male and 26 female) with no underlying medical conditions were recruited for this study, with a mean age of 22.86±5.92 years and a mean BMI of 23.18±4 kg/m². The mean 2D-SWE measurement of PWoAA was 3.87±0.99kPa (Table 1).

Table 1.

Participant characteristics (n=50).

Characteristics	Descriptive statistics (mean±SD)
Age (years)	23.86±5.92
Weight (kg)	61.39±12.33
Height (m)	1.62±0.08
BMI (kg/m^2)	23.18±4.02
SBP (mmHg)	121.92±12.88
DBP (mmHg)	77.64±10.89
HR (bpm)	76.7±13.80
2D-SWE of PWoAA (kPa)	3.87±0.99

BMI, body mass index; DBP. diastolic blood pressure; HR, heart rate; SBP, systolic blood pressure.

Intra-observer agreement of PWoAA ultrasound 2D-SWE elasticity measurements was moderate with an ICC value of 0.69 (95% CI: 0.56–0.82, *P*<0.001). Bias in intra-observer measurements was 0.18±0.92 kPa (95% LoA: -1.62–1.99) (Figure 2A, B). Similarly, inter-observer agreement was moderate with an ICC value of 0.56 (95% CI: 0.22–0.75, *P*=0.002). Bias in inter-observer measurements was -0.02±1.09 kPa (95% LoA: -2.16–2.11) (Figure 3A, B). There was no significant difference in the 2D-SWE measurements of the aortic walls, both within the same observer (mean difference [MD] 0.17, 95% CI: 0.07–0.44, *P*=0.16)) and between two different observers (MD=0.02, 95% CI: 0.33–0.28, *P*=0.86) (Figure 4).

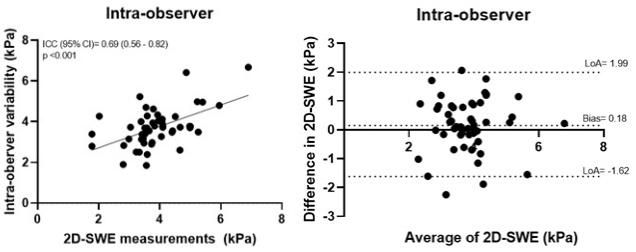

Figure 2. *Intra-observer and Bland-Altman agreement of 2D-SWE of the posterior wall of the abdominal aorta. (Reprinted by permission of Elsevier from "Reproducibility of ultrasound 2D shear-wave elastography on abdominal aortic wall" by Alsayegh et al. Ultrasound in Medicine and Biology, 2024;50:S30-S31, World Federation for Ultrasound in Medicine and Biology Congress).*

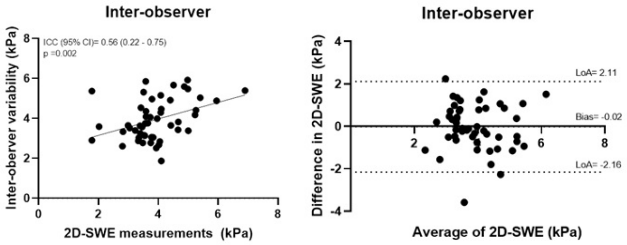

Figure 3. *Inter-observer and Bland-Altman agreement of 2D-SWE of the posterior wall of the abdominal aorta. (Reprinted by permission of Elsevier from "Reproducibility of ultrasound 2D shear-wave elastography on abdominal aortic wall" by Alsayegh et al. Ultrasound in Medicine and Biology, 2024;50:S30-S31, World Federation for Ultrasound in Medicine and Biology Congress).*

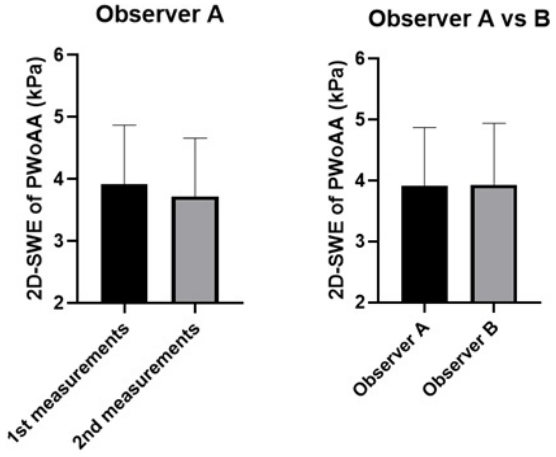

Figure 4. *Comparison within and between observers in measuring 2D-SWE of the posterior wall of the abdominal aorta (PWoAA) (mean±SD).*

Discussion

To the best of the author's knowledge, this is the first study to quantify the local stiffness of the abdominal aortic wall using ultrasound 2D-SWE and to evaluate its reproducibility in healthy subjects. The analysis revealed that the ultrasound 2D-SWE measurement of the infra-renal PWoAA is 3.87±0.99kPa, with moderate intra- and inter-observer agreement. Despite this agreement, there were no significant differences in 2D-SWE of PWoAA within or between operators These findings suggest that ultrasound 2D-SWE is a reliable method for assessing the local stiffness of the abdominal aortic wall, and that additional work is required to improve the reproducibility of this technique for measuring arterial wall stiffness and to evaluate its clinical use in patients with cardiovascular diseases, including those with abdominal aortic aneurysms.

In the present study, the local stiffness of the infra-renal PWoAA was quantified using ultrasound 2D-SWE, revealing a mean stiffness of 3.87±0.99kPa. The shear wave speed in meters per second can be converted to the Young's modulus in kilopascals using the formula $E=3(vS^2 \bullet \rho)$.[12] The AS reported in our study is notably lower than the findings

from a recent study by Elgeti et al.,[13] where a value of 19.35 kPa was found when converting the reported mean stiffness value of 2.54 m/s from healthy non-smoker and smoker subjects using time-harmonic elastography from the upper aorta. The acceleration of aortic stiffening, often associated with aging, is further exacerbated by various cardiovascular risk factors, such as diabetes, obesity, smoking, and high cholesterol.[1,13,14] This could explain the different values of AS, as the study by Elgeti et al.[13] involved an older population than ours, which could influence the stiffness measurements due to age-related changes in arterial properties. The location where AS is assessed may play a critical role in influencing study outcomes. As previously mentioned, Elgeti et al.[13] focused on the upper aorta, whereas our study targeted the infra-renal (lower) PWoAA. It has been reported that mechanical properties of the aorta exhibit significant variation along its length, with the ascending and thoracic segments typically demonstrating greater stiffness than the abdominal portion due to differences in arterial wall composition—specifically, lower elastin and higher collagen content in the abdominal aorta, and a gradient of increasing stiffness from proximal to distal aorta serving as a vital mechanism in mitigating pulsatile flow from the heart and safeguarding microcirculation.[15-17]

Furthermore, the choice of ultrasound transducer is critical for optimizing the accuracy and feasibility of elastography measurements. Various factors, including probe frequency, footprint, size, design, and placement, can significantly influence elastography outcomes. Differences in shear wave elastography technologies across systems from different manufacturers can result in varying measurements due to variations in frequencies and the algorithms used to determine tissue properties.[18,19] Consistency and reproducibility in measurements are best achieved by using the same ultrasound elastography system.[20] In this study, aortic wall elasticity for each patient was determined by averaging five 2D-SWE measurements, with an IQR/median ratio of ≤30%. This approach could lower reproducibility. Future studies with a lower IQR/median ratio could increase the agreement within and between observers. Despite moderate intra- and inter-observer agreement, we found no significant differences in aortic 2D-SWE measurements within or between operators. The reproducibility of 2D-SWE in measuring AS can be affected by the anatomical segment used for measurement, with higher stiffness values and greater variance observed in the posterior wall than in the anterior wall.[21] The higher variance in the posterior wall may be due to lower signal quality caused by the larger distance from the transducer, which induces more attenuation and presumably more reflections and reverberations from the overlying soft tissue.[19,22] Together, these factors suggest that age differences, cardiovascular risk factors, assessment locations, and ultrasound imaging systems contribute to the observed variations in AS measurements and their reproducibility. Therefore, while SWE shows promise for assessing AS, continued research and technological improvements are essential for optimizing its reproducibility and clinical application.

The current study has limitations that should be acknowledged. The inclusion criteria were restricted to young healthy adults. This limitation may limit the generalizability of the findings to older populations and those with underlying medical conditions. Patients with various comorbidities, such as hypertension, diabetes, or other chronic conditions, might exhibit different levels of AS. In this study, AS was assessed using the Philips 2D-SWE system. Therefore, the findings may not be directly comparable to those obtained using other ultrasound imaging systems. These factors should be considered when interpreting the results and their potential implications for clinical practice. Further research involving diverse populations and multiple ultrasound systems is needed to enhance the generalizability and comparability of AS measurements.

Conclusion

This study demonstrated that 2D-SWE is a promising non-invasive technique for assessing the stiffness of the abdominal aortic wall, showing moderate intra- and inter-observer reproducibility in healthy subjects, with no significant differences observed within or between observers. Further research is needed to enhance the reproducibility of this technique, particularly in clinical settings involving larger and more diverse populations, including patients with cardiovascular conditions such as abdominal aortic aneurysms.

Sources of Funding

This project was funded by the Deanship of Scientific Research (DSR) at King Abdulaziz University, Jeddah, Saudi Arabia, under grant no. (IPP: 138-142-2025). The authors, therefore, acknowledge with thanks DSR for technical and financial support.

Conflicts of Interest

The authors declare that they have no competing interests.

References

1. Sethi S, Rivera O, Oliveros R, Chilton R. Aortic stiffness: pathophysiology, clinical implications, and approach to treatment. Integr Blood Press Control. 2014 May 23;7:29-34. doi: 10.2147/IBPC.S59535. PMID: 24910511; PMCID: PMC4046515.
2. Angoff R, Mosarla RC, Tsao CW. Aortic Stiffness: Epidemiology, Risk Factors, and Relevant Biomarkers. Front Cardiovasc Med. 2021 Nov 8;8:709396. doi: 10.3389/fcvm.2021.709396. PMID: 34820427; PMCID: PMC8606645.
3. Karlsson J, Stålhand J, Carlhäll CJ, Länne T, Engvall J. Abdominal Aortic Wall Cross-coupled Stiffness Could Potentially Contribute to Aortic Length Remodeling. Artery Res. 2022;28(4):113–27.
4. Salvi P, Scalise F, Rovina M, Moretti F, Salvi L, Grillo A, Gao L, Baldi C, Faini A, Furlanis G, Sorropago A, Millasseau SC, Sorropago G, Carretta R, Avolio AP, Parati G.

Noninvasive Estimation of Aortic Stiffness Through Different Approaches. Hypertension. 2019 Jul;74(1):117-129. doi: 10.1161/HYPERTENSIONAHA.119.12853. Epub 2019 May 28. PMID: 31132954.
5. Parr S, Scheuermann B, Hammond S, Ade CJ. Abstract TP99: Non-invasive Aortic Pulse Wave Velocity Is Related To Gold Standard Carotid-femoral Pulse Wave Velocity: Implications For Monitoring Large Artery Stiffness In The Clinic. Stroke. 2023;54.
6. Calabia J, Torguet P, Garcia M, Garcia I, Martin N, Guasch B, Faur D, Vallés M. Doppler ultrasound in the measurement of pulse wave velocity: agreement with the Complior method. Cardiovasc Ultrasound. 2011 Apr 15;9:13. doi: 10.1186/1476-7120-9-13. PMID: 21496271; PMCID: PMC3098145.
7. Sigrist RMS, Liau J, Kaffas AE, Chammas MC, Willmann JK. Ultrasound Elastography: Review of Techniques and Clinical Applications. Theranostics. 2017 Mar 7;7(5):1303-1329. doi: 10.7150/thno.18650.
8. Popescu A, Sirli R, Sporea I. 2D Shear Wave Elastography for Liver Fibrosis Evaluation. IntechOpen. 2020.
9. Weiher M, Richtering FG, Dörffel Y, Müller HP. Simplification of 2D shear wave elastography by enlarged SWE box and multiple regions of interest in one acquisition. PLoS One. 2022 Sep 9;17(9):e0273769. doi: 10.1371/journal.pone.0273769. PMID: 36084083; PMCID: PMC9462759.
10. Favero G, Paganelli C, Buffoli B, Rodella LF, Rezzani R. Endothelium and its alterations in cardiovascular diseases: life style intervention. Biomed Res Int. 2014;2014:801896. doi: 10.1155/2014/801896. Epub 2014 Feb 26. PMID: 24719887; PMCID: PMC3955677.
11. Schaafs LA, Tzschätzsch H, Figiel C, van der Giet M, Reshetnik A, Hamm B, Sack I, Elgeti T. Quantitative Time-Harmonic Ultrasound Elastography of the Abdominal Aorta and Inferior Vena Cava. Ultrasound Med Biol. 2019 Sep;45(9):2349-2355. doi: 10.1016/j.ultrasmedbio.2019.05.021. Epub 2019 Jun 11. PMID: 31201021.
12. Barr RG, Ferraioli G, Palmeri ML, Goodman ZD, Garcia-Tsao G, Rubin J, Garra B, Myers RP, Wilson SR, Rubens D, Levine D. Elastography Assessment of Liver Fibrosis: Society of Radiologists in Ultrasound Consensus Conference Statement. Radiology. 2015 Sep;276(3):845-61. doi: 10.1148/radiol.2015150619. Epub 2015 Jun 16. PMID: 26079489.
13. Elgeti T, Fröhlich M, Wismayer KK, Tzschätzsch H, Hamm B, Sack I, Schaafs LA. The effect of smoking on quantification of aortic stiffness by ultrasound time-harmonic elastography. Sci Rep. 2022 Oct 22;12(1):17759. doi: 10.1038/s41598-022-22638-7. PMID: 36273020; PMCID: PMC9588008.
14. Schaafs LA, Tzschätzsch H, van der Giet M, Reshetnik A, Steffen IG, Hamm B, Braun J, Sack I, Elgeti T. Time-Harmonic Ultrasound elastography of the Descending Abdominal Aorta: Initial Results. Ultrasound Med Biol. 2017 Nov;43(11):2550-2557. doi: 10.1016/j.ultrasmedbio.2017.07.001. 1. Epub 2017 Aug 14. PMID: 28818306.
15. Collette M, Humeau A, Chevalier C, Hamel JF, Leftheriotis G. Assessment of aortic stiffness by local and regional methods. Hypertens Res. 2011 May;34(5):578-83. doi: 10.1038/hr.2010.280. Epub 2011 Jan 27. PMID: 21270814.
16. Cavalcante JL, Lima JA, Redheuil A, Al-Mallah MH. Aortic stiffness: current understanding and future directions. J Am Coll Cardiol. 2011 Apr 5;57(14):1511-22. doi: 10.1016/j.jacc.2010.12.017. PMID: 21453829.
17. Wang J, Jing C, Hu X, Cui J, Tang Q, Tu L, Zhao S, Huang J, Guo D, Li Y, Xu J. Assessment of aortic to peripheral vascular stiffness and gradient by segmented upper limb PWV in healthy and hypertensive individuals. Sci Rep. 2023 Nov 13;13(1):19859. doi: 10.1038/s41598-023-46932-0. PMID: 37963909; PMCID: PMC10645764.
18. Dietrich CF, Bamber J, Berzigotti A, Bota S, Cantisani V, Castera L, Cosgrove D, Ferraioli G, Friedrich-Rust M, Gilja OH, Goertz RS, Karlas T, de Knegt R, de Ledinghen V, Piscaglia F, Procopet B, Saftoiu A, Sidhu PS, Sporea I, Thiele M. EFSUMB Guidelines and Recommendations on the Clinical Use of Liver Ultrasound Elastography, Update 2017 (Long Version). Ultraschall Med. 2017 Aug;38(4):e48. English. doi: 10.1055/a-0641-0076. Epub 2018 Sep 3. Erratum for: Ultraschall Med. 2017 Aug;38(4):e16-e47. doi: 10.1055/s-0043-103952. PMID: 30176678.
19. Pruijssen JT, de Korte CL, Voss I, Hansen HHG. Vascular Shear Wave Elastography in Atherosclerotic Arteries: A Systematic Review. Ultrasound Med Biol. 2020 Sep;46(9):2145-2163. doi: 10.1016/j.ultrasmedbio.2020.05.013. Epub 2020 Jul 1. PMID: 32620385.
20. Sultan SR, Alghamdi A, Abdeen R, Almutairi F. Evaluation of ultrasound point shear wave elastography reliability in an elasticity phantom. Ultrasonography. 2022 Apr;41(2):291-297. doi: 10.14366/usg.21114. Epub 2021 Jul 31. PMID: 35316890; PMCID: PMC8942736.
21. Marais L, Pernot M, Khettab H, Tanter M, Messas E, Zidi M, Laurent S, Boutouyrie P. Arterial Stiffness Assessment by Shear Wave Elastography and Ultrafast Pulse Wave Imaging: Comparison with Reference Techniques in Normotensives and Hypertensives. Ultrasound Med Biol. 2019 Mar;45(3):758-772. doi: 10.1016/j.ultrasmedbio.2018.10.032.
22. Couade M, Pernot M, Prada C, Messas E, Emmerich J, Bruneval P, Criton A, Fink M, Tanter M. Quantitative assessment of arterial wall biomechanical properties using shear wave imaging. Ultrasound Med Biol. 2010 Oct;36(10):1662-76. doi: 10.1016/j.ultrasmedbio.2010.07.004. PMID: 20800942.

***Corresponding author**: Salahaden R. Sultan, E-mail: srsultan@kau.edu.sa*

International Journal of Biomedicine 15(4) (2025) 695-699
http://dx.doi.org/10.21103/Article15(4)_OA8

ORIGINAL ARTICLE

Oncology

INTERNATIONAL JOURNAL OF BIOMEDICINE

Treatment of Kidney Tumors in Albania

Aurel Janko[1], Orjent Hasanaj[1], Dritan Reovica[2]; Fatjona Pupuleku Kraja[3], Fredi Bedalli[4], Haxhire Gani[4], Zamira Hysenaj[4], Aldo Shpuza[5*]

[1]*Department of Urology, Mother Theresa University Hospital, Tirana, Albania*
[2]*Department of Abdominal Surgery, Mother Theresa University Hospital, Tirana, Albania*
[3]*Department of Oncologic Radiotherapy, Mother Theresa University Hospital, Tirana, Albania*
[4]*Department of Intensive Care-Anesthesiology, Mother Theresa University Hospital, Tirana, Albania*
[5]*Department of Public Health, University of Medicine, Tirana, Albania*

Abstract

Introduction: Kidney tumors, predominantly renal cell carcinoma (RCC), continue to pose a clinical challenge due to their asymptomatic nature in early stages and variable biological behavior.
Methods and Results: Our retrospective study included 200 patients who underwent surgical treatment for RCC between 2015 and 2024. Patients were followed at 3, 12, and 24 months using the Eastern Cooperative Oncology Group Performance Status (ECOG-PS) scale. Cox regression compared open radical nephrectomy (ORN) and open nephron-sparing surgery (NSS).
ECOG-PS score increased gradually: baseline (0.07±0.252), 3 months (0.02±0.149), 12 months (0.20±0.505), 24 months (0.24±0.570), and 36 months (0.44±0.990) (P<0.01). Kaplan-Meier curves showed better survival for tumors <4 cm. Cox regression analysis indicated a lower mortality rate with open NSS (HR = 0.148, 95% CI; 0.019–1.126), although the difference was not statistically significant. No significant difference in creatinine levels was observed between groups.
Conclusion: Patients with smaller renal tumors typically exhibit more favorable survival outcomes than those with larger masses. Current trends in kidney tumor management emphasize the use of less invasive surgical techniques, which aim to achieve comparable oncologic control while preserving overall renal function.(**International Journal of Biomedicine. 2025;15(4):695-699.**)

Keywords: renal cell carcinoma • open radical nephrectomy • nephron-sparing surgery

For citation: Janko A, Hasanaj O, Reovica D, Kraja FP, Bedalli F, Gani H, Hysenaj Z, Shpuza A. Treatment of Kidney Tumors in Albania. International Journal of Biomedicine. 2025;15(4):695-699. doi:10.21103/Article15(4)_OA8

Abbreviations

ECOG-PS, Eastern Cooperative Oncology Group Performance Status; **NSS**, nephron-sparing surgery; **ORN**, open radical nephrectomy; **RCC**, renal cell carcinoma.

Introduction

Kidney cancer is the 14th most common cancer worldwide, ranking 10th in men and 13th in women.[1] Renal cell carcinoma (RCC) is the predominant malignant tumor of the kidney, accounting for more than 90% of all renal cancers.[2] According to the American Cancer Society, the average age at diagnosis is between 55 and 74.[3] Several risk factors that are associated with kidney tumors are: smoking, obesity, hypertension, genetics, sex, polycystic renal disease, horseshoe kidney, von Hippel-Lindau syndrome, and Birt-Hogg-Dube syndrome.[4]

In the USA, there were 76,080 diagnosed patients with renal tumors in 2021, with a projection of over 81,610 patients in 2024.[3] In Europe, overall mortality rates for RCC increased up to the early 1990s, before stabilizing or declining thereafter.[5] The incidence of kidney cancer was highest in regions such as North America, Australia, New Zealand, and Northern Europe, while the lowest incidence was observed in Middle Africa, Melanesia, and South-Central Asia.[6] The 5-year relative survival for kidney cancer in the US is 93%

***Corresponding author**: Aldo Shpuza. Department of Public Health, University of Medicine, Tirana, Albania. E-mail: aldoshpuza@hotmail.com*

when diagnosed at an early stage, which accounts for about two-thirds of cases, with the overall survival for kidney and renal pelvis cancers being 75%.[7]

This study aimed to evaluate treatment outcomes and survival in patients surgically treated for RCC.

Materials and Methods

Our retrospective study included 200 patients who underwent surgical treatment for RCC between 2015 and 2024. A complete blood count was performed before surgery and 3, 6, 12, and 24 months after surgery. Results were compared for both surgical methods. A post-operative histologic report was obtained in all cases. All patients were followed for 3, 12, and 24 months to assess their Eastern Cooperative Oncology Group Performance Status (ECOG-PS) scores.[8] Descriptive statistics were initially used to analyze the distribution of various clinical variables, including age, gender, symptoms, and treatment modality. Logistic regression models, both crude and multivariable, were conducted to identify predictors of mortality, using variables such as age, low back pain, fever, and anemia.

Repeated measures analysis, specifically Friedman's test, was employed to assess changes in ECOG-PS and creatinine levels over time. Kaplan-Meier survival analysis was used to estimate survival probabilities over time. Cox proportional hazards regression was utilized to evaluate the association between surgical modality and survival, adjusting for potential confounding factors. A General Linear Model (GLM) for repeated measures was used to analyze the differences in creatinine levels over time between two treatment modalities: open radical nephrectomy (ORN) and open nephron-sparing surgery (NSS). The chi-square test was used to assess the association between treatment modality, creatinine levels, and survival status. The probability value of $P<0.05$ was considered statistically significant.

Results

The median age of the patients was 63 years, with an interquartile range (IQR) from 55 to 69 years, representing the middle 50% of the distribution. The mean age was 60.66 years with a standard deviation of 10.35.

Table 1 summarizes various clinical and demographic characteristics of RCC patients. In terms of treatment modality, 55.5% underwent ORN, 26.5% had open NSS, 16% had laparoscopic radical surgery, and 2% had laparoscopic NSS. Regarding gender, 60% were male and 40% were female. Incidental diagnosis was present in 73.7% of cases. Low back pain was reported by 30.4% of patients. Hematuria and palpable mass were present in 26.8% and 13.6% of patients, respectively. Anorexia and weight loss affected 15.2% and 14.7% of patients, respectively. Weakness was reported by 20.9% of patients. Elevated ESR level, anemia, erythrocytosis, and liver dysfunction were present in 43.5%, 22.8%, 2,7%, and 2.2% of cases, respectively. Hypertension was present in 50.3% of patients. Stauffer's syndrome was observed in 1.1% of patients. In terms of tumor size, 27.6% had tumors smaller than 4 cm, 38.7% had tumors between 4 cm and 7 cm, and 33.7% had tumors larger than 7 cm.

Table 1.
Clinical characteristics of RCC patients.

Variable	Frequency (%)*
Modality	
ORN	111 (55.5)
Open NSS	53 (26.5)
Laparoscopic Radical	32 (16)
Laparoscopic NSS	4 (2)
Gender	
Male	119 (60.7)
Female	77 (39.3)
Incidental Diagnosis	
Yes	140 (73.7)
No	50 (26.3)
Low back pain	
Yes	58 (30.4)
No	133 (69.6)
Hematuria	
Yes	51 (26.8)
No	139 (73.2)
Mass	
Yes	26 (13.6)
No	165 (86.4)
Weight Loss	
Yes	28 (14.7)
No	163 (85.3)
Fever	
Yes	7 (3.7)
No	184 (96.3)
Anorexia	
Yes	29 (15.2)
No	162 (84.8)
Weakness	
Yes	40 (20.9)
No	151 (79.1)
Anemia	
Yes	42 (22.8)
No	142 (77.2)
ESR ↑	
Yes	73 (43.5)
No	95 (56.5)
Liver Dysfunction	
Yes	4 (2.2)
No	179 (97.8)
Erythrocytosis	
Yes	5 (2.7)
No	177 (97.3)
Hypertension	
Yes	92 (50.3)
No	91 (49.7)
Stauffer's Syndrome	
Yes	2 (1.1)
No	180 (98.9)
Tumor Size	
<4 cm	50 (27.6)
4-7 cm	70 (38.7)
>7 cm	61 (33.7)

***** *The values for individual parameters may not correspond to the total number of individuals examined due to missing data.*

Initially, logistic regression models were tested for groups of variables, such as demographic factors, symptomatic indicators, and clinical examinations. From these, the most likely predictive variables were extracted, focusing on those that yielded statistical significance.

In the crude (unadjusted) logistic regression analysis predicting death from renal cancer, age was not statistically significant (B = 0.032, *P* = 0.280), with an odds ratio (OR) of 1.033 and a 95% confidence interval (CI) of 0.974 – 1.095. Low back pain was significant (B = 1.350, *P* = 0.022, OR = 3.857, 95% CI: 1.212 – 12.275), anemia approached significance (B = 1.117, *P* = 0.070, OR = 3.056, 95% CI: 0.914 – 10.217), and fever was highly statistically significant (B = 2.848, *P* = 0.017, OR = 17.250, 95% CI: 1.654 – 179.925).

In the multivariable adjusted logistic regression analysis, age became statistically significant (B = 0.076, *P* = 0.049, OR = 1.079, 95% CI: 1.000 – 1.164). However, low back pain lost significance (B = 0.627, *P* = 0.417, OR = 1.873, 95% CI: 0.411 – 8.526). Fever remained significant (B = 3.432, *P* = 0.019, OR = 30.929, 95% CI: 1.766 – 541.686), while anemia was not significant (B = 1.143, *P* = 0.133, OR = 3.135, 95% CI: 0.705 – 13.943) (Table 2).

Table 2.

Multivariable adjusted logistic regression analysis predicting death from RCC.

Predictors	B	SE	Wald	df	P-value	OR	95% CI
Age	0.076	0.039	3.888	1	0.049	1.079	1.000 – 1.164
LBP	0.627	0.773	0.658	1	0.417	1.873	0.411 – 8.526
Fever	3.432	1.461	5.519	1	0.019	30.929	1.766 – 541.686
Anemia	1.143	0.761	2.253	1	0.133	3.135	0.705 – 13.943
Constant	-6.970	2.563	7.393	1	0.007	0.001	

LBP, low back pain; B, regression coefficient; SE, standard error; Wald, Wald statistic; df, degrees of freedom; OR, odds ratio; CI, confidence interval.

The independent variable is tumor size, categorized into three groups: <4 cm, 4-7 cm, and >7 cm. The Kaplan-Meier survival plot demonstrates that patients with smaller tumors generally have better survival outcomes than those with larger tumors. Tumors smaller than 4 cm were associated with a significantly lower hazard of death (B = -1.629, *P* = 0.036, HR = 0.196, 95% CI: 0.043 – 0.898). Similarly, tumors between 4 and 7cm also showed a significantly reduced risk of death (B = -1.254, *P* = 0.015, HR = 0.285, 95% CI: 0.104 – 0.782) (Table 3). Figure 1 presents the ECOG-PS scores over time.

The descriptive statistics for ECOG-PS scores over time show that at baseline (m0), the mean score was 0.07±0.252. At 3 months (m3), the mean score decreased to 0.02±0.149, while at 12 months (m12), the mean increased to 0.20±0.505. At 24 months (m24), the mean score was 0.24± 0.570, and by 36 months, the mean had risen to 0.44±0.990, *P*<0.01 (Table 4).

Table 3.

Cox regression analysis predicting survival based on tumor size (reference: >7 cm).

Predictor	B	SE	Wald	df	P-value	HR (Exp(B))	95% CI
Size <4 cm	-1.629	0.776	4.404	1	0.036	0.196	0.043-0.898
Size 4-7 cm	-1.254	0.514	5.943	1	0.015	0.285	0.104–0.782

B, regression coefficient; SE, standard error; Wald, Wald statistic; df, degrees of freedom; HR, hazard ratio; CI, confidence interval.

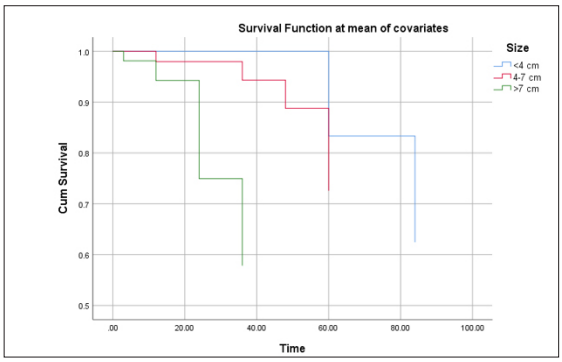

Figure 1. *ECOG-PS scores over time.*

Table 4.

Descriptive statistics and Friedman test results for ECOG-PS scores over time.

Time Point	Mean	Std. Deviation	Friedman Test (Chi-Square)
m0 (Baseline)	0.07	0.252	*P*<0.01
m3 (3 months)	0.02	0.149	
m12 (12 months)	0.20	0.505	
m24 (24 months)	0.24	0.570	
m36 (36 months)	0.44	0.990	

For patients who underwent open surgery, the mean survival time was estimated to be 70.1 months (SE = 2.8, 95% CI: 64.6 – 75.5). The estimation is limited to the largest censored survival time. This Kaplan-Meier curve reflects survival outcomes specifically for this subset of patients who underwent open surgical procedures. In this Cox regression analysis, the hazard ratio of 0.148 (95% CI: 0.019 – 1.126) suggested that the risk of death was lower for patients undergoing open NSS than for those undergoing ORN; however, the result was not statistically significant (Table 5). Survival function at the mean of covariates is presented in Figure 2.

The Friedman test for creatinine levels across four time points (0, 3, 6, and 12 months) revealed a significant difference (*P*=0.038), indicating that creatinine levels changed significantly over time (Figure 3). The descriptive statistics show that the mean creatinine levels increased slightly from 0.993 mg/dL at 0 months to 1.115 mg/dL at 12 months, with minor fluctuations across the intermediate time points.

Table 5.

Cox regression analysis predicting survival based on surgical modality (ORN vs. open NSS).

Predictor	B	SE	Wald	df	*P*-value	HR (Exp(B))	95% CI
Modality (Open NSS, Open Radical (Reference)	1.910	1.035	3.404	1	0.065	0.148	0.019 –1.126

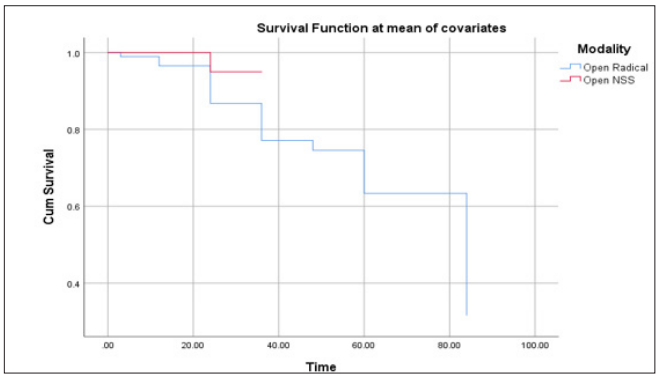

Figure 2. *Survival function at the mean of covariates.*

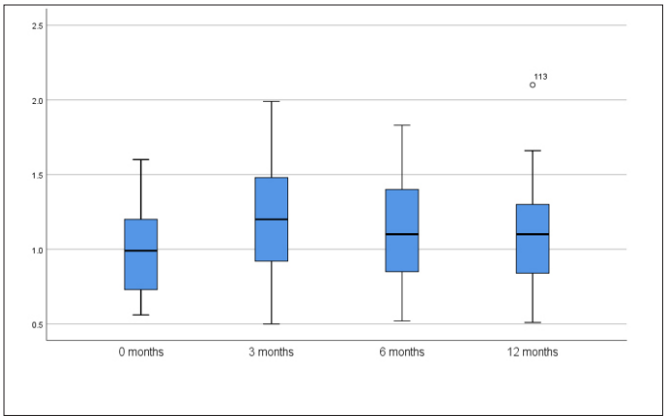

Figure 3. *The Friedman Test for creatinine levels.*

The crosstabulation of creatinine levels and event outcome (alive vs. dead) reveals that for patients in the non-risky creatinine group (<1.2 mg/dL), 83.9% were alive, while 16.1% had died. Similarly, in the risky creatinine group (>1.2 mg/dL), 81.8% were alive, and 18.2% had died (*P*=0.7).

Discussion

Staging of renal cell carcinoma based on pathological examination and radiographic examination provides important prognostic information. Stage I (T1N0M0: tumor ≤7 cm) and Stage II (T2N0M0: tumor >7 cm) tumors are limited to the kidney, whereas Stage III (T3N0, T1-3N1: tumor invades the renal vein, perinephric tissues, or has metastasized to regional lymph nodes) and Stage IV (T4NanyM0, TanyNanyM1: tumor extends beyond Gerota's fascia or has distant metastases) tumors extend beyond the kidney.[9] In a study by Kane et al.,[10] the 5-year survival rates for Stage I and II of RCC were significantly higher (90.4% and 83.4%) compared to Stage III and IV (66.0% and 9.1%).

According to another study, patients with tumors ≤7 cm had almost twice the 5-year survival compared to those with tumors of >7 cm.[11] Similarly, our study confirmed this association, showing that tumors smaller than 4 cm had around an 80% lower risk of death, while those 4–7 cm had around a 70% lower risk, both compared with tumors larger than 7cm. ECOG-PS is one of the most widely recognized prognostic indicators in renal cell carcinoma.[12,13] In our study, ECOG-PS scores improved slightly at 3 months but then gradually and significantly worsened over time, confirming its prognostic relevance in renal cell carcinoma. Our data indicated a trend toward better survival with nephron-sparing surgery. One previous study likewise found no disadvantage compared to radical surgery, supporting the oncological safety of nephron-sparing surgery.[14] Accurate postoperative prognostic models for renal cell carcinoma are critical for the development of personalized surveillance programs and adjuvant therapy design.[15-17]

Study Limitations

This study was conducted at a single center, which may limit the generalizability of the results. The retrospective design may have introduced bias and influenced the outcomes.

Conclusions

The Kaplan-Meier survival plot demonstrates that patients with smaller tumors (<4 cm) generally have better survival outcomes than those with larger tumors.

Kidney tumors can be treated with less invasive methods, including nephron-sparing surgery, compared to open radical nephrectomy, with similar oncologic results.

Today's trends in kidney tumor treatment focus on less invasive surgical techniques with similar oncologic outcomes and improved overall kidney function.

Conflicts of Interest

The author declares that there are no conflicts of interest regarding the publication of this paper.

References

1. Kidney cancer statistics [Internet]. World Cancer Research Fund. [cited 2025 Aug 19]. Available from: https://www.wcrf.org/preventing-cancer/cancer-statistics/kidney-cancer-statistics/
2. Pandey J, Syed W. Renal Cancer. In: StatPearls [Internet]. Treasure Island (FL): StatPearls Publishing; 2025 [cited 2025 Aug 19]. Available from: http://www.ncbi.nlm.nih.gov/books/NBK558975/

3. American Cancer Society. Key statistics about kidney cancer [Internet]. Atlanta; 2024 [cited 2025 Aug 19]. Available from: https://www.cancer.org/cancer/types/kidney-cancer/about/key-statistics.html
4. Risk Factors for Kidney Cancer | How Do You Get Kidney Cancer? [Internet]. [cited 2025 Aug 19]. Available from: https://www.cancer.org/cancer/types/kidney-cancer/causes-risks-prevention/risk-factors.html
5. Levi F, Lucchini F, Negri E, La Vecchia C. Declining mortality from kidney cancer in Europe. Ann Oncol. 2004 Jul;15(7):1130-5. doi: 10.1093/annonc/mdh270.
6. Cirillo L, Innocenti S, Becherucci F. Global epidemiology of kidney cancer. Nephrol Dial Transplant. 2024 May 31;39(6):920-928. doi: 10.1093/ndt/gfae036. PMID: 38341277.
7. Siegel RL, Miller KD, Jemal A. Cancer statistics, 2020. CA Cancer J Clin. 2020 Jan;70(1):7-30. doi: 10.3322/caac.21590. Epub 2020 Jan 8. PMID: 31912902.
8. Karakiewicz PI, Trinh QD, de la Taille A, Abbou CC, Salomon L, Tostain J, Cindolo L, Artibani W, Ficarra V, Patard JJ. ECOG performance status 0 or 1 and symptom classification do not improve the ability to predict renal cell carcinoma-specific survival. Eur J Cancer. 2007 Apr;43(6):1023-9. doi: 10.1016/j.ejca.2007.01.020. Epub 2007 Mar 8. PMID: 17349784.
9. Bierley J.D., Gospodarowicz M.K., Wittekind C. TNM Classification of Malignant Tumours. 8th ed. John Wiley & Sons, Inc.; Oxford, UK: Hoboken, NJ, USA: 2017.
10. Kane CJ, Mallin K, Ritchey J, Cooperberg MR, Carroll PR. Renal cell cancer stage migration: analysis of the National Cancer Data Base. Cancer. 2008 Jul 1;113(1):78-83. doi: 10.1002/cncr.23518. PMID: 18491376.
11. Abraham GP, Cherian T, Mahadevan P, Avinash TS, George D, Manuel E. Detailed study of survival of patients with renal cell carcinoma in India. Indian J Cancer. 2016 Oct-Dec;53(4):572-574. doi: 10.4103/0019-509X.204758.
12. Elçiçek ÖF, Küçüköner M, Elçiçek ÖF, Küçüköner M. Prognostic Factors and Treatment Outcomes in Renal Cell Carcinoma: A Comprehensive Analysis. Namık Kemal Med J [Internet]. 2024 Sept 20 [cited 2025 Aug 20]; Available from: https://namikkemalmedj.com/articles/prognostic-factors-and-treatment-outcomes-in-renal-cell-carcinoma-a-comprehensive-analysis/nkmj.galenos.2024.75010
13. Martini DJ, Kline MR, Liu Y, Shabto JM, Carthon BC, Russler GA, Yantorni L, Hitron EE, Caulfield S, Goldman JM, Harris WB, Kucuk O, Master VA, Bilen MA. Novel risk scoring system for metastatic renal cell carcinoma patients treated with cabozantinib. Cancer Treat Res Commun. 2021;28:100393. doi: 10.1016/j.ctarc.2021.100393. Epub 2021 May 9. PMID: 34029879; PMCID: PMC8405548.
14. Milonas D, Skulčius G, Baltrimavičius R, Auškalnis S, Kinčius M, Matjošaitis A, Gudinavičienė I, Smailytė G, Jievaltas M. Comparison of long-term results after nephron-sparing surgery and radical nephrectomy in treating 4- to 7-cm renal cell carcinoma. Medicina (Kaunas). 2013;49(5):223-8. PMID: 24247918.
15. Mattila KE, Vainio P, Jaakkola PM. Prognostic Factors for Localized Clear Cell Renal Cell Carcinoma and Their Application in Adjuvant Therapy. Cancers (Basel). 2022 Jan 4;14(1):239. doi: 10.3390/cancers14010239. PMID: 35008402; PMCID: PMC8750145.
16. Correa AF, Jegede OA, Haas NB, Flaherty KT, Pins MR, Adeniran A, Messing EM, Manola J, Wood CG, Kane CJ, Jewett MAS, Dutcher JP, DiPaola RS, Carducci MA, Uzzo RG. Predicting Disease Recurrence, Early Progression, and Overall Survival Following Surgical Resection for High-risk Localized and Locally Advanced Renal Cell Carcinoma. Eur Urol. 2021 Jul;80(1):20-31. doi: 10.1016/j.eururo.2021.02.025. Epub 2021 Mar 9. PMID: 33707112; PMCID: PMC8627688.
17. Klatte T, Rossi SH, Stewart GD. Prognostic factors and prognostic models for renal cell carcinoma: a literature review. World J Urol. 2018 Dec;36(12):1943-1952. doi: 10.1007/s00345-018-2309-4. Epub 2018 Apr 30. PMID: 29713755.

International Journal of Biomedicine 15(4) (2025) 700-703
http://dx.doi.org/10.21103/Article15(4)_OA9

ORIGINAL ARTICLE

Orthopedics

INTERNATIONAL JOURNAL OF BIOMEDICINE

Biomechanical Analysis of Newly Developed Local Hip Implant from Stainless Steel, Cobalt-Chrome, and Titanium Materials Using the Finite Element Method

Hantonius[1,2], Kukuh Dwiputra Hernugrahanto[1,2], Fahmi Mubarok[3], Dwikora Novembri Utomo[1,2*]

[1]*Department of Orthopaedics and Traumatology, Faculty of Medicine, Universitas Airlangga, Surabaya, Indonesia*
[2]*Department of Orthopaedics and Traumatology, Dr. Soetomo General Academic Hospital, Surabaya, Indonesia*
[3]*Department of Mechanical Engineering, Institut Teknologi Sepuluh Nopember, Surabaya, Indonesia*

Abstract

Background: Total hip arthroplasty (THA) is one of the most successful health interventions in the last century. However, there have been several reports of dissatisfaction with the hip implant. Most modern implants are manufactured based on Western morphology. This generalized design may not be suitable for all races, particularly Asians, who tend to have a more petite physique and distinct femoral anatomy.
Methods and Results: This study evaluated the biomechanical properties of a newly developed local hip implant using the Finite Element method based on ISO 7206-4, ISO 7206-6, and ASTM F2996-20. The implants were analyzed under static and dynamic load, and three different implant materials were used. The results showed that the titanium (Ti6Al4V) implant had the lowest von Mises stress, the cobalt-chrome (Co28Cr6Mo) implant had the lowest total deformation, and the stainless steel (SS316L) implant had the highest alternating stress and a lower life cycle. All of the materials have more than 1 (>1) safety factor value, which is considered safe for implant manufacturing.
Conclusion: This study offers insights into the performance of various materials under static and dynamic loading conditions, demonstrating that all simulated materials are deemed safe for implant manufacturing.(**International Journal of Biomedicine. 2025;15(4):700-703.**)

Keywords: biomechanical analysis • hip implant • finite element method

For citation: Hantonius, Hernugrahanto KW, Mubarok F, Utomo DN. Biomechanical Analysis of Newly Developed Local Hip Implant from Stainless Steel, Cobalt-Chrome, and Titanium Materials Using the Finite Element Method. International Journal of Biomedicine. 2025;15(4):700-703. doi:10.21103/Article15(4)_OA9

Introduction

Total hip arthroplasty (THA) is a surgical procedure that has a significant impact on restoring the function of damaged hip joints and is one of the most successful health interventions in the last century.[1] Presently, hip joint arthroplasty has a 10-year success rate and 95% survivorship for patients older than 70 years.[2] However, despite the long-term stability and functionality of the Total Hip Replacement system, a 7% rate of dissatisfaction was observed after the THA operation.[3]

The configuration of the prosthesis has been recognized as a crucial determinant of the contact condition between the implant and the bone. Most modern implants are manufactured based on Western morphology and surgical standards.[4] This generalized design template may not be adequate for all races, especially Asians, who are reported to have a more petite physique and possess smaller femoral anatomy compared to Caucasians.[5]

Institut Teknologi Sepuluh Nopember (ITS), in collaboration with the Orthopaedic Department of Dr. Soetomo Hospital, has developed a locally manufactured Indonesian hip implant (ORTHOHITS), whose design is tailored to the Mongoloid race, with a neck offset and neck length shorter than those of European brands. This implant is expected to offer more precise anatomical accuracy and improved biomechanics for Indonesians compared to European brands.

Currently, there are no other locally made Indonesian hip implants available.[6]

Biomechanical testing is a critical component in implant development, as it not only measures durability but also ensures that the implant can function optimally under realistic physiological conditions after several years of use without failure.[7] Numerous studies comparing experimental fatigue data with fatigue life simulation analysis have demonstrated that Finite Element Analysis (FEA) can accurately depict the true stress variations of the hip implant.[8-10] This study aimed to evaluate the biomechanical performance of ORTHOHITS, a newly designed hip implant adjusted for the Mongoloid race by FEA. A total of three implant materials were analyzed using Finite Element models.

Methods

This study compares the biomechanical properties of titanium (Ti6Al4V), cobalt-chrome (Co28Cr6Mo), and stainless steel (SS316L) hip implants created locally. The test was done in accordance with ISO 7206-4, ISO 7206-6, and ASTM F2996-20 standards to provide guidance to implant designers during the FEA process for hip implants.[11-13]

The ORTHOHITS hip joint implant design (Figure 1) was used in this work's geometrical analysis. Materials used in this investigation were stainless steel (SS316L), cobalt-chrome (Co28Cr6Mo), and titanium (Ti-6Al-4V).

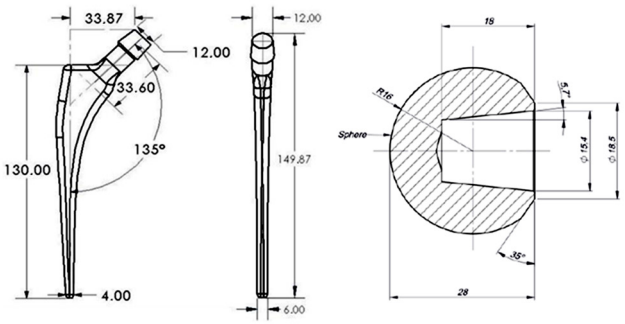

Figure 1. *ORTHOHITS hip implant design.*

The prototype implant presented in this study is a newly designed, collarless, cemented hip implant featuring a trapezoidal shape in the proximal region and a rounded stem region. Its purpose is to transmit the principal stress applied to the bone, which is an important factor for maximum principal stress distribution.

The ORTHOHITS hip joint implant stem length is 130mm with neck offset 35 mm, neck length 33.6 mm, neck-shaft angle 135-degrees, and distal stem diameter 5.4 mm. The design is based on a standard European THA brand but with 3mm shorter neck offset, 2-3 mm shorter neck length and 1.5 mm smaller stem diameter. The femoral head size is 32 mm.

The analysis method employed in this study is FEA using ANSYS Static Structural software. FEA is a numerical analysis technique for obtaining approximate solutions to a wide variety of engineering problems, ranging from complex geometries and numerical solutions to highly complicated stress problems.[14]

The commercial program Ansys Workbench 2021 R1 was used to generate the FEA model. Three-dimensional tetrahedron meshing was used because this method offers flexibility, allowing tetrahedral elements to be used to unite three-dimensional volumes regardless of their shape or topology. The optimal mesh size was estimated, and the highest von Mises stresses remained constant between 3 and 1 mm of mesh size. We used a 2 mm mesh size for rapid, precise, and reliable simulation; the total elements and nodes from the 2 mm mesh size are 15.565 and 27.388.

According to ASTM F2996-20, ORTHOHITS hip joint implant boundary condition is 90 mm from the head's center because the length of the prosthesis ranges between 120-15 0mm. Figure 2 shows the boundary conditions for the ORTHOHITS hip joint implant simulation.[13]

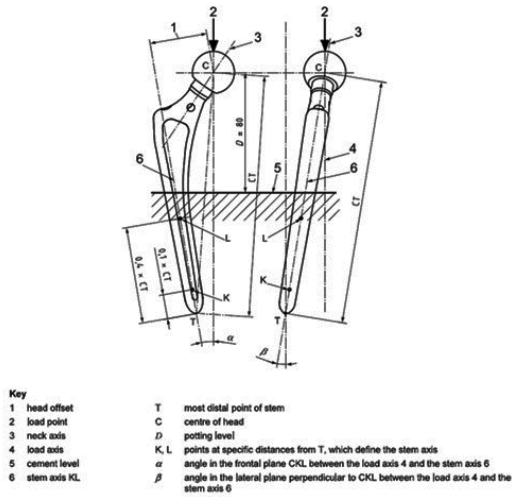

Figure 2. *Positioning of the THA implant during simulation.*

Static, dynamic, and fatigue analysis was performed according to ISO 7206-4, ISO 7206-6, and ASTM F2996-20 standards. The performance and durability of hip implants are thoroughly assessed by following ASTM F2996-20 standards and simulating loading and boundary conditions relevant to real-world situations. The hip implant model was loaded vertically with a maximum of 2300 N and a minimum of 50 N.[11-13]

Results

Static FEA was carried out on ORTHOHITS implants made of three distinct materials. The von Mises stresses induced in the implants and the total deformation obtained from the FEA calculations are shown in Table 1. The location of the maximum stress and the deformation are shown in Figure 3. The following stress distributions were induced in the implants: The maximum stress of all implants is located at the lower stem region, and the maximum deformation of all implants is located at the head.

Von Mises stresses induced in the titanium implant were lower than the stresses induced in stainless steel and cobalt

chrome implants. The displacement values in cobalt chrome are lower than those of other materials (Table 1).

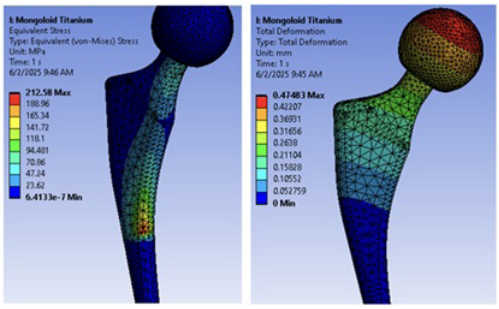

Figure 3. *Location of maximum (a) Von Mises Stress; (b) Total deformation of titanium implant.*

Tabel 1.

Von Mises stress and total deformation for the study implants

Material	Von Misses stress (MPa)	Total deformation (mm)
Stainless Steel	225.09	0.3566
Cobalt-Chrome	236.81	0.2811
Titanium	212.5	0.4748

Considering the stresses induced and the deformation that occurred, the results of the statistical analysis are equivalent based on the material's characteristics. Cobalt chrome has the highest strength, stiffness, and resistance to deformation compared to stainless steel and titanium. It is generally stiffer than other materials, making it better at withstanding deformation under stress. titanium has a relatively low Young's Modulus of elasticity compared to stainless steel and cobalt chrome. This means that it can deform more easily under stress, which means that stress can be distributed more evenly and peak stress value can be reduced.[15-17]

High-cycle fatigue FEA was performed on ORTHOHITS implants made of three distinct materials under ISO 7206-4 standard conditions. The equivalent alternating stress, the minimum life cycle of the implant, and the safety factor are presented in Table 2.

Table 2.

Fatigue Analysis Results.

Material	Alternating stress (MPa)	Life Cycle	Safey Factor
Stainless Steel	374.66	7.8938E+6	1.193
Cobalt-Chrome	119.24	1E+11	1.519
Titanium	115.86	1E+11	2.905

To understand the effects of different materials on fatigue behavior, three different implant materials were assigned to the FEA model, all of the same shape. The fatigue stress distribution and safety factor of all studied materials are shown in Figure 4.

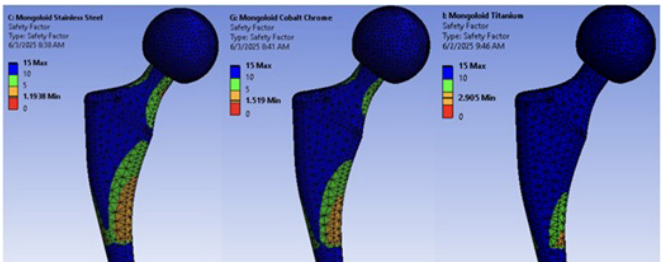

Figure 4. *Stress distribution and safety factor: (a) stainless steel, (b) cobalt-chrome, (c) titanium.*

Discussion

The equivalent alternating stress is one of the most critical parameters because it encompasses all fatigue-related calculations generally, irrespective of any material properties. Altering the characteristics of materials affects not only the fatigue alternating stresses but also the distribution of strain and displacement in the implants.[18,19] The fatigue analysis of the ORTHOHITS implant revealed the highest maximum stress at 374.66 MPa on the neck and stem region of the stainless steel implant. The lowest maximum stress was found at 115.86 MPa on the stem region of the titanium implant.

The safety factor is defined as the factor of safety for a specific design life; any value below 1 indicates that failure has occurred before the intended design life is reached. Based on simulation results, all materials' safety factor values are more than 1 (>1): 1.193 (stainless steel), 1.519 (cobalt-chrome), and 2.905 (titanium). The conclusion is that all of the materials are safe for manufacturing the ORTHOHITS hip joint implant.[20]

In this simulation, the hip implant FEA model was designed to withstand ISO 7206-4 conditions for 5×10^6 cycles without failure. Though the life cycle of the implants is well within the acceptable limit of 5 million, the stainless steel material has a significantly lower life cycle than cobalt chrome and titanium.[11]

The static structural results showed that titanium had the lowest von Mises stress at the stem, and cobalt-chrome had the lowest total deformation at the head of the implant. The material combination for the stem and head of the implant may be further studied to identify the optimal combination that offers higher factors of safety and lower damage values.[21]

The fatigue analysis showed that titanium and cobalt-chrome implants performed much better than stainless steel implants, with lower alternating stress and much higher life cycle (1E+11 vs 7.8938E+6). All of the materials have more than 1 (>1) safety factor value, which is considered safe for implant manufacturing.

The results provide insights into how different materials perform under static and dynamic loading conditions, guiding material selection for the implant productions. The real

biomechanical testing process for ORTHOHITS hip implants still needs to be carried out as validation of the Finite Element simulation results.

Acknowledgments

The authors would like to acknowledge the Indonesia Endowment Fund for Education (Ministry of Finance, Republic of Indonesia) for the support of this project through the Invitational RISPRO funding project no. PRJ-40/LPDP/2019.

Sources of Funding

This work was funded by the Indonesia Endowment Fund for Education (Ministry of Finance, Republic of Indonesia) through the Invitational RISPRO funding project no PRJ-40/LPDP/2019.

Disclosure

The authors report no conflicts of interest in this work.

References

1. Learmonth ID, Young C, Rorabeck C. The operation of the century: total hip replacement. Lancet. 2007 Oct 27;370(9597):1508-19. doi: 10.1016/S0140-6736(07)60457-7. PMID: 17964352.
2. Knight SR, Aujla R, Biswas SP. Total Hip Arthroplasty - over 100 years of operative history. Orthop Rev (Pavia). 2011 Sep 6;3(2):e16. doi: 10.4081/or.2011.e16. Epub 2011 Nov 7. PMID: 22355482; PMCID: PMC3257425.
3. Anakwe RE, Jenkins PJ, Moran M. Predicting dissatisfaction after total hip arthroplasty: a study of 850 patients. J Arthroplasty. 2011 Feb;26(2):209-13. doi: 10.1016/j.arth.2010.03.013. Epub 2010 May 11. PMID: 20462736.
4. Dundon JM, Felberbaum DL, Long WJ. Femoral stem size mismatch in women undergoing total hip arthroplasty. J Orthop. 2018 Feb 15;15(2):293-296. doi: 10.1016/j.jor.2018.02.002. PMID: 29515329; PMCID: PMC5834656.
5. Nakasone CK, Naito KT, Nishioka ST, Andrews SN. A smaller femoral stem is needed for asian females. Arch Orthop Trauma Surg. 2023 Aug;143(8):5353-5359. doi: 10.1007/s00402-022-04723-8. Epub 2022 Dec 6. PMID: 36472638.
6. Edwards K, Leyland KM, Sanchez-Santos MT, Arden CP, Spector TD, Nelson AE, Jordan JM, Nevitt M, Hunter DJ, Arden NK. Differences between race and sex in measures of hip morphology: a population-based comparative study. Osteoarthritis Cartilage. 2020 Feb;28(2):189-200. doi: 10.1016/j.joca.2019.10.014. Epub 2019 Dec 13. PMID: 31843571.
7. Kunčická L, Kocich R, Lowe T. Advances in metals and alloys for joint replacement. Prog Mater Sci. 2017;88:232-280. doi: 10.1016/j.pmatsci.2017.04.002.
8. Kaya F, İnce G. Fatigue analysis on a newly designed hip implants with finite element method. Int J Eng Innov Res. 2015;6:162-78. doi:10.47933/ijeir.1540604.
9. Pekedis M, Yildiz H. Comparison of fatigue behaviour of eight different hip stems: a numerical and experimental study. J Biomed Sci Eng. 2011;4:10. doi:10.4236/jbise.2011.410080.
10. Ploeg HL, Bürgi M, Wyss UP. Hip stem fatigue test prediction. Int J Fatigue. 2009;31:894-905. doi:10.1016/j.ijfatigue.2008.10.005.
11. The International Organization for Standardization. Implants for surgery partial and total hip prosthesis: Determination of endurance properties and performance of stemmed femoral components (ISO 7206-4). 2010. Available from: https://www.iso.org/standard/42769.html [accessed 16 July 2025].
12. The International Organization for Standardization. Implants for surgery partial and total hip prosthesis: Determination of resistance to static load of modular femoral heads (ISO 7206-10). 2018. Available from: https://www.iso.org/standard/71145.html [accessed 16 July 2025].
13. ASTM. F2996-20 Standard practice for finite element analysis (FEA) of non-modular metallic orthopaedic hip femoral stems. ASTM Int Conshohocken. 2020;22:1-11. doi:10.1520/F2996-20.
14. Jagota V, Sethi A, Kumar K. Finite element method: an overview. Walailak J Sci Technol. 2013;10:1-8. doi: 10.2004/wjst.v10i1.499.
15. Kishawy HA, Hosseini A. Titanium and titanium alloys. In: Machining difficult-to-cut materials. Materials Forming, Machining and Tribology. Springer, Cham; 2019. doi:10.1007/978-3-319-95966-5_3.
16. Colic K, Krstić D, Stanić V, Marković M, Kostić I, Radulović M, et al. Finite element modeling of hip implant static loading. Procedia Eng. 2016;149:257-62.
17. Bachtar F, Chen X, Hisada T. Finite element contact analysis of the hip joint. Med Biol Eng Comput. 2006 Aug;44(8):643-51. doi: 10.1007/s11517-006-0074-9. Epub 2006 Jul 6. PMID: 16937206.
18. Browell R. Calculating and displaying fatigue results. Ansys Sol. 2006;7:9-12.
19. Amjad M, Badshah S, Ahmad S, Badshah M, Jan S, Yasir M, Akram W, Alam Shah I, Muhammad R, Khan MI, Yasmeen T. Finite element modeling of stress distribution and safety factors in a Ti-27Nb alloy hip implant under real-world physiological loading scenarios. PLoS One. 2024 Aug 6;19(8):e0300270. doi: 10.1371/journal.pone.0300270. PMID: 39106270; PMCID: PMC11302931.
20. Taqriban R, Ismail R, Jamari J, Bayuseno A. Finite element analysis of artificial hip joint implant made from stainless steel 316L. Bali Med J. 2021;10:448-52. doi:10.15562/bmj.v10i1.2236.
21. Corda J, Chethan KN, Shenoy S, Shetty S, Shaymasunder N, Zuber M. Fatigue life evaluation of different hip implant designs using finite element analysis. J Appl Eng Sci. 2023;21:896-907. doi:10.5937/jaes0-44094.

***Corresponding author**: Prof. Dwikora Novembri Utomo, M.D., Ph.D. E-mail: dwikora-novembri-u@fk.unair.ac.id*

International Journal of Biomedicine 15(4) (2025) 704-714
http://dx.doi.org/10.21103/Article15(4)_OA10

ORIGINAL ARTICLE

Genomics and Proteomics

INTERNATIONAL JOURNAL OF BIOMEDICINE

Using Integrated Bioinformatics Strategy to Identify Differentially Expressed Genes and Hub Genes of Human Hosts with Tuberculosis

Peng Yue[1], Yan Dong[2], Fukai Bao[1,2*], Aihua Liu[1*]

[1]*Faculty of Basic Medicine, Kunming Medical University, Kunming 650500, China*
[2]*Department of Microbiology and Immunology, Haiyuan College, Kunming Medical University, Kunming 650101, China*

Abstract

Background: To date, the molecular mechanisms underlying the occurrence, development, and prognosis of tuberculosis remain incompletely understood. The study aimed to identify the host hub involved in tuberculosis.
Methods and Results: Four gene expression profiles (GSE51029, GSE52819, GSE54992, and GSE65517) were downloaded from Gene Expression Omnibus (GEO). First, the selected data sets of the *Mycobacterium tuberculosis* (MTB) infection group and the healthy control group were analyzed through GEO2R, and the genes that met the following conditions: |log FC|> 1 and P-values <0.05, are considered differentially expressed genes (DEGs). Secondly, the DEGs shared by the 4 microarray datasets were further identified. Next, Gene Ontology (GO) and Kyoto Encyclopedia of Genes and Genomes (KEGG) analyses were performed for functional enrichment analysis of these DEGs, the host hub genes were identified by the Cytohubba plugin, and module networks in DEG networks were screened by the plugin Molecular Complexity Detection (MCODE). Other bioinformatics methods were performed, including protein-protein interaction (PPI) network analysis and the construction of miRNA-hub gene networks and transcription factor (TF)-hub gene networks. Finally, the expression of the host hub genes was verified by real-time PCR.
Four GEO microarray datasets were integrated, and a total of 46 DEGs were identified. The results of the GO analysis showed that the biological functions of DEGs were primarily involved in regulating the immune response process, cytokine/chemokine activity, and receptor-ligand activity. DEGs were also significantly enriched in membrane rafts, the mitochondrial outer membrane, cytoplasmic vesicle cavities, and nuclear chromatin. KEGG enrichment analysis showed that the NOD-like receptor signaling pathway and the Toll-like receptor signaling pathway were 2 important pathways. In addition, 5 highly differentially expressed hub genes, *STAT1, TLR7, CXCL8, CCR2*, and *CCL20*, were screened out. Finally, based on the NetworkAnalyst database, we screened targeted miRNAs and TF of hub genes and found that hsa-miR-335-3p may play a key role in the regulation of these hub genes.
Conclusion: In summary, bioinformatics analyses were used to identify DEGs to find potential biomarkers that may be associated with tuberculosis. This study provides a set of candidate DEGs and 5 essential host hub genes that can be potentially useful for early detection, prognostic determination, risk assessment, and targeted tuberculosis therapy.(**International Journal of Biomedicine. 2025;15(4):704-714.**)

Keywords: tuberculosis • *Mycobacterium tuberculosis* • GEO dataset • miRNA • hub gene network • bioinformatics analysis

For citation: Yue P, Dong Y, Bao F, Liu A. Using Integrated Bioinformatics Strategy to Identify Differentially Expressed Genes and Hub Genes of Human Hosts with Tuberculosis. International Journal of Biomedicine. 2025;15(4):704-714. doi:10.21103/Article15(4)_OA10

Abbreviations

BP, biological processes; **CC**, cell components; **DEGs**, differentially expressed genes; **GEO**, Gene Expression Omnibus; **GO**, Gene Ontology; **IGRA**, interferon gamma release assay; **KEGG**, Kyoto Encyclopedia of Genes and Genomes; **MTB**, *Mycobacterium tuberculosis;* **MCODE**, Molecular Complexity Detection; **MF**, molecular functions; **PPI**, protein-protein interaction; **PBS**, phosphate-buffered saline; **STRING**, Search Tool for Retrieval of Interacting Genes; **TF**, transcription factor; **TB**, tuberculosis; **TST**, tuberculin skin test.

Introduction

Tuberculosis (TB) is a chronic infectious disease caused by *Mycobacterium tuberculosis* (MTB), which can involve many organs, but pulmonary TB is the most common infection. According to the World Health Organization, an estimated 10 million people worldwide were infected with TB in 2020, of whom 7.1 million were newly diagnosed and reported as TB cases.[1] At the same time, the incidence of TB varies from less than 5 to more than 500 cases per 100,000 population per year, and TB remains a deadly disease even in developing countries with well-established healthcare systems.

Infection with MTB causes clinical signs and symptoms when host defense is reduced or cell-mediated allergy is increased.[2] Respiratory symptoms include cough, sputum, hemoptysis, chest pain, varying degrees of chest tightness, or dyspnea. Sputum smear microscopy, bacterial culture, and MTB isolation are the most traditional, classical, and widely used diagnostic tools for TB; however, these tools require a significant amount of time, and their accuracy is not high, making it difficult to achieve early diagnosis and effective treatment of TB patients.[3] The tuberculin skin test (TST) is widely used to detect latent TB infection; however, IFN-γ release assay (IGRA), which relies on in vitro detection of a single cytokine induced by MTB-specific antigen, has been used as an alternative to the TST in the diagnosis of MTB infection.[4] However, the TST and IGRA are essentially unable to distinguish between active and latent TB infections.[5]

In recent years, rapidly developing microarray technology has been widely utilized to compare gene expression levels, predict disease progression, and facilitate accurate diagnosis and prognosis evaluations.[6,7] With the widespread use of gene expression microarray technology, a large amount of data has been published on public database platforms. The integration of these databases can be used to investigate further the molecular mechanisms involved in disease. Gene expression microarrays offer a novel approach to studying disease-related genes, providing promising prospects for molecular prediction, drug-based molecular targeting, and molecular therapy.[8] Therefore, it is essential to investigate the potential molecular mechanisms underlying TB's biological behavior to develop more effective early diagnostic techniques with high sensitivity, as well as more reliable and specific novel biomarkers to monitor recurrence and assess prognosis. There is a strong need to identify new potential diagnostic and therapeutic biomarkers for TB patients, which will not only provide new insights into the molecular and cellular processes involved in pathogenesis but also establish rapid, sensitive, and effective methods for diagnosing and treating TB.[9]

With the development of genomics technology, a large amount of data has been generated in the field of TB research.[10] In this study, we screened the differentially expressed genes(DEGs) between the MTB infection group and the healthy control group in 4 separate Gene Expression Omnibus (GEO) data sets. Then we performed Gene Ontology (GO) function enrichment analysis, Kyoto Encyclopedia of Genes and Genomes (KEGG) pathway enrichment analysis, and protein-protein interaction (PPI) network construction and module analysis. The results of this study may help to explore potential targets for the diagnosis and treatment of TB.

Materials and Methods

Microarray Dataset

The GEO database (http://www.ncbi.nlm.nih.gov/geo) is a free public genomics database that contains a variety of data, including microarray and next-generation sequencing data. We used the following keywords to search the GEO database: "tuberculosis"[MeSH Terms] OR tuberculosis [All Fields]) AND "Homo sapiens"[Organism]. The inclusion criteria of gene expression profile are as follows: The data set must include samples of peripheral blood mononuclear cells infected with MTB and normal controls; the sample size of each data set is not less than 6; there must be enough clinical information for analysis.

Based on the above search results, we obtained 4 microarray data sets from the GEO database (GSE51029, GSE52819, GSE54992, and GSE65517). The platform of GSE51029 is GPL4133 Agilent-014850 Whole Human Genome Microarray 4x44K G4112F (Feature Number version), the platform of GSE52819 is GPL6244 [HuGene-1_0-st] Affymetrix Human Gene 1.0 ST Array [transcript (gene) version], the platform of GSE54992 is GPL570 [HG-U133_Plus_2] Affymetrix Human Genome U133 Plus 2.0 Array, and the platform of GSE65517 is GPL10558 Illumina HumanHT-12 V4.0 expression beadchip. GSE51029 dataset includes 27 samples infected with MTB and 27 normal samples. GSE52819 includes 3 samples infected with MTB and 3 normal samples. GSE54992 includes 9 samples infected with MTB and 6 normal samples. GSE65517 includes 3 samples infected with MTB and 3 normal samples. The microarray data set information is shown in Table 1.

Table 1.

Detailed information about the GEO microarray data set for TB patients.

GEO profile	Source	Case	Control	Platform	Annotation platform
GSE51029	tuberculosis	27	27	GPL4133	Agilent-014850 Whole Human Genome Microarray 4x44K G4112F
GSE52819	tuberculosis	3	3	GPL6244	Affymetrix Human Gene 1.0 ST Array
GSE54992	tuberculosis	9	6	GPL570	Affymetrix Human Genome U133 Plus 2.0 Array
GSE65517	tuberculosis	3	3	GPL10558	Illumina Human HT-12 V4.0 expression beadchip

Identifying Differentially Expressed Genes

The interactive network tool GEO2R is used to analyze the gene expression data of the microarray and find DEGs.[11] In this study, the selected data sets of the MTB infection group and the healthy control group were first analyzed by GEO2R.

Subsequently, the analysis results are downloaded in Microsoft Excel format, and the genes that meet the following conditions: |log FC|>1 and P-values<0.05, were considered DEGs.[12] Finally, we used the FunRich tool (version 3.1.3) to show the intersection of DEGs. In addition, we used the R language tool (version 4.0.3) corresponding to the software R Studio to draw the heat map and correlation circle map of DEGs. The gene expression matrix data used to draw the heat map and correlation circle map was derived from GSE51029.

Function and Pathway Enrichment Analysis of DEGs

We used Metascape online software for GO analysis and KEGG pathway enrichment analysis[13] and further explored the main biological functions of the identified DEGs through functional enrichment analysis based on GO and KEGG databases.[14] The purpose of GO analysis is to identify the characteristic biological features of genes, gene products, and sequences, including biological processes (BP), cell components (CC), and molecular functions (MF).[15] KEGG pathway enrichment analysis provides a complete set of biologically interpreted genome sequence and protein interaction network information.[16] The CC, BP, and MF categories, as well as the KEGG pathway, are classified and presented in the form of bubble charts. These bubble charts are created based on the p-value using the ggplot2 R software package and the statistical software R, where $P<0.05$ is considered statistically significant.

Protein-Protein Interaction (PPI) Network Construction and Module Analysis

The Search Tool for Retrieval of Interacting Genes (STRING) database[17] (http://www.string-db.org/) is an online tool used to identify and predict interactions between genes or proteins. These interactions encompass both physical and functional associations, with data primarily derived from computational predictions, high-throughput experiments, automated text mining, and co-expression networks.[18] We mapped DEGs to the PPI network and set the interaction score>0.4 as a threshold to build a PPI analysis network for DEGs. Analysis of DEGs in the context of protein interactions can help clarify the biochemical complexes or signal transduction components that control biological output,[19] and PPI analysis is very important to explain the underlying molecular mechanisms of key cell activities in pathogenicity.[9]

Next, we used Cytoscape software (version 3.7.2) to visualize the PPI network of DEGs. Each node in the network is a gene, protein, or molecule. The connections between nodes represent the interaction of these biological molecules, which can be used to identify genes that are differentially expressed and pathway relationships between the proteins encoded by DEGs.[8] Subsequently, the modules of the PPI network were screened through the plugin MCODE in Metascape online software and Cytoscape software.[20] The default parameters are as follows: degree cutoff=2, node score cutoff=0.2, k-score=2, and max. Depth=100. Finally, Cytohubba serves as another plugin for Cytoscape.[21] Eleven methods (among which MCC shows satisfactory performance) were used to study the important nodes in the network, and the first 5 genes were selected as the target central genes.

Construction of miRNA-Hub Gene Networks and TF-Hub Gene Networks

NetworkAnalyst is a comprehensive network visualization analysis platform for gene expression analysis. The NetworkAnalyst network tool is used to find TFs of central core genes and construct TF-hub gene regulatory networks.[22] We analyzed MiRNA or TF controlled gene expressions under defined disease conditions through interaction with target genes during the post-transcriptional stage.[23,24] We also applied NetworkAnalyst (https://www.net workanalyst.ca/) to integrate miRNA databases.[25] In the study, the targeted miRNAs of hub genes were defined based on the positive results from at least 3 miRNA-target prediction databases. The targeted TF of hub genes were defined according to the positive results of the ENCODE database (http://cistrome.org/BETA/).[26,27] Finally, we visualized the target miRNA-hub gene and TF-hub gene networks using Cytoscape software.

Confirm Expression by Real-Time PCR

THP-1 is the most important immune cell line to investigate TB defense, antigen presentation, and phagocytosis. This cell line was selected for our experiment.[28] During the stimulation phase of cell culture, the standard strain MTB H37Rv was used to infect macrophages induced and differentiated from human THP-1 monocytes in vitro.[29] Trizol reagent was used to extract total RNA from cells at 24h, 48h, and 72h, respectively.

According to the manufacturer's protocol, we used the PrimeScript RT kit (Takara, Dalian, China) to reverse transcribe total RNA into cDNA and use SYBR Premix Ex Taq II (2×) to perform real-time PCR on the CFX96 PCR detection system (BioRad, California, USA). The configuration system and sample addition operations were performed on ice, and 2 replicate wells were made for detecting the target genes and the internal reference gene of each sample. The reaction volume of 25 μL contains 12.5 μL SYBR® Premix Ex Taq II (Tli RNaseH Plus) (2×), 1 μL forward primer, 1 μL reverse primer, 1 μL cDNA template, and 8.5 μL RNase-free dH_2O.The amplification conditions are as follows: 95°C for 15 s, then 40 cycles, in which the denaturation process at 95°C lasts for 5 s, and the annealing process at 58.5°C lasts for 30 s. SYBR® TB Green Premix PCR mix and primers specific to our target gene were used to amplify the target region effectively. The $2^{-\Delta\Delta}$CT method was used to calculate gene relative expression and perform statistical analysis.[30,31] The primer sequences are shown in Table 2, and the β-actin gene was used as an internal reference gene.

Statistical Analysis

The data are presented as the mean ± standard deviation (SD). GraphPad PRISM version 8.0 (GraphPad Software, Inc., San Diego, CA) was used to perform statistical calculations and prepare graphs. The inter-group comparisons were performed using an unpaired 2-tailed Student's t-test. The probability value of $P<0.05$ was considered statistically significant.

Table 2.

Primer sequence used in Real-Time PCR.

Gene	Forward	Reverse	Purification way
STAT1	ATGCTGGCACCAGAACGAATGAG	TCACCACAACGGGCAGAGAGG	PAGE
TLR7	ACCAACTGACCACTGTCCCTGAG	TCGCAACTGGAAGGCATCTTGTAG	PAGE
CCL20	AACAGCACTCCCAAAGAACTGG	GCAGAGGTGGAGTAGCAGCA	PAGE
CCR2	CCAACGAGAGCGGTGAAGAAGTC	CGAGTAGAGCGGAGGCAGGAG	PAGE
CXCL8	ACTTTCAGAGACAGCAGAGCACAC	CACACAGTGAGATGGTTCCTTCCG	PAGE
β-actin	TGGCATCCACGAAACTACCT	CAATGCCAGGGTACATGGTG	PAGE

Results

Microarray Data Information and Identification of Candidate DEGs

The 4 microarray expression datasets, GSE51029, GSE52819, GSE54992, and GSE65517, were obtained from the GEO database. The above data sets were uploaded to GEO2R and standardized (Figure 1) to screen DEGs between the TB patient group and the normal control group and create a volcano map of the distribution of these DEGs in 4 data sets. The differential expression of multiple genes in the 2 sets of sample data in each array is shown in Figure 2.

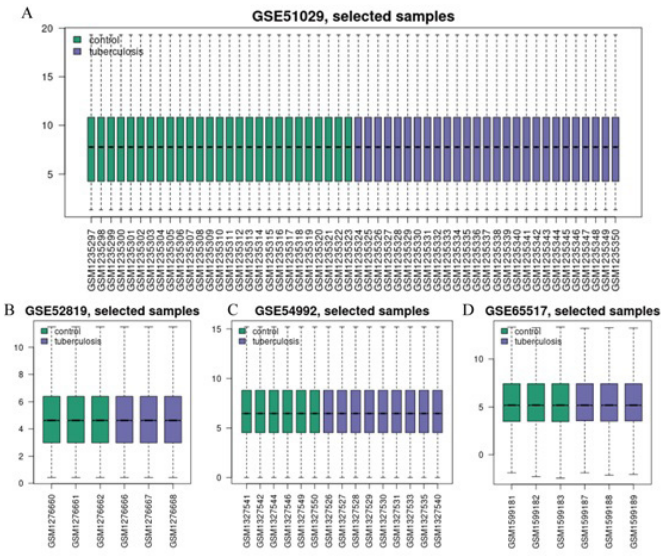

Figure 1. *Standardization of gene expression.*

(A) The standardization of GSE51029 data, (B) the standardization of GSE52819 data, (C) the standardization of GSE54992 data, and (D) the standardization of GSE65517 data. The green bars represent the normalized data for the healthy control group, and the blue bars represent those for the TB infection group.

In the GSE51029 data set, 5182 DEGs were obtained, including 1024 up-regulated genes and 4156 down-regulated genes. In the GSE52819 data set, 1959 DEGs were obtained, including 1044 up-regulated genes and 915 down-regulated genes. In the GSE54992 data set, 7461 DEGs were obtained, including 3918 up-regulated genes and 3543 down-regulated genes. In the GSE65517 data set, 2604 DEGs were obtained, including 1337 up-regulated genes and 1267 down-regulated genes.

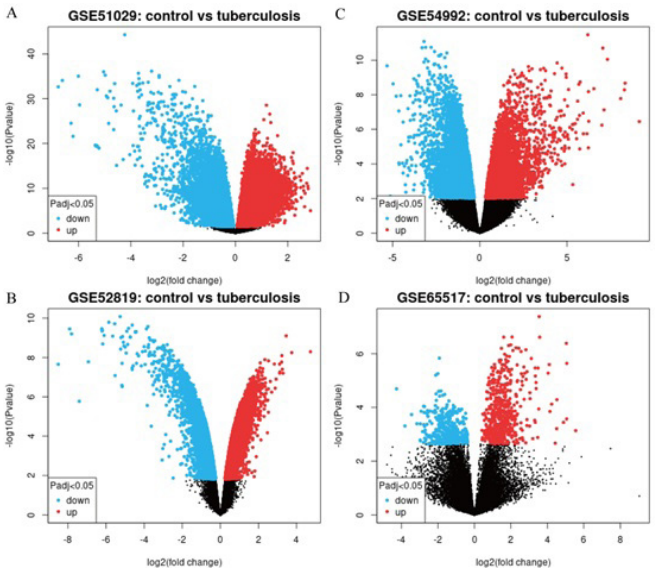

Figure 2. *Differential expression trends of data between two sets of samples.*

(A) GSE51029 data, (B) GSE52819 data, (C) GSE54992 data, and (D) GSE65517 data. The red points represent up-regulated genes screened based on \|fold change\| >1.0 and a corrected P-value of <0.05. The green points represent downregulation of gene expression, screened based on \|fold change\| >1.0 and a corrected P-value of <0.05. The black points represent genes with no significant difference.

According to the criteria of |log FC|> 1 and *P*-values <0.05, we used FunRich software to display the intersection of DEGs in the 4 microarray expression data, a total of 46 overlapping genes were found (Figure 3A), which were regarded as candidate DEGs and used for further analysis. We used the pheatmap software package in R Studio to visualize the heat map of 46 DEGs (Figore 3B). It is worth mentioning that by using the corrplot and circlize software packages in R Studio to visualize 46 DEGs, the generated correlation circle graph can show the correlation of multiple genes in one picture (Figure 3C). The outer circle represents genes, and the line between the 2 genes represents the correlation coefficient. Positive correlation is shown in red, and negative correlation is shown in green. The darker the color, the more significant the correlation.

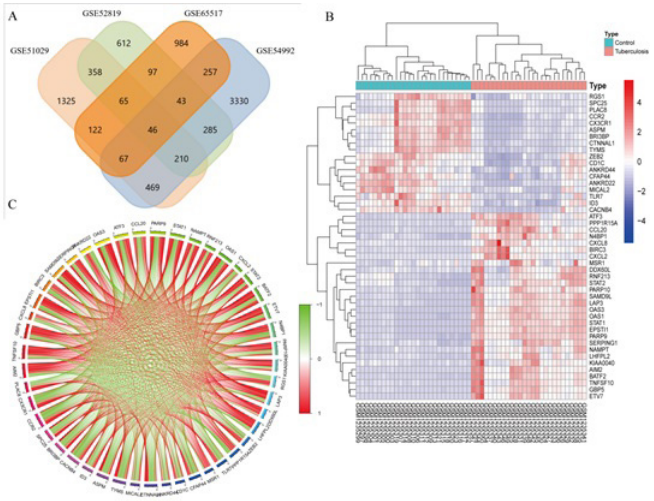

Figure 3. *Selection of candidate DEGs, hierarchical clustering heatmap, and corCircos.*
(A) Venn diagram for overlapping differentially expressed genes (DEGs) based on the four datasets, namely, GSE51029, GSE52819, GSE54992, and GSE65517. (B) The hierarchical clustering heatmap data derived from GSE51029: red indicates relatively up-regulated gene expression, and blue indicates relatively down-regulated gene expression. (C) Circos shows the relationships among multiple genes in a single picture. The positive correlation is shown in red, and the negative correlation is shown in green.

Enrichment Analysis of GO and KEGG Pathways

Enrichment analysis is the core of most existing gene annotation portals.[32] In the enrichment analysis process, the input gene list is compared with thousands of gene sets, which are defined by their participation in specific BP, protein localization, enzyme functions, pathway members, or other characteristics. We used RSQLite, org.Hs.eg.db, clusterProiler and other software packages in R software to analyze and visualize the GO function and KEGG pathway enrichment of 46 DEGs. The results are shown in Figure 4.

The top 20 most important items of enrichment analysis are illustrated in the form of bubble diagrams. The size and color of the bubbles indicate the number of DEGs and the importance of enrichment in the enrichment analysis of GO and KEGG pathways, respectively. The first 5 important terms of GO enrichment analysis indicate that in the BP category, DEGs participate in the defense response to the virus, the regulation of the immune response process, the cellular response to interferon-γ, the regulation of the innate immune response, and the mediation of the chemokine signaling pathway (Fig. 4A). For the MF category, DEGs are related to cytokine receptors, cytokine activity, G protein-coupled receptor binding, receptor ligand activity, and signal receptor activator activity (Fig. 4B). For the CC category, DEGs are significantly enriched in membrane rafts, mitochondrial outer membrane, cytoplasmic vesicle cavity, endocytic vesicles, and nuclear chromatin (Fig. 4C).

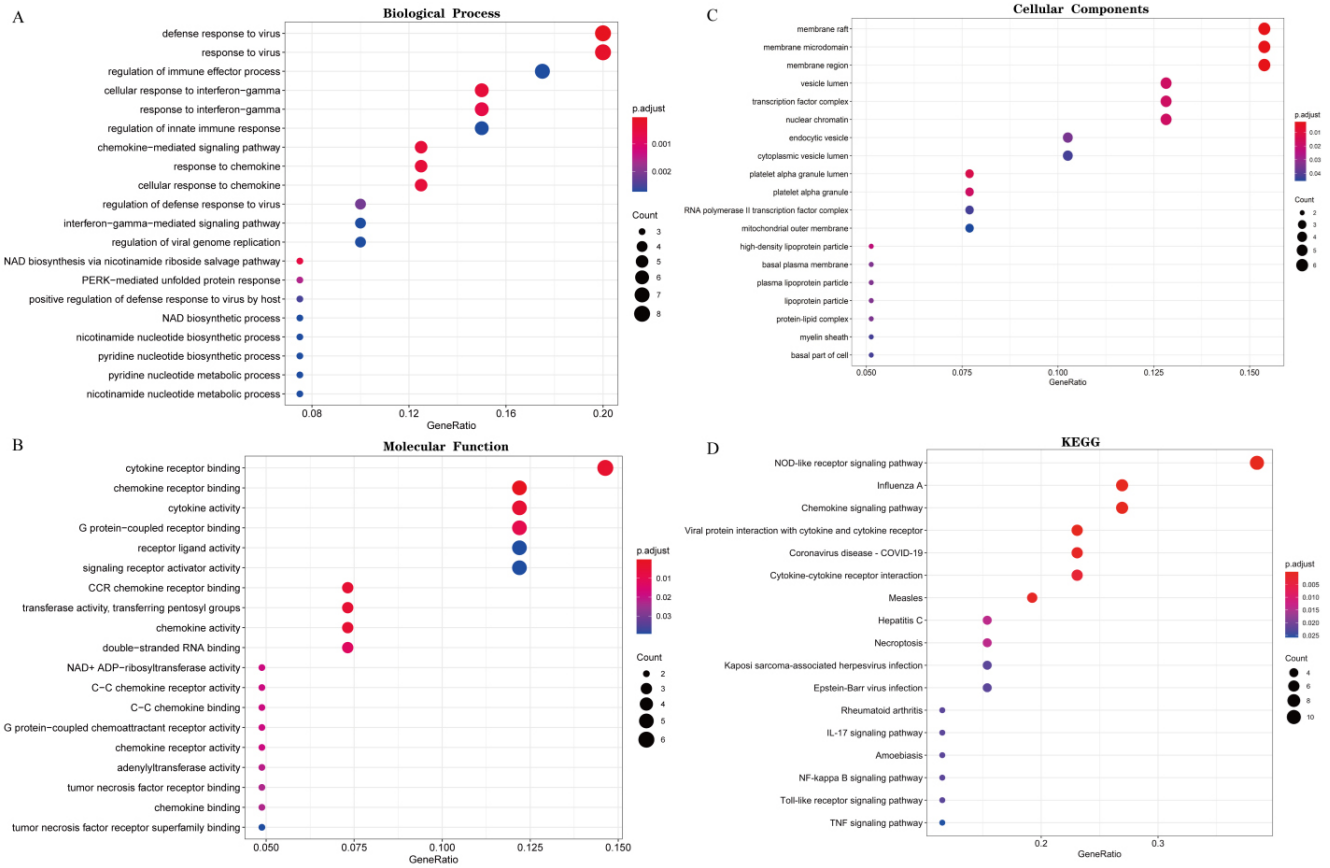

Figure 4. *Bubble map for GO and KEGG pathway analyses of DEGs.*
(A) Top 20 biological process (BP) terms, (B) Top 20 molecular functions (MF) terms, (C) Top 20 cellular components (CC) terms, and (D) Top 20 Kyoto Encyclopedia of Genes and Genomes (KEGG) pathways. The horizontal axis represents the significance of enrichment (denoted by Gene Ratio; the larger the value, the more significant the enrichment), and the vertical axis represents the GO terms enriched. The dot size and depth indicate the number of DEGs contained in the GO terms and the degree of the rich factor enrichment, respectively. We selected the top 20 GO terms according to Gene Ratio.

For KEGG pathway enrichment analysis, the first several important KEGG pathways of DEGs include the NOD-like receptor signaling pathway, influenza A, chemokine signaling pathway, COVID-19, Toll-like receptor signaling pathway, and NF-kappa B signaling pathway. To illustrate the position and significance of DEGs in the pathway in detail, based on KEGG enrichment analysis, the pathview software package in R Studio was utilized to visualize the 46 DEGs identified. The pathway diagrams are stored as the attached files.

PPI Network Construction Analysis and Host Hub Gene Selection

PPI network analysis has been regarded as a useful tool for exploring biological responses in health and disease.[33] According to the STRING database and Cytoscape software, 46 DEGs are located in the PPI network complex, including 46 nodes and 83 edges. The PPI enrichment p-value is less than 1.0e-16, and the confidence score is greater than 0.4. Finally, Cytoscape is used to visualize the PPI network of these DEGs [34] (Figure 5). After deleting isolated and partially connected nodes, a complex PPI network was successfully constructed (Figure 5A).

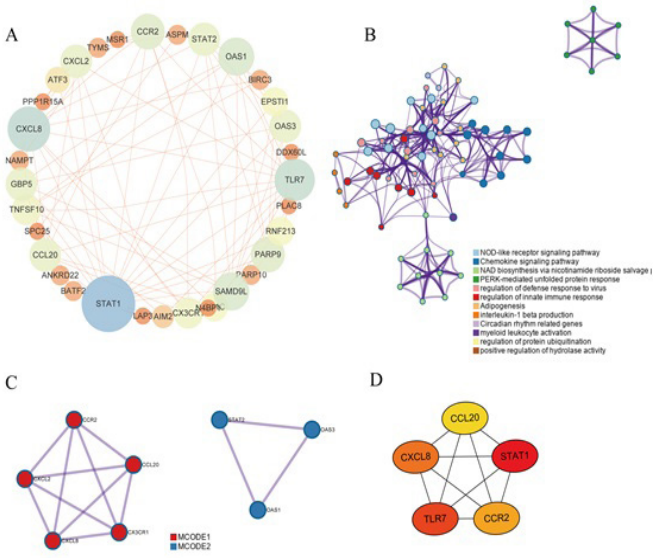

Figure 5. *Protein-protein interaction (PPI) network of differentially expressed genes and identification of hub genes.*

(A) PPI network of differentially expressed genes (DEGs). (B) Network of enriched terms of differentially expressed proteins colored by cluster ID. Each node represents an enriched term and is colored by its cluster ID. Nodes that share the same cluster ID are typically close to each other. (C) MCODE components identified in the PPI interaction network. Each node represents a gene, and different colors represent different MCODE components. (D) Subnetwork of the top five hub genes from the PPI network. Node color reflects the degree of connectivity (Red color represents a higher degree, and yellow color represents a lower degree).

The online software Metascape applies the mature complex recognition algorithm MCODE, which can automatically extract protein complexes embedded in large-scale networks.[35] It is worth mentioning that Metascape has obvious advantages in PPI network module analysis and GO enrichment analysis[36] and can directly obtain relevant data. We use Cytoscape to visualize the module analysis results generated by Metascape. The MCODE plugin of the latter filters the module network within the PPI network again (Figure 5B-C), and the options are set as default parameters. Host hub genes are a series of genes that play a vital role in diversified BP, and other genes are usually regulated by these hub genes.[37] As another plugin in Cytoscape, Cytohubba utilizes maximal clique centrality (MCC) to identify key nodes in the network and select the most relevant genes as target hub genes.[38] In this study, the top 5 hub genes with the highest degree of interaction were identified (Figure 5D), including STAT1 (Signal transducer and activator of transcription 1-alpha/beta), TLR7 (Toll-like receptor 7), CXCL8 (C-X-C motif chemokine ligand 8), CCR2 (C-C chemokine receptor type 2), CCL20 (C-C motif chemokine 20).

Construction and Analysis of the miRNA-Hub Gene Network and TF-Hub Gene Network

NetworkAnalyst was used to screen targeted miRNA and TF for hub genes.[39] For these 5 identified hub genes, the top 3 miRNA-targeted DEGs are *TLR7*, regulated by 39 miRNAs, *CXCL8*, regulated by 36 miRNAs, and *STAT1*, regulated by 19 miRNAs. The miRNA that controls the largest number of hub genes (3 genes) is hsa-mir-335-5p (Figure 6A), and other important miRNAs are shown in Table 3. Unfortunately, when the selected 5 core genes were imported into the ENCODE of the TF database, only 2 of them could be analyzed: *CCL20*, regulated by 39 TFs, and *CCR2*, regulated by 2 TFs (Figure 6B).

Table 3.

MiRNAs and its target genes.

miRNA	Hub genes targeted by miRNA	Gene count	Betweenness Centrality
hsa-mir-335-5p	*CXCL8, CCR2, CCL20*	3	0.21933622
hsa-mir-93-5p	*CXCL8, TLR7*	2	0.0620336
hsa-mir-106a-5p	*CXCL8, TLR7*	2	0.0620336
hsa-mir-203a-3p	*CXCL8, STAT1*	2	0.05025596
hsa-mir-146a-5p	*CXCL8, STAT1*	2	0.05025596
hsa-mir-150-5p	*TLR7, STAT1*	2	0.11976912
hsa-mir-155-5p	*CXCL8, STAT1*	2	0.05025596
hsa-mir-302c-3p	*CXCL8, TLR7*	2	0.0620336
hsa-mir-302d-3p	*CXCL8, TLR7*	2	0.0620336
hsa-mir-520b	*CXCL8, TLR7*	2	0.0620336

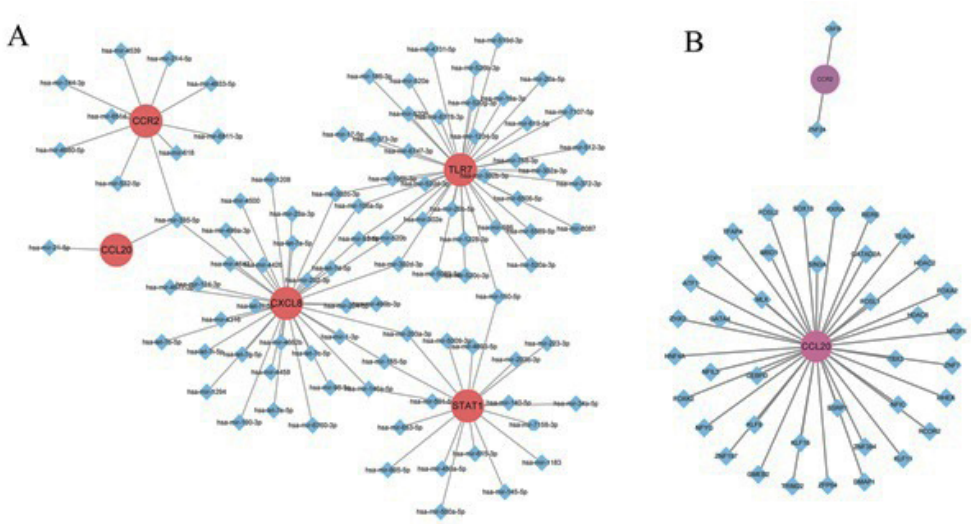

Figure 6. *Regulatory networks of miRNA-hub gene and TF-hub gene.*

The networks of (A) miRNA-hub gene and (B) TF-hub gene. The red or purple circle nodes are the hub genes, and the blue diamond nodes are the miRNAs and the TF.

Verifying the Expression Levels of Hub Genes by Real-Time PCR

To verify the accuracy of the prediction results, this study utilized real-time PCR to detect the mRNA expression levels of the 5 host hub core genes at 24-, 48-, and 72 hours after MTB infection of the cells. At least 3 biological replicates were performed for each experiment. The results showed that the expressions of core genes are generally consistent with the heat map results derived from the gene expression matrix (GSE51029_series_matrix) data. Specifically, compared with the PBS group, the mRNA expression levels of *STAT1*, *CCL20*, and *CXCL8* in the MTB group were all up-regulated at 3 time points (Figure 7A-C), while the mRNA expression levels of *TLR7* and *CCR2* at all 3 time points showed down-regulation (Figure 7D-E).

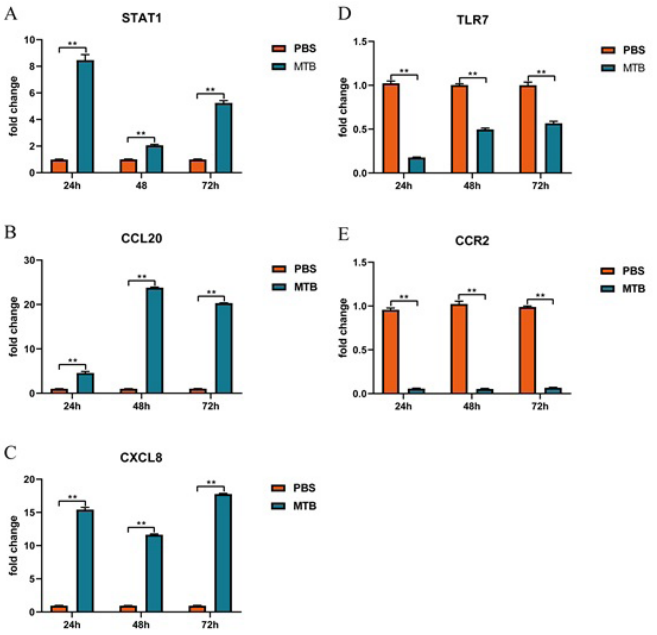

Figure 7. *The expression levels of relevant gene mRNA analyzed by Real-Time PCR, comparing the MTB infection group with the control group.*

*(A-C) STAT1, CCL20, and CXCL8 were demonstrated to be upregulated in the MTB group compared to the PBS group at 24, 48, 72 hours. (D-E) TLR7 and CCR2 were shown to be downregulated in the MTB group compared to the PBS group at 24, 48, and 72 hours. Data represent mean±SD (n=3). Asterisks denote: **P<0.01indicates significance. The yellow color represents the MTB group, and the blue color represents the PBS group.*

Discussion

TB is an infectious disease that seriously harms human health. It is caused by MTB, a bacterium that is parasitic in macrophages.[40] As an intracellular pathogen, MTB largely depends on its ability to compromise the host's innate immune defense system, specifically the macrophage.[41] As the human body's first line of immune defense, macrophages can kill MTB through phagocytosis, oxidative stress, acidification, and antigen presentation.[42] Therefore, the bioinformatics research on macrophages stimulated by MTB is particularly important.

The method of bioinformatics helps analyze the expression of key genes to reveal the potential molecular mechanisms underlying the biological behavior of TB, providing novel insights for elucidating the pathogenesis of the disease. Microarray technology enables us to investigate host genetic changes and gene expression associated with TB and has proven to be a valuable method for identifying new biomarkers in other diseases.[43] In this study, 4 GEO microarray data sets (GSE51029, GSE52819, GSE54992, and GSE65517) were integrated to identify DEGs between PBMC of TB patients and healthy people to offset the false positive rate in the analysis of independent data sets. According to the criteria of |log FC|> 1 and *P*-values <0.05,

this study used FunRich software to display the intersection of DEGs in the four-microarray expression data and found a total of 46 overlapping DEGs that can be considered as candidates. The GO function and KEGG pathway enrichment analysis, PPI network analysis, and core gene selection were carried out successively, followed by the construction of target gene-miRNA networks and target gene-TF networks, and the verification of core gene expression at the mRNA level.

According to the results of GO enrichment analysis, in the BP category, DEGs are primarily involved in regulating immune effect processes, IFN-γ-mediated signaling pathways, nicotinamide nucleotide biosynthesis processes, NAD biosynthesis processes, and chemokine-mediated signaling pathways. Studies have shown that in the case of initial infection, macrophages will encounter MTB before being stimulated by the Th1 cytokine IFN-γ.[44] However, only after stimulation with IFN-γ can the antibacterial ability and antigen presentation function of macrophages be fully activated.[45] For the MF category, DEGs are associated with cytokine/chemokine receptor binding, cytokine/chemokine activity, G protein-coupled receptor binding, receptor ligand activity, and signal receptor activator activity. MTB induces host pro-inflammatory mediators that play a crucial role in disease control;[46] among these, chemokines are small molecular-weight proteins involved in immune regulation and inflammation.[40] For the CC category, DEGs are significantly enriched in membrane rafts, mitochondrial outer membrane, cytoplasmic vesicle cavity, endocytic vesicles, and nuclear chromatin. KEGG enrichment analysis showed that the NOD-like receptor signaling pathway and the Toll-like receptor signaling pathway are 2 important pathways associated with TB. Innate immune cells utilize various pattern recognition receptors, including Toll-like receptors, C-type lectin receptors, and NOD-like receptors, to respond to pathogen components and perform a range of biological functions.[47,48] Studies have shown that experimental models of TB have highlighted the importance of TLRs in preventing MTB.[49] Additionally, antigen recognition by NOD-2 (nucleotide-binding oligomerization domain 2), a member of the NOD-like receptor family, is also crucial in conferring immunity against bacteria and viruses.[50,51] This suggests that the coordinated triggering of TLRs and NOD-2 may lead to a stronger and lasting immune response, thereby limiting the growth of MTB.[52]

By constructing a PPI network and analyzing it with MCODE and Cytohubba in Cytoscape, 5 core genes were identified. Studies have reported that in the early stage of TB infection, *STAT1* can promote the activation of downstream apoptotic factors through phosphorylation,[53] thereby activating transcription. At the same time, *STAT1* is also crucial in promoting the polarization of macrophages into the M1 phenotype. Polarized M1 macrophages can eliminate MTB infection more effectively than polarized M2 macrophages.[54] It is reported that after ssRNA upregulates TLR7, the number of MTB in macrophages is significantly reduced, and the macrophage viability is significantly increased, indicating that TLR7 can effectively inhibit the growth of MTB and improve the viability of macrophages.[42] Kane et al.[55] found that fibroblasts, through their CXCL8-dependent contribution to cell recruitment and mycobacterial killing in granulomas, have a previously unrecognized role in regulating TB inflammation. In the study by Dunlap et al.[56] the mouse model provided evidence that the *CCR2* axis is essential for protective immunity against the emerging MTB lineage infection. Another report showed that *CCL20* is overexpressed in monocytes infected by MTB and inhibits the production of reactive oxygen species (ROS).[57]

To study the molecular mechanisms of potential core gene disorders, it is necessary to identify potential miRNAs using bioinformatics methods. The miRNA is an endogenous, non-coding RNA molecule with a length of 18-22 nucleotides that targets the 3' untranslated region of a gene. It can regulate gene expression at the post-transcriptional level by degrading or inhibiting the translation of target genes.[58] miRNAs are known to regulate gene expression post-transcriptionally by either inhibiting protein synthesis or targeting mRNA for degradation.[59] Increasing evidence suggests that miRNAs are closely linked to the development and progression of cancer and other major diseases. In this study, the top 3 targeted DEGs in the miRNA gene network were *CXCL8*, *TLR7*, and *STAT1*. At the same time, we observed 10 miRNAs and found that their targeting involves at least 2 core genes. Among them, the miRNA that controls the largest number of core genes is hsa-mir-335-5p; however, there are currently few studies related to it. One study found that the gain and loss of hsa-miR-335-3p function can lead to changes in the expression of GATA4 and NKX2-5, 2 cardiac differentiation markers, during the cardiac differentiation of human embryonic stem cells.[60] In addition, hsa-miR-335-3p has been identified as an upstream regulator of 2 modules related to the recurrence of osteosarcoma patients.[61] The results of bioinformatics analysis found that hsa-mir-335-5p has high potential as a new biomarker. This study also established a hot TF-hub gene regulatory network to further explore the molecular mechanism of TB.[62] TF is the primary regulator of gene expression and is associated with the pathogenesis of TB. In our study, we also found some TFs that interact closely with hub genes (*MLX*, *TFDP1*, *RXRA*, *ZNF197*, *GMEB2*, *TRIM22*). The complex interaction between TF and hub genes has made a huge contribution to the development of the disease. Our study analyzed the miRNA/TF interactions of hub genes, providing a possibility to predict potential therapeutic agents and explore the potential mechanisms of TB. Therefore, our results lay the foundation for further research.

Conclusion

In summary, our study identified DEGs through bioinformatics analysis to discover potential biomarkers that may be related to the progression of TB. The study provides a set of candidate DEGs and 5 important hub genes. These results can provide a basis for screening candidate drugs and biomarkers for the diagnosis of TB and can be used for future research on the molecular mechanism. However, further studies, including cell and animal experiments, are

needed to elucidate the functions of DEGs in physiological and pathological processes. In the future, in-depth exploration of molecular mechanisms of new hub genes is required in TB, and related experimental models can be constructed based on these genes for early detection, prognosis judgment, risk assessment, and targeted TB therapy.

Sources of Funding

The research project was funded by grants from the National Natural Science Foundation of China (Nos. 82560396 and 82160304).

Competing Interests

The authors declare that they have no financial/commercial conflicts of interest concerning this article.

References

1. WHO. Global tuberculosis report 2020. Geneva, 2020. https://www.who.int/publications/i/item/9789240013131
2. Fan S, Zhou G, Shang P, et al. Clinical Study of 660 Cases of Pulmonary Tuberculosis. Harbin Medical Journal, 2014, 34(1):1-11.
3. Siddiqi K, Lambert ML, Walley J. Clinical diagnosis of smear-negative pulmonary tuberculosis in low-income countries: the current evidence. Lancet Infect Dis. 2003 May;3(5):288-96. doi: 10.1016/s1473-3099(03)00609-1.
4. Won EJ, Choi JH, Cho YN, Jin HM, Kee HJ, Park YW, et al. Biomarkers for discrimination between latent tuberculosis infection and active tuberculosis disease. J Infect. 2017 Mar;74(3):281-293. doi: 10.1016/j.jinf.2016.11.010. Epub 2016 Nov 19. PMID: 27871809.
5. Sharma SK, Vashishtha R, Chauhan LS, Sreenivas V, Seth D. Comparison of TST and IGRA in Diagnosis of Latent Tuberculosis Infection in a High TB-Burden Setting. PLoS One. 2017 Jan 6;12(1):e0169539. doi: 10.1371/journal.pone.0169539. PMID: 28060926; PMCID: PMC5218498.
6. Salem H, Attiya G, El-Fishawy N. Classification of human cancer diseases by gene expression profiles. Applied Soft Computing, 2017, 50:124-34.
7. Ramaswamyreddy SH, Smitha T. Microarray-based gene expression profiling for early detection of oral squamous cell carcinoma. J Oral Maxillofac Pathol. 2018 Sep-Dec;22(3):293-295. doi: 10.4103/jomfp.JOMFP_270_18. PMID: 30651668; PMCID: PMC6306598.
8. Yang X, Zhu S, Li L, Zhang L, Xian S, Wang Y, Cheng Y. Identification of differentially expressed genes and signaling pathways in ovarian cancer by integrated bioinformatics analysis. Onco Targets Ther. 2018 Mar 15;11:1457-1474. doi: 10.2147/OTT.S152238. PMID: 29588600; PMCID: PMC5858852.
9. Xie L, Chao X, Teng T, Li Q, Xie J. Identification of Potential Biomarkers and Related Transcription Factors in Peripheral Blood of Tuberculosis Patients. Int J Environ Res Public Health. 2020 Sep 24;17(19):6993. doi: 10.3390/ijerph17196993. PMID: 32987825; PMCID: PMC7579196.
10. Qin XB, Zhang WJ, Zou L, Huang PJ, Sun BJ. Identification potential biomarkers in pulmonary tuberculosis and latent infection based on bioinformatics analysis. BMC Infect Dis. 2016 Sep 21;16(1):500. doi: 10.1186/s12879-016-1822-6. PMID: 27655333; PMCID: PMC5031349.
11. Dumas J, Gargano M, Dancik GM. An online tool for biomarker analysis in Gene Expression Omnibus (GEO) datasets. Bioinform. 2016: 5292.
12. Xu Z, Zhou Y, Cao Y, Dinh TL, Wan J, Zhao M. Identification of candidate biomarkers and analysis of prognostic values in ovarian cancer by integrated bioinformatics analysis. Med Oncol. 2016 Nov;33(11):130. doi: 10.1007/s12032-016-0840-y. Epub 2016 Oct 18. PMID: 27757782.
13. Zhou Y, Zhou B, Pache L, Chang M, Khodabakhshi AH, Tanaseichuk O, et al. Metascape provides a biologist-oriented resource for the analysis of systems-level datasets. Nat Commun. 2019 Apr 3;10(1):1523. doi: 10.1038/s41467-019-09234-6. PMID: 30944313; PMCID: PMC6447622.
14. Kanehisa M, Sato Y, Kawashima M, Furumichi M, Tanabe M. KEGG as a reference resource for gene and protein annotation. Nucleic Acids Res. 2016 Jan 4;44(D1):D457-62. doi: 10.1093/nar/gkv1070. Epub 2015 Oct 17. PMID: 26476454; PMCID: PMC4702792.
15. Gene Ontology Consortium. The Gene Ontology (GO) project in 2006. Nucleic Acids Res. 2006 Jan 1;34(Database issue):D322-6. doi: 10.1093/nar/gkj021. PMID: 16381878; PMCID: PMC1347384.
16. Kanehisa M, Goto S. KEGG: kyoto encyclopedia of genes and genomes. Nucleic Acids Res. 2000 Jan 1;28(1):27-30. doi: 10.1093/nar/28.1.27. PMID: 10592173; PMCID: PMC102409.
17. Franceschini A, Szklarczyk D, Frankild S, Kuhn M, Simonovic M, Roth A, et al. STRING v9.1: protein-protein interaction networks, with increased coverage and integration. Nucleic Acids Res. 2013 Jan;41(Database issue):D808-15. doi: 10.1093/nar/gks1094. Epub 2012 Nov 29. PMID: 23203871; PMCID: PMC3531103.
18. Wang H, Zhu H, Zhu W, Xu Y, Wang N, Han B, Song H, Qiao J. Bioinformatic Analysis Identifies Potential Key Genes in the Pathogenesis of Turner Syndrome. Front Endocrinol (Lausanne). 2020 Mar 6;11:104. doi: 10.3389/fendo.2020.00104. PMID: 32210915; PMCID: PMC7069359.
19. Pizzuti C, Rombo SE. Algorithms and tools for protein-protein interaction networks clustering, with a special focus on population-based stochastic methods. Bioinformatics. 2014 May 15;30(10):1343-52. doi: 10.1093/bioinformatics/btu034. Epub 2014 Jan 22. PMID: 24458952.
20. Bandettini WP, Kellman P, Mancini C, Booker OJ, Vasu S, Leung SW, et al. MultiContrast Delayed Enhancement (MCODE) improves detection of subendocardial myocardial infarction by late gadolinium enhancement cardiovascular magnetic resonance: a clinical validation study. J Cardiovasc Magn Reson. 2012 Nov 30;14(1):83. doi: 10.1186/1532-429X-14-83. PMID: 23199362; PMCID: PMC3552709.
21. Chin CH, Chen SH, Wu HH, Ho CW, Ko MT, Lin CY. cytoHubba: identifying hub objects and sub-networks from complex interactome. BMC Syst Biol. 2014;8 Suppl 4(Suppl 4):S11. doi: 10.1186/1752-0509-8-S4-S11. Epub 2014 Dec 8. PMID: 25521941; PMCID: PMC4290687.
22. Zhou G, Soufan O, Ewald J, Hancock REW, Basu N, Xia J. NetworkAnalyst 3.0: a visual analytics platform for comprehensive gene expression profiling and meta-analysis. Nucleic Acids Res. 2019 Jul 2;47(W1):W234-W241.

doi: 10.1093/nar/gkz240. PMID: 30931480; PMCID: PMC6602507.
23. Soifer HS, Rossi JJ, Saetrom P. MicroRNAs in disease and potential therapeutic applications. Mol Ther. 2007 Dec;15(12):2070-9. doi: 10.1038/sj.mt.6300311. Epub 2007 Sep 18. PMID: 17878899.
24. Baldwin AS Jr. Series introduction: the transcription factor NF-kappaB and human disease. J Clin Invest. 2001 Jan;107(1):3-6. doi: 10.1172/JCI11891. PMID: 11134170; PMCID: PMC198555.
25. Xia J, Gill EE, Hancock RE. NetworkAnalyst for statistical, visual and network-based meta-analysis of gene expression data. Nat Protoc. 2015 Jun;10(6):823-44. doi: 10.1038/nprot.2015.052. Epub 2015 May 7. PMID: 25950236.
26. Yang D, He Y, Wu B, Deng Y, Wang N, Li M, Liu Y. Integrated bioinformatics analysis for the screening of hub genes and therapeutic drugs in ovarian cancer. J Ovarian Res. 2020 Jan 27;13(1):10. doi: 10.1186/s13048-020-0613-2. PMID: 31987036; PMCID: PMC6986075.
27. Yang W, Zhao X, Han Y, Duan L, Lu X, Wang X, et al. Identification of hub genes and therapeutic drugs in esophageal squamous cell carcinoma based on integrated bioinformatics strategy. Cancer Cell Int. 2019 May 22;19:142. doi: 10.1186/s12935-019-0854-6. PMID: 31139019; PMCID: PMC6530124.
28. Zhang YW, Lin Y, Yu HY, Tian RN, Li F. Characteristic genes in THP1 derived macrophages infected with Mycobacterium tuberculosis H37Rv strain identified by integrating bioinformatics methods. Int J Mol Med. 2019 Oct;44(4):1243-1254. doi: 10.3892/ijmm.2019.4293. Epub 2019 Jul 30. PMID: 31364746; PMCID: PMC6713430.
29. Feng Z, Bai X, Wang T, Garcia C, Bai A, Li L, et al. Differential Responses by Human Macrophages to Infection With *Mycobacterium tuberculosis* and Non-tuberculous Mycobacteria. Front Microbiol. 2020 Feb 7;11:116. doi: 10.3389/fmicb.2020.00116. PMID: 32117140; PMCID: PMC7018682.
30. Ding Z, Sun L, Bi Y, Zhang Y, Yue P, Xu X, et al. Integrative Transcriptome and Proteome Analyses Provide New Insights Into the Interaction Between Live Borrelia burgdorferi and Frontal Cortex Explants of the Rhesus Brain. J Neuropathol Exp Neurol. 2020 May 1;79(5):518-529. doi: 10.1093/jnen/nlaa015. PMID: 32196082.
31. Livak KJ, Schmittgen TD. Analysis of relative gene expression data using real-time quantitative PCR and the 2(-Delta Delta C(T)) Method. Methods. 2001 Dec;25(4):402-8. doi: 10.1006/meth.2001.1262. PMID: 11846609.
32. Li H, Long J, Xie F, Kang K, Shi Y, Xu W, et al. Transcriptomic analysis and identification of prognostic biomarkers in cholangiocarcinoma. Oncol Rep. 2019 Nov;42(5):1833-1842. doi: 10.3892/or.2019.7318. Epub 2019 Sep 17. PMID: 31545466; PMCID: PMC6787946.
33. Vella D, Marini S, Vitali F, Di Silvestre D, Mauri G, Bellazzi R. MTGO: PPI Network Analysis Via Topological and Functional Module Identification. Sci Rep. 2018 Apr 3;8(1):5499. doi: 10.1038/s41598-018-23672-0. PMID: 29615773; PMCID: PMC5882952.
34. Feng H, Gu ZY, Li Q, Liu QH, Yang XY, Zhang JJ. Identification of significant genes with poor prognosis in ovarian cancer via bioinformatical analysis. J Ovarian Res. 2019 Apr 22;12(1):35. doi: 10.1186/s13048-019-0508-2.
35. Liang J, Wu M, Bai C, Ma C, Fang P, Hou W, et al. Network Pharmacology Approach to Explore the Potential Mechanisms of Jieduan-Niwan Formula Treating Acute-on-Chronic Liver Failure. Evid Based Complement Alternat Med. 2020 Dec 30;2020:1041307. doi: 10.1155/2020/1041307. PMID: 33456481; PMCID: PMC7787753.
36. Li W, Wang S, Qiu C, Liu Z, Zhou Q, Kong D, Ma X, Jiang J. Comprehensive bioinformatics analysis of acquired progesterone resistance in endometrial cancer cell line. J Transl Med. 2019 Feb 27;17(1):58. doi: 10.1186/s12967-019-1814-6. PMID: 30813939; PMCID: PMC6391799.
37. Zhang YM, Meng LB, Yu SJ, Ma DX. Identification of potential crucial genes in monocytes for atherosclerosis using bioinformatics analysis. J Int Med Res. 2020 Apr;48(4):300060520909277. doi: 10.1177/0300060520909277. PMID: 32314637; PMCID: PMC7175059.
38. Guo C, Li Z. Bioinformatics Analysis of Key Genes and Pathways Associated with Thrombosis in Essential Thrombocythemia. Med Sci Monit. 2019 Dec 5;25:9262-9271. doi: 10.12659/MSM.918719. PMID: 31801935; PMCID: PMC6911306..
39. Zhou R, Liu D, Zhu J, Zhang T. Common gene signatures and key pathways in hypopharyngeal and esophageal squamous cell carcinoma: Evidence from bioinformatic analysis. Medicine (Baltimore). 2020 Oct 16;99(42):e22434. doi: 10.1097/MD.0000000000022434. PMID: 33080677; PMCID: PMC7571924.
40. Lyon SM, Rossman MD. Pulmonary tuberculosis. Tuberculosis and Nontuberculous Mycobacterial Infections. 2017,5(1):283-98.
41. Kumar M, Sahu SK, Kumar R, Subuddhi A, Maji RK, Jana K, et al.. MicroRNA let-7 modulates the immune response to ycobacterium tuberculosis infection via control of A20, an inhibitor of the NF-κB pathway. Cell Host Microbe. 2015 Mar 11;17(3):345-356. doi: 10.1016/j.chom.2015.01.007. Epub 2015 Feb 12. PMID: 25683052.
42. Bao M, Yi Z, Fu Y. Activation of TLR7 Inhibition of Mycobacterium Tuberculosis Survival by Autophagy in RAW 264.7 Macrophages. J Cell Biochem. 2017 Dec;118(12):4222-4229. doi: 10.1002/jcb.26072. Epub 2017 May 23. PMID: 28419514.
43. Li L, Lei Q, Zhang S, Kong L, Qin B. Screening and identification of key biomarkers in hepatocellular carcinoma: Evidence from bioinformatic analysis. Oncol Rep. 2017 Nov;38(5):2607-2618. doi: 10.3892/or.2017.5946. Epub 2017 Sep 7. PMID: 28901457; PMCID: PMC5780015.
44. Brzezinska M, Szulc I, Brzostek A, Klink M, Kielbik M, Sulowska Z, et al. The role of 3-ketosteroid 1(2)-dehydrogenase in the pathogenicity of Mycobacterium tuberculosis. BMC Microbiol. 2013 Feb 20;13:43. doi: 10.1186/1471-2180-13-43. PMID: 23425360; PMCID: PMC3599626.
45. Raja A. Immunology of tuberculosis. Indian J Med Res. 2004 Oct;120(4):213-32. PMID: 15520479.
46. Ansari AW, Kamarulzaman A, Schmidt RE. Multifaceted Impact of Host C-C Chemokine CCL2 in the Immuno-Pathogenesis of HIV-1/M. tuberculosis Co-Infection. Front Immunol. 2013 Oct 4;4:312. doi: 10.3389/fimmu.2013.00312. PMID: 24109479; PMCID: PMC3790230.
47. Akira S, Uematsu S, Takeuchi O. Pathogen recognition and innate immunity. Cell. 2006 Feb 24;124(4):783-801. doi:

10.1016/j.cell.2006.02.015. PMID: 16497588.
48. Akira S, Takeda K, Kaisho T. Toll-like receptors: critical proteins linking innate and acquired immunity. Nat Immunol. 2001 Aug;2(8):675-80. doi: 10.1038/90609. PMID: 11477402.
49. Fremond CM, Yeremeev V, Nicolle DM, Jacobs M, Quesniaux VF, Ryffel B. Fatal Mycobacterium tuberculosis infection despite adaptive immune response in the absence of MyD88. J Clin Invest. 2004 Dec;114(12):1790-9. doi: 10.1172/JCI21027. PMID: 15599404; PMCID: PMC535064.
50. PANDEY A K, YANG Y, JIANG Z, et al. NOD2, RIP2 and IRF5 play a critical role in the type I interferon response to *Mycobacterium tuberculosis* [J]. Public Library of Science Pathogens, 2009, 5(7):e1000500.
51. Lupfer C, Thomas PG, Kanneganti TD. Nucleotide oligomerization and binding domain 2-dependent dendritic cell activation is necessary for innate immunity and optimal CD8+ T Cell responses to influenza A virus infection. J Virol. 2014 Aug;88(16):8946-55. doi: 10.1128/JVI.01110-14. Epub 2014 May 28. PMID: 24872587; PMCID: PMC4136245.
52. Khan N, Pahari S, Vidyarthi A, Aqdas M, Agrewala JN. NOD-2 and TLR-4 Signaling Reinforces the Efficacy of Dendritic Cells and Reduces the Dose of TB Drugs against Mycobacterium tuberculosis. J Innate Immun. 2016;8(3):228-42. doi: 10.1159/000439591. Epub 2015 Nov 28. PMID: 26613532; PMCID: PMC6738777.
53. Yao K, Chen Q, Wu Y, Liu F, Chen X, Zhang Y. Unphosphorylated STAT1 represses apoptosis in macrophages during *Mycobacteriumtuberculosis* infection. J Cell Sci. 2017 May 15;130(10):1740-1751. doi: 10.1242/jcs.200659. Epub 2017 Mar 27. PMID: 28348106.
54. Lim YJ, Yi MH, Choi JA, Lee J, Han JY, Jo SH, et al. Roles of endoplasmic reticulum stress-mediated apoptosis in M1-polarized macrophages during mycobacterial infections. Sci Rep. 2016 Nov 15;6:37211. doi: 10.1038/srep37211. PMID: 27845414; PMCID: PMC5109032.
55. O'Kane CM, Boyle JJ, Horncastle DE, Elkington PT, Friedland JS. Monocyte-dependent fibroblast CXCL8 secretion occurs in tuberculosis and limits survival of mycobacteria within macrophages. J Immunol. 2007 Mar 15;178(6):3767-76. doi: 10.4049/jimmunol.178.6.3767. PMID: 17339475.
56. Dunlap MD, Howard N, Das S, Scott N, Ahmed M, Prince O, et al. A novel role for C-C motif chemokine receptor 2 during infection with hypervirulent Mycobacterium tuberculosis. Mucosal Immunol. 2018 Nov;11(6):1727-1742. doi: 10.1038/s41385-018-0071-y. Epub 2018 Aug 16. PMID: 30115997; PMCID: PMC6279476.
57. Rivero-Lezcano OM, González-Cortés C, Reyes-Ruvalcaba D, Diez-Tascón C. CCL20 is overexpressed in Mycobacterium tuberculosis-infected monocytes and inhibits the production of reactive oxygen species (ROS). Clin Exp Immunol. 2010 Nov;162(2):289-97. doi: 10.1111/j.1365-2249.2010.04168.x. Epub 2010 Sep 1. PMID: 20819093; PMCID: PMC2996596.
58. Sun KT, Chen MY, Tu MG, Wang IK, Chang SS, Li CY. MicroRNA-20a regulates autophagy related protein-ATG16L1 in hypoxia-induced osteoclast differentiation. Bone. 2015 Apr;73:145-53. doi: 10.1016/j.bone.2014.11.026. Epub 2014 Dec 5. PMID: 25485521.
59. Bartel DP. MicroRNAs: target recognition and regulatory functions. Cell. 2009 Jan 23;136(2):215-33. doi: 10.1016/j.cell.2009.01.002. PMID: 19167326; PMCID: PMC3794896.
60. Kay M, Soltani BM, Aghdaei FH, Ansari H, Baharvand H. Hsa-miR-335 regulates cardiac mesoderm and progenitor cell differentiation. Stem Cell Res Ther. 2019 Jun 27;10(1):191. doi: 10.1186/s13287-019-1249-2. PMID: 31248450; PMCID: PMC6595595.
61. Chen Y, Chen Q, Zou J, Zhang Y, Bi Z. Construction and analysis of a ceRNAceRNA network reveals two potential prognostic modules regulated by hsamiR3355p in osteosarcoma. Int J Mol Med. 2018 Sep;42(3):1237-1246. doi: 10.3892/ijmm.2018.3709. Epub 2018 May 29. PMID: 29845268; PMCID: PMC6089708.
62. Li T, Gao X, Han L, Yu J, Li H. Identification of hub genes with prognostic values in gastric cancer by bioinformatics analysis. World J Surg Oncol. 2018 Jun 19;16(1):114. doi: 10.1186/s12957-018-1409-3. PMID: 29921304; PMCID: PMC6009060.

Corresponding authors

Prof. Aihua Liu, Faculty of Basic Medicine, Kunming Medical University, Kunming 650500, China.liuaihua@kmmu.edu.cn; ORCID: 0000-0001-5726-6211

Prof. Fukai Bao, Faculty of Basic Medicine, Kunming Medical University, Kunming 650500, China. baofukai@kmmu.edu.cn; ORCID: 0000-0003-2652-6660

International Journal of Biomedicine 15(4) (2025) 715-721
http://dx.doi.org/10.21103/Article15(4)_OA11

ORIGINAL ARTICLE

Genomics and Proteomics

INTERNATIONAL JOURNAL OF BIOMEDICINE

Decoding Potential Mechanism of Cucurbitacin IIa Treatment on Lyme Neuroborreliosis Through Integrating Network Pharmacology-Molecular Docking Technique and Cell Experiment

Yuxin Fan[1,2,3*], Fukai Bao[1,2*/**], Hanxin Wu[1], Li Peng[1], Liangyu Zhu[1], Aihua Liu[1**]

[1]*Yunnan Province Key Laboratory of Children's Major Diseases Research, Department of Pathogen and Immunology, School of Basic Medicine, Kunming Medical University, Kunming 650030, Yunnan, China*
[2]*Research Center, Baoshan People's Hospital, Baoshan 678100, Yunan, China*
[3]*The People's Hospital of Leshan, Leshan 614003, Sichuan, China*

Abstract

Introduction: Cucurbitacin IIa (CuIIa), one of the most important active components of *Cucurbitaceae* plants, has a wide range of pharmacological effects. However, the mechanisms underlying its effects on Lyme neuroborreliosis (LNB) remain unclear. This study aimed to elucidate the potential mechanisms of CuIIa activity against LNB.

Methods and Results: Potential CuIIa targets were obtained from the Pharmmapper, Swiss Target Prediction, and Batman-Traditional Chinese medicine databases. LNB-associated genes were obtained from OMIM, GeneCards, and DisGeNET. Disease-drug intersection targets were identified using Venny. Protein-protein interaction (PPI) networks were constructed using STRING. Gene ontology (GO) and Kyoto Encyclopedia of Genes and Genomes (KEGG) pathway enrichment analyses were done on the Database for Annotation, Visualization, and Integrated Discovery (DAVID). A drug-target-pathway-disease network was constructed and Autodock software was used to verify molecular docking between active ingredients and the core targets. Finally, the key targets were experimentally validated.

A total of 574 CuIIa targets and 73 LNB-associated genes were identified, and 13 genes were common between the 2 groups. By constructing a PPI network for key targets, the top 10 core target genes were *MMP9*, *TNF*, *ALB*, *CTSG*, *TGFB1*, *CCL2*, *IL4*, *CRP*, *CCL3*, and *CCL5*. GO functional enrichment and KEGG pathway analyses identified 118 entries and 110 pathways, respectively. Molecular docking results showed that CuIIa binds to key important targets in the core network with high affinity. Validation analyses of the key targets, *CCL2* and *CCL5*, showed that CuIIa decreased their expression in a concentration-dependent manner.

Conclusion: This study revealed the potential mechanism of CuIIa activity against Lyme neuroborreliosis. Our preliminary findings using molecular docking modeling and experimental validation provide a basis for future clinical CuIIa applications. (**International Journal of Biomedicine. 2025;15(4):715-721.**)

Keywords: Cucurbitacin IIa • Lyme neuroborreliosis • network pharmacology • enrichment analysis • chemokine • molecular docking

For citation: Fan Y, Bao F, Wu H, Peng L, Zhu L, Liu A. Decoding Potential Mechanism of Cucurbitacin IIa Treatment on Lyme Neuroborreliosis Through Integrating Network Pharmacology-Molecular Docking Technique and Cell Experimen. International Journal of Biomedicine. 2025;15(4):715-721. doi:10.21103/Article15(4)_OA11

Introduction

Lyme disease (LD) is a zoonotic disease caused by the *Borrelia burgdorferi* (*Bb*) infection, which is transmitted through tick bites.[1] In the early stage of LD, *Bb* can cross the blood–brain barrier and enter the central nervous system. Due to its high neurotropism, *Bb* can remain in the central or peripheral nervous system for an extended period, causing various neuropathies. Neurological manifestations are reported in up to 12% of patients with LD.[2] Lyme neuroborreliosis (LNB) is an infectious disease of the nervous system caused by *Bb* infection.[2] The first case of LNB was reported in 1922 by Garin and Bujadoux, who described a patient in France who developed meningitis and erythema after being bitten by a tick.[2] Later, many cases with similar complications were reported, often presenting with meningitis, myelitis, painful radiculitis, cerebral palsy, and headache, with severe cases progressing to facial paralysis and dementia. The most common neurological symptoms of LNB are painful meningoencephalitis (Bannwarth syndrome) and lymphocytic meningitis.[2] Lyme disease is

mainly treated with antibiotics. Treatment with doxycycline or amoxicillin for 14–21 days is recommended for patients with early or early spread without nervous system involvement. Up to 28 days of antibiotic therapy are recommended for cases involving the central nervous system.[3,4] Although early LD can be successfully treated with doxycycline or amoxicillin, advanced LD can be refractory to antibiotic treatment when accompanied by arthritis and neurological symptoms. About 10% of LD patients experience persistent symptoms that do not resolve for several months after one or more rounds of antibiotic therapy.[5] Thus, more effective treatments for insensitive LNB, including anti-inflammatory drugs and especially antibiotics, are urgently needed.

Cucurbitacin IIa (CuIIa), a tetracyclic triterpenoid compound, is a key active component of the plant species Cucurbita. Yunnan people use the root of snow bile tuber to treat various diseases, including dysentery, enteritis, bronchitis, and acute tonsillitis. CuIIa has various effects, including lowering fever, detoxification, antibacterial, and anti-inflammatory properties.[6,7] Studies have shown that CuIIa also exhibits anti-hepatitis B virus effects, inhibits HIV replication, and possesses antidepressant properties.[8] Using high-performance liquid chromatography, a study of the antidepressant effects of CuIIa showed that it can cross the blood–brain barrier.[9] CuIIa-containing drugs, which have high developmental value, have been used clinically in China, and they can modulate a variety of signaling and metabolic pathways.

With the availability of large datasets and advances in artificial intelligence, systems biology-based network pharmacology has emerged as a valuable tool for studying the mechanisms of action of drugs. Using network pharmacology, multivariate drug–target–pathway–disease interaction networks can be constructed, and topological analysis of such networks can reveal the mechanisms of drug action against diseases.[10] In this study, we employed network pharmacology to uncover novel potential strategies for LNB treatment. We predicted the mechanisms of CuIIa activity against LNB, screened for potential CuIIa targets, and subsequently carried out experimental validation.

Materials and Methods

Flowchart of the network pharmacology analysis

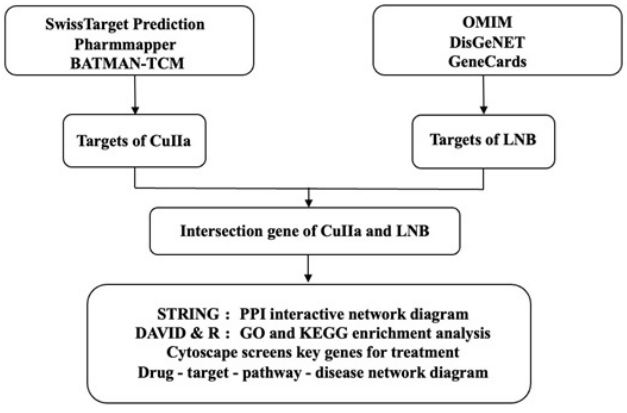

Figure 1. *Schematic representation of the network pharmacology strategy used to predict the mechanisms of CuIIa activity against LNB.*

Prediction of Potential CuIIa Targets

The 2D structure of CuIIa was obtained from PubChem (https://pubchem.ncbi.nlm.nih.gov/),[11] saved in SDF file format. It was imported into the SwissTargetPrediction (http://www.swisstargetprediction.ch/) database to select the species Homo sapiens and the top 100 targets. Import PharmMapper (http://www.lilab-ecust.cn/pharmmapper/index.html) database and select Human Protein Targets Only, number of Reserved Matched Targets (Max 1,000). 300 targets were selected for prediction.[12,13] Moreover, the BATMAN-TCM database (http://bionet.ncpsb.org/batman-tcm/) was used to identify potential CuIIa targets[14] using scores of >5 and $P<0.05$ as cutoff thresholds. Finally, the potential targets identified using the three databases were combined.

Prediction of LNB-Associated Genes

Next, to identify LNB-associated genes, DisGeNET (Score>0.01)(https://www.disgenet.org/home/), GeneCards(Relevance score≥mean value) (http://www.genecards.org/), and OMIM databases (https://omim.org/) were searched for disease-associated targets using "Lyme neuroborreliosis" as the keyword.[15-17] The potential targets identified from the three databases were then combined.

Target Gene Annotation

Potential CuIIa targets and LNB-associated genes were annotated on UniProt (https://www.uniprot.org/).[18]

Identification of Intersection Targets

Genes that were common between the CuIIa target and the LNB-associated lists were identified using Venny 2.1.0 (https://bioinfogp.cnb.csic.es/ tools/venny /index.html).[19]

Construction of a PPI Network of the Key Genes and Identification of Hub Genes

To determine the relationship between the intersecting target proteins, the key genes that may mediate the effects of CuIIa on LNB were subjected to protein-protein interaction (PPI) network analysis using STRING (https://cn.string-db.org/) with a reliability threshold of >0.4 as the cutoff.[20] Next, the network was visualized using Cytoscape (3.8.0).The top 10 interacting genes were then identified as hub genes and visualized using the Cytoscape CytoHubba plugin.[21]

GO and KEGG Pathway Enrichment Analysis

The intersection genes of the LNB treatment by CuIIa were imported into DAVID (https://david.ncifcrf.gov/) and subjected to GO and KEGG pathway enrichment analyses. [22] The GO and KEGG pathway enrichment results were then visualized using the "clusterProfiler" package in R (version 4.1.3), utilizing bar graphs and bubble plots.

Construction of the Drug–Target–Pathway–Disease Network Map

A drug–target–pathway–disease network was constructed to elucidate the synergistic mechanisms of the multi-target and multi-pathway effects of CuIIa against LNB. The top 20 KEGG pathways and the 12 co-regulatory targets associated with the pathways were selected for network file creation. They were then imported into Cytoscape (3.8.0) for network visualization.

Molecular Docking

Based on the degree value, two key target proteins were selected from the top five targets in the PPI network and used for molecular docking analysis with corresponding drugs, which also included three positive drugs: doxycycline, ceftriaxone, and cefotaxime. Through the PubChem database (https://pubchem.ncbi.nlm.nih.gov/), access to medicines, 2D structure, and application of OpenBabel software into 3D structure,[11,23] select the core target proteins of the human species with high resolution in the Protein Data Bank (PBD) database (https://www.rcsb.org/), and download the 3D model structure of the proteins.[24] Pymol 2.4.0 software was then used to remove water molecules and ligands from the core proteins. The completed core protein receptor and drug ligand files were imported into AutoDock Tools 1.5.7, a molecular docking software used to determine the rationality of target genes, and subjected to hydrogenation and charge calculation analyses using AutoDock 4.[25] The above two files were converted into. pdbpt format and imported into Autodock for molecular docking analysis of the interaction between drugs and the core proteins. The analysis results were then visualized using Pymol 2.4.0 software.[26]

Experimental Validation of the Key Targets

Cell culture

CuIIa was purchased from Yunnan Yizhihao Pharmaceutical Co. Because astrocytes are the most abundant cells in the central nervous system, the astrocyte cell line U251 was selected for the validation experiments. The U251 cells were obtained from Kunming Institute of Zoology, Chinese Academy of Sciences, Kunming, China, and cultured in DMEM (Gibco) supplemented with 10% fetal bovine serum, 100 U/mL penicillin, and 100 μg/mL streptomycin in a humidified incubator at 37 °C, 5% CO_2. To count cells, cell suspensions were mixed with trypan Blue at a 1:1 ratio, and the cells were counted using a Countstar cell counter. The U251 cells were seeded into 6-well plates at a density of 4×10^5 cells/well (in 2 mL) and treated with the negative control (PBS), *Bb*, *Bb*+1 μM CuIIa, *Bb*+25 μM CuIIa, and *Bb*+50 μM CuIIa for 6, 12, and 24 hours. The cells were then lysed using RNAiso Plus reagent (TaKaRa) and stored at -80 °C until RNA extraction. Cell culture supernatants were collected and stored at -20 °C until ELISA was carried out.

RT-qPCR

Total RNA was extracted from cells using the RNAiso Plus reagent (TaKaRa, Japan) according to the manufacturer's instructions. A PrimeScript RT Reagent Kit (TaKaRa, Japan) with a gDNA eraser was used for cDNA synthesis, following the manufacturer's protocol. RT-qPCR analysis was done using SYBR Premix Ex Taq (TaKaRa), and relative gene expression was determined using the $2^{-\Delta\Delta Ct}$ method (Livak method) using GAPDH as the reference gene. Primer sequences are shown in Table 1.

ELISA

The effect of CuIIa on CCL2 expression was analyzed using ELISA and a human CXCL2 ELISA kit (Wuhan Eliret Biotechnology Co, LTD) according to the manufacturer's protocol, followed by absorbance (450 nm) reading on a Bio-Rad microplate reader (Model 680, BioRad Laboratories, Inc, Hercules, CA, USA).

Table 1.

Table of primer sequences for qPCR.

Gene	Forward primer (5'–3')	Reverse primer (5'–3')
CCL2	GCAGCAAGTGTCCCAAAGAA	TCCTGAACCCACTTCTGCTT
CCL5	TGGGTTCGGGAGTACATCAA	AAGAGCAAGCAGAAACAGGC
GAPDH	AGCCTTTCCTTGTCCTCCAA	CAATGCCAGGGTACATGGTG

Statistical Analyses

Statistical analyses and mapping were done using GraphPad Prism 8.4.3. Data are presented as mean ± standard error of the mean, and differences between groups were compared using two-way ANOVA. $P<0.05$ indicates statistically significant differences.

Results

Prediction of Relevant Action Targets

Potential CuIIa Targets

The 2D structure of CuIIa was obtained from PubChem (Figure 2A). Potential CuIIa drug targets were predicted on SwissTargetPrediction (100 targets) and PharmMapper (412 targets), and targets were transformed on UniProt. A total of 183 potential drug targets were predicted using the BATMAN-TCM database. Combining the factors identified from the three databases found 632 common potential drug targets.

LNB-Associated Genes

LNB-associated genes were obtained from DisGeNET (11 genes), GeneCards (60 genes), and OMIM (11 genes). Combining the genes identified from the results of the three databases found 73 common LNB-associated genes (Figure 2).

Identification of Intersection Targets

To identify key genes that may underlie the effects of CuIIa against LNB, the intersection between the potential CuIIa targets and LNB-associated genes was determined using Venny 2.0.1 (Figure 2B). This analysis identified 13 (1.9%) intersection genes (*ALB*, *GSR*, *MMP9*, *PPIA*, *CTSG*, *GPI*, *TGFB1*, *CCL2*, *CCL5*, *CRP*, *TNF*, *CCL3*, and *IL4*).

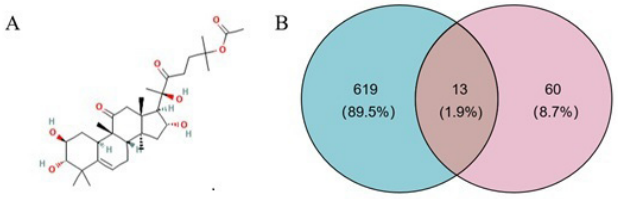

Figure 2. *The 2D structure and potential targets of CuIIa. The 2D structure of CuIIa (A). A Wayne diagram of the intersecting potential CuIIa targets (B).*

Construction of the PPI Network

To determine the relationships between the 13 intersection genes, we subjected them to PPI network analysis using STRING (Figure 3A). The nodes on the PPI network represent the proteins, whereas the different colors of the edges

indicate various types of protein interactions. Thicker edges indicate stronger protein interactions. This analysis revealed that the PPI network consisted of 13 nodes and 46 edges, with an average node degree of 7.08 and an average local clustering coefficient of 0.859.

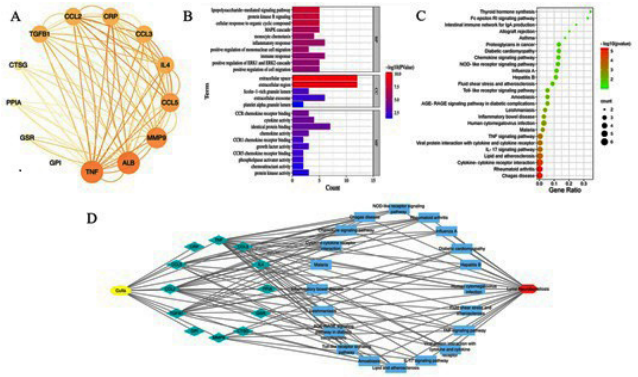

Figure 3. *The CuIIa–target pathway and CuIIa-LNB interaction network. PPI network diagram (A). GO enrichment analysis results (B). The top 20 pathways identified through KEGG enrichment analysis are shown as bubble maps (C). The CuIIa–target–pathway–LNB network (D).*

GO and KEGG Enrichment Analysis Results

A total of 118 results were obtained from the GO enrichment analysis, including 96 biological processes (BP), 10 cellular components (CC), and 12 molecular functions (MF) (Figure 3B). The BP terms were enriched for lipopolysaccharide-mediated signaling pathway, protein kinase B signal, cell response to organic cyclic compounds, MAPK cascade activation, monocyte chemotaxis, inflammatory response, positive regulation of monocyte migration, immune response, positive regulation of ERK1 and ERK2 cascade, and positive regulation of cell migration. The CC terms were mainly enriched for extracellular fluid, extracellular region, ficolin-1-rich granule lumen, extracellular body, and platelet α lumen. The MF terms were mainly enriched for cell surface, secretory granules, macromolecular complexes, secretory granule lumen, and blood particles.

KEGG analysis identified a total of 110 enriched pathways, and the top 20 were selected for further analysis (Table 2). These pathways were mainly associated with IL-17, TNF, MAPK, senescence in diabetic complications, Toll-like receptor, Nod-like receptor, and chemokine signaling pathways. A channel bubble map was made using R, with the bubble size corresponding to the number of genes and the bubble's color indicating the magnitude of the *P*-value (Figure 3C).

Hub Genes for CuIIa Treatment of LNB

The 10 genes (*ALB*, *MMP9*, *CTSG*, *TGFB1*, *CCL2*, *CCL5*, *CRP*, *TNF*, *CCL3*, and *IL4*) were identified as the PPI network's hub genes using the Cytoscape plugin cytoHubba (Figure 4A).

Construction of a CuIIa–Target–Pathway–LNB Network

The 12 key targets from the 20 main signaling pathways and the major components of their mappings were visualized on Cytoscape 3.8.0, followed by the construction of a "CuIIa–target–pathway–LNB". This analysis identified 34 nodes (1 drug, 1 disease, 12 protein targets, and 20 pathways) and 105 edges (Figure 3D).

Table 2.

The top 20 KEGG pathways.

Pathway	*P*-value	Related genes
Rheumatoid arthritis	0.00000491	*CCL2, CCL3, CCL5, TGFB1, TNF*
Chagas disease	0.00000711	*CCL2, CCL3, CCL5, TGFB1, TNF*
Cytokine-cytokine receptor interaction	0.00002311	*IL4, CCL2, CCL3, CCL5, TGFB1, TNF*
Lipid and atherosclerosis	0.00013398	*MMP9, CCL2, CCL3, CCL5, TNF*
IL-17 signaling pathway	0.00022879	*IL4, MMP9, CCL2, TNF*
Viral protein interaction with cytokine and cytokine receptor	0.00027478	*CCL2, CCL3, CCL5, TNF*
TNF signaling pathway	0.00038389	*MMP9, CCL2, CCL5, TNF*
Malaria	0.00195561	*CCL2, TGFB1, TNF*
Human cytomegalovirus infection	0.00290129	*CCL2, CCL3, CCL5, TNF*
Inflammatory bowel disease	0.00328409	*IL4, TGFB1, TNF*
Leishmaniasis	0.00457921	*IL4, TGFB1, TNF*
AGE-RAGE signaling pathway in diabetic complications	0.00761674	*CCL2, TGFB1, TNF*
Amoebiasis	0.00791437	*CTSG, TGFB1, TNF*
Toll-like receptor signaling pathway	0.00821724	*CCL3, CCL5, TNF*
Fluid shear stress and atherosclerosis	0.01434047	*MMP9, CCL2, TNF*
Hepatitis B	0.01917171	*MMP9, TGFB1, TNF*
Influenza A	0.02122703	*CCL2, CCL5, TNF*
NOD-like receptor signaling pathway	0.02435339	*CCL2, CCL5, TNF*
Chemokine signaling pathway	0.02636753	*CCL2, CCL3, CCL5*
Diabetic cardiomyopathy	0.02924612	*GSR, MMP9, TGFB1*

Molecular Docking Results

Molecular docking is a widely used method in drug discovery for predicting ligand–target interactions.[27] Because molecular docking can also be used to estimate the ligand–receptor binding free energy by evaluating the key phenomena involved in intermolecular recognition, it can elucidate molecule–target binding modes and affinities.[28] This study employed a molecular docking approach to validate the core targets *CCL2* and *CCL5*, as identified by network pharmacology, for their binding to core proteins. Because ligands and receptors bind at lower energies, the

more conformationally stable they are, the likelier they are to interact. The molecular docking analysis revealed that in CCL2, CuIIa formed one hydrogen bond with ARG-328 and two hydrogen bonds with GLU-335 and LYS-326, at a binding energy of -4.82 kcal/mol. The binding energy between CuIIa and CCL5 was -5.86 kcal/mol. The binding energies of the active chemical components to the key target proteins were all less than -4 kcal/mol. The binding energy of CuIIa with CCL2 and CCL5 was higher than that of the three positive drugs (Table 3), indicating that the compound has stable receptor binding activity. The docking pattern maps between CuIIa and the CCL2 and CCL5 proteins were visualized using the Pymol software (Figure 4).

Table 3.

Docking results of core components and core target proteins.

Core element	Binding energy (kJ/mol)			
	CuIIa	Doxycycline	Ceftriaxone	Cefotaxime
CCL2	-4.82	-1.71	-2.69	-0.72
CCL5	-5.86	-3.54	-1.19	-2.73

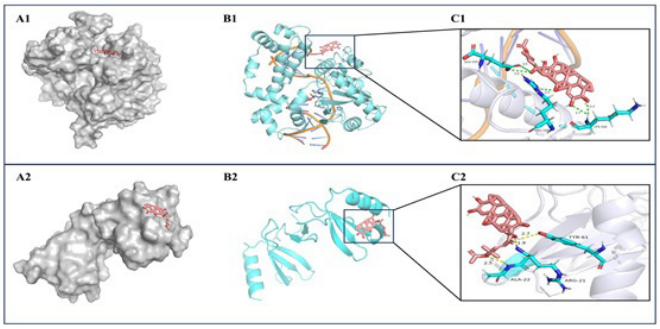

Figure 4. *An illustration of the docking between CuIIa and the CCL2 and CCL5 proteins. Schematic diagram of the three-dimensional morphology of CuIIa docking with the target proteins (A). Schematic diagram of the docking site bonds between CuIIa and the target proteins (B). Schematic diagram of the docking site energy bonds of CuIIa with target proteins (C). Hydrogen bonds are represented by yellow dotted lines, with the length indicated around the* ***lines.***

Analysis of the mRNA Levels of the Key Targets, CCL2 and CCL5

RT-qPCR analysis revealed that after 24 hours of treatment, the mRNA levels of *CCL5* and *CCL2* in U251 cells were significantly higher in the *Bb* group when compared with the negative control group (Figure 5B–C), indicating that *Bb* significantly upregulated CCL2 and CCL5 levels. When compared with the *Bb*-treated group, treatment with CuIIa significantly suppressed the expression of *CCL5* and *CCL2* in a dose-dependent manner (P<0.01 and P<0.05). ELISA revealed that *Bb* significantly increased the protein levels of CCL2 in U251 cells, and CuIIa significantly reduced CCL2 protein levels in a dose-dependent manner when compared with the *Bb* group (P<0.01 and P<0.05). These results are consistent with the findings from network pharmacology.

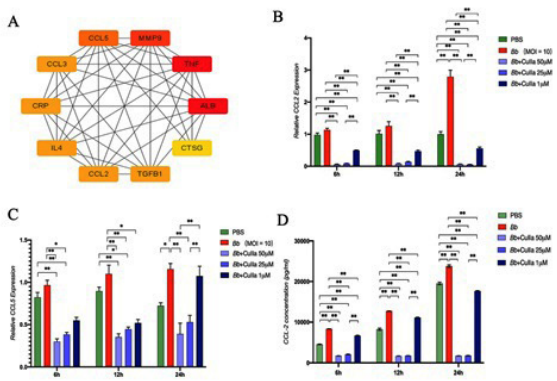

Figure 5. *Hub genes of hosts infected with Bb infection and experimental validation. Top 10 Hub genes (A). Effect of CuIIa on CCL2 and CCL5 mRNA levels and CCL2 protein levels in the human astrocyte cell line, U251. U251 cells were treated with Bb (Multiplicity of infection =10), PBS (negative control), and three drug combination groups (Bb+1 μM CuIIa, Bb+25 μM CuIIa, and Bb+50 μM CuIIa) for 6, 12, and 24 hours. The mRNA levels of CCL2 and CCL5 (B–C) and the CCL2 protein concentrations are shown (D). Values represent means ± standard error of the mean (* and ** indicate P <0.05 and <0.01, respectively.*

Discussion

Currently, LNB treatment is difficult because of poor antibiotic efficacy and post-treatment Lyme disease syndrome (PTLD). In some patients, PTLD is associated with persistent cognitive dysfunction, fatigue, and fibromuscular pain after antibiotic therapy. Moreover, clinical trials indicate that long-term antibiotic therapy does not appear to benefit patients with PTLD.[2,29] Infectious Diseases Society of America guidelines do not recommend additional antibiotic therapy for patients with persistent or recurrent nonspecific symptoms, such as fatigue, pain, or cognitive impairment, following the recommended Lyme disease treatment unless there is objective evidence of reinfection or treatment failure.[30] CuIIa has various effects, including antibacterial, anti-inflammatory, and anti-tumor activities.[7,31] Our unpublished data indicate that CuIIa was effective at alleviating Lyme disease symptoms. In this study, we employed network pharmacology to investigate further the mechanism underlying the effects of CuIIa against LNB.

To our knowledge, this is the first study to investigate CuIIa targets against LNB using network pharmacology and molecular docking analyses. The network pharmacology results suggest that CuIIa may improve LNB through its effects on several key genes, including *MMP9*, *TNF*, *ALB*, *CTSG*, *TGFB1*, *CCL2*, *IL4*, *CRP*, *CCL3*, and *CCL5*, as well as the modulation of various pathways, including IL-17, TNF, MAPK, aging, Toll-like receptor, nodal-like receptor, and chemokine signaling pathways. LNB pathogenesis is not fully understood, and immune-mediated neuroinflammation is thought to be the leading cause of LNB-associated nerve injury. Our GO enrichment analysis revealed that BPs were primarily enriched for inflammatory response, immune response, and monocyte chemotaxis, while MFs were enriched mainly for cytokine activity, chemokine activity, and protein kinase activity, suggesting that inflammatory responses play a crucial role in LNB. Recent studies have suggested that TLR activation and

the resulting production of pro-inflammatory chemokines and inflammatory cytokines may drive LNB inflammation.[32] CuIIa may exert anti-inflammatory effects by regulating the TLR pathway. Additionally, it has also been shown that the anti-inflammatory effects of CuIIa are closely associated with the mitogen-activated protein kinase (MAPK) pathway.[7]

Among the key targets identified in this study, we focused on *CCL2* and *CCL5*, which are closely associated with LNB inflammation and may contribute to the progressive exacerbation of the LNB inflammation. Characteristic monocyte infiltration is often observed in the cerebrospinal fluid of patients with LNB; however, the mechanism of their recruitment remains unclear.[2,33] Elevated *CCL2* and *CCL5* expression have been observed in the cerebrospinal fluid of LNB patients and in an animal model of Bb-induced mouse arthritis.[34] It has been demonstrated that chemokine levels, such as CCL2, CCL5, and CCL9, can induce monocytes and other immune cells to infiltrate inflammatory tissues, thereby exacerbating the progression of Lyme disease.[35] Therefore, we selected CCL2 and CCL5 for experimental validation. To this end, we infected the human astrocyte cell line, U251, with *Bb* and treated them with a negative control and three drug treatment groups. RT-qPCR and ELISA analyses revealed that *Bb* upregulated *CCL2* and *CCL5*, whereas CuIIa suppressed their expression in a concentration-dependent manner. These observations suggest that CuIIa might mediate its effects against LNB by targeting *CCL2* and *CCL5*. These preliminary findings highlight a potential strategy for treating antibiotic-unresponsive patients with LNB or PTLDS.

Conclusion

This study reveals the potential mechanism of CuIIa against Lyme disease. A total of 574 CuIIa targets and 73 LNB-related genes were identified. By constructing PPI networks of key targets, the top 10 core target genes were *MMP9*, *TNF*, *ALB*, *CTSG*, *TGFB1*, *CCL2*, *IL4*, *CRP*, *CCL3*, and *CCL5*. GO enrichment and KEGG pathway analysis identified 118 portals and 110 pathways, respectively. Molecular docking results show that CuIIa binds key and important targets in the core network with high affinity. Confirmatory analyses of key targets *CCL2* and *CCL5* showed that CuIIa reduced their expression in a concentration-dependent manner.

Financial Support

This work was supported by grants from the National Natural Science Foundation of China (No. 32060180, 82160304, 81860644, 81560596), Joint Special Project of Yunnan Science and Technology Department and Kunming Medical University [No.2019FE001(-002) and 2017FE467(-001)]. The funding institutions had no involvement in the design of the study or review of the manuscript.

Declaration of Competing Interest

The authors declare that there are no conflicts of interest.

Acknowledgements

The authors thank the Yunnan Province Key Laboratory for Tropical Infectious Diseases in Universities, the Yunnan Province Integrative Innovation Center for Public Health, Diseases Prevention, and Control, Kunming Medical University, and the Yunnan Demonstration Base of International Science and Technology Cooperation for Tropical Diseases (all located in Kunming, China) for their support of this study.

Availability of data and materials

The datasets used and/or analyzed during the current study are available from the corresponding author on reasonable request.

References

1. Mead P. Epidemiology of Lyme Disease. Infect Dis Clin North Am. 2022 Sep;36(3):495-521. doi: 10.1016/j.idc.2022.03.004.
2. Garcia-Monco JC, Benach JL. Lyme Neuroborreliosis: Clinical Outcomes, Controversy, Pathogenesis, and Polymicrobial Infections. Ann Neurol. 2019 Jan;85(1):21-31. doi: 10.1002/ana.25389.
3. Bobe JR, Jutras BL, Horn EJ, Embers ME, Bailey A, Moritz RL, et al. Recent Progress in Lyme Disease and Remaining Challenges. Front Med (Lausanne). 2021 Aug 18;8:666554. doi: 10.3389/fmed.2021.666554.
4. Wormser GP, Dattwyler RJ, Shapiro ED, Halperin JJ, Steere AC, Klempner MS, Krause PJ, Bakken JS, Strle F, Stanek G, Bockenstedt L, Fish D, Dumler JS, Nadelman RB. The clinical assessment, treatment, and prevention of lyme disease, human granulocytic anaplasmosis, and babesiosis: clinical practice guidelines by the Infectious Diseases Society of America. Clin Infect Dis. 2006 Nov 1;43(9):1089-134. doi: 10.1086/508667. Epub 2006 Oct 2. Erratum in: Clin Infect Dis. 2007 Oct 1;45(7):941.
5. Steere AC, Angelis SM. Therapy for Lyme arthritis: strategies for the treatment of antibiotic-refractory arthritis. Arthritis Rheum. 2006 Oct;54(10):3079-86. doi: 10.1002/art.22131.
6. Chen DL, Xu XD, Li RT, Wang BW, Yu M, Liu YY, Ma GX. Five New Cucurbitane-Type Triterpenoid Glycosides from the Rhizomes of Hemsleya penxianensis with Cytotoxic Activities. Molecules. 2019 Aug 13;24(16):2937. doi: 10.3390/molecules24162937.
7. Zeng Y, Wang J, Huang Q, Ren Y, Li T, Zhang X, Yao R, Sun J. Cucurbitacin IIa: A review of phytochemistry and pharmacology. Phytother Res. 2021 Aug;35(8):4155-4170. doi: 10.1002/ptr.7077.
8. Hunsakunachai N, Nuengchamnong N, Jiratchariyakul W, Kummalue T, Khemawoot P. Hunsakunachai N, Nuengchamnong N, Jiratchariyakul W, Kummalue T, Khemawoot P. Pharmacokinetics of cucurbitacin B from Trichosanthes cucumerina L. in rats. BMC Complement Altern Med. 2019 Jul 4;19(1):157. doi: 10.1186/s12906-019-2568-7.
9. Zhou SM, Guan SY, Yang L, Yang LK, Wang L, Nie HF, Li X, Zhao MG, Yang Q, Wu H. Cucurbitacin IIa exerts antidepressant-like effects on mice exposed to chronic unpredictable mild stress. Neuroreport. 2017 Mar 22;28(5):259-267. doi: 10.1097/WNR.0000000000000747.
10. Luo TT, Lu Y, Yan SK, Xiao X, Rong XL, Guo J. Network Pharmacology in Research of Chinese Medicine Formula:

Methodology, Application and Prospective. Chin J Integr Med. 2020 Jan;26(1):72-80. doi: 10.1007/s11655-019-3064-0.
11. Kim S, Chen J, Cheng T, Gindulyte A, He J, He S, Li Q, Shoemaker BA, Thiessen PA, Yu B, Zaslavsky L, Zhang J, Bolton EE. PubChem 2023 update. Nucleic Acids Res. 2023 Jan 6;51(D1):D1373-D1380. doi: 10.1093/nar/gkac956.
12. Daina A, Michielin O, Zoete V. SwissTargetPrediction: updated data and new features for efficient prediction of protein targets of small molecules. Nucleic Acids Res. 2019 Jul 2;47(W1):W357-W364. doi: 10.1093/nar/gkz382.
13. Liu X, Ouyang S, Yu B, Liu Y, Huang K, Gong J, Zheng S, Li Z, Li H, Jiang H. PharmMapper server: a web server for potential drug target identification using pharmacophore mapping approach. Nucleic Acids Res. 2010 Jul;38(Web Server issue):W609-14. doi: 10.1093/nar/gkq300.
14. Liu Z, Guo F, Wang Y, Li C, Zhang X, Li H, Diao L, Gu J, Wang W, Li D, He F. BATMAN-TCM: a Bioinformatics Analysis Tool for Molecular mechANism of Traditional Chinese Medicine. Sci Rep. 2016 Feb 16;6:21146. doi: 10.1038/srep21146.
15. Rebhan M, Chalifa-Caspi V, Prilusky J, Lancet D. GeneCards: integrating information about genes, proteins and diseases. Trends Genet. 1997 Apr;13(4):163. doi: 10.1016/s0168-9525(97)01103-7.
16. Amberger JS, Hamosh A. Searching Online Mendelian Inheritance in Man (OMIM): A Knowledgebase of Human Genes and Genetic Phenotypes. Curr Protoc Bioinformatics. 2017 Jun 27;58:1.2.1-1.2.12. doi: 10.1002/cpbi.27.
17. Piñero J, Ramírez-Anguita JM, Saüch-Pitarch J, Ronzano F, Centeno E, Sanz F, Furlong LI. The DisGeNET knowledge platform for disease genomics: 2019 update. Nucleic Acids Res. 2020 Jan 8;48(D1):D845-D855. doi: 10.1093/nar/gkz1021.
18. UniProt Consortium T. UniProt: the universal protein knowledgebase. Nucleic Acids Res. 2018 Mar 16;46(5):2699. doi: 10.1093/nar/gky092. Erratum for: Nucleic Acids Res. 2017 Jan 4;45(D1):D158-D169. doi: 10.1093/nar/gkw1099.
19. Oliveros JC. VENNY. An interactive tool for comparing lists with Venn Diagrams. http://bioinfogp.cnb.csic.es/tools/venny/index.html 2007
20. von Mering C, Jensen LJ, Snel B, Hooper SD, Krupp M, Foglierini M, Jouffre N, Huynen MA, Bork P. STRING: known and predicted protein-protein associations, integrated and transferred across organisms. Nucleic Acids Res. 2005 Jan 1;33(Database issue):D433-7. doi: 10.1093/nar/gki005.
21. Chin CH, Chen SH, Wu HH, Ho CW, Ko MT, Lin CY. cytoHubba: identifying hub objects and sub-networks from complex interactome. BMC Syst Biol. 2014;8 Suppl 4(Suppl 4):S11. doi: 10.1186/1752-0509-8-S4-S11. Epub 2014 Dec 8.
22. Dennis G Jr, Sherman BT, Hosack DA, Yang J, Gao W, Lane HC, Lempicki RA. DAVID: Database for Annotation, Visualization, and Integrated Discovery. Genome Biol. 2003;4(5):P3.
23. O'Boyle NM, Banck M, James CA, Morley C, Vandermeersch T, Hutchison GR. Open Babel: An open chemical toolbox. J Cheminform. 2011 Oct 7;3:33. doi: 10.1186/1758-2946-3-33.
24. Sehnal D, Bittrich S, Deshpande M, Svobodová R, Berka K, Bazgier V, Velankar S, Burley SK, Koča J, Rose AS. Mol* Viewer: modern web app for 3D visualization and analysis of large biomolecular structures. Nucleic Acids Res. 2021 Jul 2;49(W1):W431-W437. doi: 10.1093/nar/gkab314.
25. Trott O, Olson AJ. AutoDock Vina: improving the speed and accuracy of docking with a new scoring function, efficient optimization, and multithreading. J Comput Chem. 2010 Jan 30;31(2):455-61. doi: 10.1002/jcc.21334.
26. Abo-Zeid Y, Ismail NSM, McLean GR, Hamdy NM. A molecular docking study repurposes FDA approved iron oxide nanoparticles to treat and control COVID-19 infection. Eur J Pharm Sci. 2020 Oct 1;153:105465. doi: 10.1016/j.ejps.2020.105465. .
27. Pinzi L, Rastelli G. Molecular Docking: Shifting Paradigms in Drug Discovery. Int J Mol Sci. 2019 Sep 4;20(18):4331. doi: 10.3390/ijms20184331.
28. Ferreira LG, Dos Santos RN, Oliva G, Andricopulo AD. Molecular docking and structure-based drug design strategies. Molecules. 2015 Jul 22;20(7):13384-421. doi: 10.3390/molecules200713384.
29. Molloy PJ, Telford SR 3rd, Chowdri HR, Lepore TJ, Gugliotta JL, Weeks KE, Hewins ME, Goethert HK, Berardi VP. Borrelia miyamotoi Disease in the Northeastern United States: A Case Series. Ann Intern Med. 2015 Jul 21;163(2):91-8. doi: 10.7326/M15-0333.
30. Beck AR, Marx GE, Hinckley AF. Diagnosis, Treatment, and Prevention Practices for Lyme Disease by Clinicians, United States, 2013-2015. Public Health Rep. 2021 Sep-Oct;136(5):609-617. doi: 10.1177/0033354920973235.
31. Yu K, Yang X, Li Y, Cui X, Liu B, Yao Q. Synthesis of cucurbitacin IIa derivatives with apoptosis-inducing capabilities in human cancer cells. RSC Adv. 2020 Jan 23;10(7):3872-3881. doi: 10.1039/c9ra09113k.
32. Zhao H, Dai X, Han X, Liu A, Bao F, Bai R, Ji Z, Jian M, Ding Z, Abi ME, Chen T, Luo L, Ma M, Tao L. Borrelia burgdorferi basic membrane protein A initiates proinflammatory chemokine storm in THP 1-derived macrophages via the receptors TLR1 and TLR2. Biomed Pharmacother. 2019 Jul;115:108874. doi: 10.1016/j.biopha.2019.108874.
33. Cepok S, Zhou D, Vogel F, Rosche B, Grummel V, Sommer N, Hemmer B. The immune response at onset and during recovery from Borrelia burgdorferi meningoradiculitis. Arch Neurol. 2003 Jun;60(6):849-55. doi: 10.1001/archneur.60.6.849.
34. Grygorczuk S, Czupryna P, Dunaj J, Moniuszko-Malinowska A, Świerzbińska R, Pancewicz S. The chemotactic cytokines in the cerebrospinal fluid of patients with neuroborreliosis. Cytokine. 2021 Jun;142:155490. doi: 10.1016/j.cyto.2021.155490.
35. Ramesh G, Borda JT, Gill A, Ribka EP, Morici LA, Mottram P, Martin DS, Jacobs MB, Didier PJ, Philipp MT. Possible role of glial cells in the onset and progression of Lyme neuroborreliosis. J Neuroinflammation. 2009 Aug 25;6:23. doi: 10.1186/1742-2094-6-23.

---

*These authors contributed equally to the work.

**Correspondence:

Prof. Aihua Liu, Faculty of Basic Medical Sciences, Kunming Medical University, Kunming 650500, China. E-mail: liuaihua@kmmu.edu.cn ORCID: 0000-0001-5726-6211.

Prof. Fukai Bao, Research Center, Baoshan People's Hospital, Baoshan 678100, Yunan, China. E-mail: baofukai@kmmu.edu.cn ORCID: 0000-0003-5726-6660.

International Journal of Biomedicine 15(4) (2025) 722-726
http://dx.doi.org/10.21103/Article15(4)_OA12

ORIGINAL ARTICLE
Adolescent Health

INTERNATIONAL JOURNAL OF BIOMEDICINE

Narcotic Substance Abuse among Minors in Albania during 2020-2024

Andrin Tahiri[1], Migena Vargu[2*], Ejona Shaska-Zilja[3], Engjellushe Zenelaj[4], Ermelinda Durmishi[5], Taulant Gishto[2], Edvaldo Begotaraj[6], Petrit Vargu[2]

[1]*Toxicology Unit, University Hospital Center "Mother Teresa", Tirana, Albania*
[2]*Dermatology Unit, University Hospital Center "Mother Teresa", Tirana, Albania*
[3]*Psychiatric Hospital "Ali Mihali", Vlora, Albania*
[4]*Research Center, University College Reald, Vlore, Albania*
[5]*University "Alekander Moisiu", Durres, Albania*
[6]*Department of Psychology of Development and Socialization, Sapienza University, Rome, Italy*

Abstract

Background: The use of narcotic substances among minors represents an increasing public health concern in Albania and globally, carrying significant physical and mental health consequences. The goal of this study was to provide clinical and epidemiological evidence of psychoactive substance use among minors to inform national policy, optimize preventive strategies, and enhance therapeutic frameworks tailored to youth at risk in Albania.

Methods and Results: This study employed a retrospective observational design and was conducted at the Clinical Toxicology Service of the University Hospital Centre "Mother Teresa" in Tirana. The study included all patients who were treated for confirmed or suspected of intoxication by psychoactive substances from January 1, 2020, to December 31, 2024. Data were collected from clinical records and included types of substances used, treatment provided, and demographic factors. A total of 1,032 patients were treated for psychoactive substance intoxication. Among them, 27 (2.6%) were minors (<18 years), while 1,005 (97.4%) were adults. Among minors, 25 (92.6%) were male and 26 (96.3%) resided in urban areas. The majority of minors, 18(66.7%), lived in Tirana prefecture. Among minors, cannabis was the most prevalent substance used (37.0%), followed by opioids (22.2%), polysubstances (22.2%), and cocaine (18.5%). No alcohol-only intoxications were recorded among minors. A significantly higher proportion of minors had cannabis-related intoxication than did adults (37.0% vs. 5.7%), while cocaine use was more common among adults (39.1% vs. 18.5%). These differences were statistically significant (P<0.001).

Conclusion: This study highlights the urgent need to address narcotic substance use among minors in Albania. Strengthening national surveillance systems and integrating mental health services into prevention efforts will be key to protecting vulnerable populations and shaping effective policy responses.(**International Journal of Biomedicine. 2025;15(4):722-726.**)

Keywords: Albania • minors • narcotic substances • substance abuse • toxicology

For citation:Tahiri A, Vargu M, Shaska-Zilja E, Zenelaj E, Durmishi E, Gishto T, Begotaraj E, Vargu P. Narcotic Substance Abuse among Minors in Albania during 2020-2024. International Journal of Biomedicine. 2025;15(4):722-726. doi:10.21103/Article15(4)_OA12

Introduction

The use of narcotic substances among minors represents an increasing public health concern in Albania and globally, carrying significant physical and mental health consequences. Adolescence is a critical developmental stage characterized by neurobiological and psychosocial vulnerabilities that increase susceptibility to experimentation with psychoactive substances. Initiation of drug use during this period can lead to significant short- and long-term consequences, including academic underachievement, cognitive impairments, psychiatric disorders, and substance dependence in adulthood.[1,2]

Globally, early-onset substance use is associated with increased risk of chronic addiction, criminal behavior, and socio-occupational dysfunction in adulthood.[3,4] In Europe, approximately 11% of 15-year-olds have used cannabis at least once, with higher rates reported among boys than girls, according to the 2024 European Drug Report 2024, published by the European Monitoring Centre for Drugs and Drug Addiction (EMCDDA).[5] Despite modest reductions

in prevalence in some Western European nations over the past decade,[6,7] the availability of illicit drugs remains widespread. Adolescents today are increasingly exposed to a broader spectrum of psychoactive substances, including synthetic cannabinoids, nitrous oxide, and novel psychoactive substances, many of which are potent and poorly understood.[8,9]

In Albania, adolescent substance use remains understudied. According to the European School Survey Project on Alcohol and Other Drugs (ESPAD) reports, cannabis use among Albanian high school students increased from 5% in 2011 to 7% in 2015, which is below the European average but likely underreported due to stigma and limited screening practices.[10,11] Clinical observations and isolated toxicology reports suggest a rise in adolescent admissions due to psychoactive substances, raising concern over the actual burden of this issue on the national health system.

Cannabis is the most frequently used illicit substance among minors and is associated with a range of health complications, including cannabinoid hyperemesis syndrome, neurocognitive deficits, cardiovascular symptoms, and mental health disturbances such as depression and anxiety.[12-14] Cocaine, though less commonly used, carries a higher risk of acute toxicity and is associated with significant alterations in adolescent brain development, impulse regulation, and addiction potential.[15,16] These effects are particularly concerning given the heightened plasticity and vulnerability of the adolescent brain.

The risks of substance use are further exacerbated in adolescents with pre-existing psychiatric disorders, trauma history, or familial substance use.[17] Studies also suggest that early drug exposure is correlated with impaired educational attainment, juvenile delinquency, and risky sexual behavior.[18,19] Preventive efforts are often hampered by a lack of structured national surveillance and the absence of targeted public health campaigns addressing adolescents specifically.

Although international literature has extensively addressed substance abuse in adolescents,[20-22] regional and country-level studies, especially in the Balkans, are limited. Several case series and retrospective analyses have focused on adolescent poisoning, cannabis-induced psychosis, and polydrug toxicity in minors from Turkey, Serbia, and North Africa.[15] Such studies underscore the clinical relevance and global resonance of substance abuse in youth, but they also highlight the pressing need for Albania-specific data to guide local interventions.

This study seeks to address this research gap by analyzing data from minors treated for substance use at the Clinical Toxicology Service of the University Hospital Centre "Mother Teresa" (Tirana). The goal of this study was to provide clinical and epidemiological evidence of psychoactive substance use among minors to inform national policy, optimize preventive strategies, and enhance therapeutic frameworks tailored to youth at risk in Albania.

Materials and Methods

This study employed a retrospective observational design and was conducted at the Clinical Toxicology Service of the University Hospital Centre "Mother Teresa" in Tirana, the only national tertiary-level facility in Albania providing specialized care for substance abuse, intoxication, and overdose.

Study Population

The study included all patients who were treated for confirmed or suspected of intoxication by psychoactive substances from January 1, 2020, to December 31, 2024. Cases were identified through medical records, and patients with incomplete documentation or intoxications unrelated to psychoactive substances were excluded.

Data Collection

Clinical and demographic data were extracted from medical records using a standardized data extraction form completed by trained clinical staff. The variables included age, sex, residence, type of substance used, route of administration, clinical symptoms, diagnostic confirmation (when available, via urine or blood test), treatment interventions, and patient outcomes.

Statistical Analysis

Statistical analysis was performed using the statistical software package SPSS version 21.0 (Armonk, NY: IBM Corp.). Categorical variables were expressed as frequencies and percentages. Comparisons between minors (<18 years) and adults (≥18 years) were performed using Chi-square tests or Fisher's exact tests when appropriate. The probability value of $P \leq 0.05$ was considered statistically significant.

Results

A total of 1,032 patients were treated for psychoactive substance intoxication at the Clinical Toxicology Service from January 1, 2020, to December 31, 2024 (Table 1). Among them, 27 (2.6%) were minors (<18 years), while 1,005 (97.4%) were adults. The mean age of the entire cohort was 33.4 years (range: 10-84.9 years). Among minors, 25 (92.6%) were male and 26 (96.3%) resided in urban areas. The majority of minors, 18 (66.7%), lived in Tirana prefecture.

Table 1.

Demographic characteristics of study participants.

Variable	Number	Percentage
Gender		
Females	67	6.5
Males	965	93.5
Age		
<18 years	27	2.6
≥18 years	1005	97.4
Residence		
Rural	37	3.6
Urban	995	96.4
Region		
Tirana	564	54.7
Other regions	468	45.3
Total	1032	100.0

Analyzing the annual trend (Table 2), we found that patient admissions increased throughout the five-year study

period. In 2020, there were 92 (8.9%) cases, followed by 158 (15.3%) in 2021, 205 (19.9%) in 2022, 263 (25.5%) in 2023, and 314 (30.4%) in 2024. This steady rise suggests a growing burden of substance-related intoxications over time.

Table 2.

Annual trends in substance abuse in the study population.

Year	Number	Percentage
2020	92	8.9
2021	158	15.3
2022	205	19.9
2023	263	25.5
2024	314	30.4
Total	1032	100.0

Table 3 presents a comparative analysis of substance-related problems among minors and adults. For each substance category, the prevalence rates are reported alongside the χ^2 test values and corresponding *P*-values, indicating whether statistically significant differences exist between the two age groups.

Table 3.

Distribution of different types of substance abuse by age groups.

Substance Abuse	<18 years n (%)	≥18 years n (%)	χ^2	*P*-value
Alcohol-related problems	0 (0.0%)	20 (2.0%)	0.552	0.458
Opioid-related problems	6 (22.2%)	293 (29.2%)	0.641	0.423
Cocaine-related problems	5 (18.5%)	393 (39.1%)	6.196	0.013
Cannabis-related problems	10 (37.0%)	57 (5.7%)	40.169	<0.001
Mixed drug problems	6 (22.2%)	242 (24.1%)	0.046	0.83

Across all age groups, the most commonly abused substance was cocaine [398 (38.6%)], followed by opioids [299 (29.0%)], polysubstance use [248 (24.0%)], cannabis [67 (6.5%)], and alcohol [20 (1.9%)]. Among minors, cannabis was the most prevalent substance used [10 (37.0%)], followed by opioids [6 (22.2%)], polysubstances [6 (22.2%)], and cocaine [5 (18.5%)]. No alcohol-only intoxications were recorded among minors. A significantly higher proportion of minors had cannabis-related intoxication than did adults (37.0% vs. 5.7%), while cocaine use was more common among adults (39.1% vs. 18.5%). These differences were statistically significant ($P<0.001$).

Regarding alcohol-related problems, none of the minors reported such issues (0.0%) whereas 2.0% of adults did. The Chi-square test showed no statistically significant difference between the two groups ($\chi^2=0.552$, $P=0.458$), suggesting that alcohol use problems are similarly uncommon across both age groups in this sample.

In the case of opioid-related problems, 22.2% of minors reported use compared to 29.2% of adults. Although there is a numerical difference, it was not statistically significant ($\chi^2=0.641$, $P=0.423$), indicating that opioid use may affect both minors and adults at relatively similar rates within the studied population.

In contrast, a statistically significant difference emerged about cocaine-related problems. Among minors, 18.5% reported issues, whereas this figure rose to 39.1% among adults. The Chi-square test confirmed this difference as statistically significant ($\chi^2=6.196$, $P=0.013$), implying that adults are considerably more likely to experience problems related to cocaine use than are minors.

These findings emphasize the importance of age-specific intervention strategies, particularly in addressing the notably higher prevalence of cocaine-related issues among adults, while continuing to monitor emerging trends among youth.

Discussion

This study provides clinical and epidemiological insights into the use of psychoactive substances among minors in Albania, based on data from the only national tertiary-level toxicology service. Although minors represented a small fraction of patients (2.6%), their clinical profiles and substance use patterns reveal critical public health concerns.

Our findings show that cannabis was the most commonly used substance among minors (37.0%), followed by opioids (22.2%), multi-drug combinations (22.2%), and cocaine (18.5%). These results align with the broader European trends reported by EMCDDA in 2024,[3] which identify cannabis as the most prevalent illicit substance among adolescents across the continent. Moreover, similar patterns were observed in studies conducted in the UK by Fitzsimons & Villadsen in 2021[23] and in Western Balkan countries, such as Kosovo and North Macedonia, where cannabis and synthetic drug use among adolescents remains widespread.

The high percentage of minors presenting with cannabis-related intoxication is consistent with evidence that cannabis is often perceived as a low-risk drug by adolescents, despite its association with adverse mental and physical health outcomes. Previous research has shown that adolescent cannabis use is linked to increased risk of psychosis, depression, cannabinoid hyperemesis syndrome, and cardiovascular complications.[7,8] Our results reinforce these concerns, especially in the context of the increasing availability of high-potency cannabis products.

Cocaine use among minors (18.5%) in this study is particularly alarming, exceeding national estimates from ESPAD,[5] which reported a 2.5% usage rate among Albanian adolescents. This may reflect both increased accessibility and underreporting in national surveys. The neurodevelopmental risks associated with adolescent cocaine use, including

impaired cognitive control, addiction vulnerability, and psychiatric comorbidities, have been well documented in studies from Caffino et al.[9] and Ryan.[10] The presence of these cases in a clinical setting underscores the need for urgent intervention strategies.

Another concerning finding is that over 22% of minors were intoxicated by multiple substances. Polydrug use among adolescents increases the likelihood of unpredictable drug interactions, overdose, and severe withdrawal symptoms. This pattern mirrors findings from studies in North America and Europe showing a rise in combined use of stimulants, opioids, and alcohol among youth.[2,24] While this study contributes valuable data, several limitations must be acknowledged. Its retrospective nature restricts causal inference, and the sample may not be fully representative of the national adolescent population, given that it only includes hospital-based cases. Nevertheless, the strength of the study lies in its use of standardized clinical data from the only toxicology referral center in Albania, offering reliable insights into the most severe cases of adolescent substance use.

Conclusion

This study highlights the urgent need to address narcotic substance use among minors in Albania. Although representing a small proportion of clinical admissions, the presence of serious intoxication cases among adolescents signals broader public health challenges related to early drug initiation, particularly involving cannabis, cocaine, and drug combination use. Also, the data of the hospitalization has enabled an important conclusion that the main part of adults between the ages of 30 and 40 years who use drugs started drug abuse at a young age. Early identification, school- and community-based prevention programs, and stronger coordination between healthcare, education, and law enforcement institutions are critical for mitigating long-term risks and reducing the burden of substance abuse among youth. Strengthening national surveillance systems and integrating mental health services into prevention efforts will be key to protecting vulnerable populations and shaping effective policy responses.

Ethical Considerations

The study was approved by the Ethics Committee of the University Hospital Centre "Mother Teresa" and was conducted in accordance with the Declaration of Helsinki. All data were anonymized to ensure patient confidentiality, and no individual consent was required due to the retrospective nature of the study.

Sources of Funding

This study was funded by the National Agency for Scientific Research and Innovation of Albania (https://nasri.gov.al/).

Conflicts of Interest

The authors declare that they have no competing interests.

References

1. Charrier L, van Dorsselaer S, Canale N, et al. Health Behaviour in School-aged Children: International Report from the 2021-2022 Survey. WHO Regional Office for Europe, 2024.
2. Chen CY, Storr CL, Anthony JC. Early-onset drug use and risk for drug dependence problems. Addict Behav. 2009 Mar;34(3):319-22. doi: 10.1016/j.addbeh.2008.10.021. Epub 2008 Nov 1. PMID: 19022584; PMCID: PMC2677076.
3. European Monitoring Centre for Drugs and Drug Addiction: European Drug Report. 2024, Trends and Developments. Available at: https://www.euda.europa.eu/publications/european-drug-report/2024_en (accessed: 11 July 2025).
4. Yang J, Mejia MC, Sacca L, et al. Cannabis use among adolescents: trends and outcomes from. 20112021, 2024:872-879. doi: 10.3390/pediatric16040074.
5. ESPAD Group: ESPAD Report 2019: Results from the European School Survey Project on Alcohol and Other Drugs. Luxembourg; 2019.
6. ESPAD Group. ESPAD Report 2015: Results from the European School Survey Project on Alcohol and Other Drugs. Luxembourg; 2015.
7. Tuvel AL, Winiger EA, Ross JM. A Review of the Effects of Adolescent Cannabis Use on Physical Health. Child Adolesc Psychiatr Clin N Am. 2023 Jan;32(1):85-105. doi: 10.1016/j.chc.2022.07.005. Epub 2022 Oct 22. PMID: 36410908; PMCID: PMC10165991.
8. George T, Vaccarino F (Eds). The Effects of Cannabis Use During Adolescence. Ottawa, Canada: Canadian Centre on Substance Abuse; 2015.
9. Caffino L, Mottarlini F, Zita G, Gawliński D, Gawlińska K, Wydra K, Przegaliński E, Fumagalli F. The effects of cocaine exposure in adolescence: Behavioural effects and neuroplastic mechanisms in experimental models. Br J Pharmacol. 2022 Sep;179(17):4233-4253. doi: 10.1111/bph.15523. Epub 2021 Jun 8. PMID: 33963539; PMCID: PMC9545182.
10. Ryan SA. Cocaine Use in Adolescents and Young Adults. Pediatr Clin North Am. 2019 Dec;66(6):1135-1147. doi: 10.1016/j.pcl.2019.08.014. PMID: 31679603.
11. Volkow ND, Han B, Compton WM, Blanco C. Marijuana Use During Stages of Pregnancy in the United States. Ann Intern Med. 2017 May 16;166(10):763-764. doi: 10.7326/L17-0067. Epub 2017 Apr 18. PMID: 28418460; PMCID: PMC6984759.
12. Hall W, Lynskey M. Evaluating the public health impacts of legalizing recreational cannabis use in the United States. Addiction. 2016 Oct;111(10):1764-73. doi: 10.1111/add.13428. Epub 2016 Jun 7. PMID: 27082374.
13. Hadland SE, Levy S. Objective Testing: Urine and Other Drug Tests. Child Adolesc Psychiatr Clin N Am. 2016 Jul;25(3):549-65. doi: 10.1016/j.chc.2016.02.005. Epub 2016 Mar 30. PMID: 27338974; PMCID: PMC4920965.

14. Patrick ME, Terry-McElrath YM, Miech RA, Keyes KM, O'Malley PM. Alcohol use and marijuana use in adolescents: comparison of associations with behavior and academic outcomes. J Stud Alcohol Drugs 2017;78:65-74. doi: 10.15288/jsad.2017.78.65.
15. Atli A, Unluoglu I, Akalin H, Sahin F. Characteristics of pediatric poisoning cases in a university hospital in Turkey. Cureus 2022;14:21234. doi: 10.7759/cureus.21234.
16. Borsari A, Schiavone M, Siracusa C, et al. Cocaine intoxication in adolescents: retrospective analysis of cases from an emergency unit in Eastern Europe. Cureus 2023;15:39645. doi: 10.7759/cureus.39645.
17. Swendsen J, Burstein M, Case B, Conway KP, Dierker L, He J, Merikangas KR. Use and abuse of alcohol and illicit drugs in US adolescents: results of the National Comorbidity Survey-Adolescent Supplement. Arch Gen Psychiatry. 2012 Apr;69(4):390-8. doi: 10.1001/archgenpsychiatry.2011.1503. PMID: 22474107; PMCID: PMC3746542.
18. Schulenberg JE, Maggs JL. A developmental perspective on alcohol use and heavy drinking during adolescence and the transition to young adulthood. J Stud Alcohol Suppl. 2002 Mar;(14):54-70. doi: 10.15288/jsas.2002.s14.54. PMID: 12022730.
19. Ellickson PL, Tucker JS, Klein DJ. High-risk behaviors associated with early smoking: results from a 5-year follow-up. J Adolesc Health. 2001 Jun;28(6):465-73. doi: 10.1016/s1054-139x(00)00202-0. PMID: 11377990.
20. NIDA. Monitoring the Future Survey: High School and Youth Trends. National Institute on Drug Abuse; 2023.
21. Rakić B, Stojanović M, Todorović D, et al. Cannabis-induced psychosis in adolescents: Case series from Serbia. Cureus 2023;15:44891. doi: 10.7759/cureus.44891.
22. Bencheikh RS, Abidi A, Jidane M, et al. Pediatric emergency admissions for recreational drug toxicity in North Africa: A 5-year retrospective study. Cureus 2023;15:51002. doi: 10.7759/cureus.51002.
23. Fitzsimons E, Villadsen A. Risky behaviours among 17-year-olds: findings from the Millennium Cohort Study. London: UCL Centre for Longitudinal Studies; 2021.
24. Gil AG, Wagner EF, Tubman JG. Associations between early-adolescent substance use and subsequent young-adult substance use disorders and psychiatric disorders among a multiethnic male sample in South Florida. Am J Public Health. 2004 Sep;94(9):1603-9. doi: 10.2105/ajph.94.9.1603. PMID: 15333322; PMCID: PMC1448501.

***Corresponding author**: Dr. Migena Vargu, University Hospital Center "Mother Teresa", Tirana, Albania. E-mail: mvargu@yahoo.com*

International Journal of Biomedicine 15(4) (2025) 727-730
http://dx.doi.org/10.21103/Article15(4)_OA13

ORIGINAL ARTICLE

Antimicrobial Resistance

INTERNATIONAL JOURNAL OF BIOMEDICINE

Biofilm-Associated Genes and Antibiotic Susceptibility in Burn-Isolated *Pseudomonas aeruginosa*

Fatimah A. Abdul Jabbar[1], Mustafa S. Al-Salmani[2], Hadeer R. Kamel[3], Hasan A. Aal Owaif[1*]

[1]*Department of Applied Biological Science, College of Biotechnology, Al-Nahrain University, Baghdad, Iraq*
[2]*Department of Molecular and Medical Biotechnology, College of Biotechnology, Al-Nahrain University, Baghdad, Iraq*
[3]*College of Science, Al-Nahrain University, Baghdad, Iraq*

Abstract

Background: Burn injuries reduce skin protection and immune responses, making them a global health issue. Among the most prevalent opportunistic bacteria in burn wounds is *Pseudomonas aeruginosa*, which is drug-resistant and produces biofilms. This study investigated biofilm-associated virulence genes, antibiotic susceptibility, and the link between gene expression, biofilm production, and antibiotic resistance.

Methods and Results: Burn patients hospitalized in Baghdad between June and August 2024 provided 120 burn swabs. *P. aeruginosa* isolates were identified using biochemical tests and the VITEK-2 system. Susceptibility to antibiotics was determined using the Kirby-Bauer disk diffusion technique and interpreted in accordance with the 2024 CLSI criteria. A microtiter plate test was used to quantify the production of biofilm at an optical density (OD) of 570 nm. The *algD*, *pelA*, and *pslA* genes were detected by PCR. *P. aeruginosa* has been verified in 57 (47.5%) of the isolates. Of them, 91.2% were resistant to ceftazidime, 87.7% to imipenem, 73.7% to gentamicin, and 61.4% to ciprofloxacin. MDR was detected in 63.1% of isolates. In 49.1%, 35%, and 15.9% of the isolates, biofilm development was strong, moderate, and weak, respectively. The *algD*, *pelA*, and *pslA* genes were detected in 86.0%, 68.4%, and 59.6% of the isolates, respectively. A clear relationship was observed between these genes and biofilm production and resistance patterns.

Conclusion: The results in our study support a robust link between biofilm production, antibiotic resistance, and genes related to biofilm production by *P. aeruginosa* isolated from burn sites. Implementing gene-targeted techniques and optimal combination treatment may greatly enhance infection management and patient outcomes in burn care facilities.(**International Journal of Biomedicine. 2025;15(4):727-730.**)

Keywords: *Pseudomonas aeruginosa* • *b*urn infections • antibiotic susceptibility • biofilm production • virulence genes

For citation: Jabbar FAA, Al-Salmani MS, Kamel HR, Aal Owaif HA. Biofilm-Associated Genes and Antibiotic Susceptibility in Burn-Isolated *Pseudomonas aeruginosa*. International Journal of Biomedicine. 2025;15(4):727-730. doi:10.21103/Article15(4)_OA13

Abbreviations

CLSI, Clinical and Laboratory Standards Institute; **MDR**, multidrug resistance; **PCR**, polymerase chain reaction.

Introduction

Burn accidents are unfortunately very common and affect many individuals all over the world. Burns destroy the skin's protective barrier, leading to decreased local and systemic immune responses and creating an environment susceptible to microbial colonization and infection.[1,2] *P. aeruginosa* is known as a prevalent opportunistic bacterium responsible for severe burn wound infections, which are frequently linked with more extended hospitalization and higher morbidity.[3] This Gram-

negative bacterium demonstrates a wide range of virulence characteristics, including biofilm formation, production of exotoxins, and development of exoenzymes, which contribute to its persistence and toxicity in burn wounds.[4] *P. aeruginosa* biofilm development is a major pathogenicity mechanism, allowing the bacteria to cling securely to tissues and medical equipment while shielding themselves from host immune responses and antibiotic treatments.[5] The biofilm matrix hinders antibiotic penetration and protects bacterial cells, resulting in persistent infections that are difficult to eliminate.[6] Furthermore, *P. aeruginosa* strains generating biofilms typically exhibit multidrug resistance (MDR), limiting therapeutic choices and resulting in treatment failure.[7] Biofilm production and structural integrity depend heavily on the genetic regulating biofilm-related genes such *algD*, *pelA*, and *pslA*.[8] Higher expression of these genes corresponds with improved biofilm development and increased resistance to several medications.[9] Understanding the interactions between virulence gene expression, biofilm formation, and antibiotic sensitivity is critical for designing effective treatment methods for *P. aeruginosa* infections in burn patients. The purpose of this study was to investigate the antibiotic resistance profile, biofilm-forming potential, and expression of biofilm-associated genes in *P. aeruginosa* isolated from burn infections in hospitals in Baghdad.

Materials and Methods

Between June and August 2024, 120 burn swabs were collected from burn patients attending several hospitals in Baghdad. Conventional biochemical assays were used to identify *P. aeruginosa* isolates, which were then verified using the automated VITEK-2 system.[10] The Kirby-Bauer disk diffusion technique was used on Mueller-Hinton agar plates to determine antimicrobial susceptibility, and the data were interpreted in accordance with CLSI 2024 criteria.[11] The antibiotics examined were imipenem (10 µg), ceftazidime (30 µg), ciprofloxacin (5 µg), gentamicin (10 µg), colistin (10 µg), and amikacin (30 µg). Biofilm production was assessed using the microtiter plate assay with crystal violet staining, and optical density was evaluated at 570 nm using an ELISA reader.[6] The detection of biofilm-associated genes (*algD*, *pelA*, and *pslA)* was determined using PCR. The sequences of primers are given in Table 1.

Statistical analysis was performed using GraphPad Prism v. 8. Baseline characteristics were summarized as frequencies and percentages for categorical variables. Group comparisons were performed using the chi-square test. A *P*-value of <0.05 was considered statistically significant.

Table1.

PCR primer sequences for biofilm-related genes.[12]

Gene	Primer Sequence (5'–3')	Product size (bp)
algD	F: ATCGTCCAGCGACTACCTTC R: CGGTTGTCAGGTAGCCACTT	210
pelA	F: GCTGATGCGGTTCTTCTGTC R: CTGTTCGCCAGGAAAGTACC	195
pslA	F:TCGAGTGGAGAGACGAAGGA R: CTGGTGATCGCTGATGGTAG	182

Results

From 120 swabs, 57 (47.5%) *P. aeruginosa* isolates were identified. Antibiotic susceptibility testing revealed substantial resistance rates to imipenem (87.7%), ceftazidime (91.2%), and ciprofloxacin (61.4%), whereas resistance to colistin remained low (8.8%) (Table 2). Of the isolates, 63.1% exhibited multidrug resistance. The findings of the biofilm test categorized isolates as strong (49.1%), moderate (35%), and weak (15.9%). The *algD*, *pelA*, and *pslA* genes were detected in 86.0%, 68.4%, and 59.6% of the isolates, respectively. A substantial relationship was found between high production of biofilm and resistance to imipenem, ciprofloxacin, ceftazidime, and gentamicin (Table 3). In addition, *algD*, *pelA* and *pslA*-detected isolates had high biofilm formation in 55.1%, 56.4%, and 55.9%, respectively. (Table 4).

Table 2.

Antimicrobial susceptibility of P. aeruginosa isolates.

Antibiotic	Sensitive n (%)	Intermediate n (%)	Resistant n (%)
Ceftazidime	5 (8.8)	0 (0)	52 (91.2)
Imipenem	7 (12.3)	0 (0)	50 (87.7)
Ciprofloxacin	22 (38.6)	0 (0)	35 (61.4)
Gentamicin	25 (43.8)	5 (8.8)	27 (73.7)
Colistin	52 (91.2)	0 (0)	5 (8.8)
Amikacin	20 (35.1)	7 (12.3)	30 (52.6)

Table 3.

Biofilm production and antibiotic resistance among P. aeruginosa isolates.

Antibiotic	High production (n=28)	Intermediate production (n=20)	Low production (n=9)
	n (%)	n (%)	n (%)
Ceftazidime	27 (96.4)	18 (90)	7 (77.8)
Imipenem	26 (92.8)	15 (75)	9 (100)
Ciprofloxacin	22 (78.6)	11 (55)	2 (22.2)
Gentamicin	20 (71.4)	10 (50)	4 (44.4)
Colistin	1 (3.6)	2 (10)	2 (22.2)
Amikacin	17 (60.7)	10 (50)	3 (33.3)

Table 4.

Relationship between biofilm-associated genes and biofilm production intensity.

Gene	High production	Intermediate production	Low production	*P*-value
	n (%)	n (%)	n (%)	
algD (n=49)	27 (55.1)	14 (28.6)	8 (16.3)	<0.05
pelA (n=39)	22 (56.4)	11 (28.2)	6 (15.4)	<0.05
pslA (n=34)	19 (55.9)	10 (29.4)	5 (14.7)	<0.05

Discussion

This study has made possible the identification of important new information regarding the resistance patterns, biofilm-forming capacities, and detection of virulent factors in *P. aeruginosa* isolates from burn infections. A significant percentage (63.1%) of the 57 isolates exhibited multidrug resistance (MDR), which is in line with worldwide trends of *P. aeruginosa* resistance in burn units according to Ugwuanyi et al.[13] The overuse and misuse of antimicrobials by patients leads to resistance to antibiotics.[14] Resistance to imipenem (87.7%) and ciprofloxacin (61.4%) was positively correlated with increased biofilm formation. These results align with those reported by Heidari and colleagues, who similarly noted high resistance to carbapenems and fluoroquinolones in biofilm-producing strains.[15] Additionally, isolates exhibiting elevated levels of *algD* and *pelA* expression demonstrated increased biofilm density, consistent with the findings of Ahmed et al,[16] who noted comparable correlations between gene expression and production of biofilm.The high rate of resistance found here is a serious challenge for empirical therapy. It requires adjustments to antibiotic regimens in clinical settings, as noted by Kumar et al.[17] The incidence of biofilm development was significant, with 84.1% of isolates exhibiting moderate or high biofilm formation capacity, confirming the findings of Yang et al.[18] Biofilms increase antibiotic resistance and immunological clearance, complicating the management of burn-associated infections.[19,20] The PCR gene expression analysis revealed that robust biofilm producers exhibited elevated levels of *algD*, *pelA*, and *pslA* compared to strains that were weak or did not form biofilms at all. Our investigation revealed that *algD* was elevated in 86.0% of isolates, aligning with the observations made by Häußler et al,[21] who highlighted its significance in alginate production and its persistence within host tissues. Similarly, *pelA* and *pslA*, which play a role in the synthesis of the polysaccharide matrix, were expressed in 68.4% and 59.6% of isolates, respectively. These findings are consistent with a study by Farhan et al.,[22] highlighting their collaborative function in biofilm structure. Antibiotic susceptibility testing revealed a significant decline in sensitivity to monotherapies, with resistance rates of ceftazidime (91.2%), imipenem (87.7%), gentamicin (73.7%), and ciprofloxacin (61.4%). The findings are consistent with a publication by de Sousa et al,[23] who found higher resistance rates for these drugs. The combination therapy, particularly the combination of ceftazidime-avibactam and colistin, had a significant synergistic impact, with an increase in inhibitory zones of more than 35% when compared to the individual medications. This observation is consistent with the synergistic combination effects reported by Mikhail et al.[24] A clear relationship was observed between the *algD*, *pelA*, and *pslA* genes and biofilm production and resistance patterns, matching the results reported by Rajabi et al.[25] In addition, a robust inverse relationship was observed between the mechanical stability of the biofilm and the susceptibility to single-agent antibiotic treatment, providing further evidence that the genetic control of biofilm architecture is a central mechanism driving drug resistance in this model, as recommended by de Sousa et al.[26] Our results highlight the significance of including molecular diagnostics in standard microbiological surveillance in burn units. Customized treatment regimens can be guided by identifying high-risk MDR *P. aeruginosa* strains with a high capacity to produce biofilms, as recommended by Martinez et al.[27] Our findings support the potential use of biofilm-targeted adjuvant medications and optimized combination regimens to enhance treatment outcomes. The robustness of our conclusions is further supported by the concordance of our results with international literature, even with a moderate sample size. To further understand the molecular mechanisms behind resistance and biofilm formation, future research should concentrate on longitudinal monitoring and the insertion of more virulent genes.

Conclusion

Our data support the substantial relationship between biofilm production, antibiotic resistance, and genes related to biofilm production in *P. aeruginosa* isolates from burn sites. Implementing gene-targeted techniques and optimal combination treatments may significantly enhance the control of infections and clinical outcomes in burn care facilities.

Ethical Approval

This study was approved by the Department of Applied Biological Science Committee/College of Biotechnology, Al-Nahrain University, under the approval number: 3, 2025.

Competing Interests

The authors of this article confirm that they have no conflicting interests.

References

1. Yakupu A, Zhang J, Dong W, Song F, Dong J, Lu S. The epidemiological characteristic and trends of burns globally. BMC Public Health. 2022 Aug 22;22(1):1596. doi: 10.1186/s12889-022-13887-2. PMID: 35996116.
2. Al-Salmani MS, Shareef SA, Ali SF, Hadi SA, Owaif HAA. Virulence Factors and Antibiotic Susceptibility in Staphylococcus aureus Isolated from Burn Infections. International Journal of Biomedicine. 2025;15(1):192-195. doi:10.21103/ Article15(1)_OA24.
3. Colvin KM, Gordon VD, Murakami K, Borlee BR, Wozniak DJ, Wong GC, Parsek MR. The pel polysaccharide can serve a structural and protective role in the biofilm matrix of Pseudomonas aeruginosa. PLoS Pathog. 2011 Jan 27;7(1):e1001264. doi: 10.1371/journal.ppat.1001264.
4. Lister PD, Wolter DJ, Hanson ND. Antibacterial-resistant Pseudomonas aeruginosa: clinical impact and complex regulation of chromosomally encoded resistance mechanisms. Clin Microbiol Rev. 2009 Oct;22(4):582-610. doi: 10.1128/CMR.00040-09. PMID: 19822890; PMCID: PMC2772362.
5. Bjarnsholt T, Jensen PØ, Fiandaca MJ, Pedersen J, Hansen CR, Andersen CB, Pressler T, Givskov M, Høiby N. Pseudomonas aeruginosa biofilms in the respiratory tract of cystic fibrosis patients. Pediatr Pulmonol. 2009 Jun;44(6):547-58. doi: 10.1002/ppul.21011. PMID: 19418571.
6. Owaif HAA, Aldulaimy MK, Abdulateef SA. The

Antibiotic Resistance Genes *bla*$_{SHV}$, *bla*$_{OXA-48}$, *bla*$_{TEM}$ and *bla*$_{IMP}$ in *Pseudomonas aeruginosa* Isolated from Respiratory Tract Infections in Baghdad, Iraq. International Journal of Biomedicine.2023;13(4):341-344. doi:10.21103/Article13(4)_OA18.

7. Ma L, Conover M, Lu H, Parsek MR, Bayles K, Wozniak DJ. Assembly and development of the Pseudomonas aeruginosa biofilm matrix. PLoS Pathog. 2009 Mar;5(3):e1000354. doi: 10.1371/journal.ppat.1000354.

8. Irie Y, Starkey M, Edwards AN, Wozniak DJ, Romeo T, Parsek MR. Pseudomonas aeruginosa biofilm matrix polysaccharide Psl is regulated transcriptionally by RpoS and post-transcriptionally by RsmA. Mol Microbiol. 2010 Oct;78(1):158-72. doi: 10.1111/j.1365-2958.2010.07320.x. Epub 2010 Aug 2. PMID: 20735777; PMCID: PMC2984543.

9. Kos VN, Déraspe M, McLaughlin RE, Whiteaker JD, Roy PH, Alm RA, Corbeil J, Gardner H. The resistome of Pseudomonas aeruginosa in relationship to phenotypic susceptibility. Antimicrob Agents Chemother. 2015 Jan;59(1):427-36. doi: 10.1128/AAC.03954-14. Epub 2014 Nov 3. PMID: 25367914; PMCID: PMC4291382.

10. Pang Z, Raudonis R, Glick BR, Lin TJ, Cheng Z. Antibiotic resistance in Pseudomonas aeruginosa: mechanisms and alternative therapeutic strategies. Biotechnol Adv. 2019 Jan-Feb;37(1):177-192. doi: 10.1016/j.biotechadv.2018.11.013.

11. Hussein MH, Aal Owaif HA, Abdulateef SA. The Aminoglycoside Resistance Genes, *pehX*, *bla*$_{CTX-M}$, *bla*$_{AmpC}$, and *npsB* among *Klebsiella oxytoca* Stool Samples. International Journal of Biomedicine. 2023;13(3):127-130. doi:10.21103/Article13(3)_OA13.

12. Ali S, Assafi M. Prevalence and antibiogram of Pseudomonas aeruginosa and Staphylococcus aureus clinical isolates from burns and wounds in Duhok City, Iraq. J Infect Dev Ctries. 2024 Jan 31;18(1):82-92. doi: 10.3855/jidc.18193.

13. Ugwuanyi FC, Ajayi A, Ojo DA, Adeleye AI, Smith SI. Evaluation of efflux pump activity and biofilm formation in multidrug resistant clinical isolates of Pseudomonas aeruginosa isolated from a Federal Medical Center in Nigeria. Ann Clin Microbiol Antimicrob. 2021 Feb 2;20(1):11. doi: 10.1186/s12941-021-00417-y.

14. Abdulateef SA, Al-Salmani MS, Aal Owaif HA. Acinetobacter baumannii producing ESBLs and carbapenemases in the Intensive Care Units developing fosfomycin and colistin resistance. Journal of Applied and Natural Science. 2023;15(3):1263-1267. doi:10.31018/jans.v15i3.4872.

15. Heidari R, Farajzadeh Sheikh A, Hashemzadeh M, Farshadzadeh Z, Salmanzadeh S, Saki M. Antibiotic resistance, biofilm production ability and genetic diversity of carbapenem-resistant Pseudomonas aeruginosa strains isolated from nosocomial infections in southwestern Iran. Mol Biol Rep. 2022 May;49(5):3811-3822. doi: 10.1007/s11033-022-07225-3.

16. Ahmed Y, Mohamed F, El-Sayed HA, Fahmy YA. Correlation between biofilm formation and multidrug resistance in clinical isolates of Pseudomonas aeruginosa. Microbes Infect Dis. 2021;2(3):541–9. doi:10.21608/mid.2021.181719.

17. Kumar M, Sarma DK, Shubham S, Kumawat M, Verma V, Nina PB, Jp D, Kumar S, Singh B, Tiwari RR. Futuristic Non-antibiotic Therapies to Combat Antibiotic Resistance: A Review. Front Microbiol. 2021 Jan 26;12:609459. doi: 10.3389/fmicb.2021.609459.

18. Yang F, Liu C, Ji J, Cao W, Ding B, Xu X. Molecular Characteristics, Antimicrobial Resistance, and Biofilm Formation of *Pseudomonas aeruginosa* Isolated from Patients with Aural Infections in Shanghai, China. Infect Drug Resist. 2021 Sep 7;14:3637-3645. doi: 10.2147/IDR.S328781.

19. Al-Dulaymi AAA-M, Aal Owaif HA. Overexpression of lasB gene in *Klebsiella pneumoniae* and its effect on biofilm formation and antibiotic resistance. Al-Rafidain J Med Sci. 2024;6(2):3–8. doi:10.54133/ajms.v6i2.668.

20. Hall-Stoodley L, Costerton JW, Stoodley P. Bacterial biofilms: from the natural environment to infectious diseases. Nat Rev Microbiol. 2004 Feb;2(2):95-108. doi: 10.1038/nrmicro821.

21. Häussler S. Biofilm formation by the small colony variant phenotype of Pseudomonas aeruginosa. Environ Microbiol. 2004 Jun;6(6):546-51. doi: 10.1111/j.1462-2920.2004.00618.x.

22. Farhan RE, Solyman SM, Hanora AM, Azab MM. Molecular detection of different virulence factors genes harbor pslA, pelA, exoS, toxA and algD among biofilm-forming clinical isolates of Pseudomonas aeruginosa. Cell Mol Biol (Noisy-le-grand). 2023 May 31;69(5):32-39. doi: 10.14715/cmb/2023.69.5.6.

23. de Sousa T, Silva C, Alves O, Costa E, Igrejas G, Poeta P, Hébraud M. Determination of Antimicrobial Resistance and the Impact of Imipenem + Cilastatin Synergy with Tetracycline in *Pseudomonas aeruginosa* Isolates from Sepsis. Microorganisms. 2023 Nov 2;11(11):2687. doi: 10.3390/microorganisms11112687.

24. Mikhail S, Singh NB, Kebriaei R, Rice SA, Stamper KC, Castanheira M, Rybak MJ. Evaluation of the Synergy of Ceftazidime-Avibactam in Combination with Meropenem, Amikacin, Aztreonam, Colistin, or Fosfomycin against Well-Characterized Multidrug-Resistant Klebsiella pneumoniae and Pseudomonas aeruginosa. Antimicrob Agents Chemother. 2019 Jul 25;63(8):e00779-19. doi: 10.1128/AAC.00779-19.

25. Rajabi H, Salimizand H, Khodabandehloo M, Fayyazi A, Ramazanzadeh R. Prevalence of *algD*, *pslD*, *pelF*, *Ppgl*, and *PAPI-1* Genes Involved in Biofilm Formation in Clinical *Pseudomonas aeruginosa* Strains. Biomed Res Int. 2022 May 24;2022:1716087. doi: 10.1155/2022/1716087.

26. de Sousa T, Hébraud M, Alves O, Costa E, Maltez L, Pereira JE, Martins Â, Igrejas G, Poeta P. Study of Antimicrobial Resistance, Biofilm Formation, and Motility of *Pseudomonas aeruginosa* Derived from Urine Samples. Microorganisms. 2023 May 19;11(5):1345. doi: 10.3390/microorganisms11051345.

27. Fleitas Martínez O, Cardoso MH, Ribeiro SM, Franco OL. Recent Advances in Anti-virulence Therapeutic Strategies With a Focus on Dismantling Bacterial Membrane Microdomains, Toxin Neutralization, Quorum-Sensing Interference and Biofilm Inhibition. Front Cell Infect Microbiol. 2019 Apr 2;9:74. doi: 10.3389/fcimb.2019.00074.

***Corresponding author**: Dr. Hasan A. Aal Owaif. Department of Applied Biological Science, College of Biotechnology, Al-Nahrain University, Baghdad, Iraq. E-mail: hasan.abdulhadi@nahrainuniv.edu.iq*

International Journal of Biomedicine 15(4) (2025) 731-735
http://dx.doi.org/10.21103/Article15(4)_OA14

ORIGINAL ARTICLE

Antimicrobial Resistance

INTERNATIONAL JOURNAL OF BIOMEDICINE

Prevalence of Carbapenemase Genes *bla*$_{OXA-48}$, *bla*$_{NDM}$, and *bla*$_{IMP}$ in Multidrug Resistant *Pseudomonas aeruginosa* and *Klebsiella pneumoniae* Clinical Isolates from University Hospital Sharjah, UAE

Hassan El Sharief[1,2], Sara Mohamed Ali[1], Salsabeel Mohamed[1], Nours Abbas[2], Mera Maher[2], Praveen Kumar[1], Salma Elnour[1*]

[1]*Gulf Medical University, College of Health Science, Medical Laboratory Science Master's Program. Ajman, United Arab Emirates*
[2]*University Hospital Sharjah, Sharjah, United Arab Emirates*

Abstract

Background: Carbapenem-resistant *Pseudomonas aeruginosa* and *Klebsiella pneumoniae* are globally recognized as priority pathogens due to their association with multidrug resistance and limited therapeutic options. Carbapenemase genes, such as *bla*$_{OXA-48}$, *bla*$_{NDM}$, and *bla*$_{IMP}$, play a central role in the dissemination of resistance.
Methods and Results: This study investigated the prevalence and co-occurrence of these pathogens in 100 multidrug-resistant isolates collected from University Hospital Sharjah, between November 2024 and June 2025. PCR detection revealed *bla*$_{OXA-48}$ as the most prevalent gene (66.7% in *P. aeruginosa* and 65.5% in *K. pneumoniae*), followed by *bla*$_{IMP}$ (44.4% and 38.2%), and *bla*$_{NDM}$ (15.6% and 23.6%). Co-occurrence of two or more genes was observed in over 30% of isolates, and a small proportion carried all three. Approximately one-quarter of isolates tested negative for these targets, indicating alternative mechanisms of carbapenem resistance.
Conclusion: Our findings provide hospital-level molecular data from Sharjah that align with broader trends in the UAE, while highlighting the complexity of resistance-gene combinations. The results underscore the importance of ongoing molecular surveillance, monitoring of gene co-occurrence, and enhanced antimicrobial stewardship to mitigate the effects of multidrug-resistant, Gram-negative infections.(**International Journal of Biomedicine. 2025;15(4):731-735.**)

Keywords: β-lactamases • carbapenem resistance • metallo-beta-lactamase • infection control

For citation: Sharief HEl, Ali SM, Mohamed S, Abbas N, Maher M, Kumar P, Elnour S. Prevalence of Carbapenemase Genes *bla*$_{OXA-48}$, *bla*$_{NDM}$, and *bla*$_{IMP}$ in Multidrug Resistant *Pseudomonas aeruginosa* and *Klebsiella pneumoniae* Clinical Isolates from University Hospital Sharjah, UAE. International Journal of Biomedicine. 2025;15(4):731-735. doi:10.21103/Article15(4)_OA14

Abbreviations

CRE, carbapenem-resistant Enterobacterales; **IMP**, imipenemase; **KPC**, *Klebsiella pneumoniae* carbapenemase; **MBLs**, metallo-β-lactamases; **NDM**, New Delhi metallo-β-lactamase; **VIM**, Verona integron-encoded metallo-β-lactamase.

Introduction

The rapid emergence of multidrug-resistant (MDR) Gram-negative bacteria presents a significant global health challenge.[1] *Pseudomonas aeruginosa* and *Klebsiella pneumoniae* are associated with a wide range of infections, including bloodstream infections, ventilator-associated pneumonia, urinary tract infections, and surgical site infections,[2] which have earned them a place in the WHO's list of substantial MDR pathogens in their priority list for 2024.[3] *Pseudomonas aeruginosa* and *Klebsiella pneumoniae* possess the ability to acquire and disseminate β-lactamase genes, including carbapenemases that hydrolyze carbapenems, the last line of defence against multidrug-resistant Gram-negative infections. According to the Ambler molecular classification in 1980, β-lactamases are divided into four classes (A–D).[4] Among them, classes A, B, and D harbour the clinically

most significant carbapenemases, while class C enzymes play an indirect role.

Class A comprises serine carbapenemases such as *Klebsiella pneumoniae* carbapenemase (KPC) and, less commonly, GES-type enzymes, which are now globally disseminated in Enterobacterales.[5] Class B includes the metallo-β-lactamases (MBLs), a zinc-dependent group represented by New Delhi metallo-β-lactamase (NDM), Verona integron-encoded metallo-β-lactamase (VIM), and imipenemase (IMP), all of which confer resistance to nearly all β-lactams except monobactams.[6,7]

Class C enzymes, mainly AmpC-type cephalosporinases, are not highly efficient carbapenemases but can lead to carbapenem resistance when combined with porin loss or efflux mechanisms.[8] Finally, class D enzymes, specifically the oxacillinases, encompass the clinically significant OXA-48-like carbapenemases, which are now endemic in *K. pneumoniae* in the Middle East and North Africa.[9,10]

Recent surveillance indicates that the OXA-48 enzyme remains the most frequently detected carbapenemase globally, followed by NDM and KPC, while IMP variants continue to predominate in East Asia, particularly in Japan.[11-13] In *P. aeruginosa*, carbapenemase-mediated resistance is also escalating, with bla_{VIM} and bla_{OXA-48} being the most common, whereas bla_{IMP} and bla_{NDM} occur at lower frequencies but frequently co-exist, compounding resistance mechanisms.[14] Longitudinal studies demonstrate a significant increase in bla_{NDM} prevalence among carbapenem-resistant *P. aeruginosa* between 2021 and 2025, highlighting its expanding clinical impact.[15-18]

In the UAE, surveillance data confirm the growing clinical threat posed by carbapenem-resistant Enterobacterales (CRE). A retrospective national study analysing more than 14,500 isolates between 2010 and 2021 found that *K. pneumoniae* accounted for nearly half (48.1%) of all cases, followed by *Escherichia coli* (25.1%) and other Enterobacterales (26.8%). By 2021, resistance in *K. pneumoniae* was alarmingly high, reaching 67.6% for imipenem, 76.2% for meropenem, and 91.6% for ertapenem. bla_{NDM} and bla_{IMP} were detected across *E. coli*, *K. pneumoniae*, *P. aeruginosa*, and *A. baumannii*, often in combination with ESBL genes, while bla_{OXA-48} was notably absent.[19]

Understanding the local prevalence and interaction of carbapenemase genes is crucial for implementing effective infection control practices and antimicrobial stewardship programs. This study investigated the prevalence and co-occurrence of bla_{OXA-48}, bla_{NDM}, and bla_{IMP} genes among MDR *P. aeruginosa* and *K. pneumoniae* isolates obtained from University Hospital Sharjah in the UAE. Offering insights into the genetic architecture of resistance in this high-risk setting.

Materials and Methods

Study Design and Setting

This cross-sectional, laboratory-based study was conducted from November 2024 to June 2025 at University Hospital Sharjah in the United Arab Emirates. A total of 100 non-duplicate MDR clinical isolates, comprising 45 *Pseudomonas aeruginosa* and 55 *Klebsiella pneumoniae,* were obtained from clinical specimens, including blood, urine, sputum, wound swabs, and other sterile body fluids.

Identification and Antimicrobial Susceptibility Testing

All isolates were identified and subjected to antibiotic susceptibility testing using the VITEK® 2 Compact system (bioMérieux, France).

DNA Extraction

Genomic DNA was extracted using the G-spin Total DNA Extraction Kit from iNtRON Biotechnology, Korea, according to the manufacturer's instructions. The DNA's concentration and purity were assessed with a NanoDrop™ 2000 spectrophotometer (Thermo Fisher Scientific).

PCR Amplification of Carbapenemase Genes

PCR amplification targeting the OXA-48, IMP, and NDM genes using the primers listed in Table 1 was performed under optimized thermal cycling conditions. Each 25 µL reaction mixture contained 12.5 µL of GoTaq® Green Master Mix (Promega), 1 µL of each primer (10 µM), 2 µL of DNA template, and nuclease-free water. The thermal cycling process started with an initial denaturation at 95°C for 5 minutes, followed by 35 cycles of denaturation at 95°C for 30 seconds, annealing at variable temperatures for 30 seconds, and extension at 72°C for 1 minute, ending with a final extension at 72°C for 10 minutes (Table 2). PCR products were analyzed using 1.5% agarose gel electrophoresis and stained with ethidium bromide. Electrophoresis was conducted at 100V for 45 minutes, and bands were visualized under UV light using a Bio-Rad GelDoc XR+ Imaging System.

Statistical Analysis

Data were entered and analyzed using Microsoft Excel 2021. Descriptive statistics were used to summarize gene frequencies and co-occurrence patterns. Categorical variables were expressed as counts and percentages.

Table 1.

Primer sequences used for PCR detection of bla_{OXA-48}, bla_{IMP}, and bla_{NDM}

Gene	Sequence (5' – 3')	Length (bp)	Reference
bla_{OXA-48}	F GCGTGGTTAAGGATGAACAC R CATCAAGTTCAACCCAACCG	1080	20
bla_{IMP}	F GAAGGYGTTTATGTTCATAC R GTAMGTTTCAAGAGTGATGC	188	22
bla_{NDM}	F GGTTTGGCGATCTGGTTTTC R CGGAATGGCTCATCACGATC	621	23

Table 2.

PCR amplification parameters for each target gene.

Target Gene	Initial Denaturation	Cycles	Annealing Temperature	Extension (per cycle)	Final Extension
bla_{OXA-48}	94 °C for 6.5 min	35×	52 °C for 45 sec	72 °C for 1 min	72 °C for 5 min
bla_{IMP}	95 °C for 3.5 min	34×	48 °C for 45 sec	72 °C for 1 min	72 °C for 5 min
bla_{NDM}	95 °C for 3.5 min	34×	58 °C for 45 sec	72 °C for 1 min	72 °C for 5 min

Results

Among the 100 multidrug-resistant isolates analyzed, 45 were *P. aeruginosa* and 55 were *K. pneumoniae*.

Gene Prevalence

Among the 45 *P. aeruginosa* isolates, bla_{OXA-48} was detected in 30 (66.7%), IMP in 20 (44.4%), and bla_{NDM} in 7 (15.6%). In contrast, of the 55 *K. pneumoniae* isolates, bla_{OXA-48} was present in 36 (65.5%), bla_{IMP} in 21 (38.2%), and bla_{NDM} in 13 (23.6%) (Figure 1).

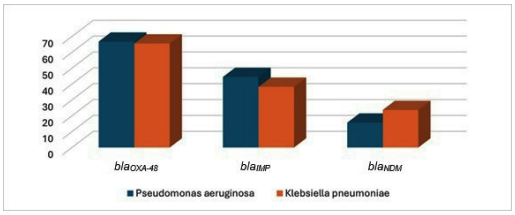

Fig. 1. *Prevalence of carbapenemase genes among multidrug-resistant clinical isolates of P. aeruginosa and K. pneumoniae. PCR detection showed* bla_{OXA-48} *as the most frequent gene in both species, followed by* bla_{IMP} *and* bla_{NDM}

Gene Co-Occurrence

The distribution of single and multiple gene positivity was as follows: In *K. pneumoniae*, the most frequent profile was single gene bla_{OXA-48} alone (29.1%), followed by bla_{OXA-48} + bla_{IMP} (21.8%), while 5.5% of isolates carried all three genes (Figure 2). In *P. aeruginosa*, the dual combination bla_{OXA-48}+ bla_{IMP} predominated (28.9%), with bla_{OXA-48} alone detected in 24.4%. Single-gene carriage of bla_{IMP} or bla_{NDM} was more frequent in *P. aeruginosa* (8.9% each) compared to *K. pneumoniae* (3.6% each). Notably, around one-quarter of isolates in both species were negative for all three genes, suggesting alternative resistance mechanisms.

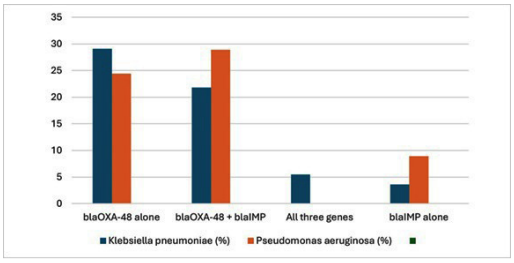

Fig.2. *Co-occurrence profiles of carbapenemase genes (*bla_{OXA-48}*,* bla_{IMP}*, and* bla_{NDM}*) among multidrug-resistant P. aeruginosa and K. pneumoniae isolates. The combination of* bla_{OXA-48} *and* bla_{IMP} *predominated in both species, while a smaller proportion carried all three genes; roughly one-quarter of the isolates were negative for all three targets, indicating the presence of alternative resistance mechanisms.*

Discussion

This study demonstrated a high prevalence of bla_{OXA-48} among both *P. aeruginosa* (66.7%) and *K. pneumoniae* (65.5%) isolates, with moderate detection of bla_{IMP} and lower but notable detection of bla_{NDM}. Gene co-occurrence was common, including isolates harbouring all three carbapenemase genes. These results underscore the dominance of bla_{OXA-48} in the UAE setting and highlight the complexity of carbapenem resistance mechanisms in clinically relevant Gram-negative pathogens.

Our findings align with reports from the Middle East and North Africa (MENA), where bla_{OXA-48} enzymes are well established as endemic.[11,20] In the UAE, Thomsen et al.[18] showed persistently high carbapenem resistance in *K. pneumoniae*, while Ragupathi et al.[19] identified bla_{NDM} and bla_{IMP} but did not detect bla_{OXA-48} in the Northern Emirates, suggesting geographic variation within the country. The recent emergence of bla_{OXA-48} in *E. coli* ST167 reported by Al-Marzooq et al.[21] further illustrates the genetic diversity of carbapenemase enzymes in the UAE. Compared to global trends, our results confirm the widespread dissemination of bla_{NDM} across Asia and the Middle East, as well as the continued prominence of bla_{IMP} in East Asia.

The predominance of bla_{OXA-48} is of particular concern, as it is often difficult to detect with routine laboratory methods and may appear susceptible in vitro, leading to inappropriate carbapenem use and therapeutic failure.[22] The co-occurrence of multiple carbapenemase genes within the same isolate raises the risk of horizontal transfer and limits the efficacy of last-line antibiotics. These findings are consistent with clinical observations from,[23] who reported high mortality rates in patients with CRE bacteremia in the UAE despite treatment with ceftazidime–avibactam and aztreonam. Together, these data highlight the urgent need for enhanced antimicrobial stewardship and optimized treatment strategies.

The detection of high rates of carbapenemase genes in both pathogens underscores the critical threat they pose to healthcare systems in the UAE. bla_{OXA-48} and bla_{NDM} are both recognized by the World Health Organization as priority resistance determinants requiring urgent attention. Our results underscore the importance of robust molecular surveillance, routine screening for gene co-occurrence, and regional collaboration in monitoring the spread of high-risk clones.

This study is limited by its sample size and single-center scope, which may not fully reflect the national distribution of resistance genes. Moreover, the absence of sequencing data restricts insights into the genetic context of these genes, such as plasmid associations or integron carriage. Finally, clinical data were not analyzed, precluding an assessment of gene presence in relation to patient outcomes.

Future research should incorporate whole-genome sequencing to explore the genetic environments of bla_{OXA-48}, bla_{NDM}, and bla_{IMP} in UAE isolates. Larger multicenter studies across the Emirates and the broader Gulf Cooperation Council (GCC) region are needed to assess epidemiological trends. Linking molecular findings to patient-level clinical outcomes will be crucial in informing treatment guidelines. Finally, investigation of novel therapeutic strategies, such as cefiderocol or optimized CAZ-AVI combinations, should be prioritized in this context.

Ethical Approval

This study was approved by the University Hospital Sharjah Research and Ethics Committee (Approval No. UHS-

HERC-176-16092025) and the Gulf Medical University Institutional Review Board (Approval No. IRB-COHS-STD-98-NOV-2024).

Acknowledgments

The authors thank the staff of the Microbiology Laboratory at University Hospital Sharjah for their technical assistance and support during specimen collection and processing.

Competing Interests

The authors declare that there are no conflicts of interest or competing interests regarding the publication of this paper.

Funding Source

The institutional resources of Gulf Medical University and University Hospital Sharjah provided support for the work.

References

1. Thompson W, Cieplik F, Teoh L, Jakubovics N, Benzian H. Fighting the Antimicrobial Resistance Global Emergency: The Lifesaving Role of Dentistry. J Dent Res. 2025 Aug;104(9):933-935. doi: 10.1177/00220345251324162. Epub 2025 Mar 19. PMID: 40108748; PMCID: PMC12209544.
2. Balkhair A, Saadi KA, Adawi BA. Epidemiology and mortality outcome of carbapenem- and colistin-resistant *Klebsiella pneumoniae, Escherichia coli, Acinetobacter baumannii*, and *Pseudomonas aeruginosa* bloodstream infections. IJID Reg. 2023 Jan 8;7:1-5. doi: 10.1016/j.ijregi.2023.01.002. PMID: 36936715; PMCID: PMC10014253.
3. Sati H, Carrara E, Savoldi A, Hansen P, Garlasco J, Campagnaro E, et al.; WHO Bacterial Priority Pathogens List Advisory Group. The WHO Bacterial Priority Pathogens List 2024: a prioritisation study to guide research, development, and public health strategies against antimicrobial resistance. Lancet Infect Dis. 2025 Sep;25(9):1033-1043. doi: 10.1016/S1473-3099(25)00118-5. Epub 2025 Apr 14. PMID: 40245910; PMCID: PMC12367593.
4. Ambler RP. The structure of beta-lactamases. Philos Trans R Soc Lond B Biol Sci. 1980 May 16;289(1036):321-31. doi: 10.1098/rstb.1980.0049. PMID: 6109327.
5. Galdadas I, Qu S, Oliveira ASF, Olehnovics E, Mack AR, Mojica MF, Agarwal PK, Tooke CL, Gervasio FL, Spencer J, Bonomo RA, Mulholland AJ, Haider S. Allosteric communication in class A β-lactamases occurs via cooperative coupling of loop dynamics. Elife. 2021 Mar 23;10:e66567. doi: 10.7554/eLife.66567. PMID: 33755013; PMCID: PMC8060031.
6. Bush K. Classification for β-lactamases: historical perspectives. Expert Rev Anti Infect Ther. 2023 May;21(5):513-522. doi: 10.1080/14787210.2023.2194633. Epub 2023 Apr 6. PMID: 36951174.
7. Oelschlaeger P. β-Lactamases: Sequence, Structure, Function, and Inhibition. Biomolecules. 2021 Jul 5;11(7):986. doi: 10.3390/biom11070986. PMID: 34356610; PMCID: PMC8301796.
8. Philippon A, Arlet G, Labia R, Iorga BI. Class C β-Lactamases: Molecular Characteristics. Clin Microbiol Rev. 2022 Sep 21;35(3):e0015021. doi: 10.1128/cmr.00150-21. Epub 2022 Apr 18. PMID: 35435729; PMCID: PMC9491196.
9. Baig MA. DOMINANCE OF blaOXA-48-LIKE AMONG CARBAPENEM RESISTANT KLEBSIELLA PNEUMONIAE ISOLATED FROM ABU DHABI HOSPITALS. Thesis United Arab Emirates University, 2023.
10. Lascols C. Global Molecular Characterization of Extended-Spectrum ß-lactamases and carbapenemases in Enterobacterales: Université Paris-Saclay; 2024.
11. Boyd SE, Holmes A, Peck R, Livermore DM, Hope W. OXA-48-Like β-Lactamases: Global Epidemiology, Treatment Options, and Development Pipeline. Antimicrob Agents Chemother. 2022 Aug 16;66(8):e0021622. doi: 10.1128/aac.00216-22. Epub 2022 Jul 20. PMID: 35856662; PMCID: PMC9380527.
12. Dong H, Li Y, Cheng J, Xia Z, Liu W, Yan T, et al. Genomic Epidemiology Insights on NDM-Producing Pathogens Revealed the Pivotal Role of Plasmids on bla_{NDM} Transmission. Microbiol Spectr. 2022 Apr 27;10(2):e0215621. doi: 10.1128/spectrum.02156-21. Epub 2022 Feb 28. PMID: 35225688; PMCID: PMC9049954.
13. Falagas ME, Asimotou CM, Zidrou M, Kontogiannis DS, Filippou C. Global Epidemiology and Antimicrobial Resistance of Klebsiella Pneumoniae Carbapenemase (KPC)-Producing Gram-Negative Clinical Isolates: A Review. Microorganisms. 2025 Jul 19;13(7):1697. doi: 10.3390/microorganisms13071697. PMID: 40732206; PMCID: PMC12300886.
14. Di Pilato V, Pollini S, Miriagou V, Rossolini GM, D'Andrea MM. Carbapenem-resistant *Klebsiella pneumoniae*: the role of plasmids in emergence, dissemination, and evolution of a major clinical challenge. Expert Rev Anti Infect Ther. 2024 Jan-Jun;22(1-3):25-43. doi: 10.1080/14787210.2024.2305854. Epub 2024 Feb 12. PMID: 38236906.
15. Chen X, Liu X, Ren W, Li H, Yang S. Distribution patterns and evolution of antimicrobial resistance in Gram-negative bacteria within the intensive care unit of a tertiary hospital from 2019 to 2024. Front Microbiol. 2025 May 15;16:1587132. doi: 10.3389/fmicb.2025.1587132. PMID: 40444004; PMCID: PMC12119562.
16. Liu L, Liu S, Yang Z, Wang F, Yuan H, Xu H, Chen J, Li X. Shifts in hospital-associated pathogens and prevalence trends of carbapenem-resistant Escherichia coli infections, 2021-2023. J Infect Dev Ctries. 2025 Jul 28;19(7):1100-1107. doi: 10.3855/jidc.20930. PMID: 40720467.
17. Wise MG, Karlowsky JA, Mohamed N, Hermsen ED, Kamat S, Townsend A, et al. Global trends in carbapenem- and difficult-to-treat-resistance among World Health Organization priority bacterial pathogens: ATLAS surveillance program 2018-2022. J Glob Antimicrob Resist. 2024 Jun;37:168-175. doi: 10.1016/j.jgar.2024.03.020. Epub 2024 Apr 10. PMID: 38608936.
18. Thomsen J, Abdulrazzaq NM; UAE AMR Surveillance Consortium; Everett DB, Menezes GA, Senok A, Ayoub Moubareck C. Carbapenem resistant *Enterobacterales* in the

United Arab Emirates: a retrospective analysis from 2010 to 2021. Front Public Health. 2023 Dec 7;11:1244482. doi: 10.3389/fpubh.2023.1244482. PMID: 38145078.
19. Ragupathi P, Khamisani V, Sadiq AF, Mobiddo MA, Rahamathullah N, Bagchi S, et al. Prevalence of class A ESBL, class B and D carbapenemase encoding genes (CTX-M, TEM, SHV, NDM, IMP, OXA-48) in gram-negative bacterial pathogens isolated from various clinical samples collected from northern region of United Arab Emirates. medRxiv. 2024:2024.01. 26.24301841.
20. Ziadi H, Chougrani F, Cheriguene A, Carballeira L, García V, Mora A. Phenotypic and Genotypic Characterization of ESBL-, AmpC-, and Carbapenemase-Producing *Klebsiella pneumoniae* and High-Risk *Escherichia coli* CC131, with the First Report of ST1193 as a Causative Agent of Urinary Tract Infections in Human Patients in Algeria. Antibiotics (Basel). 2025 May 9;14(5):485. doi: 10.3390/antibiotics14050485. PMID: 40426551; PMCID: PMC12108494.
21. Al-Marzooq F, Ghazawi A, Allam M, Collyns T. Deciphering the genetic context of the emerging OXA-484-producing carbapenem-resistant *Escherichia coli* from ST167 high-risk clone in the United Arab Emirates. European Journal of Clinical Microbiology & Infectious Diseases.2025; 44(5):1155-1166. doi:10.1007/s10096-025-05082-z
22. Rujaibi AA, Jabri ZA, Jardani AA, Rashdi AA, Mamari AA, Sumri SA, et al. Assessment of Phenotypic Tools for Detection of OXA-48, KPC, and NDM in *Klebsiella pneumoniae* in Oman. Diagnostics (Basel). 2025 Apr 8;15(8):949. doi: 10.3390/diagnostics15080949. PMID: 40310344; PMCID: PMC12025575.
23. Agha A, Al Hassani A, Shubbar A, Al Hassani Z, Al Hassani A, Saleem A. Prognosis and Outcome of Carbapenem-Resistant Enterobacterales Bacteremia Managed With Ceftazidime-Avibactam and Aztreonam Combination Therapy in Tawam Hospital, UAE: A Retrospective Study. Cureus. 2025 Jun 10;17(6):e85689. doi: 10.7759/cureus.85689. PMID: 40642711; PMCID: PMC12243072.

***Corresponding author**: Dr. Salma Elnour Rahma, PhD. E-mail: dr.salmaelnour@gmu.ac.ae*

International Journal of Biomedicine 15(4) (2025) 736-740
http://dx.doi.org/10.21103/Article15(4)_OA15

ORIGINAL ARTICLE

Dentistry

INTERNATIONAL JOURNAL OF BIOMEDICINE

Impact of Increment Thickness, Preheating and Light Exposure Duration on Surface Hardness of Bulk-Fill Composite Cured in Covered Slot

Timur V. Melkumyan[1,2*], Surayo Sh. Sheraliyeva[1], Zurab S. Khabadze[2], Maria K. Makeeva[2], Gerhard K. Seeberger[3], Shahnoza K. Musashaykhova[1], Nuriddin Kh. Kamilov[1], Diyoraxon A. Inoyatova[1], Angela D. Dadamova[1]

[1]*Tashkent State Medical University, Tashkent, Uzbekistan*
[2]*Peoples' Friendship University of Russia (RUDN University), Moscow, Russia*
[3]*Order of Physicians and Dentists of the Province of Cagliari, Sardinia, Italy*

Abstract

Background: Experimental methods for evaluating composite filling materials and their use are essential for achieving reliable, predictable clinical results in tooth restoration. This study aimed to evaluate the impact of bottom increment thickness, preheating, and light exposure duration on microhardness and depth of cure of bulk-fill resin composite after polymerization in a covered slot.
Methods and Results: A total of 32 filling samples were made using Tetric® N-PowerFill 2 bulk-fill resin composite material (Ivoclar Vivadent AG). Composite filling samples were made in opaque plastic molds with isosceles trapezoidal slots. The slot was 1.5 mm wide. The lower and upper bases of the trapezoid were 3 and 6 mm, respectively. The height of the trapezoidal slot was 5 mm. Filling samples were divided into 8 groups of 4 each. All trapezoidal slots were filled with 2 successive layers of different thicknesses. In Groups 1, 3, 5, and 7, the height of the bottom horizontal layer was ~1 mm, the top horizontal layer ~ 4 mm. In Groups 2, 4, 6, and 8, the height of the bottom horizontal layer was ~ 4 mm, the top horizontal layer ~ 1 mm. Every layer was cured individually. In Groups 1, 2, 5, and 6, the light exposure for each layer was 20 sec, while in Groups 3, 4, 7, and 8, it was 40 sec. Filling samples in Groups 1, 2, 3, and 4 were made from a room-temperature composite (22-24 °C). In Groups 5, 6, 7, and 8, the material was polymerized after heating in the slot up to 55-60 °C. Photoactivation was performed with the Valo X LED lamp (Ultradent, USA) in standard mode. The surface microhardness of composite filling samples was assessed using the Vickers hardness tester after exposure to light and storage in a dark container for 24 hours. Measurements were performed using a "ПМТ-3" tester with an indenter at a 50 g load for a 15-second dwell time. Indentations were made in a linear order at levels of 0.5, 1.5, 2.5, 3.5, and 4.5 mm from the top surface.
Doubling the photoactivation time of the room-temperature composite from 20 seconds to 40 seconds increased the Vickers hardness number (VHN) of composite fillings at depths of 1.5, 2.5, 3.5, and 4.5 mm by 55%, but mostly insignificantly. The only difference of ~1.6 times was noted in the VHN at a depth of 4.5 mm between the filling samples from Group 3 and Group 2 (P=0.0071), indicating the importance of both low increment thickness and prolonged irradiance. The surface hardness of fillings at 0.5 mm in samples from Groups 1, 2, 3, and 4 was relatively high and did not show significant statistical differences among them. It was another confirmation of the crucial importance of close light source adjustment to the surface of light-cured material. Photoactivation of a heated composite material in a covered slot had certain advantages over using a room-temperature composite, as demonstrated by the VHN of filling samples at different depths. For example, at all depths, the VHN of composite fillings in Group 8 was statistically greater than in Group 2, regardless of the thickness of the bottom increment. Moreover, the difference increased with depth, from 1.4 (P=0.0431) [at 0.5 mm] to 1.8 (P=0.0001) [at 4.5 mm]. However, it was noteworthy that prolonged irradiance of a 4 mm-thick layer of resin composite is beneficial and may offset the low polymerization kinetics of a room-temperature filling material.
Conclusion: Lowering the thickness of the bottom layer of bulk-fill composite, along with its preheating and prolonged photoactivation, cumulatively contributed to a significant increase in depth of cure and microhardness of filling samples made in a covered slot. (**International Journal of Biomedicine. 2025;15(4):736-740.**)

Keywords: bulk-fill resin composite • preheating • covered slot • class II restorations

For citation: Melkumyan TV, Sheraliyeva SSh, Khabadze ZS, Makeeva MK, Seeberger GK, Musashaykhova ShK, Kamilov NKh, Inoyatova DA, Dadamova AD. Impact of Increment Thickness, Preheating and Light Exposure Duration on Surface Hardness of Bulk-Fill Composite Cured in Covered Slot. International Journal of Biomedicine. 2025;15(4):736-740. doi:10.21103/Article15(4)_OA15

Introduction

The optimal physical and aesthetic properties of modern composite filling materials have significantly widened the indications for direct dental restorations. However, despite the widespread acceptance, the high probability of suboptimal polymerization is one of the main reasons for unsatisfactory tooth treatment and the poor state of composite restorations.[1,2] The desirable degree of conversion of light-cured composites can be achieved by placing the tip of the light source as close as possible to the surface of the light-cured resin to ensure light transmission through the composite layer to its deepest areas, initiating polymerization.

It is clear that the light intensity emitted by the curing device gradually decreases as it penetrates deeper into the composite material. As a result, the degree of conversion of the resin monomers gradually decreases with increasing distance from the irradiated surface. A low degree of conversion worsens the physical properties of composite restorations and promotes the release of unreacted monomers, which can pose a potential threat to pulp cells and the oral mucosa.[3,4]

In restorative dentistry, the evaluation of surface microhardness is used to predict the wear resistance of any restorations subject to occlusal loading. However, only for direct composite materials is the bottom-to-top ratio of surface microhardness measured, given its great clinical value. Thus, it has been accepted that a favorable prognosis for the composite restoration remains possible when the ratio equals 0.8 or 0.85. In contrast, lower values do not guarantee the mechanical and chemical stability of the filling.[5]

Numerous factors influence the depth of cure. These include the type of composite resin, its color and transparency, the layer thickness and distance from the radiation source, the size and distribution of the filler particles, the intensity and exposure time of the material, the wavelength of the light, and the temperature of the composite.[2,4,6,7]

Temperature is known to affect the rate of chemical reactions significantly. Therefore, preheating composite materials before light-curing has become popular at times in modern restorative dentistry. A wide variety of methods and devices have been designed and proposed for heating. Most studies have demonstrated a significant impact of preheating on conversion rate and microhardness of composite fillings.[8]

However, despite the significant opportunity to improve the strength and chemical stability of composite restorations, the preheating method has not been widely adopted due to several clinical issues. Among them, the predominant stickiness of heated composite to instruments during placement of the material into the cavity and the rapid loss of temperature have been emphasized, which significantly reduced the feasibility of using this method for direct restorations.[9]

On the other hand, there is a large amount of experimental data indicating a high degree of conversion and microhardness of the top and bottom surfaces of composite filling samples that were light-activated at 55-60 ºC.[8] A high degree of conversion of resin composite materials contributes to a better seal, prevents leakage and the occurrence of secondary caries, promotes the vitality of the tooth, and prevents pulp alterations. Those are specific goals that are difficult to achieve in the direct restoration of Class II cavities with dental composites.[5]

Filling deep tooth cavities in contact areas and the lack of a light source close to the surface of the resin composite create unfavorable conditions for adequate polymerization of the restorative material.[5] To achieve optimal conversion of a composite in poorly illuminated areas, bulk-fill resin materials can be used, thanks to a greater depth of cure supported by the polymer matrix's special properties, the quality of filler particles, and an advanced initiator system.

However, despite significant supportive data indicating the efficacy of bulk-fill composites in the restoration of large and deep tooth cavities, the issue of depth of cure for this type of composite remains under discussion.[8]

Given the indisputable priority of high conversion of composite materials and the high prevalence of disruptive factors, the development of new methods and techniques for the application of light-cured materials remains relevant.

This study aimed to evaluate the impact of bottom increment thickness, preheating, and light exposure duration on microhardness and depth of cure of bulk-fill resin composite after polymerization in a covered slot.

Materials and Methods

Composite filling samples were made in opaque plastic molds with isosceles trapezoidal slots (Figure 1). The slot was 1.5mm wide. The lower and upper bases of the trapezoid were 3 and 6 mm, respectively. The height of the trapezoidal slot was 5mm. Before inserting the filling material into the mold, the slot's outer surface was covered with a metal strip matrix spanning its entire height to prevent side light from entering and to ensure unidirectional light-curing of the composite from above (Figure 2).

Fig.1. *Plastic molds with trapezoidal slots for a composite material.*

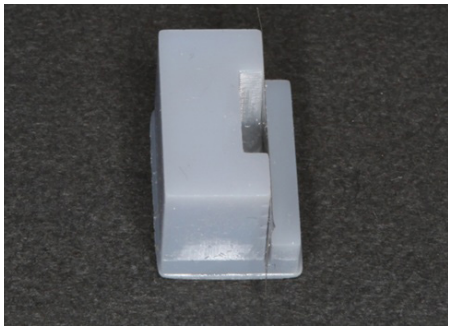

Fig.2. *Plastic mold with a trapezoidal slot covered with a metal strip.*

Photoactivation was performed with the Valo X LED lamp (Ultradent, USA) in standard mode. Filling samples were made using Tetric® N-PowerFill 2 bulk-fill resin composite material (Ivoclar Vivadent AG). They were divided into 8 groups of 4 each. All trapezoidal slots were filled with 2 successive layers of different thicknesses. In Groups 1, 3, 5, and 7, the height of the bottom horizontal layer was ~1 mm, the top horizontal layer ~4 mm (Figure 3). In Groups 2, 4, 6, and 8, the height of the bottom horizontal layer was ~ 4 mm, the top horizontal layer ~ 1 mm (Figure 4). Every layer was cured individually. In Groups 1, 2, 5, and 6, the light exposure for each layer was 20 sec, while in Groups 3, 4, 7, and 8, it was 40 sec. Filling samples in Groups 1, 2, 3, and 4 were made from a room-temperature composite (22-24 °C). In Groups 5, 6, 7, and 8, the material was polymerized after heating in the slot by applying the heating device's working part to the surface of the metal matrix. The material was heated to 55-60 °C and kept at this temperature during photoactivation.

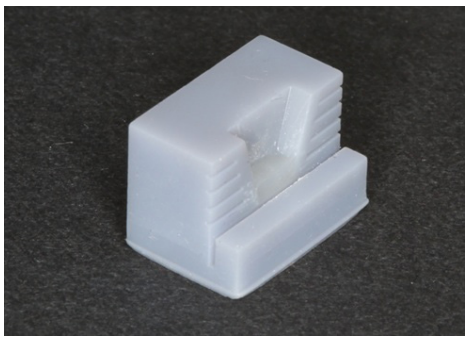

Fig. 3. *Plastic mold with a trapezoidal slot filled with the bottom horizontal layer ~ 1 mm.*

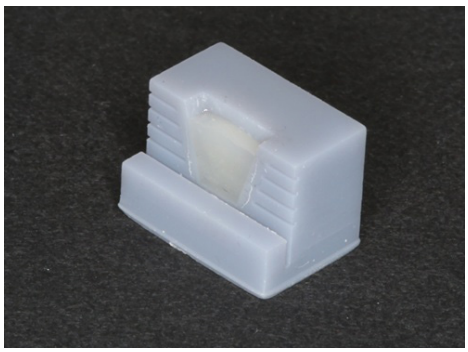

Fig. 4. *Plastic mold with a trapezoidal slot filled with the bottom horizontal layer ~ 4 mm.*

The surface microhardness of composite filling samples (n=32) was assessed using the Vickers hardness tester after exposure to light and storage in a dark container for 24 hours. Measurements were performed using a "ПМТ-3" tester with an indenter at a 50 g load for a 15-second dwell time. Indentations were made in a linear order at levels of 0.5, 1.5, 2.5, 3.5, and 4.5 mm from the top surface. Three indentations were made at each level.

The Vickers hardness number (VHN) was calculated according to the following formula: $VHN = 1.854 \times (F/D^2)$, where F is the applied load (kg), and D is the mean diagonal of the indentation (mm), which yields the VHN units (kg/mm^2).

Statistical analysis was performed using the statistical software package SPSS version 21.0 (Armonk, NY: IBM Corp). For descriptive analysis, results are presented as mean ± standard deviation. Multiple comparisons were performed with one-way ANOVA with Tukey's pairwise comparisons. The probability value of $P<0.05$ was considered statistically significant.

Results

Depth of cure was expressed as the ratio of the microhardness numbers of the top and bottom layers of the fillings and was presented as a percentage.

Analysis of data on the surface hardness of filling samples cured in a covered slot showed that the depth of cure of the bulk-fill composite material depends on the thickness of the bottom layer, the material temperature, and the duration of photoactivation.

At a depth of 4.5 mm, the VHN of composite fillings in Group 1 was 1.3 times greater than in Group 2. These samples were made from a room-temperature composite, and photoactivation of each layer was performed for 20 seconds. However, the thick first increment in Group 2 samples may have prevented light from reaching deeper portions of the composite, which could explain its low conversion, but without statistical significance (Table 1). Also, at the same depth, the VHN of composite fillings in Group 6 was 1.8 times greater than in Group 2, with statistical significance ($P=0.0001$). It should be noted that the samples from Group 6 were made in a similar layering sequence to those from Group 2, but they were heated to 55-60 °C and maintained at this temperature for 20 seconds during photoactivation. Moreover, the bottom-to-top ratio of surface hardness in Group 5 filling samples was ~95%, whereas in Group 2 samples, it was ~71%.

Doubling the photoactivation time of the room-temperature composite from 20 seconds to 40 seconds resulted in an increase in the VHN of composite fillings at depths of 1.5, 2.5, 3.5, and 4.5 mm up to 55%, but mostly insignificantly. The only difference of ~1.6 times was noted in VHN at a depth of 4.5 mm between the filling samples from Group 3 and Group 2 ($P=0.0071$), indicating the importance of both low increment thickness and prolonged irradiance. Also, increased light exposure of the resin composite contributed to improvements in the bottom-to-top ratio of surface hardness in samples from Groups 3 and 4, reaching 93% and 98%, respectively.

The surface hardness of fillings at 0.5mm in samples from Groups 1, 2, 3, and 4 was relatively high and did not show significant statistical differences among them. It was another confirmation of the crucial importance of close light source adjustment to the surface of light-cured material.

Photoactivation of a heated composite material in a covered slot had certain advantages over using a room-temperature composite, as demonstrated by the VHN of filling samples at different depths. For example, at all depths, the VHN of composite fillings in Group 8 was statistically greater than in Group 2, regardless of the thickness of the bottom

increment. Moreover, the difference increased with depth, from 1.4 (P=0.0431) [at 0.5 mm] to 1.8 (P=0.0001) [at 4.5 mm]. However, it was noteworthy that prolonged irradiance of a 4 mm-thick layer of resin composite is beneficial and may offset the low polymerization kinetics of a room-temperature filling material. Also, the bottom-to-top ratio of surface hardness of fillings in samples of Groups 5, 6, 7, and 8 ranged from 91% to 96%, which could be of great clinical value.

Discussion

Experimental methods for evaluating composite filling materials and their use are essential for achieving reliable, predictable clinical results in tooth restoration. Although there are only 5 classes of tooth lesions, each clinical situation has its own characteristics that can significantly affect the quality of direct restorations and the treatment outcome.

According to many studies, a low conversion rate of light-cured materials is often observed in the restoration of Class II lesions.[5,10-12] Narrow and deep cavities that prevent the normal transmission of light through the thickness of the filling material are the main reasons for insufficient composite polymerization.

Polymerization of light-cured resin composite in a covered slot most closely resembles the clinical situation of Class II restoration, guarantees a unidirectional transmission of a light beam, and can be considered as the most suitable and feasible laboratory technique to serve the purpose of the present study.[12]

In conclusion, lowering the thickness of the bottom layer of bulk-fill composite, along with its preheating and prolonged photoactivation, cumulatively contributed to a significant increase in depth of cure and microhardness of filling samples made in a covered slot.

Table 1.

Surface hardness of composite filling samples measured at different depths after photo activation in a covered slot.

Depth (mm)	Group 1	Group 2	Group 3	Group 4	Group 5	Group 6	Group 7	Group 8	Statistical data
0.5	40.2 ±2	38.9 ±7.6	46.6 ±11	43.6 ±7.3	52.4 ±6.3	55.1 ±7.3	54.4 ±5.8	55.8 ±6.1	F=3.8345; P=0.0062 P_{1-2}=1.0000; P_{1-3}=0.8975; P_{1-4}=0.0068; P_{1-5}=0.2676; P_{1-6}=0.0997; P_{1-7}=0.1312; P_{1-8}=0.0750; P_{2-3}=0.7789; P_{2-4}=0.9786; P_{2-5}=0.1706; P_{2-6}=0.0583; P_{2-7}=0.0782; P_{2-8}=0.0431; P_{3-4}=0.9985; P_{3-5}=0.9356; P_{3-6}=0.6871; P_{3-7}=0.7680; P_{3-8}=0.6010; P_{4-5}=0.6506; P_{4-6}=0.3334; P_{4-7}=0.4080; P_{4-8}=0.2676; P_{5-6}=0.9993; P_{5-7}=0.9999; P_{5-8}=0.9968; $P_{6-7=}$1.0000; P_{6-8}=1.0000; P_{7-8}=1.0000
1.5	36.2 ±4.5	39.9 ±5.7	45.9 ±3.2	49.9 ±8.9	49.7 ±6.4	62 ±5.4	55.9 ±6.4	61.8 ±7.5	F=9.2634; P=0.0000 P_{1-2}=0.9886; P_{1-3}=0.3831; P_{1-4}=0.0759; P_{1-5}=0.0833;P_{1-6}=0.0001; P_{1-7}=0.0033; P_{1-8}=0.0001; P_{2-3}=0.8643;P_{2-4}=0.3470; P_{2-5}=0.3708; P_{2-6}=0.0009; P_{2-7}=0.0243; P_{2-8}=0.0010; P_{3-4}=0.9822; P_{3-5}=0.9867; P_{3-6}=0.0231; P_{3-7}=0.3470; P_{3-8}=0.0256; P_{4-5}=1.0000; P_{4-6}=0.1554; P_{4-7}=0.8643; P_{4-8}=0.1690; P_{5-6}=0.1427; P_{5-7}=0.8442; P_{5-8}=0.1554; P_{6-7}=0.8544; P_{6-8}=1.000; P_{7-8}=0.8738
2.5	36.1 ±5.5	32.3 ±4.6	42.9 ±3.8	44.9 ±7.9	47.2 ±7.4	53.2 ±6	52.1 ±7.4	55.7 ±9.3	F=6.0841; P=0.0004 P_{1-2}=0.9914; P_{1-3}=0.8333; P_{1-4}=0.5921; P_{1-5}=0.3142; P_{1-6}=0.0262; P_{1-7}=0.0439; P_{1-8}=0.0077; P_{2-3}=0.3678; P_{2-4}=0.1851; P_{2-5}=0.0720; P_{2-6}=0.0040; P_{2-7}=0.0070; P_{2-8}=0.0011; P_{3-4}=0.9999; P_{3-5}=0.9825; P_{3-6}=0.4023; P_{3-7}=0.5397; P_{3-8}=0.1715; P_{4-5}=0.9996; P_{4-6}=0.6574; P_{4-7}=0.7911; P_{4-8}=0.3458; P_{5-6}=0.9031; P_{5-7}=0.9644; P_{5-8}=0.6314; P_{6-7}=1.0000; P_{6-8}=0.9994; P_{7-8}=0.9938
3.5	32.4 ±4.7	31.5 ±5.8	40.9 ±5.4	43.5 ±8.3	44.3 ±7.4	50.3 ±6.5	51.2 ±7.8	52.1 ±8.7	F=5.3548; P=0.0009 P_{1-2}=1.0000; P_{1-3}=0.6706; P_{1-4}=0.3561; P_{1-5}=0.2772; P_{1-6}=0.0243; P_{1-7}=0.0159; P_{1-8}=0.0104; P_{2-3}=0.5572; P_{2-4}=0.2682; P_{2-5}=0.2036; P_{2-6}=0.0159; P_{2-7}=0.0104; P_{2-8}=0.0067; P_{3-4}=0.9994; P_{3-5}=0.9965; P_{3-6}=0.5572; P_{3-7}=0.4463; P_{3-8}=0.3456; P_{4-5}=1.0000; P_{4-6}=0.8565; P_{4-7}=0.7654; P_{4-8}=0.6581; P_{5-6}=0.9181; P_{5-7}=0.8475; P_{5-8}=0.7541; P_{6-7}=1.0000; P_{6-8}=0.9990; P_{7-8}=1.0000
4.5	35.5 ±2.8	27.5 ±3	43.2 ±4.9	42.7 ±8.2	49.7 ±2.8	50.4 ±6.9	52.1 ±3	50.3 ±7.4	F=10.5695; P=0.0000 P_{1-2}=0.4295; P_{1-3}=0.4762; P_{1-4}=0.5574; P_{1-5}=0.0181; P_{1-6}=0.0117; P_{1-7}=0.0040; P_{1-8}=0.0125; P_{2-3}=0.0071; P_{2-4}=0.097; P_{2-5}=0.0001; P_{2-6}=0.0001; P_{2-7}=0.0000; P_{2-8}=0.0001; P_{3-4}=1.0000; P_{3-5}=0.6724; P_{3-6}=0.5574; P_{3-7}=0.3036; P_{3-8}=0.5739; P_{4-5}=0.5904; P_{4-6}=0.4762; P_{4-7}=0.2449; P_{4-8}=0.4922; P_{5-6}=1.0000; P_{5-7}=0.9979; P_{5-8}=1.0000; $P_{6-7=}$0.9998; P_{6-8}=0.9907; P_{7-8}=0.9997
B/T, %	88	71	93	98	95	91	96	90	

Competing Interests

The authors declare that they have no competing interests.

References

1. Santos A, Proença L, Polido M, Cristina Azul A. Depth of cure of bulk-fill light cured composite resins with different initiators. Ann Med. 2019 May 28;51(Suppl 1):141. doi: 10.1080/07853890.2018.1561985. PMCID: PMC7888906.
2. Tapety CM, Carneiro YK, Chagas YM, Souza LC, Souza NO, Valadas LA. Degree of Conversion and Mechanical Properties of a Commercial Composite with an Advanced Polymerization System. Acta Odontol Latinoam. 2023 Aug 31;36(2):112-119. doi: 10.54589/aol.36/2/112. PMID: 37776508; PMCID: PMC10557085.
3. Khabadze Z, Dolzhikov N, Bagdasarova I, Badalov F, Dashtieva M, Karapetian E, Umarova A, Generalova Yu, Kulikova A, Umarov A, Starodubtseva E, Tursunboev S, Aude R. Cytotoxicity of Methacrylate – Based Resin Materials in Dentistry. J Int Dent Med Res. 2025;18(2):904-913).
4. Khabadze Z, Generalova Yu, Abdulkerimova S, Dashtieva M, Borlakova M, Meremkulov R, Mordanov O, Magomedova Kh, Kulikova A, Bakaev Yu, Golubenkova A, Voskressensky L, Melkumyan T. Analysis of the Anaerobic Conversion Efficiency of Various Group Composite Material. Journal of International Dental and Medical Research. 2023;16(3):975-982.
5. Musavinasab SM, Norouzi Z. Hardness and Depth of Cure of Conventional and Bulk-Fill Composite Resins in Class II Restorations with Transparent and Metal Matrix Strips. Front Dent. 2023 Jun 13;20:20. doi: 10.18502/fid.v20i20.12912. PMID: 37701657; PMCID: PMC10493112.
6. Melkumyan TV, Sheraliava SSh, Mendosa EYu, Khabadze ZS, Makeeva MK, Musoshayhova ShK, Dadamova AD, Shakirov ShM, Mukhamedov AA, Tojinazarov FM, Iskandarov NE. Impact of Different LED Units, Tip Distance and Time of Light Exposure on Microhardness of Resin-Based Composite for Posterior Teeth. International Journal of Biomedicine. 2024;14(4):700-703. doi:10.21103/Article14(4)_OA27
7. Melkumyan TV, Sheraliava SSh, Mendosa EYu, Khabadze ZS, Makeeva MK, Kamilov NKh, Musoshayhova ShK, Dadamova AD, Shakirov ShM, Mukhamedov AA. Effect of Preheating on Mechanical Properties of Different Commercially Available Dental Resin Composites. International Journal of Biomedicine. 2023;13(4):317-322. doi:10.21103/ Article13(4)_OA14.
8. Singha A, Dhanesha A, Nair S, Patel R, Behera S, Nanda S. Pre-heating effect on micro-hardness and depth of cure for three bulk-fill composite resins: An *in vitro* study. Bioinformation. 2024 Sep 30;20(9):1128-1131. doi: 10.6026/97320630020011128. PMID: 39917230; PMCID: PMC11795488.
9. Asani RN, Gade VJ, Umale KG, Gawande R, Amburle RR, Kusumbe RR, Kale PP, Kosare PR. Preheated composite: Innovative approach for aesthetic restoration [Internet]. Arch Dent Res. 2021 [cited 2025 Oct 04];11(2):103-107. Available from: doi: 10.18231/j.adr.2021.017.
10. Poggio C, Chiesa M, Scribante A, Mekler J, Colombo M. Microleakage in Class II composite restorations with margins below the CEJ: in vitro evaluation of different restorative techniques. Med Oral Patol Oral Cir Bucal. 2013 Sep 1;18(5):e793-8. doi: 10.4317/medoral.18344. PMID: 23722121; PMCID: PMC3790654.
11. Haddad M, Lugassy D, Barhum M, Brosh T, Matalon S. The Influence of Posterior Class II Composite Restoration Location and Techniques on Marginal Sealing. Dent J (Basel). 2025 Jan 17;13(1):39. doi: 10.3390/dj13010039. PMID: 39851615; PMCID: PMC11763528.
12. Brent W Church, Daranee Tantbirojn, Thuydung Do, Martha H Wells, Antheunis Versluis. Depth-of-cure of Bulk-fill Composites Cured in Tooth or Opaque Substrate. International Journal of Experimental Dental Science, July-December 2017;6(2):68-73

***Corresponding author:** *Prof. Timur V. Melkumyan, PhD, ScD. Tashkent State Dental Institute Tashkent, Uzbekistan. Peoples' Friendship University of Russia (RUDN University), Moscow, Russia. E-mail: t.dadamov@gmail.com*

International Journal of Biomedicine 15(4) (2025) 741-745
http://dx.doi.org/10.21103/Article15(4)_OA16

ORIGINAL ARTICLE

Experimental Biology

INTERNATIONAL JOURNAL OF BIOMEDICINE

The Effect of Direct Electric Current on Some Parameters of Human Blood Coagulation

Anzhela Z. Galstyan[1], Zoya Kh. Paronyan[1*], Narine S. Piloyan[1], Hasmik A. Stepanyan[1], Davit A. Poghosyan[1], Lusine R. Arakelyan[1], Torgom Ye. Seferyan[1]

[1]*Institute of Biochemistry after H. Buniatyan, NAS RA, Yerevan, Armenia*

Abstract

Background: Direct current (DC) is increasingly used in medical applications, yet its effects on blood plasma hemostasis remain underexplored. This study systematically examines the effects of DC exposure on key coagulation parameters and plasma pH, highlighting their potential physiological relevance and implications for electrotherapeutic strategies.

Methods and Results: The experiments used a pooled plasma sample from healthy donors, which was subjected to electrolysis using platinum point electrodes and a DC with a voltage range of 11-19 V. A number of parameters characterizing plasma hemostasis were measured to assess the coagulation process, including recalcification time, prothrombin time, thrombin time, activated partial thromboplastin time, international normalized ratio index, fibrinogen level, pH, and absorbed current strength. Experimental data showed that, with increasing current voltage during electrolysis, plasma coagulation time exhibits nonlinear changes, some parameters change significantly, and plasma hemostasis slows down beyond a certain current voltage threshold. The obtained data can be helpful for both therapeutic and other research in this field. (**International Journal of Biomedicine. 2025;15(4):741-745.**)

Keywords: plasma • hemostasis • fibrinogen • anticoagulant action

For citation: Galstyan AZ, Paronyan ZKh, Piloyan NS, Stepanyan HA, Poghosyan DA, Arakelyan LR, Seferyan TYe. The Effect of Direct Electric Current on Some Parameters of Human Blood Coagulation. International Journal of Biomedicine. 2025;15(4):741-745. doi:10.21103/Article15(4)_OA16

Abbreviations

aPTT, activated partial thromboplastin time; **FL**, fibrinogen level; **ISI**, international sensitivity index; **INR**, international normalized ratio; **PH**, plasma hemostasis; **PT**, prothrombin time; **RT**, recalcification time; **TT**, thrombin time.

Introduction

To maintain the fluid state of blood with optimal viscosity, the body has a special functional system that includes coagulation and anticoagulation mechanisms, which are normally in a state of balance (hemostasis). It is known that disruption of hemostasis leads to undesirable pathological conditions, such as bleeding or the formation of blood clots.

Currently, numerous studies examine the effects of various physical factors on blood physiological parameters. The effects of electric current on the body are used for various purposes, such as electrotherapy, electrocoagulation, muscle stimulators, oncotherapy methods, neuropsychology, and more.[1-5] It is known that electric current affects not only tissue cells but also tissue fluids, particularly blood. Hemostasis, one of the primary physiological indicators of blood, can be altered by electrical current, with significant physiological implications when used for therapeutic purposes. Its disruptions are particularly hazardous for patients with concomitant conditions such as cancer, infectious diseases, severe trauma, and diabetes mellitus.[6,7]

The effects of direct current (DC) on body tissues can be considered the result of simplified basic reactions and phenomena of electrolysis, such as electrode reactions, a reduction in calcium concentration in the medium, and the generation of free radicals.[8]

Electrolysis of a physiological buffer solution initiates chemical reactions. Combined both half-reactions in electrodes is: $2NaCl(aq)+2H_2O(l)\rightarrow H_2(g)+Cl_2(g)+2NaOH(aq)$

During the electrolysis of saline solutions, different compounds form (O_3, O_2, H_2O_2, HClO, $HClO_2$, ClO, ClO_2, Cl_2, H_2, HO_2^-, O_2^-, H^-, ClO^-, ClO_3^-, ClO_4^-, H^-, O^-, Cl^-, OH^-, HO_2^-, $^1O_2$, ClO^-, O_2^{-}).[9-11] These compounds may affect hemostasis.[12] Even the electrolysis of saline, which can be considered a simple model of blood electrolysis, has many reactions.

Since Scudamore's work in 1824,[13] the effect of DC on blood coagulation has been a subject of inquiry. Hayashi[14] reviewed all relevant studies conducted between 1824 and 1964. His paper notes that Schwartz[15] found that applying a DC of 4.5 V and 5 mA for 1 hour induced thrombus formation in the superficial femoral vein of dogs. Kravitze and Wagner [16] demonstrated that a DC of 12 to 16 mA applied for 7 to 10 minutes typically resulted in coagulation on diffusely bleeding surfaces. Hayashi also reported that applying 6 V and 4 to 4.5 mA of positive DC for 9 to 12 minutes initiated thrombus formation in the mesenteric plexus blood vessels of rabbits.

Recent studies have shown that DC prolongs coagulation time and acts as a non-chemical anticoagulant.[17-19] Until now, existing studies have not systematically examined the dynamic changes in hemostasis parameters under the influence of electric current at different exposure time doses. Based on the above considerations, this study aimed to investigate the effects of DC on the main indicators of PH, including prothrombin time (PT), international normalized ratio (INR), activated partial thromboplastin time (aPTT), thrombin time (TT), recalcification time (RT), fibrinogen level (FL), and plasma pH. It is known that the pH of the medium is crucial for hemostasis; even a minor change of 0.5 can alter the timing of thrombosis by more than 25%.[19] The current intensity (mA) required for these effects was also examined.

Plasma hemostasis is part of the overall hemostatic system, which includes a cascade of protein reactions in blood plasma and is closely related to the vascular-platelet interaction and the anticoagulant system. Since the traumatic factor of hemostasis change is not present in the case of electric current exposure, it is not considered in this work.

Materials and Methods

Human plasma was obtained from the Hematology Center named after Prof. R. Yeolyan (Yerevan, Armenia). The purchase was conducted through an open sale transaction. Samples were collected in PVC bags and remained unexposed to any freeze–thaw cycles. CPDA-1 (citrate-phosphate-dextrose; RAVIMED, Poland) was used as the anticoagulant.

Plasma samples were collected from 10 healthy donors (5 men, 5 women) aged 18–50 years. No personal information was provided beyond sex and age. Equal volumes of individual plasma samples were pooled to create a composite sample. Each experiment was performed in 6 replicates.

Thromboplastin with ISI of 1.75 was obtained from Delta LTD (Armenia).Thrombin time reagents were obtained from RPA 'RENAM' (Russia). aPTT-Kaolin set was produced by BIOLABO (France).

Electrolysis and pH Measurement

Plasma electrolysis was performed using a custom electrolytic chamber consisting of a cylindrical glass cup (total volume of 15 mL) sealed with a cap housing 2 platinum dot electrodes (Gomel, Belarus) spaced 15 mm apart. A DC power supply with precise voltage regulation was connected to the electrodes. During electrolysis, the chamber was placed on a magnetic stirrer operating at low speed (30 rpm).

A volume of 4 mL of pooled plasma was placed in the electrolysis cell. DC ranging from 11 to 19 V was applied for 10 minutes. For recalcification analysis, electrolysis was performed at 11, 13, 15, 17, and 19 V. For other hemostasis parameters, voltages of 11, 15, and 19 V were used. pH and current measurements were conducted across a voltage range of 11, 13, 15, 17, 19, and 24 V. No electrolyzed plasma pool was used as a control.

The pH values of plasma were measured using a Hanna HI2002-01 pH/ORP meter (Hanna Instruments, USA). To determine the dependence of plasma pH on the duration of electrolysis, the measurement was performed directly on the electrolyzed plasma at room temperature.

Consumed power was measured using a multimeter connected in series with the electrolysis circuit. Electric current was recorded at one-minute intervals throughout the 10-minute electrolysis period at applied voltages of 11, 13, 15, 17, 19, and 24 V.

Biochemical Methods

Plasma coagulation effectiveness was measured using clot-based tests, such as RT,[20] PT/INR,[21] TT, aPTT, and FL.[22] Hemostasis parameters (RT, PT, INR, TT and aPTT) were measured using a biochemical analyzer STart Max (Stago, France).

Prothrombin time was measured using thromboplastin with an ISI of 1.75. Electrolyzed and control plasma samples were preincubated in a water bath at 37°C for 4 min. Thromboplastin was added with fast stirring, and the time was measured until fibrin filaments were observed.[23] International normalized ratio (INR) was calculated using the following formula:[21]

$$INR = \left(\frac{PT\ exp.}{PT\ control}\right)^{ISI}$$

where "PT exp." and "PT control" are prothrombin time for electrolyzed and control plasma, respectively, and ISI is the International Sensitivity Index of Thromboplastin (provided with the reagent).

For TT assay, plasma was prewarmed for 3 minutes in a 37°C water bath. The TT detection reagent ("RENAM" RPA, Russia) was prepared according to the manufacturer's instructions and added to the electrolyzed and control plasma samples. Coagulation time was measured after the addition of the thrombin reagent.

aPTT was measured using the BIO-CK aPTT-Kaolin kit (BIOLABO, France). The reagent was prepared according to the manufacturer's instructions, prewarmed to 37°C, and added to the plasma. After 3 minutes of incubation at 37°C in a water bath, 0.227% $CaCl_2$ was added, and the coagulation time was measured.

For recalcification measurement, plasma samples were mixed with 5% $CaCl_2$ (in ratio 10:1) and incubated at room

temperature without any activating factors. Coagulation time was measured from the time of $CaCl_2$ addition.

The level of fibrinogen was measured by a slightly modified gravimetric method, described in Saxena.[24] Briefly, clots were carefully removed from plasma samples after recalcification assay, compressed to expel residual plasma and reagents, thoroughly dried using filter paper, and weighed on an analytical balance.

Statistical Analysis

The results are reported as the mean ± standard error of the mean (SEM). Data were analyzed using one-way ANOVA with GraphPad Prism v.9.3 (GraphPad Software Inc., La Jolla, CA, USA). Statistical significance is indicated as follows, * - $P \leq 0.05$, ** - $P \leq 0.01$, *** - $P \leq 0.001$, and **** - $P \leq 0.0001$.

Results

Plasma hemostasis is necessary to maintain the normal fluid state of the blood and effectively stop bleeding. To obtain information on overall blood coagulation, the RT determination method was used, which correlates with the total clotting time.

Preliminary studies have shown that increasing the applied DC voltage did not result in significant changes in RT within the studied range (Figure 1A). Further studies focused on evaluating the dependence of the investigated parameters on voltage variation. When recording the RT, it was observed that as the current voltage increased during electrolysis (11–15 V), the RT initially decreased slightly (by 4.5%); a further increase in voltage (19 V) resulted in a twofold increase (by 104.2%) (Figure 1B). This suggests that within a specific voltage range, the plasma coagulation system is partially activated, but higher voltages can damage coagulation factors or alter the plasma pH, slowing down coagulation.

We found that as the current voltage increased, the rate of fibrin formation from fibrinogen decreased (from 44.2% to -62%) (Figure 1C). These changes may be the reason for the decrease in thrombin activity or structural changes in fibrinogen.

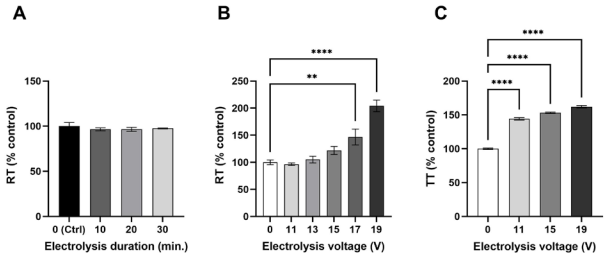

Fig. 1. *The effect of electrolysis on RT for 11V 0-30min (A), RT (B), and TT (C). Data are normalized to control and presented as the mean ± SEM, n=6. *P<0.05; **P<0.01; ***P<0.001; ****P<0.0001*

One of the important laboratory parameters characterizing the state of the blood coagulation system is PT, which is used to assess the activity of the extrinsic pathway of blood coagulation and the deficiency of factors II, X, VII, and V. Initially, PT was slightly reduced (11 V) (Figure 2A), possibly due to mild activation, but at 15 V and especially at 19 V it increased significantly, by 11% and 42.8%, respectively. This indicates the possibility of inhibiting the extrinsic pathway of blood coagulation or decreasing the activity of factors under the influence of high voltage.

Along with PT, aPTT is an essential indicator for monitoring coagulation processes (both the extrinsic and intrinsic pathways). A significant increase in aPTT (Figure 2B) during electrolysis (38.3%) at high voltages (19 V) indicates a disruption of the intrinsic coagulation pathway, which may be due to a deficiency of coagulation factors I, II, V, VII and X, as well as prekallikrein or one of the intrinsic coagulation pathway factors (VIII, IX, XI and/or XII), which may occur as a result of electrochemical reactions during electrolysis or as a result of change in pH.

The INR at 11V decreased to 0.79, which may indicate a temporary increase in prothrombin activity or partial stimulation of the coagulation system. At 15 V, the INR increased to 1.21, and at 19 V, it increased to 1.88, indicating a slowdown or disruption of the extrinsic coagulation pathway (Figure 2C).

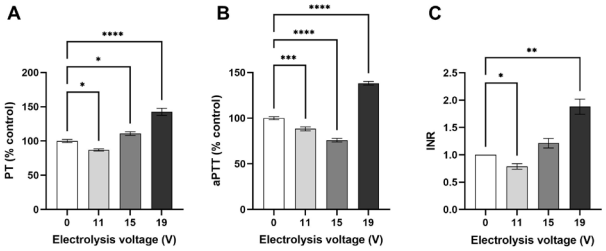

Fig. 2. *The effect of electrolysis on PT (A), aPTT (B), and INR (C). Data are presented as the mean ± SEM, n=6. *P<0.05; **P<0.01; ***P<0.001; ****P<0.0001. For PT and aPTT data, the values are normalized to the control.*

It is believed that high voltage during electrolysis can oxidize or inactivate some components of the prothrombin complex, weakening the coagulation process. When studying FL, we found that at 11 V, it decreased by 18.8%, which may be associated with fibrinogen degradation or structural changes. However, at voltages of 15 V and 19 V, FL increased by 13.6% and 23.1%, respectively (Figure 3A).

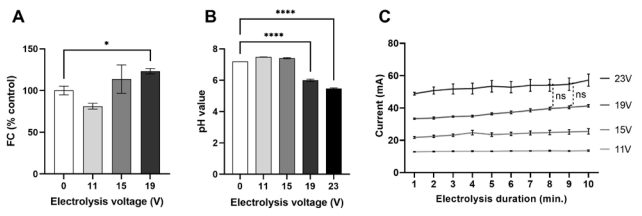

Fig. 3. *The effect of electrolysis on FL (A) and pH of plasma (B). FL is normalized to control. (C) shows power consumption during the electrolysis at different voltages. Data are presented as the mean ± SEM, n=6. *P<0.05; **P<0.01; ***P<0.001; ****P<0.0001. For (C), all differences between groups are significant except marked as "ns."*

Given the importance of pH in coagulation reactions, the possible change in pH under DC influence was observed. The pH at 11 V and 15 V shows a relative increase of 0.278 and 0.206, respectively, (Figure 3B) and at 19 V a decrease of 1.73 points, reaching 5.998. To further examine the trend in the pH indicator change, the pH indicator was also observed at 23 V, registering a lower value than those recorded at 19 V (5.462). The obtained data indicate that under the influence of electrolysis, an intensive formation of acidic or basic substances occurs, leading to disruption of the acid-base balance and exceeding the plasma's buffering capacity.

In plasma electrolysis, water is decomposed, producing hydrogen and hydroxide ions that can alter the pH balance. Plasma contains buffer systems (e.g., bicarbonate), but their ability to neutralize pH changes is limited.

Electrolysis can produce carbonic acid from carbon dioxide dissolved in water, which itself is a weak acid. Still, during intensive hydrolysis, its concentration increases, and the system becomes overloaded, which, in blood plasma, can lead to a rise in acidity and slow down the blood clotting process, especially at high voltages.[19,25]

To assess the possible correlation between the obtained data and the energy introduced into the electrolytic system and the dynamics of energy absorbed by the system, amperometric recordings of plasma electrolysis were also performed (Figure 3C). The obtained data indicate that the current in the system increases proportionally with voltage, showing a slight increase over time, reaching a maximum of 8.4 mA at 23 V. Large amperometric values and the most significant changes in the obtained indicators characterizing hemostasis are observed mainly at high voltages.

Discussion

The effect of electrolysis on the blood coagulation system has not been sufficiently studied. Our results show that changes in current voltage during electrolysis can affect hemostasis mechanisms in different ways, causing both coagulant and anticoagulant effects. The results also indicate that DC can directly affect the main PH parameters.

In electrolysis at a moderate current (up to 15 V), a slight increase in pH was observed. In contrast, at high voltages (19 V), prolonged clotting time, increased INR, increased FL, and significant changes in the intrinsic and extrinsic coagulation pathways were observed. These effects likely result from pH changes during electrolysis or from reduced activity of some coagulation factors due to the electrochemical effects. An increase in FL resulting from electrolysis, along with a rise in INR, may indicate activation of hemostasis in response to plasma damage. The INR measures the efficiency of the extrinsic coagulation pathway, and its increase may indicate a reduced activity of coagulation factors. Fibrinogen, a key component of the thrombus, may increase as part of a protective mechanism to sustain thrombus formation.[26] When low-voltage DC electricity is applied, ionized calcium, an essential element in blood coagulation, is absorbed by the negative electrode. In contrast, most blood proteins, including coagulation factors that are negatively charged at normal blood pH, can be adsorbed onto the positive electrode.[27,28] Calcium is a vital cofactor for many coagulation factors, while blood pH significantly affects the concentration of ionized calcium and the function of these factors. In acidosis, hydrogen ions displace calcium from proteins, increasing the ionized calcium concentration. Changes in calcium ion concentration can affect the activation of coagulation factors, and changes in protein concentration can affect their capacity to form clots. Conversely, as the intensity of plasma electrolysis increases, the pH decreases, creating an acidic environment that disrupts the function of enzymes and other proteins involved in hemostasis.[29]

Acidity affects the activity of clotting factors and can impair fibrinolytic activity; together, these effects create an imbalance that may increase the risk of both bleeding and thrombosis, depending on the degree and nature of the disorder.

The data indicate that, at low voltages, the examined blood plasma parameters—except TT—tend to decrease, whereas at higher voltages they increase. This suggests that plasma can resist the effects of the applied current up to a specific limit, beyond which all parameters increase along with voltage and current strength. The obtained data can be helpful for both therapeutic and other research in this field.

Sources of Funding

This work was made possible by a research grant from the Armenian National Science and Education Fund (ANSEF) based in New York, USA (hubio-3936).

Competing Interests

The authors declare that they have no competing interests.

References

1. Zhong S, Yao S, Zhao Q, Wang Z, Liu Z, Li L, et al. Electricity-Assisted Cancer Therapy: From Traditional Clinic Applications to Emerging Methods Integrated with Nanotechnologies. Advanced NanoBiomed Research. 2023 Mar;3(3):2200143.
2. Watson T. The role of electrotherapy in contemporary physiotherapy practice. Man Ther. 2000 Aug;5(3):132-41. doi: 10.1054/math.2000.0363. PMID: 11034883.
3. Hills A, Stebbing J. Electrotherapy: enlightening modern medicine. Lancet Oncol. 2014 Sep;15(10):1060-1. doi: 10.1016/S1470-2045(14)70423-1. PMID: 25186041.
4. Shin YI, Foerster Á, Nitsche MA. Transcranial direct current stimulation (tDCS) - application in neuropsychology. Neuropsychologia. 2015 Mar;69:154-75. doi: 10.1016/j.neuropsychologia.2015.02.002. Epub 2015 Feb 3. PMID: 25656568.
5. Ushimaru Y, Odagiri K, Akeo K, Ban N, Hosaka M, Yamashita K, Saito T, Tanaka K, Yamamoto K, Makino T, Takahashi T, Kurokawa Y, Eguchi H, Doki Y, Nakajima K. Efficacy of electrocoagulation hemostasis: a study on the

optimal usage of the very-low-voltage mode. Surg Endosc. 2022 Nov;36(11):8592-8599. doi: 10.1007/s00464-022-09492-4. Epub 2022 Aug 5. PMID: 35931893.
6. Mruthunjaya AKV, Torriero AAJ. Electrochemical Monitoring in Anticoagulation Therapy. Molecules. 2024 Mar 24;29(7):1453. doi: 10.3390/molecules29071453. PMID: 38611733; PMCID: PMC11012951.
7. Falanga A, Marchetti M, Vignoli A. Coagulation and cancer: biological and clinical aspects. J Thromb Haemost. 2013 Feb;11(2):223-33. doi: 10.1111/jth.12075. PMID: 23279708.
8. Jahanbani A, Eskandari Roozbahani N. Electrochemical Anticoagulant Method. In: Qi X, Shao X, editors. Anticoagulation - An Update. IntechOpen; 2024.
9. Okada F, Nay K. Electrolysis for Ozone Water Production. In: Kleperis J, editor. Electrolysis. InTech; 2012. p. 243–72.
10. Wang YH, Chen QY. Anodic Materials for Electrocatalytic Ozone Generation. International Journal of Electrochemistry. 2013;2013:1–7.
11. Jackson CV, Mickelson JK, Stringer K, Rao PS, Lucchesi BR. Electrolysis-induced myocardial dysfunction. A novel method for the study of free radical mediated tissue injury. J Pharmacol Methods. 1986 Jul;15(4):305-20. doi: 10.1016/0160-5402(86)90010-0. PMID: 3724201.
12. Nencini F, Giurranna E, Borghi S, Taddei N, Fiorillo C, Becatti M. Fibrinogen Oxidation and Thrombosis: Shaping Structure and Function. Antioxidants (Basel). 2025 Mar 26;14(4):390. doi: 10.3390/antiox14040390. PMID: 40298646; PMCID: PMC12024030.
13. Scudamore C, Scudamore C, St. Thomas's Hospital. Medical School Library former owner, King's College London. An essay on the blood. London : printed for the author, and published by Longman, Hurst, Rees, Orme, Brown, and Green; 1824. 194 p.
14. Hayashi H. Fundamental studies on the electrical potential difference across blood vessel walls and applications of direct current coagulation. Nagoya J Med Sci. 1968 Mar;30(4):399-418. PMID: 5662367.
15. SCHWARTZ SI. Prevention and production of thrombosis by alterations in electric environment. Surg Gynecol Obstet. 1959 May;108(5):533-6. PMID: 13647208.
16. KRAVITZ HM, WAGNER KJ. APPLICATIONS OF DIRECT CURRENT COAGULATION IN PLASTIC SURGERY. Plast Reconstr Surg. 1964 Apr;33:361-7. doi: 10.1097/00006534-196404000-00006. PMID: 14142134.
17. Jahanbani A, Dezfouli SMS, Javaherifar A, Yourdkhani MR, Goudarzi M. To Delay the Process of Blood Coagulation Using Electrolysis Technique in Sheep Blood. International Journal of Scientific & Engineering Research. 2017 Mar;8(3).
18. Kahn NN, Feldman SP, Bauman WA. Lower-extremity functional electrical stimulation decreases platelet aggregation and blood coagulation in persons with chronic spinal cord injury: a pilot study. J Spinal Cord Med. 2010;33(2):150-8. doi: 10.1080/10790268.2010.11689690. PMID: 20486534; PMCID: PMC2869270.
19. Gissel M, Brummel-Ziedins KE, Butenas S, Pusateri AE, Mann KG, Orfeo T. Effects of an acidic environment on coagulation dynamics. J Thromb Haemost. 2016 Oct;14(10):2001-2010. doi: 10.1111/jth.13418. Epub 2016 Sep 12. PMID: 27431334.
20. Lee RI, White PD. A CLINICAL STUDY OF THE COAGULATION TIME OF BLOOD. The American Journal of the Medical Sciences. 1913 Apr;145(4):495–503.
21. Dorgalaleh A, Favaloro EJ, Bahraini M, Rad F. Standardization of Prothrombin Time/International Normalized Ratio (PT/INR). Int J Lab Hematol. 2021 Feb;43(1):21-28. doi: 10.1111/ijlh.13349. Epub 2020 Sep 26. PMID: 32979036.
22. Walker HK, Hall WD, Hurst JW, editors. Clinical Methods: The History, Physical, and Laboratory Examinations. 3rd ed. Boston: Butterworths; 1990. PMID: 21250045.
23. Ruggeri ZM. Von Willebrand factor, platelets and endothelial cell interactions. J Thromb Haemost. 2003 Jul;1(7):1335-42. doi: 10.1046/j.1538-7836.2003.00260.x. PMID: 12871266.
24. Saxena KK, Srivastava RK, Kulshrestha VK, Prasad DN. A simple gravimetric method for estimation of plasma fibrinogen. Indian J Physiol Pharmacol. 1979 Apr-Jun;23(2):137-9. PMID: 489096.
25. Naceradska J, Pivokonska L, Pivokonsky M. On the importance of pH value in coagulation. Journal of Water Supply: Research and Technology-Aqua. 2019 May;68(3):222–30.
26. Luyendyk JP, Schoenecker JG, Flick MJ. The multifaceted role of fibrinogen in tissue injury and inflammation. Blood. 2019 Feb 7;133(6):511-520. doi: 10.1182/blood-2018-07-818211. Epub 2018 Dec 6. PMID: 30523120; PMCID: PMC6367649.
27. Wilson K, Walker J, editors. Principles and Techniques of Biochemistry and Molecular Biology. 7th ed. Cambridge University Press; 2010.
28. Berg JM, Tymoczko JL, Gatto GJ, Stryer L, editors. Biochemistry. 8. ed. New York, NY: W.H. Freeman/ Macmillan; 2015.
29. Scharbert G, Franta G, Wetzel L, Kozek-Langenecker S. Effect of pH levels on platelet aggregation and coagulation: a whole blood in vitro study. Crit Care. 2011 Feb;15(S1):P446, cc9866.

***Corresponding author:** *Zoya Kh. Paronyan, PhD. Laboratory of Biomedical Research, Institute of Biochemistry after H. Buniatyan, NAS RA. E-mail: aregarpi4@gmail.com.*

International Journal of Biomedicine 15(4) (2025) 746-751
http://dx.doi.org/10.21103/Article15(4)_OA17

ORIGINAL ARTICLE

Experimental Biology

INTERNATIONAL JOURNAL OF BIOMEDICINE

Curcumin Analogue EF-24 Induces Ferroptosis in Human Multiple Myeloma Cells MM.1S

Liu-Qing Cui, Meng-Yi Yang, Jia-Jun Zhao, Shi-Wei Ma, Guang-Zhou Zhou*

College of Bioengineering, Henan University of Technology, Zhengzhou 450001, China

Abstract

Myeloma is a type of malignant tumor that originates from plasma cells. The curcumin analog EF-24 has demonstrated promising antitumor activity. However, its role in myeloma cell proliferation was unclear. In this study, we found that EF-24 could inhibit the proliferation of multiple myeloma cells (MM.1S) by morphological observation and CCK-8 assay. RNA-sequencing analysis indicated that several genes associated with ferroptosis exhibited differential transcription, which was confirmed by RT-qPCR. Therefore, following detection of ferroptosis-related proteins (GPX4 and SLC7A11) and upregulation in the destruction of mitochondrial cristae and other ferroptosis factors, including MDA, GSH, ROS, and Fe^{2+} concentrations, were conducted in EF-24-treated MM.1S cells, which concluded that EF-24 could induce ferroptosis in myeloma cells. Conversely, the addition of the ferroptosis inhibitor (ferrostatin-1) could reverse the above changes activated by EF-24. Moreover, NOD/SCID mice grafted with MM.1S cells were constructed, and intravenous injection of EF-24 effectively decreased tumor growth and protected normal tissues, as observed by Hematoxylin-Eosin staining. In summary, our results confirm the EF-24-induced ferroptosis in myeloma cells and exhibited a protective role in model mice grown from implanted MM.1S cells in vivo.(**International Journal of Biomedicine. 2025;15(4):746-751.**)

Keywords: Curcumin analogue • ferroptosis • multiple myeloma

For citation: Cui L-Q, Yang M-Y, Zhao J-J, Ma S-W, Zhou G-Z. Curcumin Analogue EF-24 Induces Ferroptosis in Human Multiple Myeloma Cells MM.1S. International Journal of Biomedicine. 2025;15(4):746-751. doi:10.21103/Article15(4)_OA17

Introduction

Multiple myeloma (MM) is a clonal plasma cell malignancy originating from the bone marrow that accounts for approximately 13% of all hematologic cancers and is associated with a range of symptoms, including anemia, bone damage, hypercalcemia, and renal impairment.[1,2] The treatment of MM has changed dramatically in recent years, with a series of advances in therapeutic approaches that have led to improved survival rates; however, the majority of patients eventually relapse.[3] One of the major advances in the treatment of MM in the last decade has been the introduction of the novel drugs thalidomide, bortezomib, and lenalidomide.[4] But obviously, it is not enough, and many more molecules or drugs against multiple myeloma need to be explored.

Curcumin (Cur) is a bioactive polyphenolic compound found in turmeric, which has a variety of pharmacological activities, including anti-inflammatory, antiaging, antidiabetic, and antitumor functions, and so on.[5,6] Although a large number of clinical trials have confirmed curcumin's safety, its low water solubility, rapid metabolism, and poor bioavailability have not yet led to approval as a clinically applicable drug, limiting its application. As a result, beneficial curcumin derivatives or analogues are now being developed to replace curcumin.[7] Among them, curcumin analog EF-24 shows potent antitumor activity and induces autophagy or apoptosis in various tumor cells.[8-10] However, the effect of EF-24 on myeloma cell proliferation is unknown.

Ferroptosis is an oxidative, iron-dependent form of regulated cell death (RCD) that differs from other types in its morphology, biochemistry, and core regulators, as first proposed by Scott Dixon in 2012.[11,12] Ferroptosis can be induced by inhibiting the cystine/glutamate transporter protein (SLC7A11/xCT) and the enzyme glutathione peroxidase 4 (GPX4), which are critical for preventing ferroptosis.[13] Studies have shown that ferroptosis is an adaptive response with tumor suppressive function.[14] The discovery of ferroptosis as a new mode of cell death has opened a new way to think about and treat many diseases.[15] In this study, the curcumin analogue EF-24 was first used to treat human multiple myeloma cells (MM.1S), and the current study demonstrated that EF-24 could inhibit cell proliferation and induce ferroptosis. Furthermore, the in vivo

antitumor effect of EF-24 was investigated in NOD/SCID mice grafted with MM.1S cells.

The present study provided additional information and laid a solid foundation for future research on the antitumor properties of curcuminoids.

Materials and Methods

Cell Culture and Chemicals

The human multiple myeloma cell line MM.1S was purchased from Sebachem (Shanghai Biotechnology Co. Ltd.) and cultured in RPMI-1640 medium containing 10% FBS at 37°C with 5% CO_2.

Cur analogue EF-24 (Sigma-Aldrich, Shanghai, China) was dissolved in dimethyl sulfoxide (DMSO) to prepare a 40 mM master stock solution, which was stored at -20°C before use. Ferrostatin-1 (abbreviated Fer-1, HY-100579), Z-VAD-FMK (HY-16658B), and wortmannin (HY-12420) were purchased from MedChemExpress (MCE, Shanghai, China). Anti-GPX4, SLC7A11, and α-tubulin primary antibodies were bought from ProteinTech (Wuhan, China). The IRDye® 800CW Goat anti-mouse IgG(H+L) and IRDye® 800CW Goat anti-rabbit IgG(H+L) secondary antibodies were provided by Li-Cor Biotechnology (Lincoln, NE, USA).

Cell Viability Assay

MM.1S cells were inoculated into 6-well plates (6×10^5/well) and incubated overnight after treating the cells with different concentrations of EF-24 (0, 200, 400, 600, 800, and 1000 nM) for different times. Morphological changes in treated cells were observed with an inverted microscope and photographed.

For cell viability analysis, MM.1S cells were inoculated into 96-well plates (1×10^4/well) overnight and treated with DMSO and a range of concentrations of EF-24 (0-1000 nM) for different times, respectively. Then, 10 μL of CCK-8 (Uelandy, Suzhou, China) was added to each well and incubated for another 4 h at 37 °C. Finally, cell absorbances were measured with a microplate spectrophotometer at 450 nm.

cDNA Extraction and RNA-Sequencing

MM.1S cells were treated with EF-24 (600 nM) for 24 h, then total RNA was extracted using TRIzol kit (Thermo Fisher, CA, USA). Transcriptome data were obtained using Illumina NovaseqTM 6000 (LC Bio Technology CO., Ltd., Hangzhou, China). GO function analysis, pathway function analysis, cluster analysis, and other in-depth mining analyses were performed on the selected differentially expressed genes. Quantitative analysis of three randomly selected cell death signal-related genes (*p62/SQSTM1, FTL*, and *GJA1*) was conducted using quantitative real-time PCR (qRT-PCR).

qRT-PCR

MM.1S cells were inoculated into 6-well plates and cultured overnight, and then treated with EF-24 at different concentrations for 24 h. The total RNA samples were extracted from the treated cells using a conventional protocol. The RNA samples were reverse transcribed into cDNA. RT-qPCR was performed using a SYBR Green real-time fluorescence quantitative PCR system. The following primer sequences were used for the PCR procedures:

p62/SQSTM1-F: TACGACTTGTGTAGCGTCTGC, *p62/SQSTM1*-R: GTGTCCGTGTTTCACCTTCC

FTL-F: CACGGACCCCCATCTCTGTG, *FTL*-R: TAGTCGTGCTTGAGAGTGAGC

GJA1-F: CCAGCACCGTTTTTGTGGTT, *GJA1*-R: GGTCGAAATAGAAGCCCAGAGA.

GAPDH (F: AATGACCCCTTCATTGAC, R: TCCACGACGTACTCAGCGC) was used as an internal control gene for mRNA quantification. The relative mRNA values for each group were calculated using the $2^{-\Delta\Delta}$Ct method.

Western Blot

The treated MM.1S cells were lysed in lysis buffer containing 2% SDS, 25 mM Tris-HCl (pH 6.8), 2 mM PMSF, 6% glycerol, 0.02% bromophenol blue, 1% β-mercaptoethanol, and protease inhibitors. Proteins were separated by SDS-PAGE, and the target proteins in the gel were transferred to a nitrocellulose membrane (NC), which was then incubated with a primary antibody at 4°C overnight. After washing with TBST, the membranes were incubated with the appropriate secondary antibody for 1 h at room temperature. Immunoblots were processed using an Odyssey CLX infrared imaging system (LI-COR Biosciences, Cambridge, UK), and the fluorescence intensity of the blot was analyzed using the Odyssey application.

MDA and GSH Assay

After MM.1S cells came to approximately 80% confluence in 6-well plates, the cells were exposed to EF-24 (2.5-20 μM) with Fer-1 (2 μM), or Z-VAD-FMK (5 μM), or wortmannin (5 μM) for 24 h, respectively. Total malondialdehyde in treated cells was determined using a malondialdehyde assay kit (Nanjing Jiancheng, China) and normalized to protein concentration according to the manufacturer's instructions. Similarly, for the detection of GSH in treated cells, the total amount of glutathione was determined using a glutathione assay kit (Beyotime Biotechnology, Shanghai, China) and normalized to protein concentration according to the manufacturer's instructions.

Transmission Electron Microscopy (TEM)

After treatment with EF-24 (600 nM) for 24 h, the cells were fixed with a 2% paraformaldehyde-2.5% glutaraldehyde fixation mixture. Next, the cells were dehydrated continuously with graded concentrations (30%, 50%, 70%, 80%, 90%, and 95%) of ethanol solution for 15 min. Anhydrous ethanol and acetone were then used to treat the cells for 20 min, respectively. After embedding, the cell samples were sectioned with a UC7 Ultrathin Section Ultrathin Slicer. Finally, the cells were stained with uranyl acetate and alkaline lead citrate, respectively. The samples were observed and photographed using a transmission electron microscope (JEOL-JEM-1200EX, Japan).

ROS and Fe^{2+} Fluorescence Assay

MM.1S cells were inoculated into 6-well plates (1×10^5/well) and cultured overnight. The cells were treated with EF-24

or EF-24 (5 μM) + Fer-1 (1 μM) for 24 h, respectively (Rousp-treated cells for 30 min were used as a positive control). After aspiration of the waste liquid, DCFH-DA probe (10 mM, diluted in serum-free culture medium at 1:1000) was added to the wells for 15 min at 37°C. The cells were then thoroughly washed with serum-free cell culture solution and resuspended in PBS. ROS levels in different samples were measured using flow cytometry (BD FACSCanto™ II, USA).

As for the detection of Fe^{2+} concentrations in cells treated with the above-described methods, the cell supernatant was discarded, and the cells were washed three times with PBS. Finally, FerroOrange working solution (1 μM) was added into the wells, and the cell plates were visualized using a fluorescence microscope (ZEISS AxioObserver 3, Germany).

Hematoxylin-Eosin (HE) Staining

SPF-grade female NOD/SCID mice (Beijing Viton Lever, n=6, 4-6 weeks old, weight 20~25 g) were purchased and fed in a SPF-grade sterile laminar flow animal rearing system. The density of MM.1S was adjusted to 7×10^7 cells/mL, and each mouse was inoculated with 150 μL subcutaneously on the dorsal surface of the left hind limb. The modeled mice were injected with saline and EF-24 (200 μL/per mouse, 20 mg/kg) into the tail vein every 3 days, according to standard procedures. After 7 injections, the treated mice were sacrificed for histochemical analysis. Then, the heart, liver, spleen, lung, kidney, and tumor tissues of the mice were dissected for ultrathin sectioning. The tissue sections were stained with HE and photographed under a microscope.

Statistical Analysis

The significance of differences between groups was tested using t-test. GraphPad Prism 7.0c software was used for statistical analysis. A *P*-value <0.05 was considered statistically significant.

Results

EF-24 Inhibits MM.1S Cell Proliferation

Inverted microscopy revealed that the morphology of the EF-24-treated cells in the experimental group underwent significant changes, including fragmentation, shrinkage, and death, whereas the control group showed normal cell growth (Figure 1A). As the concentration increases, the damage to the treated cells gradually intensifies. In addition, we examined the effect of EF-24 on MM.1S cell proliferation using the CCK-8 assay (Figure 1B). The results showed that higher concentrations and longer treatment times were associated with greater decreases in cell viability, suggesting that EF-24 inhibits MM.1S cell proliferation in a time- and concentration-dependent manner.

EF-24 Induces the Expression of Ferroptosis-related Genes Differently in MM.1S Cells

To explore the potential antitumor mechanism of EF-24 against MM.1S, we first used transcriptomic analysis to identify differentially expressed genes in EF-24-treated MM. 1S cells. Three replicate samples from the EF-24-treated groups or the blank control groups were collected for RNA-seq analysis. The present results showed that 292 genes were upregulated and 539 were downregulated. Heat map and volcano plot analyses showed that among the upregulated genes, *GJA1*, *FTL*, and *p62/SQSTM1* were the most differentially expressed (Figure 2A).

Therefore, qRT-PCR was performed to identify transcriptional changes in the three genes in EF-24-treated MM.1S cells. Current results confirmed that *GJA1*, *FTL*, and *p62/SQSTM1* mRNA levels were elevated compared with the blank control group (Figure 2B), consistent with transcriptome sequencing analysis. Given that genes such as *GJA1* and *FTL* are involved in ferroptosis, we speculated that differential expression of ferroptosis-related genes in MM.1S cells may be associated with EF-24 treatment.

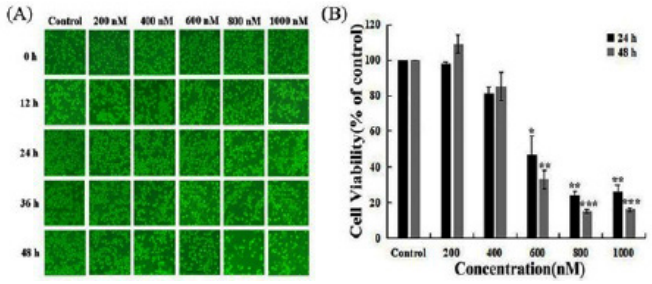

Fig. 1. *Effect of EF-24 on the proliferation of MM.1S cells. (A) Morphological changes of MM.1S cells after treatment with different concentrations of EF-24 for different times (original magnification, ×100). (B) Cell viability analysis of MM.1S cells treated with different concentrations of EF-24 for 24 and 48 h (n=3; *-P<0.05, **-P<0.01, and ***-P<0.001).*

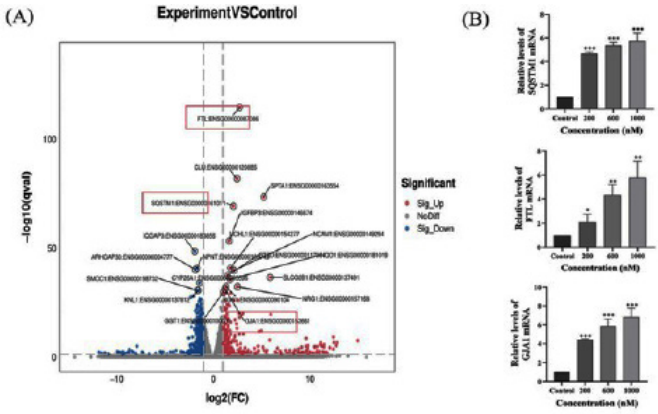

Fig.2. *Transcriptomic analysis of cell-death-related genes in EF-24-treated MM.1S cells. (A) Volcano map analysis of transcriptome sequencing differential gene clustering after EF-24 treatment of MM.1S cells. Several cell death-related genes were outlined in red. (B) RT-qPCR analysis of FTL, GJA1, and p62/SQSTM1 mRNA after 24 h of treatment with different concentrations of EF-24 (n=3; **- P<0.01 and *** - P<0.001).*

EF-24 Induces Ferroptosis in MM.1S Cells

When ferroptosis occurs, several changes occur within the cell, including the accumulation of MDA, ROS, and Fe^{2+}, depletion of GSH, and changes in mitochondrial morphology. Here, we firstly treated MM.1S cells with various concentrations of EF-24 and assessed changes in cellular MDA and GSH levels. Relative to the untreated cells, the experimental group

exhibited increased MDA levels and decreased GSH levels with a concentration-dependent effect (from 200 nM to 1000 nM) (Figure 3A; 3B), respectively. Subsequently, following treatment with EF-24 (600 nM), fluorescence microscopy analysis showed stronger orange-red fluorescence in the experimental group compared to the control (Figure 3C), suggesting elevated Fe^{2+} levels in the experimental group. Moreover, flow cytometry analysis was applied to detect the production of ROS in EF-24-treated MM.1S cells, which showed that the ROS level had an increasing trend in a concentration-dependent manner (from 200 nM to 1000 nM of EF-24) (Figure 3D). Additionally, transmission electron microscopy of MM.1S cells treated with EF-24 (600 nM) showed that mitochondrial volume and cristae decreased or disappeared. At the same time, there were no apparent changes in the control group (Figure 3E). In summary, these results suggested that EF-24 indeed induced ferroptosis in MM.1S cells.

Furthermore, we continued to detect the expression of two key regulatory factors of ferroptosis, GPX4 and SLC7A11, which are considered upstream regulators of ferroptosis. The present study indicated that, after EF-24 treatment, the expressions of GPX4 and SLC7A11 were downregulated overall (Figure 3F), further supporting EF-24-induced ferroptosis.

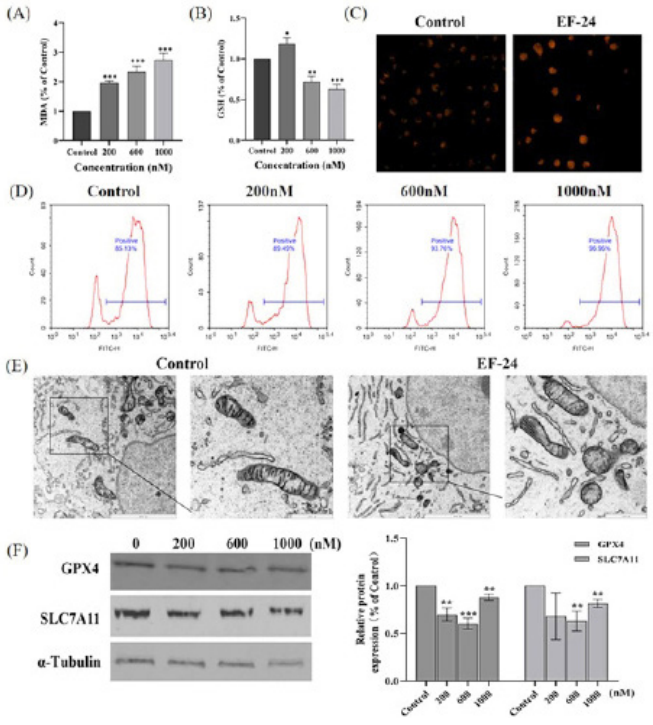

Fig.3. *EF-24 induces ferroptosis in MM.1S cells. (A) and (B) Changes of MDA and GSH content in cells treated with different concentrations of EF-24 for 24 h, respectively. (C) Cells were treated with EF-24 (600 nM) for 24 h. The Fe^{2+} concentrations (yellow color) were observed by fluorescence microscopy. (D) Cells were treated with different concentrations of EF-24 for 24 h, and ROS levels were detected using flow cytometry. (E) Cells were treated with EF-24 (600 nM) for 24 h, and the changes in mitochondria were observed by transmission electron microscopy. (F) Western blot analysis (Left) and statistical analysis (Right) of GPX4 and SLC7A11 after treatment with different concentrations of EF-24 for 24 h. Bars represent densitometric analysis of the ratio of GPX4 or SLC7A11 to GAPDH expression levels. (n=3; *-P<0.05, **-P<0.01, and ***- P<0.001).*

Addition of Inhibitors Suppresses Ferroptosis in MM.1S Cells

To further confirm ferroptosis induced by EF-24 in MM.1S cells, after combination treatment with EF-24 (600 nM) and the ferroptosis inhibitor ferrostatin-1 (2 μM), we found that MDA levels were reduced, while GSH levels were significantly increased compared to the EF-24-alone treatment group. However, the MDA levels in the groups treated with the combination of EF-24 and either the autophagy inhibitor wortmannin (5 μM) or the apoptosis inhibitor Z-VAD-FMK (5 μM) remained essentially unchanged or even slightly increased, while GSH levels remained essentially unchanged or even decreased (Figure 4A; 4B). Additionally, the number of intracellular orange-red fluorescence signals was significantly reduced in the combination treatment group with ferrostatin-1 (Figure 4C), indicating that the addition of ferrostatin-1 led to a significant decrease in cellular Fe^{2+} levels in EF-24-treated MM.1S cells. Moreover, flow cytometry analysis showed that the ROS level in the combination treatment group was significantly lower than in the EF-24-alone treatment group. These results further confirmed that EF-24 induced ferroptosis in MM.1S cells.

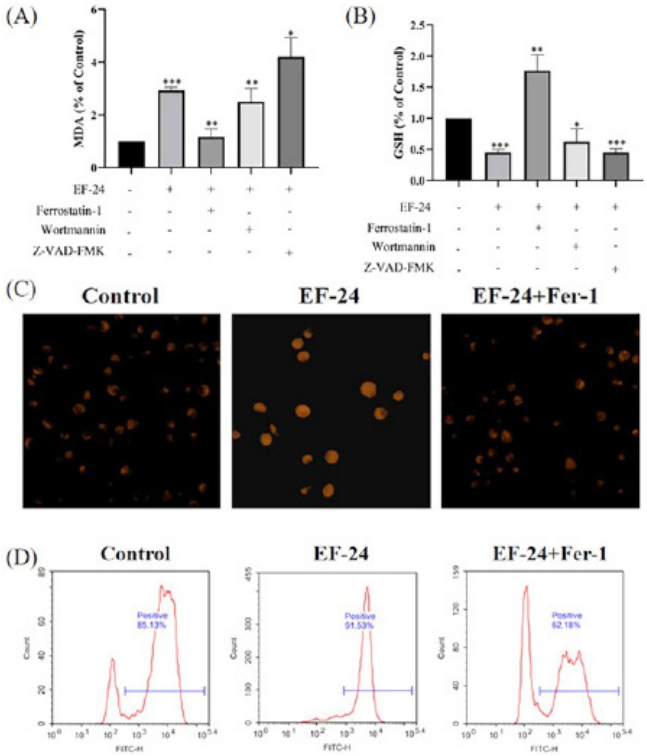

Fig. 4. *Ferrostatin-1 (Fer-1) inhibits EF-24-inducing ferroptosis in MM.1S cells. Expression of MDA (A) and GSH (B) in cells treated with EF-24 (600 nM), and EF-24 (600 nM) in combination with Ferrostatin-1 (2 μM), Z-VAD-FMK (5 μM), or Wortmannin (5 μM) for 24 h, respectively. (C) Fluorescence microscopy for Fe^{2+} content after co-treatment of cells with EF-24 (600 nM) or EF-24 (600 nM) with Fer-1 (2 μM), respectively. (D) ROS expression was detected by flow cytometry after cells were co-treated with EF-24 (600 nM) or EF-24 (600 nM) with Fer-1 (2 μM), respectively (n=3; *-P<0.05, **-P<0.01, and ***-P<0.001).*

EF-24 Can Resist Tumor Progress *in vivo*

To further determine the in vivo antitumor proliferation ability of EF-24, NOD/SCID mouse models grafted with

MM.1S cells were constructed, and EF-24 was administered to treat the mice. After 15 days of treatment, the overall tumor inhibition rate reached 47.25% in EF-24-injected mice, with tumor volumes and sizes significantly reduced compared to control mice. The current study suggested that EF-24 could block tumor progression in vivo.

In addition, tumor tissue from mice and normal organ tissue were collected for HE staining analysis. The results showed that normal heart, liver, spleen, lung, and kidney tissue from mice treated with EF-24 retained a relatively compact structure and had fewer cavities compared to the control groups (Figure 5). Tumor tissue from mice treated with EF-24 was significantly damaged by EF-24 and had more cavities per section (Figure 5). These results clearly demonstrated the ability of EF-24 to suppress tumor cell proliferation in vivo.

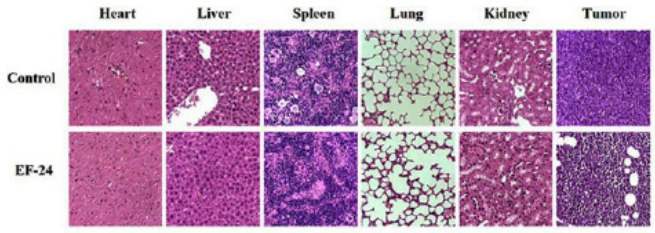

Fig.5. *HE-staining analysis of tissues from NOD/SCID mouse models grafted with MM.1S cells. EF-24 treatment could effectively protect normal organs while damaging tumor tissues in mice.*

Discussion

Although significant progress has been made over the past two decades in the study of the physiopathological mechanisms underlying myeloma,[16] myeloma remains a hitherto incurable plasma cell malignancy. Developing more antimyeloma strategies or drug molecules has become an urgent task.

In our previous study, we confirmed the anti-proliferative and anti-migratory activities of the curcumin analogue EF-24 against breast cancer cells.[17,18] Even recently, we have discovered that EF-24 has antiviral effects on rhabdovirus replication.[19] In fact, compared with curcumin, EF-24 exhibited better bioavailability and antitumor activity. Several studies have demonstrated that EF-24 can inhibit cancer development through various pathways, including inhibition of the NF-κB and p38 pathways and regulation of ROS production.[20,21] However, its role in myeloma remains unexplored. Therefore, this study aimed to investigate the mechanism of EF-24 against myeloma cell proliferation.

The current study confirmed that EF-24 had the ability to inhibit the proliferation of human multiple myeloma cells, MM.1S. Transcriptomic sequencing and subsequent qRT-PCR analysis suggested that ferroptosis-related genes were regulated following EF-24 treatment in MM.1S cells. As a type of cell death caused by lipid peroxidation, ferroptosis plays an important role in tumor suppression and can provide new ideas and methods for cancer treatment.[22] When ferroptosis occurs, a series of physiological and biochemical changes occurs within the cell.[23] Therefore, experiments were performed to verify cell ferroptosis in EF-24-treated MM.1S cells by fluorescence microscopy, transmission electron microscopy, and flow cytometry. By promoting Fe^{2+} and ROS accumulation, increasing MDA levels, suppressing GSH, and reducing mitochondrial cristae, EF-24 triggers ferroptosis in MM.1S cells. GPX4 and SLC7A11, key regulators of ferroptosis, were also assessed by western blot, which showed downregulation of their expression in EF-24-treated MM. 1S cells, further confirming EF-24-Induced ferroptosis in MM.1S cells.

In fact, for multiple myeloma (MM), some potential antitumor molecules or extracts had been developed and characterized in previous reports. Zhong et al.[24] found that fingolimod (FTY720), a novel immunosuppressant, could induce ferroptosis and autophagy via the PP2A/AMPK pathway in myeloma cell lines U266 and RPMI8266, providing a new perspective on the MM treatment. Recently, Li et al.[25] also identified several molecules or compounds that can significantly induce ferroptosis in MM cells, including ethanol extract of Eclipta prostrata, andrographolide,[26] and shikonin.[27] Liang et al.[28] also found that the antimalarial drug artesunate (ART) could inhibit nuclear localization of SREBP2, downregulate IPP and GPX4, and eventually trigger ferroptosis in myeloma cells. All these compounds could be considered as potential drug candidates against myeloma. Our present study on the mediation of ferroptosis in MM.1S by EF-24 may identify a new candidate molecule for antimyeloma therapy.

We should note that although some compounds that sensitize myeloma cells to ferroptosis have been screened and are appealing alternative treatment strategies for multiple myeloma and other malignancies, only a limited number of ferroptosis regulators or factors have been identified.[29] Further research should aim to elucidate the detailed mechanism of interaction between ferroptosis and myeloma-targeting drugs. Our current study certainly opens new possibilities for myeloma treatment and potential clinical applications.

Funding Statement

This research was supported by the Natural Science Foundation of Henan (232300420018) and the High-level talents Fund from Henan University of Technology (2023BS001).

Competing Interests

The authors declare that they have no financial/commercial conflicts of interest concerning this article.

References

1. Kyle RA, Rajkumar SV. Multiple myeloma. Blood. 2008 Mar 15;111(6):2962-72. doi: 10.1182/blood-2007-10-078022.
2. Joshua DE, Bryant C, Dix C, Gibson J, Ho J. Biology and therapy of multiple myeloma. Med J Aust. 2019 May;210(8):375-380. doi: 10.5694/mja2.50129.
3. Pawlyn C, Davies FE. Toward personalized treatment in multiple myeloma based on molecular characteristics.

Blood. 2019 Feb 14;133(7):660-675. doi: 10.1182/blood-2018-09-825331.
4. Moreau P, Attal M, Facon T. Frontline therapy of multiple myeloma. Blood. 2015 May 14;125(20):3076-84. doi: 10.1182/blood-2014-09-568915.
5. Yavarpour-Bali H, Ghasemi-Kasman M, Pirzadeh M. Curcumin-loaded nanoparticles: a novel therapeutic strategy in treatment of central nervous system disorders. Int J Nanomedicine. 2019 Jun 17;14:4449-4460. doi: 10.2147/IJN.S208332.
6. Anand P, Kunnumakkara AB, Newman RA, Aggarwal BB. Bioavailability of curcumin: problems and promises. Mol Pharm. 2007 Nov-Dec;4(6):807-18. doi: 10.1021/mp700113r.
7. Tomeh MA, Hadianamrei R, Zhao X. A Review of Curcumin and Its Derivatives as Anticancer Agents. Int J Mol Sci. 2019 Feb 27;20(5):1033. doi: 10.3390/ijms20051033.
8. Hsiao PC, Chang JH, Lee WJ, Ku CC, Tsai MY, Yang SF, Chien MH. The Curcumin Analogue, EF-24, Triggers p38 MAPK-Mediated Apoptotic Cell Death via Inducing PP2A-Modulated ERK Deactivation in Human Acute Myeloid Leukemia Cells. Cancers (Basel). 2020 Aug 4;12(8):2163. doi: 10.3390/cancers12082163.
9. Skoupa N, Dolezel P, Ruzickova E, Mlejnek P. Apoptosis Induced by the Curcumin Analogue EF-24 Is Neither Mediated by Oxidative Stress-Related Mechanisms nor Affected by Expression of Main Drug Transporters ABCB1 and ABCG2 in Human Leukemia Cells. Int J Mol Sci. 2017 Oct 31;18(11):2289. doi: 10.3390/ijms18112289.
10. Shi YY, Zhou GZ, Li AF, Zhou YH. Review on the cellular anti-proliferation research development of curcumin analogs. Biotechnology. 2017; **27**, 192-197.
11. Li J, Cao F, Yin HL, Huang ZJ, Lin ZT, Mao N, Sun B, Wang G. Ferroptosis: past, present and future. Cell Death Dis. 2020 Feb 3;11(2):88. doi: 10.1038/s41419-020-2298-2.
12. Tang D, Chen X, Kang R, Kroemer G. Ferroptosis: molecular mechanisms and health implications. Cell Res. 2021 Feb;31(2):107-125. doi: 10.1038/s41422-020-00441-1.
13. Lei ZY, Li ZH, Lin DN, Cao J, Chen JF, Meng SB, et al. Med1 inhibits ferroptosis and alleviates liver injury in acute liver failure via Nrf2 activation. Cell Biosci. 2024 Apr 27;14(1):54. doi: 10.1186/s13578-024-01234-4.
14. Guo L, Wang Z, Fu Y, Wu S, Zhu Y, Yuan J, Liu Y. MiR-122-5p regulates erastin-induced ferroptosis via CS in nasopharyngeal carcinoma. Sci Rep. 2024 May 1;14(1):10019. doi: 10.1038/s41598-024-59080-w.
15. Lai L, Tan M, Hu M, Yue X, Tao L, Zhai Y, Li Y. Important molecular mechanisms in ferroptosis. Mol Cell Biochem. 2025 Feb;480(2):639-658. doi: 10.1007/s11010-024-05009-w.
16. Bazou D, Dowling P. Editorial: Multiple Myeloma: Molecular Mechanism and Targeted Therapy. Int J Mol Sci. 2024 Mar 28;25(7):3799. doi: 10.3390/ijms25073799.
17. Li J, Wang SH, Liu YT, Zhang Q, Zhou GZ. Inhibition of autophagic flux by the curcumin analog EF-24 and its antiproliferative effect on MCF-7 cancer cells. J Biochem Mol Toxicol. 2023 Apr;37(4):e23307. doi: 10.1002/jbt.23307.
18. Zhao YY, Li J, Wang HQ, Zheng HB, Ma SW, Zhou GZ. Activation of autophagy promotes the inhibitory effect of curcumin analog EF-24 against MDA-MB-231 cancer cells. J Biochem Mol Toxicol. 2024 Feb;38(2):e23642..
19. Ju PM, Ma SW, Li YY, Zhang SF, Li J, Zhou GZ. Investigation of the antiviral mechanism of curcumin analog EF-24 against *Siniperca cachuatsi* rhabdovirus. Fishes. 2024; 9, 179.
20. Lee CY, Ho YC, Lin CW, Hsin MC, Wang PH, Tang YC, Yang SF, Hsiao YH. EF-24 inhibits TPA-induced cellular migration and MMP-9 expression through the p38 signaling pathway in cervical cancer cells. Environ Toxicol. 2023 Feb;38(2):451-459. doi: 10.1002/tox.23709.
21. Su SC, Hsin CH, Lu YT, Chuang CY, Ho YT, Yeh FL, Yang SF, Lin CW. EF-24, a Curcumin Analog, Inhibits Cancer Cell Invasion in Human Nasopharyngeal Carcinoma through Transcriptional Suppression of Matrix Metalloproteinase-9 Gene Expression. Cancers (Basel). 2023 Mar 1;15(5):1552. doi: 10.3390/cancers15051552.
22. Shao L, Zhu L, Su R, Yang C, Gao X, Xu Y, Wang H, Guo C, Li H. Baicalin enhances the chemotherapy sensitivity of oxaliplatin-resistant gastric cancer cells by activating p53-mediated ferroptosis. Sci Rep. 2024 May 10;14(1):10745. doi: 10.1038/s41598-024-60920-y.
23. Zhang W, Li Q, Zhang Y, Wang Z, Yuan S, Zhang X, Zhao M, Zhuang W, Li B. Multiple myeloma with high expression of SLC7A11 is sensitive to erastin-induced ferroptosis. Apoptosis. 2024 Apr;29(3-4):412-423. doi: 10.1007/s10495-023-01909-2.
24. Zhong Y, Tian F, Ma H, Wang H, Yang W, Liu Z, Liao A. FTY720 induces ferroptosis and autophagy via PP2A/AMPK pathway in multiple myeloma cells. Life Sci. 2020 Nov 1;260:118077. doi: 10.1016/j.lfs.2020.118077.
25. Li W, Yin X, Fu H, Liu J, Weng Z, Mao Q, Zhu L, Fang L, Zhang Z, Ding B, Tong H. Ethanol extract of Eclipta prostrata induces multiple myeloma ferroptosis via Keap1/Nrf2/HO-1 axis. Phytomedicine. 2024 Jun;128:155401. doi: 10.1016/j.phymed.2024.155401.
26. Li W, Fu H, Fang L, Chai H, Ding B, Qian S. Andrographolide induced ferroptosis in multiple myeloma cells by regulating the P38/Nrf2/HO-1 pathway. Arch Biochem Biophys. 2023 Jul 1;742:109622. doi: 10.1016/j.abb.2023.109622.
27. Li W, Fu H, Fang L, Chai H, Gao T, Chen Z, Qian S. Shikonin induces ferroptosis in multiple myeloma *via* GOT1-mediated ferritinophagy. Front Oncol. 2022 Oct 25;12:1025067. doi: 10.3389/fonc.2022.1025067.
28. Liang D, Minikes AM, Jiang X. Ferroptosis at the intersection of lipid metabolism and cellular signaling. Mol Cell. 2022 Jun 16;82(12):2215-2227. doi: 10.1016/j.molcel.2022.03.022.
29. Logie E, Van Puyvelde B, Cuypers B, Schepers A, Berghmans H, Verdonck J, Laukens K, Godderis L, Dhaenens M, Deforce D, Vanden Berghe W. Ferroptosis Induction in Multiple Myeloma Cells Triggers DNA Methylation and Histone Modification Changes Associated with Cellular Senescence. Int J Mol Sci. 2021 Nov 12;22(22):12234. doi: 10.3390/ijms222212234.

***Corresponding author**: Guang-Zhou Zhou, E-mail: gzzhou@163.com*

International Journal of Biomedicine 15(4) (2025) 752-755
http://dx.doi.org/10.21103/Article15(4)_OA18

ORIGINAL ARTICLE

Experimental Biology

INTERNATIONAL JOURNAL OF BIOMEDICINE

NLRP3 Inflammasome Activation in Endothelial Cells and the Potential Modulatory Role of Riociguat in the Nitric Oxide Pathway

Nita Kutllovci[1], Alajdin Salihu[2], Burim Neziri[1,2*]

[1]*Faculty of Medicine, University of Prishtina, Prishtina, Kosovo*
[2]*Institute of Pathophysiology, University Clinical Centre of Kosovo, Prishtina, Kosovo*

Abstract

Background: The NOD-like receptor protein 3 (NLRP3) inflammasome is a cytoplasmic protein complex activated by damage-associated molecular patterns (DAMPs) and pathogen-associated molecular patterns (PAMPs), resulting in the release of pro-inflammatory cytokines such as IL-1β and IL-18. In this pathway, the activation of NF-κB plays a key role. Many studies have demonstrated the significant role of IL-1β in activating NF-κB. The aim of this study: We hypothesized that the activation of the nitric oxide (NO)- (sGC)-(cGMP)-PKG through the vasodilator-stimulated phosphoprotein (VASP) pathway may lead to anti-inflammatory effects through (NFκB)-NLRP3 inhibition on endothelial cells.

Methods and Results: This experimental research was conducted using human pulmonary artery endothelial cells (HPAEC). The growth and monitoring of cell cultures were done according to strict guidelines and protocols. In our study, we added TNFα (10 mg/mL) to activate the inflammasome. Ten minutes later, riociguat (RCG) was added at six different concentrations (50 μM, 10 μM, 5 μM, 1 μM, 0.5 μM, and 0.1 μM) to activate the NO pathway, followed by 15 mM of ATP. Incubation is continued at different times (60, 90, and 120 minutes). The measurement of caspase-1 activity was performed using a luminescence assay. Our results have once again demonstrated the successful activation of the inflammasome by TNFα. We suggest that the highest concentration of RCG, 50 μM, in our study was insufficient to trigger the NO pathway; additionally, more complex molecular pathways may be involved, and further investigations are warranted to clarify the underlying complex mechanism.(**International Journal of Biomedicine. 2025;15(4):752-755.**)

Keywords: NLRP3 inflammasome • endothelial cells • nitric oxide • riociguat

For citation: Kutllovci N, Salihu A, Neziri B. NLRP3 Inflammasome Activation in Endothelial Cells and the Potential Modulatory Role of Riociguat in the Nitric Oxide Pathway. International Journal of Biomedicine. 2025;15(4):752-755. doi:10.21103/Article15(4)_OA18

Abbreviations

DAMPs, damage-associated molecular patterns; **HPAEC**, human pulmonary artery endothelial cells; **IL**, interleukin; **NLRP3,** NOD-like receptor protein 3; **NF-κB**, nuclear factor-κB; **PAMPs**, and pathogen-associated molecular patterns; **RCG**, riociguat; **VASP**, the vasodilator-stimulated phosphoprotein.

Introduction

The NOD-like receptor protein 3 (NLRP3) inflammasome is a large and complex cytoplasmic protein that is activated when cells are exposed to pathogens or in response to cellular damage. The activation of caspase-1, a proteolytic enzyme, leads to the release of pro-inflammatory cytokines such as IL-1β and IL-18, thereby playing a crucial role in inflammation and tissue damage (Figure 1). Extended activation of the NLRP3 inflammasome may contribute to the development of chronic inflammatory diseases, including preeclampsia. [1-6]

Within this scope, extensive research has been conducted on the significant levels of IL-1β in the activation of nuclear factor-κB (NF-κB), as observed in the pathogenesis of essential hypertension, pulmonary hypertension, gestational

***Corresponding author**: Burim Neziri, MD, PhD. Institute of Pathophysiology, University Clinical Centre of Kosovo, Prishtina, Kosovo E-mail: burim.neziri@uni-pr.edu*

hypertension, and preeclampsia. These studies have highlighted the important role of NF-κB in the inflammatory response and thrombosis.[7-9]

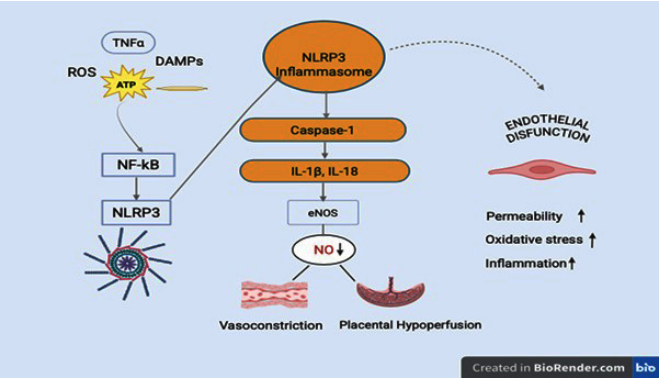

Fig. 1. *NLRP3 inflammasome role in the pathogenesis of inflammation and vasoconstriction*

Despite numerous publications suggesting that cyclic guanosine monophosphate (cGMP) inhibits NF-κB activation, the entire complex pathway, including the dynamics underlying this mechanism, remains incompletely understood.

The NO–(cGMP)–(PDE-5) pathway is investigated in nearly all physiological, inflammatory, and neoplastic pathways. This molecular pathway is highly complex, and clarifying the role of any of its components would be greatly appreciated. This was further explained by recent publications, which have linked the phosphorylation of VASP (vasodilator-stimulated phosphoprotein) by cGMP-activated protein kinase G (PKG) to the NLRP3 inflammasome in hepatic cells.[10] In this study, a connection between VASP phosphorylation status and NLRP3 activation, as well as the release of IL-β1 and IL-18, has been investigated. Since the role (cGMP) is now explained above, the role of its stimulants on the relaxation of smooth muscle cells in blood vessels is crucial (Figure 2). Therefore, we used riociguat (RCG), which directly stimulates soluble guanylyl cyclase (sGC), increasing so cGMP. This is particularly beneficial in cases where NO levels are decreased, such as in preeclampsia.[11,12]

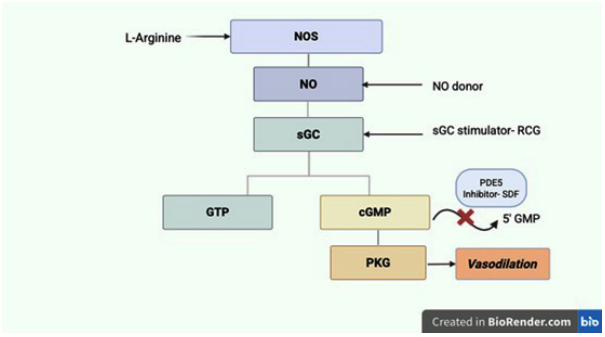

Fig. 2. *The cGMP-dependent pathway, initiated by nitric oxide (NO), is involved in vasodilation.*

Our study aimed to investigate the potential modulatory effects of RCG on endothelial cells through the NO pathway and cellular response via sGC stimulation. A possible molecular diagram describing the relationship between NO pathway activation and NLRP3 inflammasome activation was also reviewed to predict potential modulatory effects of new drugs.

Methods

This experimental research was conducted using human pulmonary artery endothelial cells (HPAEC), which were thawed in a water bath. The special media were prepared with supplements, including fetal calf serum (0.02 ml/ml), growth supplement for endothelial cells (0.004 ml/ml), epidermal growth factor (recombinant), fibroblast growth factor (recombinant), heparin, and hydrocortisone, as well as antibiotics (penicillin & streptomycin). Cells were seeded and incubated at 37°C with a carbon dioxide concentration of 5%. Medium changes were performed 24 hours after incubation and then every 2-3 days. After being confluent, about 70-90%, cells were detached with Trypsin/EDTA and centrifuged for 5 min at 1500. A laminin coating was performed using laminin at a concentration of 1mg/mL and incubated for 2 hours. Cells were cultured in 96-well plate culture and 6-well plate boxes, incubation followed. Cell treatment is as follows: initially, TNFα (10 µg/mL) is added, followed after 10 minutes by the addition of RCG in six concentrations (50 µM; 10 µM; 5 µM; 1 µM; 0.5 µM; 0.1 µM) and incubated for 12h at 37 °C with 5% CO_2. Then, 15 mM of ATP is added, and the incubation is continued for 2 hours. Caspase-1 activity measurement is done via Caspase-Glo® Inflammasome Assay. Statistical analysis was performed using an ANOVA test followed by Tukey post hoc tests. The probability value of $P<0.05$ was considered statistically significant.

Results and Discussion

After seeding and incubating the endothelial cells and treating them with ATP (15 µM), TNFα (10 µg/mL), and RCG at six different concentrations, we measured caspase-1 activity at 60, 90, and 120 minutes. These measurements reflect the results of NLRP3 inflammasome activation. We analyzed only the caspase-1 activity under the highest concentration of RCG, 50 µM, for further analysis (Figure 3).

The Tukey post-hoc analysis (Table 1) above shows that administering RCG at its maximum concentration of 50 µM, with or without TNFα, results in a significant increase of inflammasome activity when compared to the control. The anti-inflammatory properties of RCG become evident only when administered at very high concentrations, as previously demonstrated and confirmed.[13] The experiment did not reveal any significant difference between control cells and cells treated with TNFα alone. The experimental results indicate that TNFα produces only a minor inflammatory response during this study.

The data presented in Figure 3 and Table 1 show that a sustained increase in caspase-1 activity becomes evident after prolonged incubation, particularly when measured after 120 minutes. The continuous increase suggests that

the inflammasome remains activated. The rising pattern throughout the observed period could indicate that RCG requires an extended incubation time for complete NLRP3 inflammasome inhibition, possibly because the activation of the nitric oxide (NO) signaling pathway occurs later.

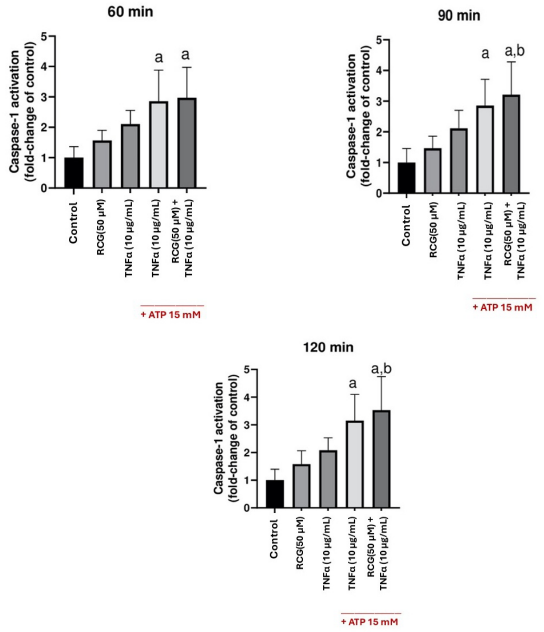

Fig. 3. *Caspase-1 activity at 60, 90, and 120 minutes after treating with ATP, TNFα, and RCG (50 µM).*
a - different from control; b - different from RCG.

Table 1.

The Tukey post-hoc analysis of the highest concentration of RCG (50 µM) effects with 120 min incubation on inflammasome activity.

Tukey's multiple comparisons test	Mean Diff.	95% CI of Diff.	Below threshold	*P*-value
Control vs. RCG (50 µM)	-0.58	-2.45 to 1.29	No	0.8804
Control vs. TNFα (10 µg/mL)	-1.08	-2.95 to 0.79	No	0.4369
Control vs. TNFα (10 µg/mL) + ATP (15 mM)	-2.15	-4.02 to -0.28	Yes	0.0196
Control vs. RCG 50 (µM) + TNFα (10 µg/mL) + ATP (15 mM)	-2.53	-4.15 to -0.91	Yes	0.0013
RCG (50 µM) vs. TNFα (10 µg/mL)	-0.50	-2.37 to 1.37	No	0.9265
RCG (50 µM) vs. TNFα (10 µg/mL) + ATP (15 mM)	-1.57	-3.44 to 0.30	No	0.1266
RCG ((50 µM) vs.RCG 50 µM + TNFα (10 µg/mL)	-1.95	-3.57 to -0.33	Yes	0.0139
TNFα (10 µg/mL) vs. TNFα (10 µg/mL)+ ATP (15 mM)	-1.07	-2.94 to 0.80	No	0.4450
TNFα (10 µg/mL) vs. RCG (50 µM) + TNFα (10 µg/mL) +ATP (15 mM)	-1.45	-3.07 to 0.17	No	0.0928
Control vs. RCG (50 µM)	-0.37	-2.00 to 1.24	No	0.9531

In our experiment, TNFα (10 µg/mL) and ATP (15 mM) induced inflammasome activation, leading to the activation of caspase-1, as shown in Figure 3 at different time frames (60, 90, and 120 min). According to the literature, activation of the NLRP3 inflammasome leads to the conversion of pro-IL-1β into its active form by caspase-1.[14-17] Our results support the successful activation of the NLRP3 inflammasome by TNFα and ATP, as demonstrated in other publications.[18-20]

The results obtained under our experimental conditions have shown that treatment of cells with low concentrations of RCG, at varying concentrations, and also considering only the highest concentration of 50 µM, resulted in a modest activation, but not a statistically significant inhibition of the NLRP3 inflammasome. This suggests that the potential modulatory effect of RCG as a possible inhibitor of NLRP3 Activation in endothelial cells is not sufficient under these conditions. Higher RCG concentrations and a more extended incubation period are suggested. Almost similar to those in literature, which show that the NO-cGMP-PDE5 pathway should be further explained, and other related complex vascular mechanisms should be taken into consideration regarding NLRP3 inflammasome inhibition.[21,22]

Conclusions

Data from the literature imply that TNFα, induced by DAMPs or PAMPs, contributes to the priming and activation of the NLRP3 inflammasome, ultimately leading to the conversion of pro-IL-1β into its active state via caspase-1.

Our findings are consistent with those observations, adding strength to the intense pro-inflammatory activity of TNFα for inflammasome activation. The NO–sGC–cGMP–PKG–VASP pathway exhibits anti-inflammatory effects and interferes with the inflammatory pathways, including NF-κB, NLRP3, IL-1β, and IL-18.

In our experiment, however, the maximum dose of RCG (50 µM) appeared insufficient to stimulate this anti-inflammatory pathway most effectively. The decreased or slowed phosphorylation of VASP under these conditions suggests that higher doses or longer incubation times may be necessary to suppress inflammasome activation via the NO signal pathway. Considering these molecular pathways are very complex, further assays targeting them are warranted to clarify the underlying complex mechanism.

Due to their vasodilatory effects, RCG can be used in the research of many diseases and disorders. Despite the numerous potential benefits, significant fetal risks and side effects significantly limit its use.

Conflicts of Interest

The author declares that there are no conflicts of interest regarding the publication of this paper.

Informed Consent Statement

Not applicable.

References

1. Scott TE, Kemp-Harper BK, Hobbs AJ. Inflammasomes: a novel therapeutic target in pulmonary hypertension? Br

J Pharmacol. 2019 Jun;176(12):1880-1896. doi: 10.1111/bph.14375. Epub 2018 Jun 27. PMID: 29847700; PMCID: PMC6534811.
2. Latz E, Xiao TS, Stutz A. Activation and regulation of the inflammasomes. Nat Rev Immunol. 2013 Jun;13(6):397-411. doi: 10.1038/nri3452. PMID: 23702978; PMCID: PMC3807999.
3. Swanson KV, Deng M, Ting JP. The NLRP3 inflammasome: molecular activation and regulation to therapeutics. Nat Rev Immunol. 2019 Aug;19(8):477-489. doi: 10.1038/s41577-019-0165-0. PMID: 31036962; PMCID: PMC7807242.
4. Zhou F, Li C, Zhang SY. NLRP3 inflammasome: a new therapeutic target for high-risk reproductive disorders? Chin Med J (Engl). 2020 Nov 4;134(1):20-27. doi: 10.1097/CM9.0000000000001214. PMID: 33395071; PMCID: PMC7862815.
5. Shirasuna K, Karasawa T, Takahashi M. Role of the NLRP3 Inflammasome in Preeclampsia. Front Endocrinol (Lausanne). 2020 Feb 25;11:80. doi: 10.3389/fendo.2020.00080. PMID: 32161574; PMCID: PMC7053284.
6. Pasqua T, Pagliaro P, Rocca C, Angelone T, Penna C. Role of NLRP-3 Inflammasome in Hypertension: A Potential Therapeutic Target. Curr Pharm Biotechnol. 2018;19(9):708-714. doi: 10.2174/1389201019666180808162011.
7. Lawrence T. The nuclear factor NF-kappaB pathway in inflammation. Cold Spring Harb Perspect Biol. 2009 Dec;1(6):a001651. doi: 10.1101/cshperspect.a001651. Epub 2009 Oct 7. PMID: 20457564; PMCID: PMC2882124.
8. Vaughan JE, Walsh SW. Activation of NF-κB in placentas of women with preeclampsia. Hypertens Pregnancy. 2012;31(2):243-51. doi: 10.3109/10641955.2011.642436. Epub 2012 Mar 1. PMID: 22380486; PMCID: PMC3542769.
9. Mussbacher M, Salzmann M, Brostjan C, Hoesel B, Schoergenhofer C, Datler H, Hohensinner P, Basílio J, Petzelbauer P, Assinger A, Schmid JA. Cell Type-Specific Roles of NF-κB Linking Inflammation and Thrombosis. Front Immunol. 2019 Feb 4;10:85. doi: 10.3389/fimmu.2019.00085. PMID: 30778349; PMCID: PMC6369217.
10. Laban H, Weigert A, Zink J, Elgheznawy A, Schürmann C, Günther L, Abdel Malik R, Bothur S, Wingert S, Bremer R, Rieger MA, Brüne B, Brandes RP, Fleming I, Benz PM. VASP regulates leukocyte infiltration, polarization, and vascular repair after ischemia. J Cell Biol. 2018 Apr 2;217(4):1503-1519. doi: 10.1083/jcb.201702048. Epub 2018 Mar 5. PMID: 29507126; PMCID: PMC5881493.
11. Benza R, Mathai S, Nathan SD. sGC stimulators: Evidence for riociguat beyond groups 1 and 4 pulmonary hypertension. Respir Med. 2017 Jan;122 Suppl 1:S28-S34. doi: 10.1016/j.rmed.2016.11.010. Epub 2016 Nov 14. PMID: 27890470.
12. Ghofrani HA, Galiè N, Grimminger F, Grünig E, Humbert M, Jing ZC, Keogh AM, Langleben D, Kilama MO, Fritsch A, Neuser D, Rubin LJ; PATENT-1 Study Group. Riociguat for the treatment of pulmonary arterial hypertension. N Engl J Med. 2013 Jul 25;369(4):330-40. doi: 10.1056/NEJMoa1209655.
13. Kutllovci N. Investigating the correlation between activation of the Nitric Oxide pathway and inhibition of the NLRP3 inflammasome in endothelial cells in preeclampsia. Italian Journal JOC. 2024;36 (Supplement No. 2):25. doi: 10.36129/jog.2024.S63
14. Kahlenberg JM, Lundberg KC, Kertesy SB, Qu Y, Dubyak GR. Potentiation of caspase-1 activation by the P2X7 receptor is dependent on TLR signals and requires NF-kappaB-driven protein synthesis. J Immunol. 2005 Dec 1;175(11):7611-22. doi: 10.4049/jimmunol.175.11.7611. PMID: 16301671.
15. Usui F, Shirasuna K, Kimura H, Tatsumi K, Kawashima A, Karasawa T, Hida S, Sagara J, Taniguchi S, Takahashi M. Critical role of caspase-1 in vascular inflammation and development of atherosclerosis in Western diet-fed apolipoprotein E-deficient mice. Biochem Biophys Res Commun. 2012 Aug 24;425(2):162-8. doi: 10.1016/j.bbrc.2012.07.058. Epub 2012 Jul 20. PMID: 22819845.
16. Lopez-Pastrana J, Ferrer LM, Li YF, Xiong X, Xi H, Cueto R, Nelson J, Sha X, Li X, Cannella AL, Imoukhuede PI, Qin X, Choi ET, Wang H, Yang XF. Inhibition of Caspase-1 Activation in Endothelial Cells Improves Angiogenesis: A NOVEL THERAPEUTIC POTENTIAL FOR ISCHEMIA. J Biol Chem. 2015 Jul 10;290(28):17485-94. doi: 10.1074/jbc.M115.641191. Epub 2015 Jun 2. PMID: 26037927; PMCID: PMC4498083.
17. Melton E, Qiu H. Interleukin-1β in Multifactorial Hypertension: Inflammation, Vascular Smooth Muscle Cell and Extracellular Matrix Remodeling, and Non-Coding RNA Regulation. Int J Mol Sci. 2021 Aug 11;22(16):8639. doi: 10.3390/ijms22168639. PMID: 34445357; PMCID: PMC8395428.
18. Kim JH, Kim JY, Park M, Kim S, Kim T, Kim J, Choi S, Park W, Hwang JY, Choe J, Ha KS, Won MH, Ryoo S, Kwon YG, Kim YM. NF-κB-dependent miR-31/155 biogenesis is essential for TNF-α-induced impairment of endothelial progenitor cell function. Exp Mol Med. 2020 Aug;52(8):1298-1309. doi: 10.1038/s12276-020-0478-x. Epub 2020 Aug 7. PMID: 32770080; PMCID: PMC8080610.
19. Gao Q, Tang J, Li N, Zhou X, Li Y, Liu Y, Wu J, Yang Y, Shi R, He A, Li X, Zhang Y, Chen J, Zhang L, Sun M, Xu Z. A novel mechanism of angiotensin II-regulated placental vascular tone in the development of hypertension in preeclampsia. Oncotarget. 2017 May 9;8(19):30734-30741. doi: 10.18632/oncotarget.15416. PMID: 28430615; PMCID: PMC5458163.
20. Zhou R, Yazdi AS, Menu P, Tschopp J. A role for mitochondria in NLRP3 inflammasome activation. Nature. 2011 Jan 13;469(7329):221-5. doi: 10.1038/nature09663. Epub 2010 Dec 1. Erratum in: Nature. 2011 Jul 7;475(7354):122. PMID: 21124315.
21. Tanase DM, Valasciuc E, Gosav EM, Ouatu A, Buliga-Finis ON, Floria M, Maranduca MA, Serban IL. Portrayal of NLRP3 Inflammasome in Atherosclerosis: Current Knowledge and Therapeutic Targets. Int J Mol Sci. 2023 May 3;24(9):8162. doi: 10.3390/ijms24098162. PMID: 37175869.
22. Benz PM, Frömel T, Laban H, Zink J, Ulrich L, Groneberg D, Boon RA, Poley P, Renne T, de Wit C, Fleming I. Cardiovascular Functions of Ena/VASP Proteins: Past, Present and Beyond. Cells. 2023 Jun 28;12(13):1740. doi: 10.3390/cells12131740. PMID: 37443774; PMCID: PMC10340426.

International Journal of Biomedicine 15(4) (2025) 756-758
http://dx.doi.org/10.21103/Article15(4)_CR1

CASE REPORT

INTERNATIONAL JOURNAL OF BIOMEDICINE

Regenerative Capacity of Anterior Chamber Injection of Eye Platelet-Rich Plasma for Pseudophakic Bullous Keratopathy

Anita Syla Lokaj[1*]

[1]*Department of Ophthalmology, Eye Clinic, University Center Clinic of Kosovo, Prishtina, Kosovo*

Abstract

Purpose: To present successful management of moderate corneal edema following cataract surgery by using the application of eye platelet-rich plasma (E-PRP) in the anterior chamber in a case of pseudophakic bullous keratopathy.
Methods and Results: A 44-year-old male presented to our clinic with a year of diminution of vision in the right eye, associated with intermittent photophobia and colored halos around lights, primarily upon waking in the morning. The patient had cataract surgery ten years ago. We use AS-OCT, slit lamp, and corneal pachymetry, which reveal multiple small subepithelial micro- and macrobullae involving the entire cornea, diffuse stromal edema, and mild thickening of Descemet's membrane with folds. We administer 0.3 mL of E-PRP into the anterior chamber under sterile conditions.
Various medical treatments involving numerous drops have been unsuccessful. A sterile 0.3 mL of E-PRP was injected into the anterior chamber every 2 weeks for 1 month. Clinical and anatomical improvement began from the first week, and corneal edema resolved at 2 months. Postoperatively, no significant side effect was noted. We followed up with Slit lamp, anterior segment OCT, and corneal pachymetry, which showed improvement in corneal transparency and total disappearance of fluid in the cystic superficial epithelium. The patient is in a follow-up procedure.
Conclusion: This study suggests that the therapeutic response to intracameral injection of E-PRP was satisfactory in moderate pseudophakic bullous keratopathy. In this case, intraocular E-PRP was a promising, safe, and effective treatment option for managing bullous keratopathy, for which conventional approaches had failed.(**International Journal of Biomedicine. 2025;15(4):756-758.**)

Keywords: bullous keratopathy • eye platelet-rich plasma • treatment

For citation: Lokaj AS. Regenerative Capacity of Anterior Chamber Injection of Eye Platelet-Rich Plasma for Pseudophakic Bullous Keratopathy. International Journal of Biomedicine. 2025;15(4):756-758. doi:10.21103/Article15(4)_CR1

Introduction

Pseudophakic bullous keratopathy (PBK) is a postoperative complication that arises after cataract extraction and intraocular lens implantation, characterized by endothelial cell loss leading to corneal edema, epithelial bullae formation, and, in advanced cases, irreversible vision loss.[1] The most common causes include intraoperative trauma, placement of anterior chamber or iris-supported intraocular lenses, and pre-existing conditions such as Fuchs endothelial dystrophy.[2] Several studies have reported that endothelial cell loss may persist and even progress over time, years after cataract surgery.[4]

Conventional treatment approaches include topical hypertonic solutions, lubricating ointments, bandage contact lenses, autologous serum, and, in more severe cases, penetrating keratoplasty or endothelial keratoplasty (e.g., Descemet Stripping Endothelial Keratoplasty, DSEK).[4] However, these treatments often provide only temporary relief or require complex surgical procedures. In this context, autologous blood-derived therapies such as platelet-rich plasma (PRP) have gained significant attention due to their regenerative potential and ability to promote wound healing on the ocular surface.[5]

Case Report

A 44-year-old man presented to our clinic complaining of foreign body sensation, pain, redness, photophobia, and decreased vision in his right eye for a year. The patient had

***Corresponding author**: Anita Syla Lokaj, MD, PhD. E-mail: anitasyla@live.com*

previously been treated with non-preservative artificial tears, antibiotic eye drops, and therapeutic bandage contact lenses to protect the cornea. Treatment in various hospitals was unsuccessful.

Objective examination revealed epithelial and subepithelial bullae that developed and ruptured, resulting in severe pain as underlying nerve endings were exposed and severe corneal thickening (688 μm) measured by anterior segment OCT and pachymetry (Fig. 1). Visual acuity was 20/100 due to corneal edema and irregular astigmatism.

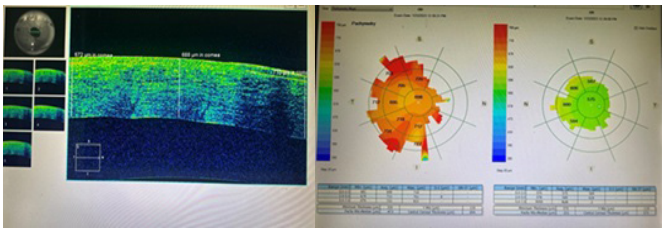

Fig. 1. *Anterior segment OCT and pachymetry.*

With the patient's consent, a novel PRP solution was accepted as treatment. Autologous 0.3 ml of PRP was administered intracameral and subconjunctival to the patient in the operating room in sterile conditions every 2 weeks for one month, along with preservative-free 50% PRP eye drops.(Fig. 2, Fig. 3). After just 30 days, resolution of the corneal lesion was observed, and all topical medications were gradually reduced. The OCT scan and pachymetry demonstrated resolution of the corneal edema, with normalization in corneal morphology, compared to before the injections (Fig. 4). The subjective symptoms, including burning, grittiness, and ocular discomfort, noticeably reduced, and the conjunctival congestion slowly resolved (Fig. 5). Postoperatively, no significant side effect was noted except an early transient moderate (25 mm Hg) intraocular pressure peak. Visual acuity improved from 20/100 to 20/50 on the Snellen chart.

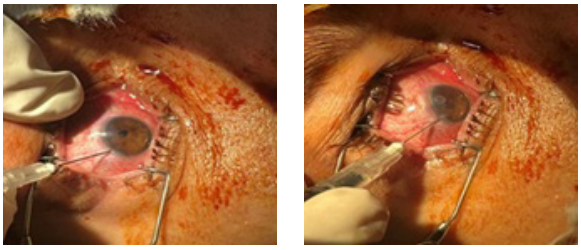

Fig. 2. *Injection of PRP into the anterior chamber.*

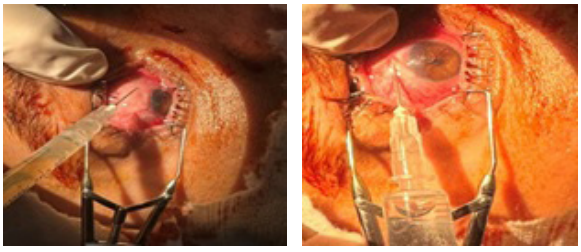

Fig. 3. *Subconjunctival injection of PRP.*

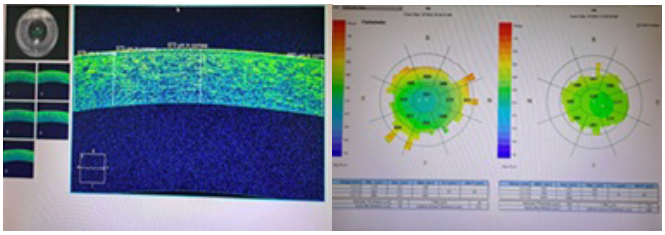

Fig. 4. *AS-OCT and pachymetry - 1 month after surgery.*

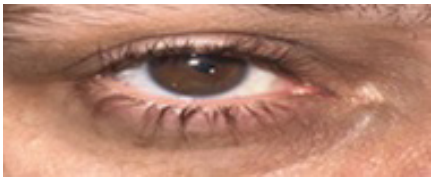

Fig. 5. *Slit lamp biomicroscopy.*

Discussion

Platelet-rich plasma is an autologous, preservative-free preparation that contains a high concentration of platelets and numerous growth factors essential for tissue regeneration and wound repair.[5,6] Compared to autologous serum (AS), PRP has a higher concentration of biologically active components, including platelet-derived growth factor (PDGF), transforming growth factor-beta (TGF-β1 and β2), insulin-like growth factor (IGF-1), vascular endothelial growth factor (VEGF), epidermal growth factor (EGF), and fibroblast growth factor-2 (FGF-2).[7] These molecules play critical roles in promoting epithelial cell proliferation, collagen synthesis, angiogenesis, and tissue remodeling.

Additionally, PRP contains cytokines such as PF4 and CD40L that contribute to immune modulation and cellular adhesion.[8] This composition supports a favorable environment for epithelial regeneration and corneal surface stability, especially in conditions characterized by chronic or recurrent epithelial defects.

Kheirkhah et al.[9] compared the clinical effects of PRP and AS in treating ocular surface diseases. They reported superior outcomes with PRP in terms of epithelial healing and symptom relief, particularly in cases of dry eye disease and neurotrophic keratopathy. Similarly, Alio et al.[10] demonstrated that PRP eye drops improved healing in patients with persistent epithelial defects and ocular surface disorders, suggesting its potential as a safe and effective therapy. In the context of PBK, where chronic corneal edema and epithelial instability are common, PRP may offer significant advantages by providing essential growth signals that support re-epithelialization and tissue repair. Although the application of PRP specifically for PBK remains underexplored, the evidence from related ocular surface conditions strongly supports its potential efficacy. Further randomized controlled trials are warranted to establish standardized treatment protocols and assess the long-term safety and effectiveness of PRP in PBK management.

Conclusion

Pseudophakic bullous keratopathy remains a challenging postoperative complication with limited long-term therapeutic options. While conventional treatments provide symptomatic relief, they often fail to promote lasting regeneration of the corneal endothelium. Autologous PRP, due to its high concentration of growth factors and bioactive molecules, offers a promising adjunct or alternative therapy. Evidence from similar ocular surface diseases supports its regenerative potential, particularly in promoting epithelial healing and reducing inflammation. Although further clinical trials are necessary to validate its efficacy and safety in PBK specifically, early findings suggest that injection in the anterior chamber or topical PRP could become an innovative and biologically sound strategy in the management of corneal decompensation following cataract surgery. Its autologous origin, low risk of immune reaction, and ease of preparation make it a valuable option for personalized, regenerative ocular care.

Patient Consent

The patient has provided written informed consent. This report does not contain any personal information that could be used to identify the patient.

Conflicts of Interest

The author declares no competing interests.

References

1. Johnson R, Kim D, Lee M. Long-term endothelial cell loss after cataract surgery. J Cataract Refract Surg. 2015;41(4):512–9.

2. Singh A, Patel H. Risk factors in pseudophakic bullous keratopathy: a clinical review. Int J Ophthalmol. 2018;11(2):123–30.

3. Bourne WM. Biology of the corneal endothelium in health and disease. Eye (Lond). 2003 Nov;17(8):912-8. doi: 10.1038/sj.eye.6700559. PMID: 14631396.

4. Gain P, Jullienne R, He Z, Aldossary M, Acquart S, Cognasse F, Thuret G. Global Survey of Corneal Transplantation and Eye Banking. JAMA Ophthalmol. 2016 Feb;134(2):167-73. doi: 10.1001/jamaophthalmol.2015.4776. PMID: 26633035.

5. Everts PA, Knape JT, Weibrich G, Schönberger JP, Hoffmann J, Overdevest EP, Box HA, van Zundert A. Platelet-rich plasma and platelet gel: a review. J Extra Corpor Technol. 2006 Jun;38(2):174-87. PMID: 16921694; PMCID: PMC4680757.

6. Martinez R, Gomez E, Alvarez M. Use of platelet-rich plasma in ocular surface disease: a review of clinical outcomes. Br J Ophthalmol. 2019;103(5):645–50.

7. Anitua E, Andía I, Sanchez M, Azofra J, del Mar Zalduendo M, de la Fuente M, Nurden P, Nurden AT. Autologous preparations rich in growth factors promote proliferation and induce VEGF and HGF production by human tendon cells in culture. J Orthop Res. 2005 Mar;23(2):281-6. doi: 10.1016/j.orthres.2004.08.015. PMID: 15779147.

8. Sundman EA, Cole BJ, Fortier LA. Growth factor and catabolic cytokine concentrations are influenced by the cellular composition of platelet-rich plasma. Am J Sports Med. 2011 Oct;39(10):2135-40. doi: 10.1177/0363546511417792. Epub 2011 Aug 16. PMID: 21846925.

9. Kheirkhah A, Raju VK, Tseng SC. Comparison of autologous serum and platelet-rich plasma for the treatment of ocular surface disease. Am J Ophthalmol. 2011;152(4):734–40.e1

10. Alio JL, Colecha JR, Pastor S, Rodriguez A, Artola A. Symptomatic dry eye treatment with autologous platelet-rich plasma. Ophthalmic Res. 2007;39(3):124-9. doi: 10.1159/000100933. Epub 2007 Mar 19. PMID: 17374962.

International Journal of Biomedicine 15(4) (2025) 759-762
http://dx.doi.org/10.21103/Article15(4)_CR2

CASE REPORT

INTERNATIONAL JOURNAL OF BIOMEDICINE

Interdisciplinary Management of One or Two Missing Maxillary Incisors: A Clinical Case Series

Miranda Sejdiu Abazi[1], Arben Abazi[2*], Agim Prokshaj[1], Tetore Olloni[3], Egzon Veliu[2]

[1]*Department of Dentistry, Faculty of Dentistry, UBT College, Pristina, Kosovo*
[2]*Department of Dentistry, Faculty of Medicine, University of Pristina, Pristina, Kosovo*
[3]*Department of Prosthodontics, Faculty of Dentistry, "Hasan Prishtina" University, Prishtina, Kosovo*

Abstract

Congenital absence of one or both maxillary lateral incisors is a common dental anomaly that significantly impacts a patient's facial aesthetics, oral function, and occlusal development. Given the anterior location of these teeth, their absence necessitates careful, individualized treatment planning. The choice between orthodontic space closure and prosthetic replacement depends on a range of dental, skeletal, and aesthetic factors. Therefore, an interdisciplinary approach—typically involving orthodontists, prosthodontists, and occasionally oral surgeons—is essential to achieve optimal functional and aesthetic results.

This article presents clinical outcomes from a case series involving patients with one or two missing maxillary lateral incisors. Each case was managed through customized treatment plans based on the patient's age, occlusal relationship, space conditions, and aesthetic considerations. Treatment modalities included either orthodontic space closure or space opening, followed by prosthetic rehabilitation using supported crowns or resin-bonded prostheses. Diagnostic records, treatment duration, aesthetic results, and patient satisfaction were evaluated.

The management of missing maxillary lateral incisors requires a personalized approach that considers the clinical, aesthetic, and psychosocial aspects of each case. No universal solution exists; thus, decisions between space closure and prosthetic replacement should be made collaboratively through interdisciplinary planning. The presented cases highlight that individualized orthodontic-prosthetic strategies can yield excellent functional and aesthetic outcomes.(**International Journal of Biomedicine. 2025;15(4):759-762.**)

Keywords: maxillary incisor • space management • orthodontic space • interdisciplinary treatment

For citation:Abazi MS, Abazi A, Prokshaj A, Olloni T, Veliu E. Interdisciplinary Management of One or Two Missing Maxillary Incisors: A Clinical Case Series. International Journal of Biomedicine. 2025;15(4):759-762. doi:10.21103/Article15(4)_CR2

Introduction

Maxillary lateral incisor agenesis is one of the most prevalent forms of congenital tooth absence in the anterior maxilla, accounting for approximately 20% of all dental anomalies.[1] Overall, dental agenesis affects around 4.2% of the population and represents a significant developmental condition in the permanent dentition.[2]

The absence of maxillary lateral incisors presents both aesthetic and functional challenges, particularly due to their prominent position in the smile zone. As a result, treatment planning must be highly individualized, considering each patient's clinical characteristics, occlusal relationship, aesthetic expectations, and psychological profile. There is no universally ideal solution; thus, treatment modalities should be selected based on case-specific functional, periodontal, and aesthetic parameters, with a strong emphasis on long-term success.[3]

A retrospective study by Robertsson and Mohlin compared two primary treatment strategies for managing maxillary lateral incisor agenesis: orthodontic space closure using canine substitution and space opening followed by prosthetic rehabilitation. Their results indicated higher patient satisfaction and superior periodontal health in the group treated with space closure.[4]

Spear et al.[5] emphasized that the successful management of anterior aesthetics should be guided by aesthetic principles and executed through interdisciplinary collaboration. Treatment should begin with a comprehensive aesthetic analysis and incorporate considerations of function, structure, and biological

***Corresponding author:** Dr. Arben Abazi. E-mail: arbenabazi033@gmail.com*

health, requiring coordinated efforts among orthodontists, prosthodontists, periodontists, and oral surgeons.

Maxillary lateral incisor agenesis is often not an isolated anomaly. It frequently coexists with other dental irregularities, including microdontia of the lateral incisors, agenesis of other permanent teeth, ectopic eruption of maxillary canines, and distoangulation of mandibular second premolars.[6] These associated anomalies complicate diagnosis and must be carefully considered during both orthodontic and prosthetic treatment planning.

Furthermore, as highlighted by Kavadia et al.,[7] current evidence is insufficient to definitively endorse one treatment modality over another for maxillary lateral incisor agenesis. Therefore, a multidisciplinary diagnostic approach and individualized treatment-planning process are essential for selecting the most appropriate therapeutic strategy for each patient.

This study is a retrospective clinical case series aimed at evaluating treatment options for patients presenting with the congenital absence of one or two maxillary incisors. All patients were managed using a combination of orthodontic and prosthetic interventions. A total of four patients were included; all treated at the Panacea Clinic in Ferizaj. The sample consisted of two female patients aged 15 and 19 years, and two male patients aged 17 and 23. Inclusion criteria were congenital absence of one or two maxillary incisors and availability of complete diagnostic documentation, including radiographs and clinical photographs. The study adhered to the ethical principles outlined in the Declaration of Helsinki. All patients provided informed consent for participation in this study and the use of their clinical data.

Each case was evaluated individually, and treatment was planned through interdisciplinary collaboration involving orthodontists and prosthodontists. The therapeutic approach—either space closure with canine substitution or space opening for prosthetic replacement—was selected based on the specific clinical, aesthetic, and functional needs of each patient.

This study presents four clinical cases treated at our clinic, involving patients with congenital absence of one or two maxillary incisors. Each patient underwent a comprehensive clinical, radiographic, and aesthetic evaluation. The therapeutic approach varied from orthodontic space closure with aesthetic reshaping of the canines to space opening followed by prosthetic rehabilitation, depending on the individual needs of each case. Treatment was planned in close collaboration between the orthodontist, the prosthodontist, and maxillofacial surgeon. Post-treatment follow-up lasted at least six months.

Case 1

A female patient presented with agenesis of both maxillary lateral incisors. After a thorough clinical evaluation, an interdisciplinary treatment plan was developed, combining orthodontics with prosthetics. Given the patient's young age and ongoing skeletal growth, it was decided to open the spaces orthodontically and to maintain them using a removable, acrylic partial denture with two lateral incisors. Orthodontic therapy focused on creating space for prosthetic replacements and aligning the canines in their proper anatomical positions to ensure correct interdigitation with the mandibular dentition (Figures 1,2).

(a) (b)

Fig. 1. *(a) The beginning of the treatment; (b) The removable acrylic partial denture, replacing the missing incisors.*

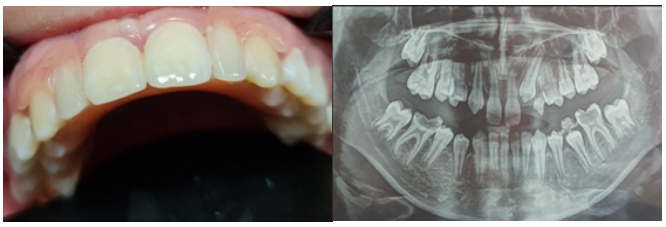

(a) (b)

Fig. 2. *(a) Occlusal view; (b) Panoramic radiograph.*

Case 2

A 19-year-old female patient presented with agenesis of the maxillary left lateral incisor. Following a comprehensive clinical evaluation, an interdisciplinary treatment plan combining orthodontic and prosthetic approaches was formulated. One of the primary objectives of orthodontic treatment was to correct a midline deviation that had shifted to the left. After orthodontic space opening and alignment of the left canine into proper occlusion, the midline was successfully corrected. To replace the missing lateral incisor, a multilayer zirconia-bonded appendix bridge was placed. The patient opted for this conservative prosthetic solution and declined implant placement. The final aesthetic and functional outcomes were satisfactory, and occlusal harmony was restored (Figure 3).

(a) (b)

(c) (d)

Fig. 3. *(a) Before treatment; (b) The beginning of the orthodontic treatment; (c) The end of the orthodontic treatment; (d) The final treatment.*

Case 3

A male patient aged 17 years presented to our clinic seeking orthodontic treatment. Clinical and radiographic

evaluation revealed agenesis of the left maxillary lateral incisor , along with atypical crown morphology, Angle's Class II malocclusion, deep bite, and a pronounced curve of Spee. The treatment plan involved distalization of the left canine to create space for the prosthetic replacement of the missing lateral incisor. On the right side, a multilayer zirconia crown was planned following orthodontic treatment. After correction of the malocclusion to a stable Angle's Class I relationship, prosthetic rehabilitation was completed with a Maryland bridge on the left side, following the patient's preference. As a dental technician, he opted for a conservative, adhesive solution. A zirconia crown was fabricated for the right side. Final impressions were taken to fabricate retention splints and maintain the achieved results (Figures 4,5).

(a) (b)

Fig. 4. *(a) The beginning of the orthodontic treatment; (b) The final treatment.*

Fig. 5. *The panoramic radiograph.*

Case 4

A male patient aged 23 years presented for aesthetic concerns related to the spacing between his anterior teeth. Clinical and radiological evaluation confirmed the bilateral congenital absence of maxillary lateral incisors as the primary cause of the diastemas (Figures 6,7). Orthodontic treatment was chosen to close the spaces, as this solution was both aesthetically optimal and preferred by the patient. Canine substitution will be used to achieve a harmonious smile line, and the treatment outcome will meet both functional and aesthetic expectations. The patient is undergoing fixed therapy (Figure 8).

Fig. 6. *The panoramic radiograph.*

(a)

(b) (c)

Fig. 7. *(a) The frontal view; (b) Right view; (c) Left view.*

Fig. 8. *(a, b) The beginning of the orthodontic treatment; (c, d) Closed space with power chain.*

Discussion

Hypodontia, excluding third molars, is the most common dental developmental disorder, with a reported prevalence ranging from 1.6% to 6.9%. The teeth most frequently missing are the mandibular second premolars and maxillary lateral incisors.[7,2] The global prevalence of maxillary lateral incisor agenesis, according to Polder et al.,[8] is 1.55%, whereas Aktan et al.[11] found that the prevalence of lateral incisor agenesis in

the Turkish population is approximately 2.4%. Polder et al.,[8] in their meta-analysis on the prevalence of permanent tooth agenesis, found that its occurrence is significantly lower in North America than in Europe and Australia. The most frequently missing teeth are the mandibular second premolars, followed by the maxillary lateral incisors and the maxillary second premolars. Agenesis typically occurs unilaterally, except in the case of maxillary lateral incisors, which are more likely to be missing bilaterally.

According to Garib et al.,[6] congenital absence of maxillary lateral incisors is frequently associated with other dental anomalies such as microdontia of lateral incisors (38.8%), agenesis of maxillary premolars (10.3%) and mandibular premolars (7.9%), as well as palatal displacement of canines. These associated findings significantly complicate the treatment-planning process and underscore the need for a multidisciplinary approach.

Muhamad and Abdulgani[2] emphasized the importance of collaborative management in cases involving maxillary lateral incisor agenesis. They concluded that such cases require personalized planning and close cooperation among orthodontists, prosthodontists, and periodontists to achieve a predictable and aesthetically acceptable result for the patient, as in the cases we presented in this article.

Lateral incisor agenesis is primarily a genetic anomaly, although environmental factors may also contribute. It significantly affects oral aesthetics and function. As there is no universally applicable treatment approach, each case requires an individualized, multidisciplinary solution.[6,10]

Wright and colleagues, in their study using dental models, compared the tooth dimensions in patients with agenesis of maxillary lateral incisors to those with complete dentition. They concluded that patients missing one or more maxillary lateral incisors exhibited a generalized reduction in tooth size—not only in the maxilla but also in the mandible—thereby supporting a broader genetic influence on dental development.[9]

Conclusion

The management of one or two missing maxillary incisors requires a comprehensive and patient-specific approach. Treatment planning should be guided by a thorough evaluation of clinical, occlusal, aesthetic, and psychological factors unique to each individual.

Given the variability in presentation and patient expectations, there is no universally optimal treatment modality. Therefore, the decision between orthodontic space closure and prosthetic rehabilitation must be made collaboratively through interdisciplinary consultation among orthodontists, prosthodontists, and other relevant specialists.

The clinical cases presented in this series illustrate that personalized, combined orthodontic-prosthetic treatment strategies can lead to highly favorable aesthetic and functional outcomes. These findings underscore the importance of individualized care protocols and reinforce the value of multidisciplinary teamwork in addressing anterior dental agenesis.

Ethical Statements

All patients have provided written informed consent. These reports do not contain any personal information that could be used to identify the patient.

Acknowledgments

We want to express our sincere gratitude to all Panacea staff for their support and contributions.

Conflicts of Interest

The authors declare that they have no competing interests.

References

1. Pini NI, De-Marchi LM, Gribel BF. Missing maxillary lateral incisors: A clinical approach. J Esthet Restor Dent. 2014;26(5):302–13.
2. Muhamad AH, Abdulgani A. Congenitally Missing Teeth: A Multidisciplinary Approach. Lambret, June 2015. ISBN: 978-3-659-54508-5
3. Kinzer GA, Kokich VO Jr. Managing congenitally missing lateral incisors. Part II: tooth-supported restorations. J Esthet Restor Dent. 2005;17(2):76-84. doi: 10.1111/j.1708-8240.2005.tb00089.x. PMID: 16036123.
4. Robertsson S, Mohlin B. The congenitally missing upper lateral incisor. A retrospective study of orthodontic space closure versus restorative treatment. Eur J Orthod. 2000 Dec;22(6):697-710. doi: 10.1093/ejo/22.6.697. PMID: 11212605.
5. Spear FM, Kokich VG, Mathews DP. Interdisciplinary management of anterior dental esthetics. J Am Dent Assoc. 2006 Feb;137(2):160-9. doi: 10.14219/jada.archive.2006.0140.
6. Garib DG, Alencar BM, Lauris JR, Baccetti T. Agenesis of maxillary lateral incisors and associated dental anomalies. Am J Orthod Dentofacial Orthop. 2010 Jun;137(6):732.e1-6; discussion 732-3. doi: 10.1016/j.ajodo.2009.12.024.
7. Kavadia S, Papadiochou S, Papadiochos I, Zafiriadis L. Agenesis of maxillary lateral incisors: a global overview of the clinical problem. Orthodontics (Chic.). 2011 Winter;12(4):296-317. PMID: 22299104.
8. Polder BJ, Van't Hof MA, Van der Linden FP, Kuijpers-Jagtman AM. A meta-analysis of the prevalence of dental agenesis of permanent teeth. Community Dent Oral Epidemiol. 2004 Jun;32(3):217-26. doi: 10.1111/j.1600-0528.2004.00158.x. PMID: 15151692.
9. Wright J, Bosio JA, Chou JC, Jiang SS. Maxillary lateral incisor agenesis and its relationship to overall tooth size. J Prosthet Dent. 2016 Feb;115(2):209-14. doi: 10.1016/j.prosdent.2015.07.010.
10. Al-Ani AH, Antoun JS, Thomson WM, Merriman TR, Farella M. Hypodontia: An Update on Its Etiology, Classification, and Clinical Management. Biomed Res Int. 2017;2017:9378325. doi: 10.1155/2017/9378325.
11. Aktan AM, Kara S, Şener I, Bereket C, Çiftçi ME. An evaluation of agenesis of permanent teeth excluding third molars in a sample of Turkish population. Int J Paediatr Dent. 2010;20(3):209–15.

International Journal of Biomedicine 15(4) (2025) 763-766
http://dx.doi.org/10.21103/Article15(4)_CR3

CASE REPORT

INTERNATIONAL JOURNAL OF BIOMEDICINE

Maxillary Permanent Canine with One Root and Three Canals: A Case Report

Nexhmije Ajeti[1*], Miranda Stavileci[2], Donika Bajrami[2], Shqipe Buleshkaj[1]

[1]*Department of Dental Pathology and Endodontics, Dental School, University of Business and Technology, Prishtina, Kosovo*
[2]*Department of Dental Pathology and Endodontics, Faculty of Medicine, University of Prishtina, Prishtina, Kosovo*

Abstract

Typically, the maxillary canine possesses a single root and a single root canal. However, anatomical variations have been documented in several in vitro and in vivo studies. The presence of two roots and two canals in maxillary canines is rare, and the occurrence of three canals within one root is even more exceptional. Dentists must have comprehensive knowledge of root canal morphology and its potential variations to ensure successful treatment outcomes. This report presents a rare case of a maxillary canine with one root and three canals. Accurate diagnosis of such uncommon anatomical variations is crucial for the success of endodontic therapy.(**International Journal of Biomedicine. 2025;15(4):763-766.**)

Keywords: maxillary permanent canine • root canal • anatomical variation

For citation:Ajeti N, Stavileci M, Bajrami D, Buleshkaj S. Maxillary Permanent Canine with One Root and Three Canals: A Case Report. International Journal of Biomedicine. 2025;15(4):763-766. doi:10.21103/Article15(4)_CR3

Introduction

Understanding the root canal morphology of teeth is vital for achieving successful endodontic treatment. One of the primary reasons for root canal treatment failure is the inability to detect and properly manage additional canals.[1,2]

Vertucci classified human permanent tooth canal systems into several configurations, ranging from one to three distinct canals.[3] While the maxillary canine typically has one root and one canal,[4] anatomical variations, such as additional roots or canals, have also been reported.

Several cases in the literature have documented maxillary canines with two canals.[5,1,6] Asiry[7] reported the presence of two distinct roots (mesial and distal) in a permanent maxillary canine, emphasizing bilateral differences.

Furthermore, Uchiyama et al.[8] studied 250 extracted maxillary canines in vitro, revealing accessory canals in 40% of the specimens, many of which were difficult to access and treat. Reports describing three-canal maxillary canines remain extremely rare. Vertucci's Type III configurations[3] in maxillary canines are scarcely documented.

The etiology behind such anatomical anomalies is not well understood. Hypotheses include differential development of Hertwig's epithelial root sheath trauma,[9] disturbances in morpho-differentiation,[10] genetic factors,[11] or defects in the dental lamina during root formation.[12]

In the past, various methodologies used to study canal anatomy were histopathological studies,[13] intraoral periapical radiographs, cleaning and demineralizing method,[14] and surgical operating microscopy.[15]

Various methodologies have been employed to study canal morphology, including histological analysis,[13] radiographic imaging, canal staining and clearing, and cone-beam computed tomography (CBCT). CBCT offers non-invasive, three-dimensional imaging and is now considered a valuable tool for detecting rare root canal variations.[16,17]

There were limited studies in the literature evaluating the root and canal morphology of canine teeth in different populations using CBCT.[3,18,19]

The objective of this case report is to present and analyze a rare anatomical variation of a maxillary canine with one root and three distinct canals using CBCT imaging.

***Corresponding author**: Prof. Nexhmije Ajeti, E-mail: nexhmije.ajeti@ubt-uni.net*

Materials and Methods

A 46-year-old male patient presented with spontaneous, sharp pain in the region of the upper jaw at the Department of Endodontics, University Dental Clinical Center of Kosovo. Clinical examination revealed a deep carious lesion. According to the patient's history, the pain began a week prior, with episodes lasting 20–30 minutes, followed by one-hour intervals. Cold stimuli exacerbated pain. The tooth was not sensitive to percussion, and vitality testing was positive.

Radiographic examination included a periapical radiograph (Sirona Siemens, Germany) and 3D CBCT imaging (Orthophos SL, Dentsply, Sirona, Germany). No anatomical abnormalities of the pulp chamber were detected in the conventional radiograph (Figure 1).

Fig. 1. *Retro-alveolar radiograph with only one root canal.*

Local anesthesia was administered using Articaine HCl 4% with Epinephrine 1:100,000 (Septocain, Septodont, France). Rubber dam isolation was applied, and the access cavity was prepared. Upon entering the pulp chamber, three distinct canal orifices were observed: one palatal and two buccal (mesiobuccal and distobuccal), confirmed radiographically using 3D CBCT. After the instrumentation of the tooth root canals, a 3D radiographic scan (cone beam computed tomography, CBCT) was performed to assess the condition of the canals more accurately. The 3D radiographic scan revealed three entrances to root canals within the pulp chamber. (Figures 2,3,4)

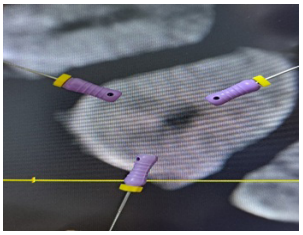

Fig. 2. *Localization of the root canal orifices of the maxillary canine.*

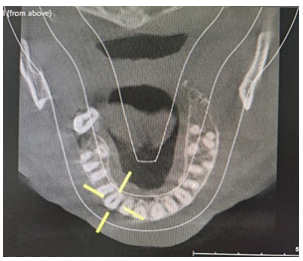

Fig. 3. *The canine in the axial projection.*

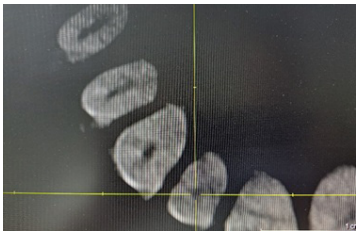

Fig. 4. *The canine in the tangential projection.*

After 3 D radiographic scan, working lengths were determined with an apex locator (DentaPort, Morita, Japan): 19.24 mm for the palatal canal, 17.97 mm for the disto buccal canal, and 15 mm for the mesiobuccal canal. The canals were instrumented with a rotary system (Endo Smart Cordless Endo Motor, Germany). Irrigation was performed with 2.5% sodium hypochlorite (Chlorax, Cerkamed, Poland) to remove organic tissue, followed by 17% EDTA (I EDTA, Lithuania) for one minute to eliminate inorganic components. Final irrigation was done with 0.9% saline solution (NaCl, B. Braun, Germany).

After drying with absorbent paper points (Korea), a trial obturation was performed using gutta-percha cones to confirm the presence of the canal (Figure 5).

Fig. 5. *Test radiograph with gutta-percha.*

Then, the canals were obturated using a bio-ceramic sealer (One-Fil, Korea), confirmed with a final radiograph (Figure 6).

Fig. 6. *Root canal obturation.*

The patient, residing abroad, was monitored remotely at 1, 3, and 12 months post-treatment. No symptoms or complications were reported during the follow-up period.

Discussion

Maxillary canines typically present with one root and one canal, making this case of a single-rooted tooth with three canals a rare anatomical variant.

During the discussion of this presentation, there is one aspect to consider: the presence of unusual morphology in the maxillary canine with one root and three canals.

Our presentation aligns with the clinical research of Supritha et al., who also reported the presence of a permanent maxillary canine with one root and three canals (buccal, mesiobuccal, and palatal).[20]

Such configurations are difficult to detect in conventional radiographs due to two-dimensional limitations.[21] Multi-angled radiographic views and advanced imaging, such as CBCT, are vital tools for accurately diagnosing such complex cases.[22]

Only a few cases have been described in the literature regarding the maxillary canine with three canals based on Vertucci classification.[23]

Kandasamy et al. also reported a maxillary canine with three roots and three canals, considered the first of its kind.[24] Galhotra et al.[25] and Bolla & Kavuri[26] reported multirooted variations in maxillary canines, while Wolf et al. estimated that three canals in maxillary canines occur in just 0.1–0.2% of cases.[27]

Studies by Martins et al.[28] and Masyakhy[29] suggested that 1.4% of maxillary canines may contain two canals, emphasizing the rarity of three canal occurrences. Further highlighted were accessory canals found in 40% of maxillary canines in vitro, many of which were inaccessible for proper cleaning and shaping.[8]

These anatomical deviations may arise from multiple factors, including abnormal root sheath development,[9] trauma,[10] genetic predisposition,[30] and disturbances during root formation.[12]

Given these complexities, CBCT is essential when conventional imaging is inconclusive. It provides accurate, three-dimensional insight into canal configurations, helping to ensure complete cleaning and obturation.[16,17]

Conclusion

Anatomical variations in the maxillary permanent canine, including the presence of one root and three canals, are extremely rare but clinically significant. Precise identification of such anomalies is critical for effective endodontic treatment. While conventional radiographs remain useful, cone-beam computed tomography should be employed in cases where anatomical complexity is suspected or when standard imaging proves inadequate. Accurate diagnosis and management of these unusual cases can significantly enhance the success of root canal therapy.

Conflicts of Interest

The authors declare that they have no competing interests.

References

1. Bhadora A, Nikhil V, Iha P, Mishra P. An intriguing case of maxillary canine with two canals: A rare entity. International Journal of Research and Review.2021:8(5).
2. Shin DR, Kim JM, Kim DS, Kim SY, Abbot PV, Park SH. A maxillary canine with two separated root canals: a case report. JKACD. September 2011;36(5):431-434.
3. Vertucci FJ. Root canal anatomy of the human permanent teeth. Oral Surg Oral Med Oral Pathol. 1984 Nov;58(5):589-99. doi: 10.1016/0030-4220(84)90085-9. PMID: 6595621.
4. Plascencia H, Cruz Á, Palafox-Sánchez CA, Díaz M, López C, Bramante CM, Moldauer BI, Ordinola-Zapata R. Micro-CT study of the root canal anatomy of maxillary canines. J Clin Exp Dent. 2017 Oct 1;9(10):e1230-e1236. doi: 10.4317/jced.54235. PMID: 29167714; PMCID: PMC5694153.
5. Muppalla JN, Kavuda K, Punna R, Vanapatla A. Management of an Unusual Maxillary Canine: A Rare Entity. Case Rep Dent. 2015;2015:780908. doi: 10.1155/2015/780908. Epub 2015 Dec 8. PMID: 26779354; PMCID: PMC4686623.
6. Dong Ryul Shin, Jin- Man Kim, Duk- Su Kim, Su Youg Kim, Paul V Abbot, FRACDS, FPFA, FADI, FICD, FACD, San Hjuk Park. A maxillary canine with two separated root canals: a case report. Restorative Dentistry&Endodontics. 2011, Sept 36(5):435.
7. Assiry A. Bi-rooted primary maxillary canines: a case report. J Med Case Rep. 2019 Aug 7;13(1):261. doi: 10.1186/s13256-019-2174-9. PMID: 31387625; PMCID: PMC6685265.
8. Uchiyama M, Anzai M, Yamamoto A, Uchida K, Utsuno H, Kawase Y, Kasahara E. Root canal system of the maxillary canine. Okajimas Folia Anat Jpn. 2011 Feb;87(4):189-93. doi: 10.2535/ofaj.87.189. PMID: 21516985.
9. Kelly JR. Birooted primary canines. Oral Surg Oral Med Oral Pathol. 1978 Dec;46(6):872. doi: 10.1016/0030-4220(78)90323-7. PMID: 282552.
10. Orhan AI, Sari S. Double-rooted primary canines: A report of three cases. J Indian Soc Pedod Prev Dent. 2006 Dec;24(4):204-8. doi: 10.4103/0970-4388.28079. PMID: 17183186.
11. Almulhim B. Bilateral occurrence of bimaxillary bi-rooted primary canines: a rare case report with review of the literature. Surg Radiol Anat. 2021 Jun;43(6):997-1000. doi: 10.1007/s00276-020-02633-1. Epub 2021 Jan 3. PMID: 33388946.
12. Talebi M, Parisay I, Khorakian F, Bagherian M. Bi-rooted Primary Maxillary Canines: A Case Report. J Dent Res Dent Clin Dent Prospects. 2010 Summer;4(3):101-3. doi: 10.5681/joddd.2010.026. Epub 2010 Sep 16. PMID: 22991609; PMCID: PMC3429982.
13. Sert S, Bayirli GS. Evaluation of the root canal configurations of the mandibular and maxillary permanent teeth by gender in the Turkish population. J Endod. 2004 Jun;30(6):391-8. doi: 10.1097/00004770-200406000-00004. PMID: 15167464.
14. Velmurugan N, Sandhya R. Root canal morphology of mandibular first premolars in an Indian population: a laboratory study. Int Endod J. 2009 Jan;42(1):54-8. doi: 10.1111/j.1365-2591.2008.01494.x. PMID: 19125980.
15. Schwarze T, Baethge C, Stecher T, Geurtsen W. Identification of second canals in the mesiobuccal root of

maxillary first and second molars using magnifying loupes or an operating microscope. Aust Endod J. 2002 Aug;28(2):57-60. doi: 10.1111/j.1747-4477.2002.tb00379.x. PMID: 12360670.
16. Kim Y, Lee SJ, Woo J. Morphology of maxillary first and second molars analyzed by cone-beam computed tomography in a korean population: variations in the number of roots and canals and the incidence of fusion. J Endod. 2012 Aug;38(8):1063-8. doi: 10.1016/j.joen.2012.04.025. Epub 2012 Jun 20. PMID: 22794206.
17. Cotton TP, Geisler TM, Holden DT, Schwartz SA, Schindler WG. Endodontic applications of cone-beam volumetric tomography. J Endod. 2007 Sep;33(9):1121-32. doi: 10.1016/j.joen.2007.06.011. Epub 2007 Jul 19. PMID: 17931947.
18. Somalinga Amardeep N, Raghu S, Natanasabapathy V. Root canal morphology of permanent maxillary and mandibular canines in Indian population using cone beam computed tomography. Anat Res Int. 2014;2014:731859. doi: 10.1155/2014/731859. Epub 2014 May 6. PMID: 24895538; PMCID: PMC4033413.
19. Neelakantan P, Subbarao C, Ahuja R, Subbarao CV, Gutmann JL. Cone-beam computed tomography study of root and canal morphology of maxillary first and second molars in an Indian population. J Endod. 2010 Oct;36(10):1622-7. doi: 10.1016/j.joen.2010.07.006. Epub 2010 Aug 30. PMID: 20850665.
20. A Supritha, Ashwija Shetty, Sriekha A, Lekha S, Chapa C. An Unusual Entity of Three Canals in a Maxillary Canine: A Case Report. Journal of Dental and Medical Sciences. 2021;20(2): 06-09.
21. Hildebolt CF, Vannier MW, Pilgram TK, Shrout MK. Quantitative evaluation of digital dental radiograph imaging systems. Oral Surg Oral Med Oral Pathol. 1990 Nov;70(5):661-8. doi: 10.1016/0030-4220(90)90419-s. PMID: 2234888.
22. Peters OA. Current challenges and concepts in the preparation of root canal systems: a review. J Endod. 2004 Aug;30(8):559-67. doi: 10.1097/01.don.0000129039.59003.9d. PMID: 15273636.
23. Gehlot PM, Murali B, Ghosh S, Shafiq SM. Non-surgical Endodontic Management of a Permanent Maxillary Canine With Vertucci Type 3 Canal Configuration: A Case Report. Cureus. 2024 Oct 28;16(10):e72565. doi: 10.7759/cureus.72565. PMID: 39606508; PMCID: PMC11602104.
24. Kandasamy S, Balakrishnan N, Chandrasekar M. A Three-Rooted Permanent Maxillary Canine: A Rare Anatomical Variant. J Pharm Bioallied Sci. 2019 May;11(Suppl 2):S485-S487. doi: 10.4103/JPBS.JPBS_292_18. PMID: 31198392; PMCID: PMC6555322.
25. Galhotra V, Pandit IK, Srivastava N, Gugnani N. Endodontic treatment of a multirooted permanent maxillary canine. J Dent Child (Chic). 2007 Jan-Apr;74(1):73-5. PMID: 18430359.
26. Bolla N, Kavuri SR. Maxillary canine with two root canals. J Conserv Dent. 2011 Jan;14(1):80-2. doi: 10.4103/0972-0707.80726. PMID: 21691513; PMCID: PMC3099122.
27. Wolf TG, Rempapi T, Wierichs RJ, Waber AL. Morphology and root canal configuration of maxillary canines: a systematic review and meta-analysis. BMC Oral Health. 2024 Aug 15;24(1):944. doi: 10.1186/s12903-024-04682-z. PMID: 39143543; PMCID: PMC11325658.
28. Martins JNR, Marques D, Mata A, Caramês J. Root and root canal morphology of the permanent dentition in a Caucasian population: a cone-beam computed tomography study. Int Endod J. 2017 Nov;50(11):1013-1026. doi: 10.1111/iej.12724. Epub 2017 Jan 3. PMID: 27883205.
29. Mashyakhy M. Prevalence of a Second Root and Canal in Mandibular and Maxillary Canines in a Saudi Arabian Population: A Cone-beam Computed Tomography Study. J Contemp Dent Pract. 2019 Jul 1;20(7):773-777. PMID: 31597794.
30. Almulhim B. Bilateral occurrence of bimaxillary bi-rooted primary canines: a rare case report with review of the literature. Surg Radiol Anat. 2021 Jun;43(6):997-1000. doi: 10.1007/s00276-020-02633-1. Epub 2021 Jan 3. PMID: 33388946.

International Journal of Biomedicine 15(4) (2025) 767
http://dx.doi.org/10.21103/Article15(4)_ER1

RETRACTION

INTERNATIONAL JOURNAL OF BIOMEDICINE

RETRACTED: Morphological Substantiation for the Effectiveness of the Proposed Method of Gastrostomy using a Polypropylene Endoprosthesis

International Journal of Biomedicine

Editorial Retraction

International Journal of Biomedicine has retracted the article titled "Morphological Substantiation for the Effectiveness of the Proposed Method of Gastrostomy using a Polypropylene Endoprosthesis" (Shurygin SN, Vaganov AG, Tsulaya AS, Asratyan SA, Sazhin IV, Alimov AN, Safonov LV, Volkov DA. Morphological Substantiation for the Effectiveness of the Proposed Method of Gastrostomy using a Polypropylene Endoprosthesis. International Journal of Biomedicine. 2020;10(1):45-49. doi: 10.21103/Article10(1)_OA6.) The above article has been retracted due to concerns regarding the reliability of the data. All authors agree with the retraction of the article. The retracted article will remain online to maintain the scholarly record, but each page will be digitally watermarked with the label "Retracted." (International Journal of Biomedicine. 2025;15(4):767.)

For citation: International Journal of Biomedicine. RETRACTED: Morphological Substantiation for the Effectiveness of the Proposed Method of Gastrostomy using a Polypropylene Endoprosthesis. International Journal of Biomedicine. 2025;15(4):767. doi: 10.21103/Article15(4)_ER1.

International Journal of Biomedicine 15(4) (2025) 768
http://dx.doi.org/10.21103/Article15(4)_ER2

RETRACTION

INTERNATIONAL JOURNAL OF BIOMEDICINE

RETRACTED: Experimental Substantiation for the Effectiveness of Gastrostomy using a Polypropylene Endoprosthesis Based on a Comparative Morphological Assessment of the State of the Hollow Organs of the Gastrointestinal Tract

International Journal of Biomedicine

Editorial Retraction

International Journal of Biomedicine has retracted the article titled "Experimental Substantiation for the Effectiveness of Gastrostomy using a Polypropylene Endoprosthesis Based on a Comparative Morphological Assessment of the State of the Hollow Organs of the Gastrointestinal Tract" (Shurygin SN, Vaganov AG, Tsulaya AS, Asratyan SA, Sazhin IV, Alimov AN, Safonov LV, Volkov DA. Morphological Substantiation for the Effectiveness of the Proposed Method of Gastrostomy using a Polypropylene Endoprosthesis. International Journal of Biomedicine. 2020;10(3):251-256. doi: 10.21103/Article10(3)_OA10). The above article has been retracted due to concerns regarding the reliability of the data. All authors agree with the retraction of the article. The retracted article will remain online to maintain the scholarly record, but each page will be digitally watermarked with the label "Retracted." (International Journal of Biomedicine. 2025;15(4):768.)

For citation: International Journal of Biomedicine. RETRACTED: Experimental Substantiation for the Effectiveness of Gastrostomy using a Polypropylene Endoprosthesis Based on a Comparative Morphological Assessment of the State of the Hollow Organs of the Gastrointestinal Tract. International Journal of Biomedicine. 2025;15(4):768. doi: 10.21103/Article15(4)_ER2.

IJBM

INTERNATIONAL JOURNAL OF BIOMEDICINE

Instructions for Authors

International Journal of Biomedicine (IJBM) publishes peer-reviewed articles on the topics of basic, applied, and translational research on biology and medicine. International Journal of Biomedicine welcomes submissions of the following types of paper: Original articles, Reviews, Perspectives, Viewpoints, and Case Reports.

All research studies involving animals must have been conducted following animal welfare guidelines such as *the National Institutes of Health (NIH) Guide for the Care and Use of Laboratory Animals*, or equivalent documents. Studies involving human subjects or tissues must adhere to the *Declaration of Helsinki and Title 45, US Code of Federal Regulations, Part 46, Protection of Human Subjects*, and must have received approval of the appropriate institutional committee charged with oversight of human studies. Informed consent must be obtained.

Pre-submissions

Authors are welcome to send an abstract or draft manuscript to obtain a view from the Editor about the suitability of their paper. Our Editors will do a quick review of your paper and advise if they believe it is appropriate for submission to our journal. It will not be a full review of your manuscript.

Manuscript Submission

Manuscript submissions should conform to the guidelines set forth in the Recommendations for the Conduct, Reporting, Editing and Publication of Scholarly Work in Medical Journals (ICMJE Recommendations), available from www.ICMJE.org.

Original works will be accepted with the understanding that they are contributed solely to the Journal, are not under review by another publication, and have not previously been published except in abstract form.

All manuscripts must be submitted through the International Journal of Biomedicine`s online submission system (www.ijbm.org/submission.php). Manuscripts must be typed, double-spaced using a 14-point font, including references, figure legends, and tables. Leave 1-inch margins on all sides. Assemble the manuscript in this order: Title Page, Abstract, Key Words, Text (Introduction, Methods, Results, and Discussion), Acknowledgments, Sources of Funding, Disclosures, References, Tables, Figures, and Figure Legends. References, figures, and tables should be cited in numerical order according to first mention in the text.

The preferred order for uploading files is as follows: Cover letter, Full Manuscript PDF (PDF containing all parts of the manuscript including references, legends, figures and tables), Manuscript Text File (MS Word), Figures (each figure and its corresponding legend should be presented together), and Tables. Files should be labeled with appropriate and descriptive file names (e.g., SmithText.doc, Fig1.eps, Table3.doc). Text, Tables, and Figures should be uploaded as separate files. (Multiple figure files can be compressed into a Zip file and uploaded in one step; the system will then unpack the files and prompt the naming of each figure. See www.WinZip.com for a free trial.)

Authors who are unable to provide an electronic version or have other circumstances that prevent online submission must contact the Editorial Office prior to submission to discuss alternate options (editor@ijbm.org).

Cover Letter

The cover letter should be saved as a separate file for upload. In it, the authors should (1) state that the manuscript, or parts of it, have not been and will not be submitted elsewhere for publication; (2) state that all authors have read and approved the manuscript; and (3) disclose any financial or other relations that could lead to a conflict of interest. If a potential conflict exists, its nature should be stated for each author. When there is a stated potential conflict of interest a footnote will be added indicating the author's equity interest in or other affiliation with the identified commercial firms.

The corresponding author should be specified in the cover letter. All editorial communications will be sent to this author. A short paragraph telling the editors why the authors think their paper merits publication priority may be included in the cover letter.

Types of articles

Original articles

Original articles present the results of original research. These manuscripts should present well-rounded studies reporting innovative advances that further knowledge about a topic of importance to the fields of biology or medicine. These can be submitted as either a full-length article (no more than 6,000 words, 4 figures, 4 tables) or a Short Communication (no more than 2,500 words, 2 figures, 2 tables). An original

article may be Randomized Control Trial, Controlled Clinical Trial, Experiment, Survey, and Case-control or Cohort study.

Case Reports

Case reports describe an unusual disease presentation, a new treatment, a new diagnostic method, or a difficult diagnosis. The author must make it clear what the case adds to the field of medicine and include an up-to-date review of all previous cases in the field. These articles should be no more than 5,000 words with no more than 6 figures and 3 tables. Case Reports should consist of the following headings: Abstract (no more than 100 words), Introduction, Case Presentation (clinical presentation, observations, test results, and accompanying figures), Discussion, and Conclusions.

Reviews

Reviews analyze the current state of understanding on a particular subject of research in biology or medicine, the limitations of current knowledge, future directions to be pursued in research, and the overall importance of the topic. Reviews could be non-systematic (narrative) or systematic. Reviews can be submitted as a Mini-Review (no more than 2,500 words, 3 figures, and 1 table) or a long review (no more than 6,000 words, 6 figures, and 3 tables). Reviews should contain four sections: Abstract, Introduction, Topics (with headings and subheadings, and Conclusions and Outlook.

Perspectives

Perspectives are brief, evidenced-based and formally structured essays covering a wide variety of timely topics of relevance to biomedicine. Perspective articles are limited to 2,500 words and usually include ≤10 references, one figure or table. Perspectives contain four sections: Abstract, Introduction, Topics (with headings and subheadings), Conclusions and Outlook.

Viewpoints

Viewpoint articles include academic papers, which address any important topic in biomedicine from a personal perspective than standard academic writing. Maximum length is 1,200 words, ≤70 references, and 1 small table or figure.

Manuscript Preparation

Title Page

The first page of the manuscript (title page) should include (1) a full title of the article, (2) a short title of less than 60 characters with spaces, (3) the authors' names, academic degrees, and affiliations, (4) the total word count of the manuscript (including Abstract, Text, References, Tables, Figure Legends), (5) the number of figures and tables, and (6) the name, email address, and complete address of corresponding author.

Disclaimers. An example of a disclaimer is an author's statement that the views expressed in the submitted article are his or her own and not an official position of the institution or funder.

Abstract

The article should include a brief abstract of no more than 200 words. Limit use of acronyms and abbreviations. Define at first use with acronym or abbreviation in parentheses. The abstract should be structured with the following headings: Background, Methods and Results, and Conclusions. The Background section should describe the rationale for the study. Methods and Results should briefly describe the methods and present the significant results. Conclusions should succinctly state the interpretation of the data. Authors should supply a list of up to four key words not appearing in the title, which will be used for indexing. The key words should be listed immediately after the Abstract. Use terms from the Medical Subject Headings (MeSH) list of Index Medicus when possible.

Main text in the IMRaD format

Introduction should describe the purpose of the study and its relation to previous work in the field; it should not include an extensive literature review.

Methods should be concise but sufficiently detailed to permit repetition by other investigators. Previously published methods and modifications should be cited by reference. A subsection on statistics should be included in the Methods section.

Results should present positive and relevant negative findings of the study, supported when necessary by reference to Tables and Figures.

Discussion should interpret the results of the study, with emphasis on their relation to the original hypotheses and to previous studies. The importance of the study and its limitations should also be discussed.

The IMRaD format does not include a separate Conclusion section. The conclusion is built into the Discussion. More information on the structure and content of these sections can be found in the Recommendations for the Conduct, Reporting, Editing and Publication of Scholarly Work in Medical Journals (ICMJE Recommendations), available from www.ICMJE.org.

Acknowledgments, Sources of Funding, and Disclosures

Acknowledgments : All contributors who do not meet the criteria for authorship should be listed in an acknowledgments section. Examples of those who might be acknowledged include a person who provided purely technical help, writing assistance, or a department chairperson who provided only general support. Authors should declare whether they had assistance with study design, data collection, data analysis, or manuscript preparation. If such assistance was available, the authors should disclose the identity of the individuals who provided this assistance and the entity that supported it in the published article.

Sources of Funding: All sources of financial support for the study should be cited on the title page, including federal or state agencies, nonprofit organizations, and pharmaceutical or other commercial sources.

Disclosure and conflicts of interest: All authors must disclose any financial or other relations that could lead to a conflict of interest. If a potential conflict exists, its nature should be stated for each author. All sources of financial support for the study should be cited, including federal or state agencies, nonprofit organizations, and pharmaceutical or other commercial sources. Please use ICMJE Form for Disclosure of Potential Conflicts of Interest (http://www.icmje.org/conflicts-of-interest/).

References

References should follow the standards summarized in the NLM's International Committee of Medical Journal Editors (ICMJE) Recommendations for the Conduct,

Reporting, Editing and Publication of Scholarly Work in Medical Journals: Sample References webpage (www.nlm.nih.gov/bsd/uniform_requirements.html) and detailed in the NLM's Citing Medicine, available from www.ncbi.nlm.nih.gov/books/NBK7256/. MEDLINE abbreviations for journal titles (www.ncbi.nlm.nih.gov/nlmcatalog/journals) should be used.

References should be presented in the Vancouver style. The first six authors should be listed in each reference citation (if there are more than six authors, "et al" should be used following the sixth). Periods are not used in authors' initials or journal abbreviations. Examples of journal reference style:

Journal Article: Serruys PW, Ormiston J, van Geuns RJ, de Bruyne B, Dudek D, Christiansen E, et al. A Polylactide Bioresorbable Scaffold Eluting Everolimus for Treatment of Coronary Stenosis: 5-Year Follow-Up. J Am Coll Cardiol. 2016;67(7):766-76. doi: 10.1016/j.jacc.2015.11.060.

Book: Murray PR, Rosenthal KS, Kobayashi GS, Pfaller MA. Medical Microbiology. 4th ed. St. Louis: Mosby; 2002.

Chapter in Edited Book: Meltzer PS, Kallioniemi A, Trent JM. Chromosome alterations in human solid tumors. In: Vogelstein B, Kinzler KW, editors. The Genetic Basis of Human Cancer. New York: McGraw-Hill; 2002:93–113.

References should be numbered consecutively in the order in which they are first mentioned in the text. Identify references in text, tables, and legends by Arabic numerals in parentheses and listed at the end of the article in citation order.

Tables

Tables should be comprehensible without reference to the text and should not be repetitive of descriptions in the text. Every table should consist of two or more columns; tables with only one column will be treated as lists and incorporated into the text. All tables must be cited in the text and numbered in order of appearance. Tables should include a short title. Place explanatory matter in footnotes, not in the heading. Explain all nonstandard abbreviations in footnotes, and use symbols to explain information if needed. Each table submitted should be double-spaced, each on its own page. Each table should be saved as its own file as a Word Document. Explanatory matter and source notations for borrowed tables should be placed in the table footnote.

Figures and Legends

All illustrations (line drawings and photographs) are classified as figures. All figures should be cited in the text and numbered in order of appearance. Figures should be provided in .tiff, .jpeg or .eps formats. Color images must be at least 300 dpi. Gray scale images should be at least 300 dpi. Line art (black and white or color) and combinations of gray scale images and line art should be at least 1,000 dpi. The optimal size of lettering is 12 points. Symbols should be of a similar size. Figures should be sized to fit within the column (86 mm) or the full text width (180 mm). Line figures must be sharp, black and white graphs or diagrams, drawn professionally or with a computer graphics package. Legends should be supplied for each figure and should be brief and not repetitive of the text. Any source notation for borrowed figures should appear at the end of the legend. Figures should be uploaded as individual files.

Units of Measurement

Measurements of length, height, weight, and volume should be reported in metric units (meter, kilogram, or liter) or their decimal multiples. Temperatures should be in degrees Celsius. Blood pressures should be in millimeters of mercury. All measurements must be given in SI or SI-derived units. Drug concentrations may be reported in either SI or mass units, but the alternative should be provided in parentheses where appropriate.

Style and Language

The journal accepts manuscripts written in English. Spelling should be US English only. The language of the manuscript must meet the requirements of academic publishing. Reviewers may advise rejection of a manuscript compromised by grammatical errors. Non-native speakers of English may choose to use a copyediting service.

Abbreviations and Symbols

Use only standard abbreviations; use of nonstandard abbreviations can be confusing to readers. Avoid abbreviations in the title of the manuscript. The spelled-out abbreviation followed by the abbreviation in parenthesis should be used on first mention unless the abbreviation is a standard unit of measurement.

Drugs should be referred to by their generic names. If proprietary drugs have been used in the study, refer to these by their generic name, mentioning the proprietary name, and the name and location of the manufacturer, in parentheses.

Permissions

To use tables or figures borrowed from another source, permission must be obtained from the copyright holder, usually the publisher. Authors are responsible for applying for permission for both print and electronic rights for all borrowed materials and are responsible for paying any fees related to the applications of these permissions. This is necessary even if you are an author of the borrowed material. It is essential to begin the process of obtaining permission early, as a delay may require removing the copyrighted material from the article. The source of a borrowed table should be noted in a footnote and of a borrowed figure in the legend. It is essential to use the exact wording required by the copyright holder. A copy of the letter granting permission, identified by table or figure number, should be sent along with the manuscript. A permission request form is provided for the authors use in requesting permission from copyright holders.

Page Proofs

Page proofs are sent from the Publisher electronically and must be returned within 72 hours to avoid delay of publication. Generally, peer review is completed within 4-5 weeks.

It is important to note that when citing an article from IJBM, the correct citation format is **International Journal of Biomedicine.**

IJBM

INTERNATIONAL JOURNAL OF BIOMEDICINE

International Journal of Biomedicine (IJBM) is an open access journal. IJBM publishes peer-reviewed articles on aspects of basic, applied, and translational research in biology and medicine. The main purpose of IJBM is to establish a scientific platform for targeted promotion of new scientific ideas and biomedical technologies focused on the applied aspects of biomedicine.

The journal publishes articles on:

Internal Medicine
Cardiology
Pulmonology
Endocrinology
Neurology
Hepatology
Gastroenterology
Nephrology
Ophthalmology
Otorhinolaryngology
Radiology
Surgery
Obstetrics and Gynecology
Pediatrics
Dermatology and STD
Clinical Immunology
Oncology
Genomics and Proteomics
Population Genetics
Epidemiology and Population Health
Reproductive Health
Adolescent Health
Cell Biology
Experimental Biology
Biotechnology
Dentistry
Infectious Diseases
Sports Medicine

Authors are invited to submit:

Original articles
Review articles
Case reports
Perspectives
Viewpoints